

Design, synthesis and biological assessment of SERS guided cell surface glycan modifications and anti- calcification properties of nano-rhein

by

MADHUKRISHNAN M.

10CC18A39004

A thesis submitted to the
Academy of Scientific & Innovative Research
for the award of the degree of

DOCTOR OF PHILOSOPHY
in
SCIENCE

Under the supervision of

Dr. KAUSTABH KUMAR MAITI



**CSIR-National Institute for Interdisciplinary
Science and Technology (CSIR-NIIST)
Thiruvananthapuram, Kerala- 695 019, India**



**Academy of Scientific and Innovative Research
AcSIR Headquarters, CSIR-HRDC campus
Sector 19, Kamla Nehru Nagar,
Ghaziabad, U.P. – 201 002, India**

JULY-2024

Dedicated to my beloved Family



CSIR- National Institute for Interdisciplinary
Science and Technology

(Formerly Regional Research laboratory)

Council of Scientific & Innovative Research (CSIR)


Industrial Estate P.O., Trivandrum-695 019

Kerala, INDIA

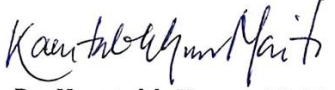


CERTIFICATE

This is to certify that the work incorporated in this PhD thesis entitled, “**Design, synthesis and biological assessment of SERS guided cell surface glycan modifications and anti-calcification properties of nano-rhein**” submitted by Mr. Madhukrishnan M., to the Academy of Scientific and Innovative Research (AcSIR) in fulfilment of the requirements for the award of the Degree of *Doctor of Philosophy* in Science, embodies original research work carried out by the student. We further certify that this work has not been submitted to any other University or Institution in part or full for the award of any degree or diploma. Research materials obtained from other sources and used in this research work has been duly acknowledged in the thesis. Images, illustrations, figures, tables etc., used in the thesis from other sources, have also been duly cited and acknowledged.


Madhukrishnan M.

July 31, 2024


Dr. Kaustabh Kumar Maiti

(Supervisor)

July 31, 2024

STATEMENTS OF ACADEMIC INTEGRITY

I, Madhukrishnan M. a Ph.D student of the Academy of Scientific and Innovative Research (AcSIR) with Registration No. 10CC18A39004 hereby undertake that, the thesis entitled **“Design, synthesis and biological assessment of SERS guided cell surface glycan modifications and anti-calcification properties of nano-rhein”** has been prepared by me and that the document reports original work carried out by me and is free of any plagiarism in compliance with the UGC Regulations on *“Promotion of Academic Integrity and Prevention of Plagiarism in Higher Educational Institutions (2018)”* and the CSIR guidelines for *“Ethics in Research and in Governance (2020)”*.

July 31, 2024


Madhukrishnan M.

Thiruvananthapuram

It is here by certified that the work done by the student, under our supervision, is plagiarism free in accordance with the UGC Regulations on *“Promotion of Academic Integrity and Prevention of Plagiarism in Higher Educational Institutions (2018)”* and the CSIR guidelines for *“Ethics in Research and in Governance (2020)”*.


Dr. Kaustabh Kumar Maiti

July 31, 2024

Thiruvananthapuram

DECLARATION

I, **Madhukrishnan M.**, bearing AcSIR Registration No. 10CC18A39004 declare that, my thesis entitled, “**Design, synthesis and biological assessment of SERS guided cell surface glycan modifications and anti-calcification properties of nano-rhein**” is plagiarism free in accordance with the UGC Regulations on “*Promotion of Academic Integrity and Prevention of Plagiarism in Higher Educational Institutions (2018)*” and the CSIR guidelines for “*Ethics in Research and in Governance (2020)*”.

I would be solely held responsible if any plagiarised content in my thesis is detected, which is violative of the UGC regulations 2018.

July 31, 2024

Thiruvananthapuram



Madhukrishnan M.

ACKNOWLEDGEMENTS

*It is with great respect that I express my deep sense of gratitude and obligation to my mentor and research supervisor **Dr. Kaustabh Kumar Maiti** for suggesting the research topic and also for their excellent guidance, constant encouragement, and constructive criticism.*

I am grateful to Dr. C. Anandharamakrishnan and Dr. A. Ajayaghosh, present and former Directors of, the CSIR-National Institute for Interdisciplinary Science and Technology, for providing all infrastructural facilities to carry out this work.

My sincere thanks are also due to:

- ❖ *Dr. P. Jayamurthy, Dr. V. Karunakaran and Dr. C. H. Suresh, present and former AcSIR programme coordinator, CSIR-NIIST for the timely help and advice for the academic procedures of AcSIR*
- ❖ *Dr. K. V. Radhakrishnan, Dr. B.S. Sasidhar, and Dr. S. Priya (my Doctoral Advisory Committee members) for their valuable suggestions and evaluations throughout my Ph. D. period.*
- ❖ *Dr. K. V. Radhakrishnan, Dr. P. Sujatha Devi, Dr. R. Luxmi Varma, present and former Heads, Chemical Sciences and Technology Division for their endless support.*
- ❖ *Dr. K. V. Radhakrishnan, Dr. B. S. Sasidhar, Dr L Ravi Sankar, Dr. Sunil Varughese, and Dr. Jubi John Scientists of Organic Chemistry Section for the stimulation and assistance.*
- ❖ *Prof. Elambalassery Jayasree, CUSAT for the wonderful collaboration in computational studies.*
- ❖ *Dr. Manu M Joseph, Dr. Vishnu Priya Murali and Dr. Varsha Karunakaran for teaching me the initial lessons of research.*
- ❖ *Dr. Shamjith S, Mr. Vimal Kumar, for helping me to conduct some of the experiments in laboratory.*
- ❖ *Dr. Maniganda, Dr. Saranya, Dr. Ramya A N., Dr. Jyothi B Nair, Dr. Arya J S, Dr. Sujai P T, my seniors for the valuable suggestions and support throughout my work.*
- ❖ *Dr. Drishya Elizabeth, Mr. Vijayakumar Swamiyappan, Dr. Aswathy M for the fruitful discussions and support.*
- ❖ *Mrs. Saumini Mathew, Mr Saran for NMR analysis, Mrs. Viji S. for HRMS, Mr. Kiran Mohan for TEM analysis, Mr. Harish for SEM analysis.*

- ❖ *Mrs. Theresa George, Mrs Soumya Rajan, Ms. Sharmida Bhanu, Mr. Harishankar M S, Mr. Vishnu Prasad M M for helping me to complete some of the lab works.*
- ❖ *All the present and former members of K.K.M group.*
- ❖ *All present and former members of Organic Chemistry Section for their friendship and creative inspirations.*
- ❖ *All my friends at CSIR-NIIST.*
- ❖ *All my teachers in S.N. College, Nattika for the care and support.*

Words are inadequate to express my feelings for the love, care, support, and encouragement shown by my parents (Mrs. Ajitha K and Late. Mr. Murali P) Sister (Aswathy M.), Partner (Dr. Aswathy M.) throughout my academic career.

I am grateful to University Grants Commission (UGC), for the financial assistance.

And above all, I thank Almighty for all his blessings.

Madhukrishnan M.

TABLE OF CONTENTS

	Page
Certificate	i
Statements of academic integrity	ii
Declaration	iii
Acknowledgements	iv
Table of contents	vi
List of Abbreviations	xi
Preface	xix
CHAPTER 1: Insights of surface enhanced Raman scattering in glycan recognition and hypercalciuria-induced nephropathies	01-32
1.1. Abstract	1
1.2. Surface Enhanced Raman Scattering (SERS)	2
1.2.1. SERS imaging	3
1.2.2. Cellular imaging utilising SERS	3
1.2.3. In vivo imaging	5
1.3. Bioorthogonal chemistry	6
1.4. Glycans and their detection	11
1.4.1. Biological functions of glycans and glycoconjugates	11
1.4.2. Glycan in cancer progression	12
1.4.3. Detection of glycans	13
1.5. Metabolic labelling	15
1.5.1. Metabolic labelling strategies to evaluate different modalities	16
1.5.2. Metabolic glycan labelling through the fluorescent modality	19
1.5.3. Raman-assisted metabolic labelling (RAML) techniques	21

1.6.	Vascular calcification and its involvement in chronic kidney disease	23
1.6.1.	Pathophysiology of VC in CKD	24
1.6.2.	Involvement of calcium oxalate in VC	24
1.6.3.	Therapeutic approaches and involvement of SERS in recognising VC	25
1.7.	Conclusion	26
1.8.	Objectives of the present investigation	27
1.9.	References	28
CHAPTER 2:	Exploring cell surface glycan imbalance via SERS-guided metabolic glycan labelling: assessing metastatic potential in cancer cells	33-67
2.1.	Abstract	33
2.2.	Introduction	34
2.2.1.	An overview of metabolic labelling of glycans	36
2.3.	Aim and scope of the study	37
2.4.	Result and Discussion	38
2.4.1.	Synthesis and characterization	38
2.4.1.1.	General procedure for the synthesis of alkynylated glucosamine derivatives	39
2.4.1.2.	Synthesis of GlcNAlk	41
2.4.2.	SERS analysis of alkynylated glucosamine analogues	44
2.4.3.	Cytotoxicity studies of alkynylated compounds	47
2.4.4.	Metabolic glycan labelling of glucosamine analogues	48
2.4.5.	Complementary glycan labelling through fluorescence and western blot Analysis	49
2.4.5.1.	Synthesis of azidonaphthalimide derivative	50

2.4.5.2.	Cu catalysed click reaction between alkynylated glucosamine and azido naphthalimide flourophore	51
2.4.6.	Metastatic potential and cell-surface glycosylation in cancer cells	54
2.4.7.	Glycosylation inhibition through SERS Assessment	56
2.5.	Conclusion	57
2.6.	Experimental methods	58
2.6.1.	Materials and methods	58
2.6.2.	Synthesis of gold nanoparticle	59
2.6.3.	Cellular studies	59
2.6.3.1.	Cytotoxicity studies of alkynylated compounds	59
2.6.3.2.	Cell culture and metabolic labelling of cell surface glycans	59
2.6.3.3.	Thiobarbituric acid (TBA) method for sialic acid quantification	60
2.6.3.4.	Western blotting	60
2.6.3.5.	Live cell imaging	61
2.6.3.5.1.	SERS evaluation of molecules and metabolic labelling	61
2.6.3.5.2.	Comparative analysis method of Raman intensity of tags	61
2.6.3.5.3.	Generation of secondary images from Raman field images using commands	61
2.6.3.5.4.	Fluorescence microscopy and imaging	62
2.7.	Spectral data	62
2.8.	Reference	63
CHAPTER 3:	Investigation into the substrate promiscuity of hexosamine biosynthetic enzymes using unnatural sugar derivatives	68-102
3.1.	Abstract	68
3.2.	Introduction	69
3.3.	Aim and scope of the study	73
3.4.	Results and Discussion	74

3.4.1.	Synthesis and characterisation of hexosamine derivatives	74
3.4.1.1.	Synthesis of GlcNPhAlk, ManNPhAlk	75
3.4.1.2.	Synthesis of GlcNAcPhAlk and ManNAcPhAlk	78
3.4.1.3.	Synthesis of GlcNAcOPhAlk and ManNAcOPhAlk	82
3.4.2.	SERS analysis of glycan precursors	85
3.4.3.	Cytotoxicity studies of glycan precursors	86
3.4.4.	Metabolic labelling of glycan precursors	87
3.4.5.	Inhibitor studies on metabolic labelling of glycan precursors	88
3.4.6.	Confirmation of protein glycosylation by far-western blot analysis	91
3.4.7.	Inhibitor studies on metabolic labelling of glycan precursors by far-western blot analysis	92
3.5.	Conclusion	94
3.6.	Experimental section	95
3.6.1.	General Experimental Methods	95
3.6.2.	Synthesis of gold nanoparticle	95
3.6.3.	Cellular studies	95
3.6.3.1.	Cell culture and metabolic labelling of cell surface glycans	95
3.6.3.2.	Far-western blotting	96
3.6.3.3.	Live cell imaging	97
3.6.3.3.1.	SERS evaluation of molecules and metabolic labelling	97
3.7.	Spectral data	97
3.8.	References	100
CHAPTER 4:	Repurposing nano-dimensions of a small phytomolecule, rhein into nano-rhein, to investigate its efficacy on hypercalciuria-induced nephropathies by SERS-imaging	103-130
4.1.	Abstract	103
4.2.	Introduction	104

4.3.	Aim and scope of the study	107
4.4.	Results and Discussion	108
4.4.1.	Synthesis and morphological characterization of nano-rhein (NR)	108
4.4.2.	The self-assembly mechanism of rhein nanoparticles	110
4.4.3.	Anti-calcification property of rhein and NR	112
4.4.4.	Mechanism of CaOx inhibition by NR	115
4.4.5.	SERS-imaging platform for monitoring calcification processes	118
4.4.6.	Transcriptomic assessment of vascular calcification processes and anti-calcification responses by NR	121
4.5.	Conclusion	124
4.6.	Experimental Section	125
4.6.1.	Materials and methods	125
4.6.2.	Scanning Electron Microscopy (SEM)	125
4.6.3.	Cell based studies	126
4.6.3.1.	Cytotoxicity studies of rhein and NR	126
4.6.3.2.	Cell culture and metabolic labelling of cell surface glycans	126
4.6.4.	RNA Sequencing	127
4.6.5.	Bioinformatics analyses	127
4.6.6.	DFT studies	128
4.6.7.	Spectral data of Rhein	128
4.7.	References	128
	Abstract of the thesis	131
	List of publications	132
	List of Posters & Conferences	133
	Attachment of the Photocopy of Publications	

ABBREVIATIONS

Å	:	Angstrom
α	:	Alpha
Ac	:	Acetyl
AFM	:	Atomic force microscopy
AKI	:	acute kidney injury
apps	:	Apparent singlet
APEX	:	Ascorbate peroxidase
ARS	:	Alizarin Red S assays
Asn	:	Asparagine
AuNPs	:	gold nanoparticles
AuNRs	:	Gold nanorods
β	:	Beta
BCA	:	Bicinchoninic acid
BioID	:	Biotin ligase
Bn	:	Benzyl
BrdU	:	5-bromo-2'-deoxyuridine
BSA	:	Bovine serum albumin
¹³ C	:	Carbon-13
Ca	:	Calcium
CaCl ₂	:	Calcium chloride
CaOx	:	Calcium oxalate

CARS	:	Coherent anti-stokes Raman scattering
CB	:	4-cyanobenzaldehyde
CC	:	Column chromatography
CCD	:	Charge coupled device
CD ₃ OD	:	Deuterated methanol
CF	:	<i>Cassia fistula</i> Linn.
CKD	:	Chronic kidney disease
cm	:	Centimetre
CMP	:	Cytidine-5'-monophospho- <i>N</i> -acetylneuraminic acid
COD	:	Calcium oxalate dihydrate
COM	:	Calcium oxalate monohydrate
CO ₂	:	Carbon dioxide
CuAAC	:	Copper (1)-catalysed azide-alkyne cycloaddition
CuSO ₄	:	Copper sulphate
d	:	Doublet
DEGs	:	Differentially expressed genes
DFT	:	Density functional theory
DIPEA	:	Diisopropylethylamine
DLS	:	Dynamic light scattering
DMEM	:	Dulbecco's modified Eagle medium
DMF	:	<i>N,N</i> -Dimethylformamide
DMSO-d ₆	:	Dimethyl sulfoxide-d ₆
DNA	:	Deoxyribonucleic acid

DOX	:	Doxorubicin
ECM	:	Extracellular matrix
ECL	:	Enterochromaffin-like cells
EDTA	:	Ethylenediaminetetraacetic acid
EGFR	:	Epidermal growth factor receptor
EM	:	Electromagnetic wave
EMT	:	Epithelial-mesenchymal transition
ER	:	Endoplasmic reticulum
ERSD	:	End-stage renal diseases
ESI	:	Electrospray ionization
EtOAc	:	Ethyl acetate
FBS	:	Fetal bovine serum
FPKM	:	Fragments per kilo base of exon model per million reads mapped
GAG	:	Glycosaminoglycan
Gal	:	D-Galactose
GalNAc	:	N-acetylgalactosamine
GlcNAz	:	<i>N</i> -azidoacetylglucosamine
GlcNAc	:	N-acetylglucosamine
GlcN-6-P	:	glucosamine-6-P
GlcNPhAlk	:	<i>N</i> -alkyl derivative of glucosamine
Gln-Fruc-6-P-T	:	fructose-6-P amidotransferase
GFP	:	Green fluorescent protein
GFR	:	Glomerular filtration rate

GNE	:	GlcNAc 2-epimerase
HBP	:	Hexosamine biosynthetic pathway
HBTU	:	1H-benzotriazol-1-yl 1,1,3,3-tetramethyluronium tetrafluoroborate
GPs	:	Glycan precursors
H	:	Hydrogen
HBSS	:	Hanks' balanced salt solution
HeLa	:	Henrietta Lacks
HP116	:	Human Fibrosarcoma
HRMS	:	High resolution mass spectrometry
HRP	:	Horse radish peroxidase
H ₂ SO ₄	:	Sulphuric acid
iEDDA	:	inverse Electron-demand Diels-Alder reaction
IL6R	:	Interleukin-6 signaling
INHBA	:	Inhibitin A
IP6	:	<i>myo</i> -Inositol hexaphosphate
IR	:	Infrared
J	:	Coupling Constant
KV	:	Kilovolt
kcal	:	Kilo calorie
LSPR	:	Localised surface plasmon resonance
m	:	Multiplet
M ⁺	:	Molecular ion
ManNAc	:	<i>N</i> -acetylmannosamine

ManNAz	:	<i>N</i> -azidoacetylmannosamine
MeCN	:	Acetonitrile
MGAT5	:	β -1,6- <i>N</i> -acetylglucosaminyltransferase V
MGL	:	Metabolic Glycan Labelling
MGP	:	Matrix Gla-protein
MHz	:	Mega Hertz
min	:	Minutes
mg	:	Milligram
MGE	:	Metabolic glycoengineering
MNK	:	ManNAc-kinase
ml	:	Millilitre
ML	:	Metabolic labelling
mM	:	Millimolar
MMI	:	Multimodal imaging
MOE	:	metabolic oligosaccharide engineering
mol	:	mole
MRI	:	Magnetic resonance imaging
MRS	:	magnetic resonance spectroscopy
MTT	:	3-(4,5-dimethylthiazol-2-yl)-2,5-diphenyltetrazolium bromide
mW	:	milliwatt
Na	:	Sodium
NaAsO ₂	:	Sodium arsenite
NaBH ₃ CN	:	Sodium cyanoborohydride

NaCl	:	Sodium chloride
Na ₂ C ₂ O ₄	:	Sodium oxalate
NaIO ₄	:	Sodium periodate
NGF	:	Nerve growth factor
NANS	:	<i>N</i> -acetylneuraminic acid synthase
NaOx	:	sodium oxalate
NMR	:	Nuclear Magnetic Resonance
Na ₂ SO ₄	:	Sodium sulphate
Neu5Ac	:	<i>N</i> -Acetylneuraminic acid
NIR	:	Near infrared
nm	:	Nanometre
NPs	:	Nanoparticles
TPL	:	two-photon luminescence
NR	:	Nano rhein
NTRKs	:	Neurotrophic tyrosine receptor kinase
NTs	:	Nanotags
OD	:	Optical density
ON	:	Oxalate nephropathy
PBS	:	phosphate-buffered saline
PEG	:	Polyethylene glycol
PET	:	positron emission tomography
PPM	:	Parts per million
PTT	:	Photothermal therapy
PVDF	:	Polyvinylidene fluoride

PDT	:	photodynamic therapy
RAML	:	Raman-assisted metabolic labelling techniques
RIC	:	Relative Raman intensity
RNA	:	Ribonucleic acid
rpm	:	Rotation per minute
s	:	Second
SDS-PAGE	:	Sodium dodecylsulfate polyacrylamide gel electrophoresis
SEM	:	scanning electron microscopy
Ser	:	Serine
SERS	:	Surface-enhanced Raman Scattering
SPAAC	:	Strain promoted azide-alkyne cycloaddition
SiaNAI	:	Alkyne modified sialic acid
SILAC	:	Stable isotope labelling with amino acids in cell culture
SMLM	:	Single-molecule localisation microscopy
SRS	:	Stimulated Raman scattering
STED	:	stimulated emission depletion microscopy
TBA	:	Thiobarbituric acid
TEM	:	Transmission electron microscope
TGA	:	Thermogravimetric analysis
TGF- β	:	transforming growth factor-beta
THF	:	Tetrahydrofuran
Thr	:	Threonine

TLC	:	Thin Layer Chromatography
TLD	:	Thermoluminescent Detector
TNAP	:	Tissue-nonspecific alkaline phosphatase
TNFSF	:	TNF receptor superfamily members
TNFRSF12A	:	Tumour necrosis factor receptor superfamily 12A
Tun	:	Tunicamycin
µg	:	Microgram
µl	:	Micro litre
UDP	:	Uridine diphosphate
UV	:	Ultraviolet
VC	:	vascular calcification
VSMC	:	vascular smooth muscle cell

PREFACE

Understanding biological processes is essential for detecting diseases and initiating appropriate treatments. There is a need for methods that enable fast, specific, and sensitive detection in complex biological environments. Glycosylation is a major post-translational modification that is prevalent in most eukaryotes. Notably, glycans cover the cell surface and play a decisive role in cell-cell interactions and cell migration during various physiological processes such as fertilization, embryogenesis and immune responses.^[1,2] Raman imaging has emerged as a promising technique for glycan detection due to its high sensitivity. When combined with non-destructive Raman spectroscopy, metabolic labeling allows for the visualization and identification of specific biomolecules within the cells, facilitating the study of intricate biological processes at a molecular level.

Vascular calcification (VC) significantly contributes to cardiovascular diseases, particularly among individuals with chronic kidney disease (CKD) and metabolic disorders.^[3] CKD involves a progressive decline in renal function, leading to the accumulation of waste products and excess fluids in the body, which can result in various complications, including the formation of calcium oxalate crystals in the kidney tubules.^[4] While, effective treatments to reverse calcifications are currently unavailable, certain therapies can slow down their progression. Surface-Enhanced Raman Spectroscopy (SERS) holds promise for rapid, reliable, and non-invasive disease diagnosis, including the study of vascular calcification.

Out of the four chapters in the thesis, the **first chapter** provides an overview of the current advancements of SERS in biomedical applications especially in glycan recognition and hypercalciuria-induced nephropathies. This chapter also discusses a literature overview on metabolic labelling, specifically glycans, and Raman-based metabolic labelling studies. This chapter also discusses nephrolithiasis and CaOx inhibitors and their potential applications in therapy against kidney stones.

The intricate nature of cell-surface glycans makes it challenging to track metabolic changes in cells. In **chapter 2**, we utilized the metabolic glycan labelling (MGL) technique along with surface-enhanced Raman scattering (SERS) to investigate the distinct glycosylation patterns in cancer cell lines. This work introduces an N-alkyl derivative of glucosamine (GlcNPhAlk) as a precursor for glycan labelling. We assessed the extent of labelling using Raman imaging

and confirmed our findings through complementary fluorescence and western blot analysis. The MGL-SERS approach allowed us to compare and evaluate the imbalance of cell surface glycans in different cancer cells, establishing a direct correlation between glycan expression and metastatic potential. Furthermore, we demonstrated the incorporation of GlcNPhAlk into terminal glycans through the sialic acid biosynthetic pathway by studying the effect of the sialyltransferase inhibitor, P-3Fax-Neu5Ac, on the metabolic labelling of GlcNPhAlk. This methodology sheds light on the understanding of metastatic progression in cancer cells with aberrant glycosylation.

In **chapter 3**, it has shown that modified forms of N-acetyl hexosamine can be incorporated into mammalian cell surfaces, leading to altered cell surface glycans. This chapter is investigating the tolerance levels of the hexosamine biosynthetic pathway for structural modifications. Various analogues have been synthesized and tested using the MGL-SERS technique, with findings indicating differences in labelling efficiency. Inhibitor studies revealed that the analogues predominantly label N-glycans.

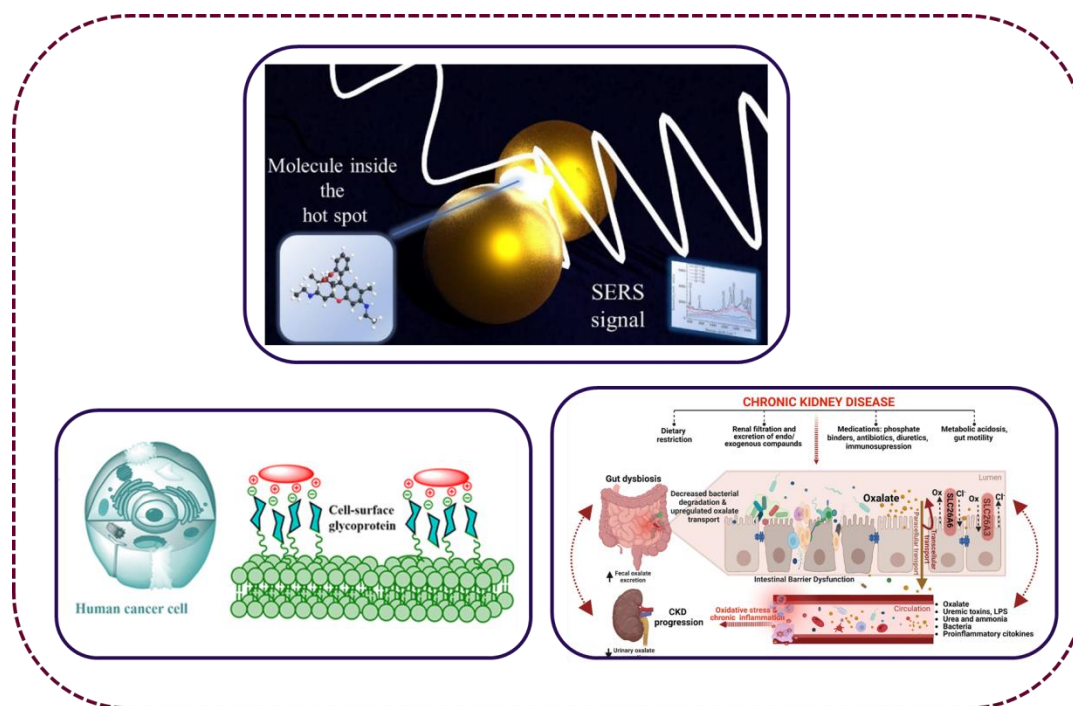
In **chapter 4**, a study was conducted to convert a bioactive herbal compound, rhein, into nano-rhein to enhance its inhibitory efficacy against CaOx. A robust imaging platform was established using surface-enhanced Raman scattering (SERS) to monitor calcification processes, and transcriptomic modifications induced by CaOx exposure and the mitigating effects of Rhein/Nano-Rhein were validated through comprehensive RNA sequencing followed by Reactome pathway analysis. The study provides insights into the potential of rhein, particularly in its nano form, as a promising therapeutic agent for CaOx-induced nephropathies.

References

- (1) Ohtsubo, K.; Takamatsu, S.; Minowa, M. T.; Yoshida, A.; Takeuchi, M.; Marth, J. D. Dietary and Genetic Control of Glucose Transporter 2 Glycosylation Promotes Insulin Secretion in Suppressing Diabetes. *Cell* **2005**, *123*, 1307-1321.
- (2) Cha, S.; Ortega, B.; Kurosu, H.; Rosenblatt, K. P.; Kuro-o, M.; Huang, C. Removal of Sialic Acid Involving Klotho Causes Cell-Surface Retention of TRPV5 Channel via Binding to Galectin-1. *Proc. Natl. Acad. Sci.* **2008**, *105* (28), 9805-9810.
- (3) A. Singh, S. Tandon, C. Tandon, An update on vascular calcification and potential therapeutics, *Mol. Biol. Rep.* **2021**, *48*, 887.
- (4) M. R. Hayden, S. C. Tyagi, L. Kolb, J. R. Sowers, R. Khanna, Vascular ossification-calcification in metabolic syndrome, type 2 diabetes mellitus, chronic kidney disease, and calciphylaxis-calcific uremic arteriopathy: the emerging role of sodium thiosulfate, *Cardiovasc. Diabetol.* **2005**, *4*, 1.

CHAPTER 1

Insights of surface enhanced Raman scattering in glycan recognition and hypercalciuria-induced nephropathies



1.1. Abstract

Surface-Enhanced Raman Scattering (SERS) has become a critical analytical technique, offering exceptional sensitivity and specificity in the detection and characterisation of biomolecules. This chapter discusses the dual application of SERS in glycan recognition and the study of hypercalciuria-induced nephropathies. Glycans, the complex carbohydrates found on cell surfaces and secreted molecules, play vital roles in various biological processes, such as cell signalling and pathogen recognition. With the enhanced Raman signals provided by SERS, researchers can now achieve high-resolution, real-time imaging of glycan structures and interactions, leading to deeper insights into their functional roles in health and disease. Excessive excretion of calcium in the urine characterises hypercalciuria, a medical condition that often leads to nephropathies, including kidney stones and chronic kidney disease. The chapter explores how SERS technology is used to identify and quantify biomarkers associated with hypercalciuria-induced nephropathies. By leveraging SERS, clinicians and researchers can detect subtle changes in biochemical compositions preceding the onset of nephropathic conditions, enabling early diagnosis and improved patient

outcomes. The incorporation of SERS into these fields not only highlights its versatility but also its potential to transform diagnostic and therapeutic approaches. This chapter's goal is to give a thorough summary of current methodologies, advancements, and applications of SERS in glycan recognition and the study of hypercalciuria-induced nephropathies, while also discussing the future prospects and challenges in these emerging areas of research.

1.2. Surface Enhanced Raman Scattering (SERS)

Surface-enhanced Raman spectroscopy, which is also referred to as surface-enhanced Raman scattering (SERS), is a technique that boosts Raman scattering by molecules that are adsorbed on rough metal surfaces or nanostructures. Rayleigh (elastic) scattering involves the interaction of photons with a material, whereas Raman (inelastic) scattering occurs with a minimal number of photons. This significant insight was originally established by Sir C.V. Raman and K.S. Krishnan in 1928.^[1,2] The Raman signal strength is limited by its lower cross section compared to its emission cross-section, constraining its broader applications due to inherent weakness. Fleischmann *et al.*, made a ground-breaking discovery when they observed a significant enhancement of Raman signals from pyridine molecules on the rough surface of silver.^[3] This discovery marked the inception of SERS, a sophisticated variant of Raman scattering. Nano-roughened metal surfaces in SERS amplify Raman signals by many orders of magnitude when analytes are tuned in proximity. This amplification requires the involvement of a strong localised surface plasmon resonance (LSPR) peak of metal nanostructures (NPs) when exposed to the incident electromagnetic (EM) wave. It is possible to achieve ultrasensitive detection down to the level of a single molecule when light passes through the "hot spots" formed by tiny areas on the surface of plasmon-coupled metallic nanoparticles, where the field enhancement is at its maximum. Raman spectroscopy experiences less interference from water compared to infrared (IR) and surface-enhanced infrared absorption spectroscopy, making it a more suitable platform for biological research. Moreover, the capacity for multimodal imaging (MMI) could be achieved by integrating the SERS modality with complementary methods such as fluorescence microscopy, magnetic resonance imaging (MRI), and two-photon luminescence (TPL), enabling full clinical translation. SERS has wide-ranging biomedical applications including labelled and label-free molecular detection, imaging, and theranostics modalities such as photothermal therapy (PTT), photodynamic therapy (PDT), and chemotherapy. It is also used in *in vivo* spectroscopic evaluation, monitoring biomolecular events, and image-guided surgery (**Figure 1.1**).

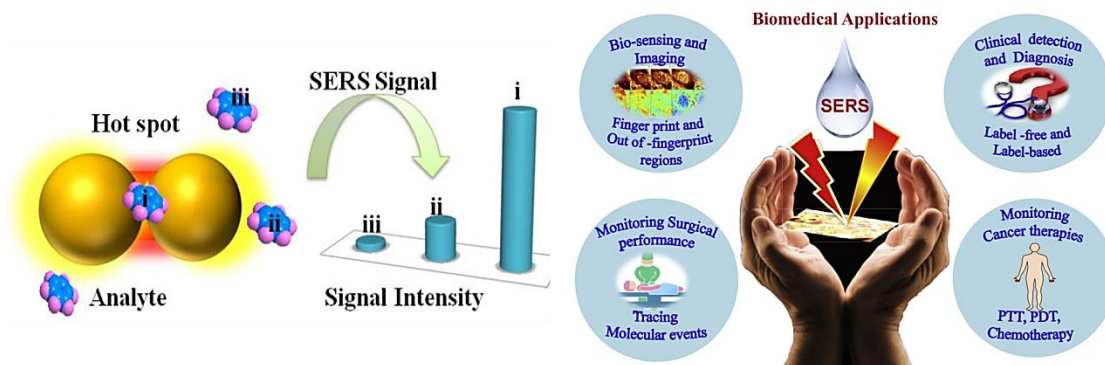


Figure 1.1: Schematic representation of SERS signal amplification and demonstrating diverse biomedical applications of SERS. (Adapted from *Biomaterials*, 2018, 181, 140-181)

1.2.1. SERS imaging

Despite being widely used in biology, fluorescence-based imaging modalities have several drawbacks, including a) broad fluorescence band; b) poor chemical selectivity; c) photobleaching of labels; d) weak Stokes shift; e) phototoxicity; and many more.^[4] SERS imaging combines optical imaging techniques with Raman scattering to reveal the spatial distribution of a specific analyte in a heterogeneous environment. The fundamental concept of SERS imaging is to isolate the Raman scattered photons from the SERS spectrum of a specific analyte that represents its unique signal to determine the spatial distribution of the analyte. SERS imaging can be performed in any desired combination along all three directions (X, Y, and Z). The most commonly used form of SERS imaging, referred to as two-dimensional (2D) imaging, utilises variations in colour or brightness to represent changes in the composition or structure of the sample. Z-stack of XY images is utilized in three-dimensional (3D) SERS imaging to provide detailed chemical information about a sample's internal features.

1.2.2. Cellular imaging utilising SERS

It is crucial to obtain precise data on biomolecules for research related to cellular functions. It is important to gather accurate data on biomolecules for research related to cellular functions. Ramaiah *et al.*, reported on a SERS nanoprobe coupled with an anti-EGFR (Epidermal Growth Factor Receptor) monoclonal antibody, a well-known cancer-targeting motif against overexpressed cell-surface receptor expressed of many cancer cells including human fibrosarcoma (HP116) (**Figure 1.2 a**). This nanoprobe left normal cells unharmed while effectively targeting the surface marker of HP116 cells, confirming its usefulness as an

ultrasensitive Raman probe for detection and targeted imaging This study was the first to identify the distinctive Raman signatures of aza-BODIPY dyes, which had not been studied before because of their low solubility and challenges integrating them with nanomaterial substrates like gold or silver NPs.^[5]

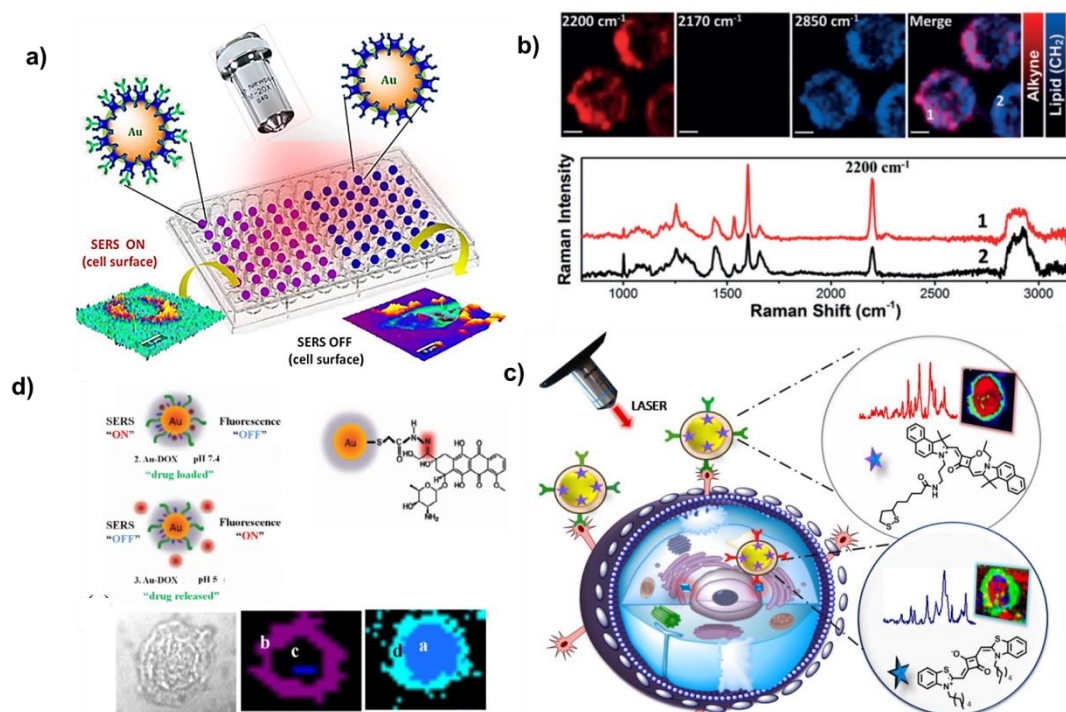


Figure 1.2: Cellular imaging through SERS modality. a) cellular imaging of aza-BODIPY^[5], b) usage of conjugated polymers with intrinsic alkyne groups for cell silent Raman imaging^[6] c) Schematic illustration of cancer cell recognition by SERS by nanotags.^[8] d) efficient monitoring of drug release with targeted delivery from the nanoconstructs^[7].

Poly (phenylene ethynylene) derivatives, incorporating intrinsic alkyne groups as a fundamental structural component, have demonstrated notable Raman scattering characteristics, specifically manifesting a Raman signal at 2200 cm^{-1} . This unique feature has been utilised in Raman imaging studies targeting HeLa cells, particularly focusing on regions of the cells traditionally considered 'silent' in terms of Raman activity (**Figure 1.2 b**). The findings from these investigations underscore the exceptional imaging capabilities of this polymer, presenting a promising avenue for advanced cellular imaging applications.^[6]

A novel folate receptor-targeted nano-delivery system, termed Au@SiO₂-DOXeCSeFA, was developed featuring a gold core and a SiO₂ shell, functionalised with chitosan-FA for efficient doxorubicin (DOX) delivery. This study utilised bimodal SERS/fluorescence nanoprobe to monitor cellular biochemical changes and DOX release over time. SERS

spectral analysis revealed distinct nucleic acid peaks in the nuclear regions (1487, 1510, and 1534 cm^{-1}) and highlighted molecular vibrations corresponding to RNA, carotenoids, and various biomolecules in the cytoplasm, aiding in the understanding of the nano-envelope's impact at the molecular level (Figure 1.2 d).^[7]

In another research, the team utilised nanotags (NTs) tagged with EGFR and p16/Ki-67 antibodies for early detection of cervical cancer, focusing on SERS imaging of HeLa cells. When these NTs, targeting an over-expressed nuclear receptor, were applied, it led to the predominant localisation of nanoparticles (NPs) within the nucleus, effectively confirming HeLa cell identification. Raman imaging further corroborated these findings by highlighting NP localisation on the cell surface, verified through traditional immunocytochemistry (Figure 1.2 c).^[8]

1.2.3. *In vivo* imaging

Gambhir *et al.*, used the SERS imaging platform was chosen to identify the tumour margins for image-guided excision, 24 hours after injection.^[9]

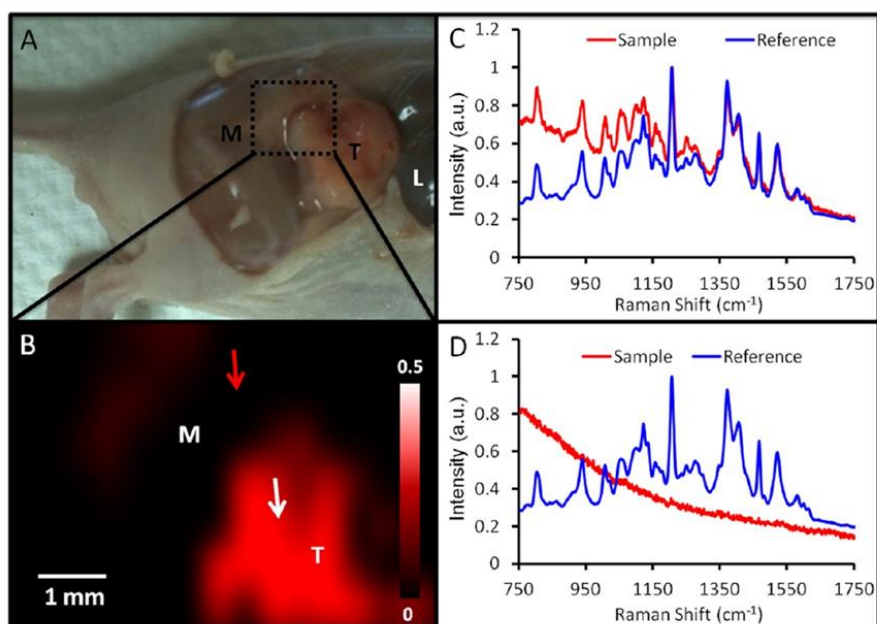


Figure 1.3: Tumour margin identification with SERS imaging. (a) Snapshot of mouse bearing a tumour and (b) corresponding SERS spectral image of the tumour area. (c, d) comparison of the SERS spectra at various spatial positions (red curve) to reference spectra (blue curve) collected *ex vivo*, (adapted from ACS Nano, 2012, 6, 10366-10377)

generation of non-toxic by-products, positioning it as a quintessential tool for cellular surface engineering amongst other intracellular applications.

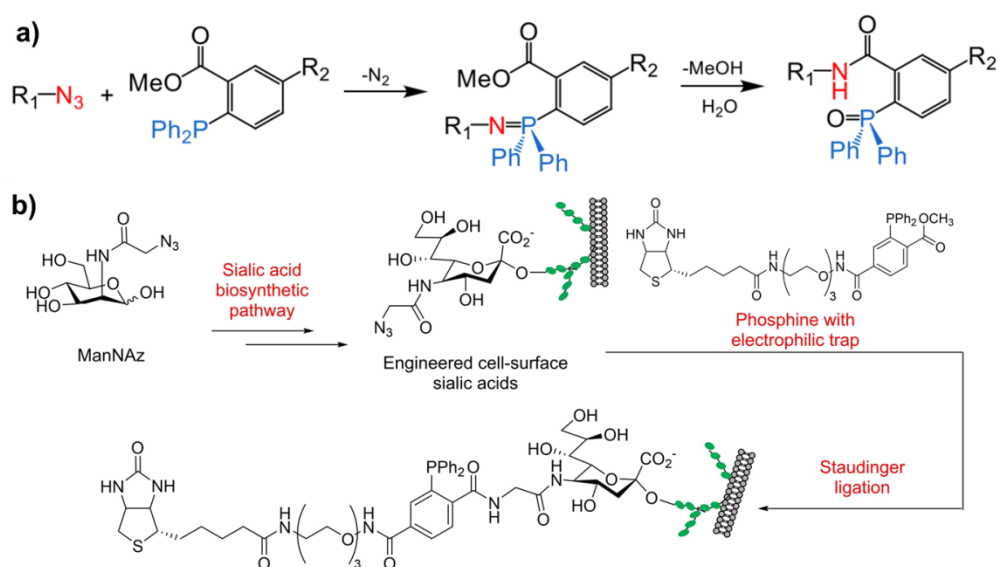


Figure 1.5: a) Staudinger reaction and b) the first application of the Staudinger ligation for cell-surface glycan labelling. (Adapted from Science, 2007, 80, 287)

Subsequent to the Staudinger ligation, the copper-catalysed azide-alkyne cycloaddition (CuAAC), often dubbed the “click” reaction, has emerged as a mainstay in the domain of bioorthogonal chemistry. According to Rostovtsev *et al.*, this reaction entails the copper-facilitated cycloaddition of an azide and a terminal alkyne, yielding a stable triazole ring. Owing to its high specificity and efficiency, the CuAAC reaction has firmly established itself as a fundamental pillar of bioorthogonal chemistry, acclaimed for its robustness and applicability across a spectrum of biological contexts.^[11]

For interventions pertaining to live-cell applications, the strain-promoted azide-alkyne cycloaddition (SPAAC) represents a crucial advancement. This copper-free variant of the click reaction, as delineated by Agard *et al.*, involves the cycloaddition of an azide to a strained alkyne, for instance, dibenzocyclooctyne. SPAAC's exclusion of copper underscores its significance, circumventing the cytotoxicity associated with the metal and thus facilitating the safe labelling and imaging of live cells.^[12]

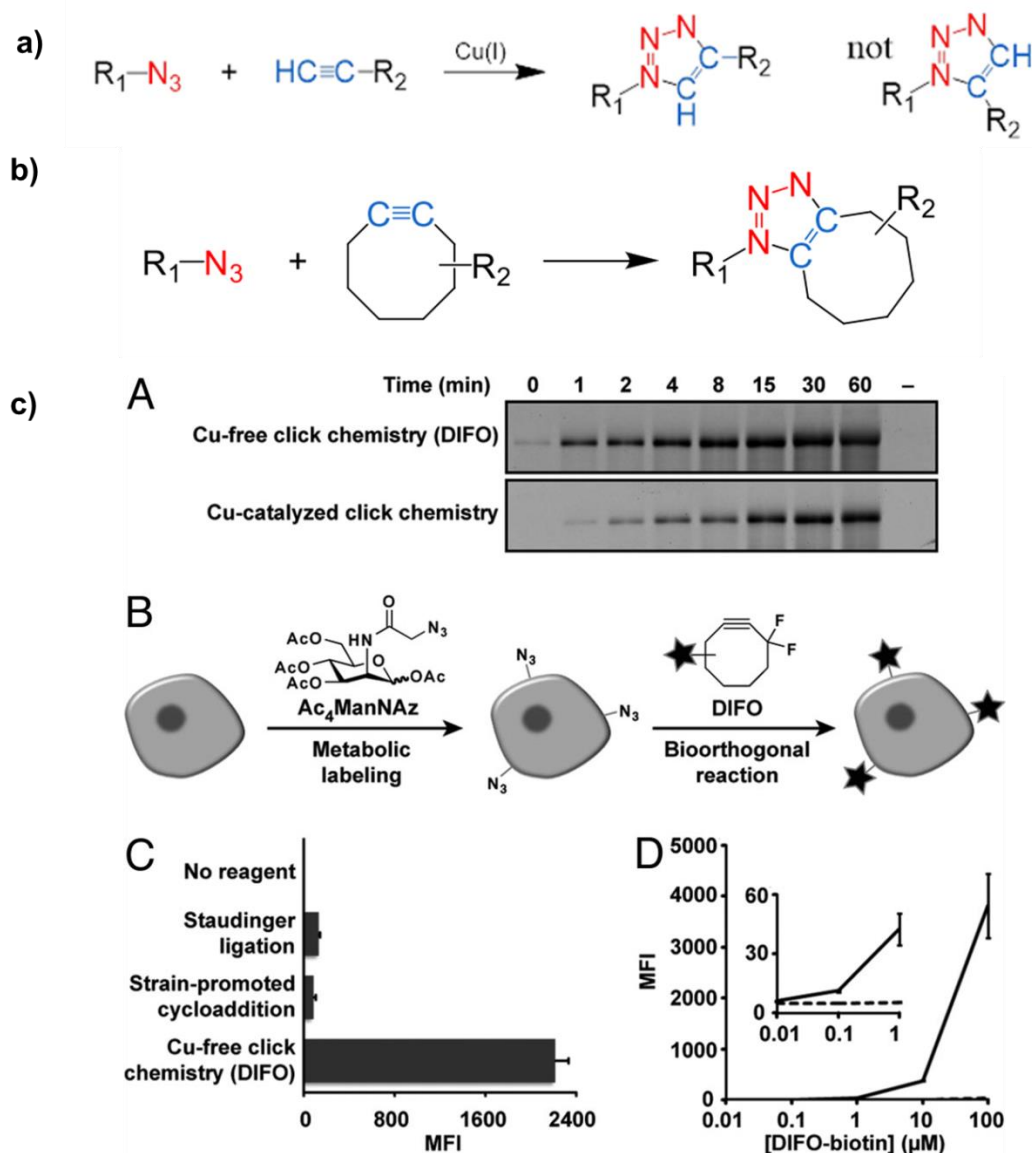


Figure 1.6: a) CuAAC reaction and b) Cu free click chemistry/SPAAC and c) Comparison of CuAAC, SPAAC and Staudinger ligation. (Adapted from J. Am. Chem. Soc. 2004, 126, 15046)

Moreover, the tetrazine ligation has been identified as another rapid and effective bioorthogonal reaction. Predicated on the inverse electron-demand Diels-Alder reaction between a tetrazine and a trans-cyclooctene, this reaction, as reported by Blackman *et al.*, is among the fastest bioorthogonal reactions discovered to date. Its accelerated reaction kinetics and specificity make the tetrazine ligation especially advantageous for dynamic imaging endeavours, where the swift tagging of biomolecules is imperative.^[13]

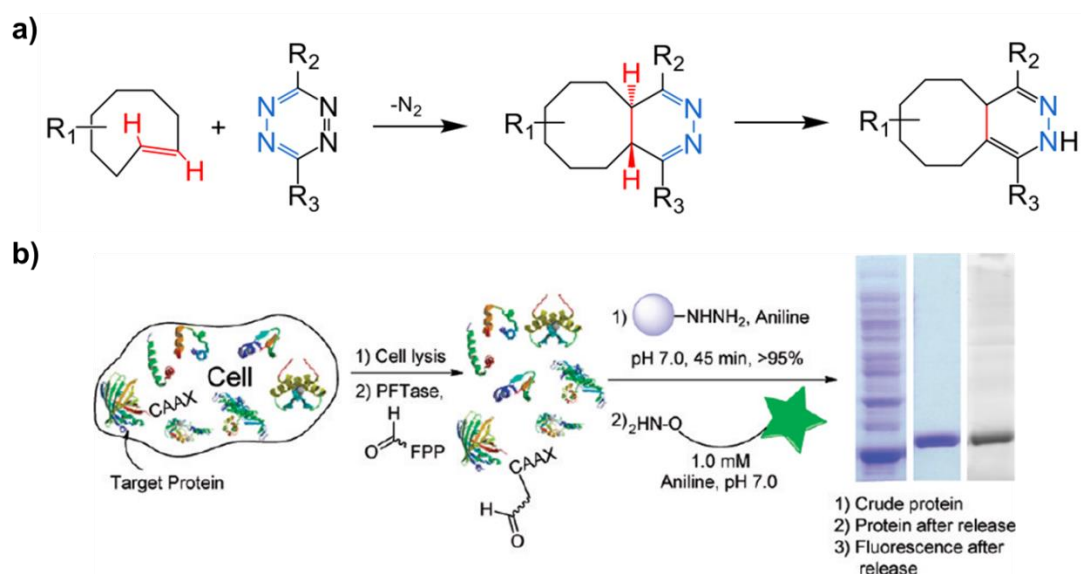


Figure 1.7: a) Tetrazine ligation chemistry and b) Oxime reaction for labelling of proteins. (Adapted from Science, 80, 1994, 27)

Furthermore, the oxime ligation, which forges an oxime bond between an aldehyde or ketone and an aminoxy compound, merits attention. Initially articulated by Dawson *et al.*,^[14] this reaction is noteworthy for its reversibility under specific conditions, though it can be rendered stable. The oxime ligation extends a versatile methodology for conjugating biomolecules, especially in scenarios where reversible linkage is advantageous.

Collectively, these bioorthogonal reactions constitute a seminal augmentation to the chemical biology toolkit, enabling the precise, selective, and minimally invasive modification of biomolecules within complex biological matrices. The continuous development and refinement of bioorthogonal methodologies are instrumental in advancing our understanding and manipulation of biological systems at the molecular level.

Any chemical reaction that may take place inside of biological systems without affecting natural biochemical processes is referred to as bioorthogonal chemistry and such functional groups which are orthogonal to biological systems are known as bioorthogonal functional groups.^[15] The bioorthogonal Raman reporters identified in biological systems to date are alkynes, azides, cyanides, deuterium etc.^[16] These functional groups also have the advantage of having Raman signal from the “cell silent region” which is in the range of 1800-2800 cm^{-1} where inherent Raman signals of endogenous biomolecules are absent (**Figure 1.8**).

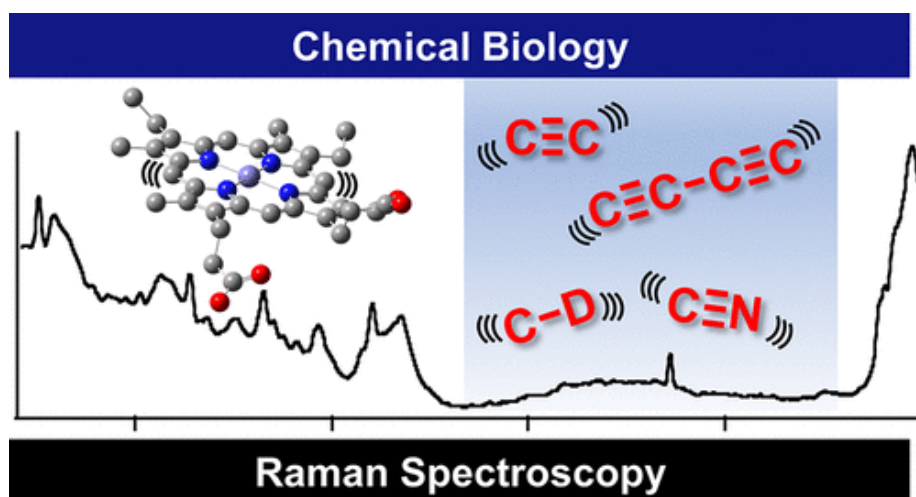


Figure 1.8: Depiction of fingerprint region and cell-silent region (Adapted from J. Am. Chem. Soc. 2022, 144, 43, 19651–19667).

Yamakhoshi and colleagues made one of the earliest and most significant contributions in this field when they developed the alkyne group 5-Ethynyl-2-deoxyuridine (EdU), which is labelled as a thymidine analogue for the visualisation of live DNA synthesis in cellular systems.^[17] Chen and colleagues utilised the alkyne group tagged artificial monosaccharide analogue *N*-(4-Pentynoyl)mannosamine to visualise cell surface glycans in this study (**Figure 1.9**).^[18]

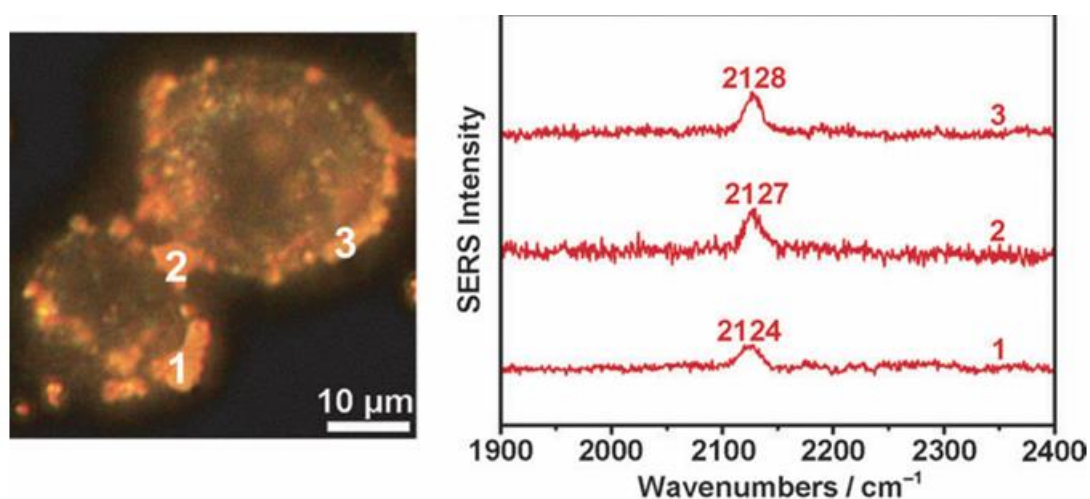


Figure 1.9: SiaNAI on the surface of cells detected by SERS. HeLa cells treated with Ac4ManNAI in a dark field picture, after which MPBA-AuNPs were incubated (Adapted from Angew. Chem. Int. Ed. 2013, 52, 7266–7271).

1.4. Glycans and their detection

All living organisms require carbohydrates as their main energy source to support their daily activities. Additionally, proteins or lipids can be modified to form glycoproteins or glycolipids, which act as both structural and functional components. The carbohydrate portion of these conjugates, known as glycans, consists of different monosaccharides arranged in various sequences.

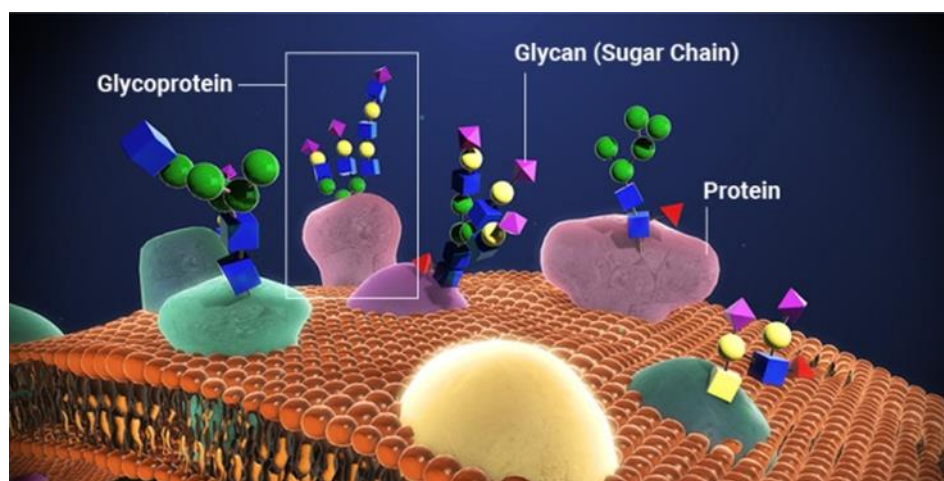


Figure 1.10: Schematic representation of glycans and glycoconjugates

1.4.1 Biological functions of glycans and glycoconjugates

Cell membranes predominantly consist of glycoconjugates. Glycans play a vital role in various biological functions necessary for the development, growth, maintenance, and survival of organisms.^[19] Glycans are present in all cells and living forms due to their ubiquity, structural variety, and participation in intercellular communication, evolutionary conservation, homeostasis, and host-pathogen interactions. Glycans are ubiquitous and play a crucial role in numerous living forms. Monosaccharides, the basic building blocks of complex structures, are fundamental to biology. Monosaccharides combine to generate oligosaccharides, which facilitate cellular communication, recognition, and signalling. Covalently linked oligosaccharide chains in glycoproteins have important roles in cellular communication, adhesion, and immunological recognition. Glycolipids play a crucial role in maintaining membrane integrity and cell recognition. Proteoglycans, which connect core proteins to lengthy glycosaminoglycan (GAG) chains, contribute to continued evolution.

This partnership forms the basis of the extracellular matrix, providing essential structural support for tissues. GAGs play a key role in determining the structure of connective tissue.

The structures of *N*- and *O*-linked glycans guide protein folding and stability (**Figure 1.11**). Additionally, Lewis blood group antigens and sialic acids have a notable impact on immune responses, blood compatibility, and cellular communication.^[20]

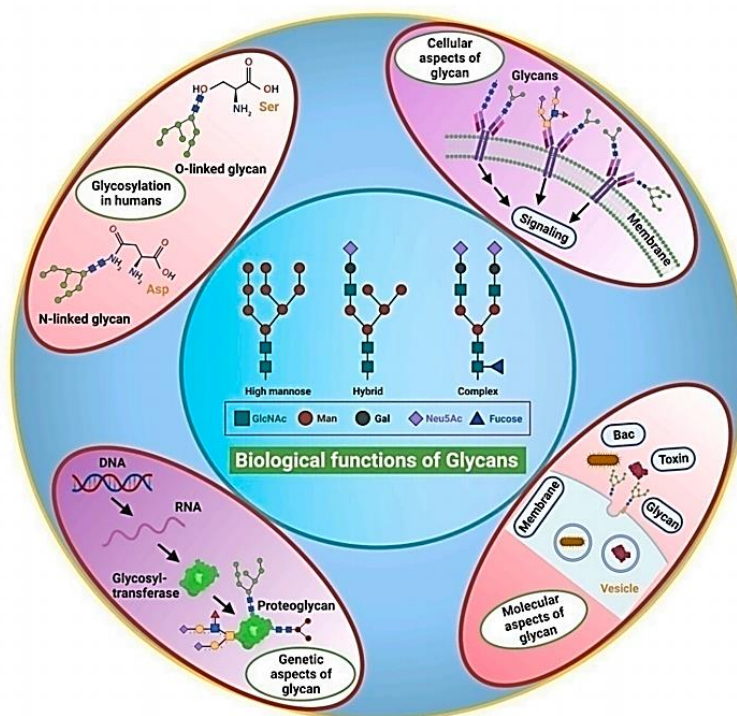


Figure 1.11: Shows an insightful schematic that highlights the biological activities of glycans, illustrating their vital involvement in cellular communication, adhesion, immunological regulation, and signalling pathways (Adapted from Int. J. Biol. Macromol. 2024, 268, 131511).

1.4.2. Glycan in cancer progression

Glycans play vital roles in cell biology and structural biology, particularly in cancer cells. These functions include signalling within cells, cell detachment of tumour and spread, interaction between tumour cells and the surrounding matrix, formation of blood vessels, regulation of the immune system, and the progression of metastatic cancer.^[21] Glycosylation is a vital post-translational modification process that involves adding sugar molecules to proteins and lipids. It is involved in many essential biological functions, including cell communication and immunological responses. In the field of cancer, glycoproteins serve as important diagnostic and prognostic tools. They are widely used as biomarkers in cancer patients, aiding in the detection and assessment of cancer in various organs such as the prostate, ovaries, stomach (CA19-9), and pancreas (CA19-9). The utilisation of glycoproteins

contributes significantly to the development of diagnostic and prognostic techniques in cancer research and patient care.^[22,23]

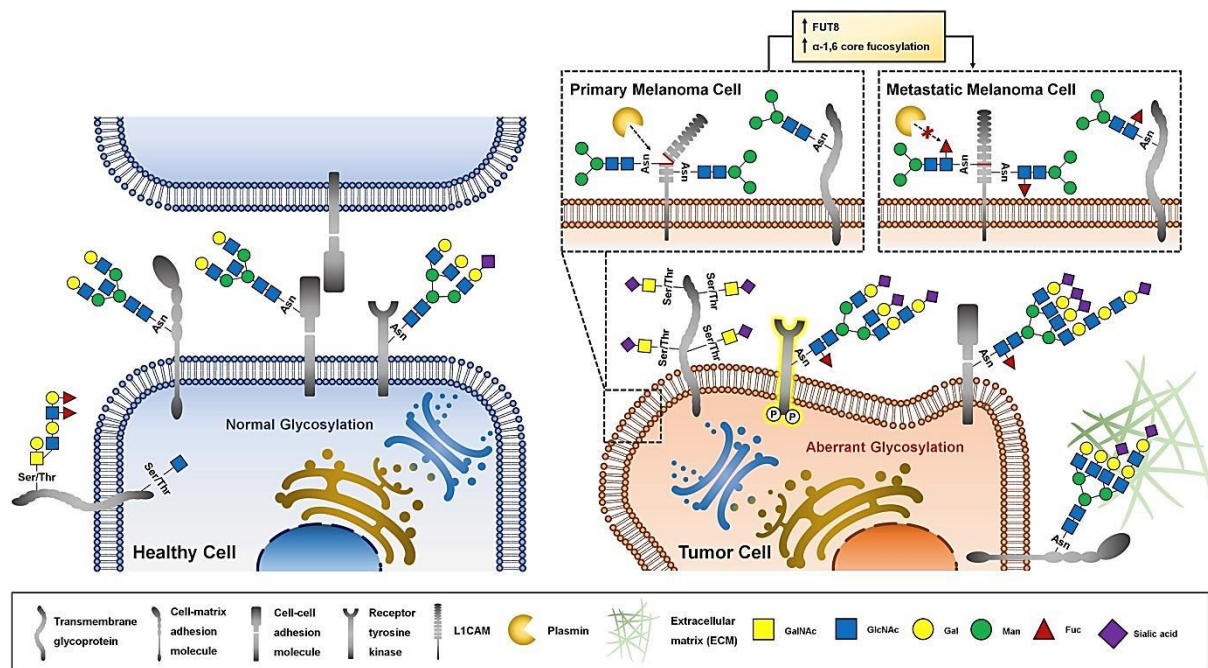


Figure 1.12: Aberrant glycosylation of cells in cancer cells compared to healthy cells (Adapted from Cancer Cell, 2017, 31(6), 737-754).

Variations in the composition of glycans can play a role in different stages of cancer development which is known as aberrant glycosylation (**Figure 1.12**). The mechanisms responsible for the changes in glycan structures within cancer cells are not fully understood but are likely to involve modifications in epigenetics, genetic mutations, dysregulated expression of glycosyltransferase and chaperone genes, and incorrect localisation of glycosyltransferases.^[24,25]

1.4.3. Detection of glycans

Glycans are potentially important biomarkers with significant research implications and vast applications in illness diagnosis and therapy. Developing glycan labelling technologies and implementing specific sensing methodologies will help in obtaining spatial and temporal glycan expression data, which is critical for understanding the regulatory mechanisms and biological consequences of glycans on cell surfaces. By using glycan sensing technologies, it is possible to understand the changing characteristics of glycans during the onset and progression of illnesses, as well as provide novel biomarkers and diagnostic procedures for early detection.^[26]

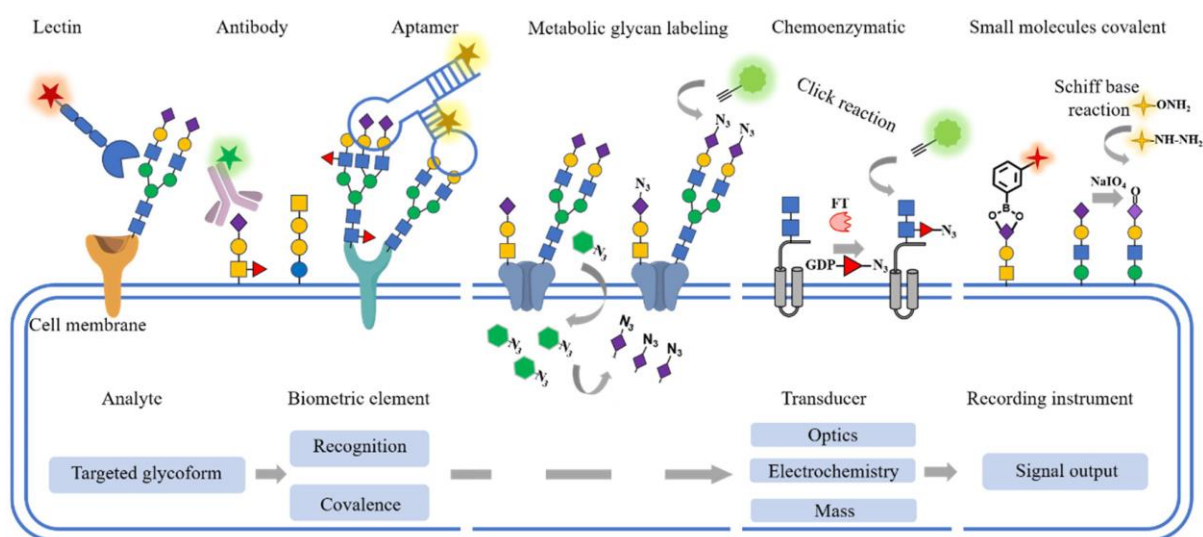


Figure 1.13: Cell-surface glycan labelling and sensing methods

Detecting glycans on cell membrane surfaces is challenging for several reasons: (1) carbohydrate isomers are diverse and hard to distinguish from one another; (2) glycosylation is a non-template synthesis process that results in microscopic variability in modification sites; and (3) glycoconjugates on cell membrane surfaces are functionally complex and sparse. Glycan identification and detection rely heavily on their unique recognition and stable binding. Common glycan recognition molecules include lectins, aptamers, and antibodies (Figure 1.13).

Method	Description	Detection Principle	References
Fluorescence-based HPLC	Separation of glycans by HPLC with fluorescence detection	Fluorescent labels on glycans	[27]
Mass Spectrometry (MS)	Separation and identification of glycans based on mass-to-charge ratio	Ionisation and mass analysis	[27–29]
Glycosyltransferase Labelling	Radiolabelled nucleotide sugars or unnatural sugars enable detection	Enzymatic labelling	[28]
Metabolic Labelling	Radiolabelled or unnatural sugars incorporated into glycans	Metabolic pathways	[27–29]

Periodate Oxidation	Oxidation followed by colorimetric or fluorescent detection	Oxidation of glycan structures	[27–29]
Lectins and Antibodies	Binding reagents for glycans	Specific lectins or antibodies	[29]

Table 1.1: Cell-surface glycan labelling and sensing methods with its principles.

1.5. Metabolic labelling

Metabolic reprogramming is a well-known characteristic of several disorders, including cancer and neurodegenerative diseases. Metabolic alterations occur early in the progression of the disease, making them a more sensitive indicator of treatment response than the reduction in tumour size. Metabolic labelling is a technique in molecular biology and biochemistry used to study the synthesis, modification, and degradation of biomolecules within cells. This method involves introducing labelled precursors, such as amino acids, nucleotides, or sugars, into newly synthesised compounds. These labels can take the form of radioactive or stable isotopes, or other chemical tags, which facilitate the identification and quantification of labelled biomolecules. Clinical techniques such as PET (positron emission tomography) and MRS (magnetic resonance spectroscopy) are well-established but they are expensive, time-consuming, and have poor sensitivity, particularly in detecting diseased cells at an early stage like the pre-metastatic niche. Raman spectroscopy addresses these limitations by offering a rapid, label-free, low-cost, and high-throughput approach for detecting multiple metabolites. Metabolic labelling (ML) has emerged as a powerful tool in biological research, allowing the study of dynamic cellular processes in real-time. It involves incorporating externally supplied molecules, such as amino acids, nucleotides, or sugars, into cellular biomolecules during their biosynthesis.^[30] The labelled molecules act as probes, enabling the tracking and quantification of newly synthesized biomolecules within living cells or organisms. ML is widely employed in molecular biology and biomedical research to study various cellular processes, such as protein synthesis, trafficking, and turnover. The diverse modalities used for their detection have significantly advanced our understanding of cellular functions and provided invaluable insights into complex biological systems.^[31–33] Overall, metabolic labelling, combined with diverse detection methods, has made significant contributions to various fields, including cancer research, neurobiology, and drug discovery.

1.5.1. Metabolic labelling strategies to evaluate different modalities

Stable isotope labelling has played a crucial role in identifying metabolic changes specific to cancer, while click chemistry has made it possible to accurately label proteins for proteomic studies. The use of radioisotopes, such as [^{35}S] methionine or [^3H] leucine, which emit detectable radiation, has been one of the leading methods in metabolic labelling.^[33] However, the application of radio isotopic labelling is limited due to safety concerns related to radiation exposure and disposal. To address safety issues, non-radioactive alternatives have emerged, including stable isotopes like [^{13}C] or [^{15}N]-labelled amino acids. Stable isotopes allow for precise quantification of newly synthesised proteins using techniques like stable isotope labelling with amino acids in cell culture (SILAC) or ^{15}N metabolic labelling. Furthermore, non-protein biomolecules have also become part of metabolic labelling techniques. For example, nucleoside analogues like EdU and 5-bromo-2'-deoxyuridine (BrdU) are used to label newly synthesised DNA during cell proliferation.^[17] Click chemistry-based methods enable specific visualisation of EdU or BrdU-labelled DNA, providing insights into cell cycle dynamics and DNA replication processes. In addition to nucleic acids and proteins, metabolic labelling approaches can also be used to study lipid metabolism. For instance, alkyne- or azide-tagged fatty acids can be integrated into cellular lipids and then visualised using bioorthogonal chemistry-based methods. Advances in detection techniques have greatly improved the precision and versatility of metabolic labelling methods.

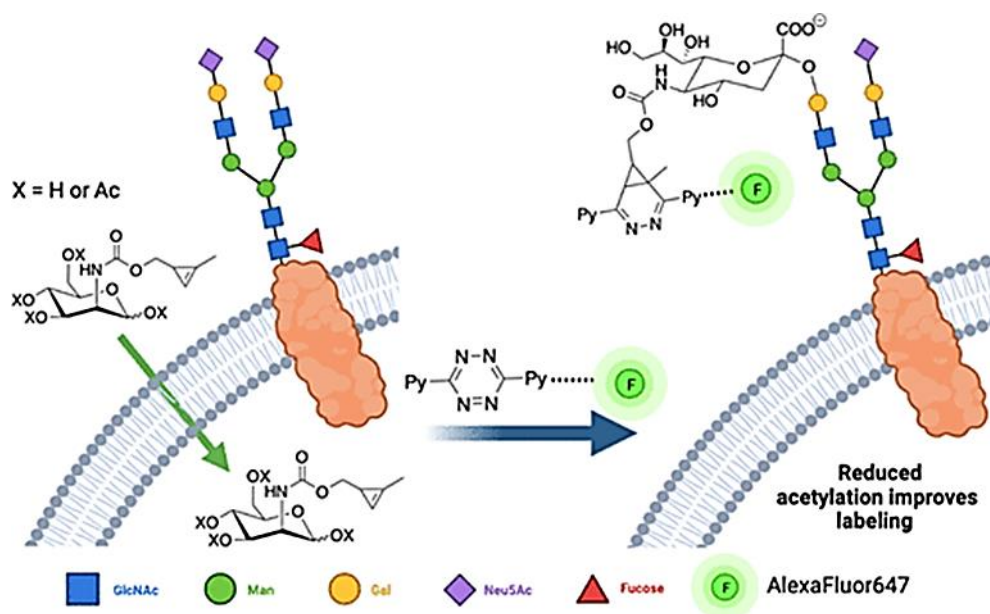


Figure 1.14: Metabolic labelling of glycans with bioorthogonal reaction and subsequent fluorescent detection (Adapted from ACS Chem. Biol. 2014, 9, 592).

Fluorescent labelling, for example, enables the high spatial and temporal resolution monitoring of cellular processes in real time. Fluorescent proteins, or its derivatives, like green fluorescent protein (GFP), can be genetically encoded or bound to biomolecules to visualise them within live cells.^[34] Furthermore, proximity-based labelling methods like BioID (biotin ligase) and APEX (ascorbate peroxidase) enable the identification of protein-protein interactions and the subcellular localisation of proteins within the cellular environment. These methods involve fusing a promiscuous biotin ligase to a protein of interest, making it possible to covalently attach biotin molecules to nearby proteins for subsequent enrichment and identification using mass spectrometry.^[35–37] Recent advancements in super-resolution microscopy have transformed the visualisation of cellular structures and molecular interactions beyond the diffraction limit.^[38] Single-molecule localisation microscopy (SMLM) and stimulated emission depletion (STED) microscopy techniques offer an unparalleled spatial resolution, allowing for precise localisation of labelled biomolecules within subcellular compartments.^[39]

Generally in imaging platforms both fluorescence as well as SERS have its pros and cons which is listed below:-

Features	SERS modality	Fluorescence modality
Advantages of SERS over fluorescent detection platform		
High Sensitivity	Can detect single molecules due to enhancement effect ^[40,41]	Can detect low concentrations of fluorescently labelled molecules ^[42]
Specificity	Provides unique molecular fingerprints for precise identification ^[40,41,43,44]	Wide range of fluorescent dyes and probes available for various applications ^[42]
Non-Destructive	Does not typically damage the sample, suitable for real-time	Fluorescent dyes can degrade over time under

	monitoring of dynamic processes in live cells ^[40]	light exposure, reducing signal intensity (photo bleaching). ^[42]
Multiplexing Capability	Can simultaneously detect multiple analytes. ^[41,44]	Capable of rapid imaging, making it suitable for high-throughput screening. ^[42]
Minimal Interference	Less affected by water interference, suitable for biological samples. ^[43]	Auto fluorescence from biological samples can interfere with signal detection. ^[42]
Disadvantages		
Complex Sample Preparation	Requires use of metallic nanoparticles or surfaces. ^[40,43]	Requires optimisation of concentrations of fluorescent dyes
Reproducibility Issues	Variability in enhancement factor due to inconsistent surface preparations. ^[43]	Difficulties in absolute quantification due to variations in dye uptake and photobleaching. ^[42]
Depth Penetration	Limited depth penetration but can obtain SERS signals at depths up to 45–50 mm in tissues by using NIR lasers. ^[44]	Typically lower spatial resolution compared to techniques like SERS or electron microscopy. ^[42]
Technical Expertise	Requires specialized knowledge for sample preparation and interpretation of spectra. ^[43]	Proper handling and usage of fluorescent dyes, setting up and calibrating the microscope, and accurately interpreting the imaging data all require specialized knowledge and experience.

Table 1.2: Advantages and disadvantages of SERS modality over fluorescent detection platform.

1.5.2. Metabolic glycan labelling through the fluorescent modality

The detection of metabolic glycan labelling through fluorescent modalities is a cutting-edge technique essential for studying cellular glycosylation processes. Glycans, complex carbohydrates attached to proteins and lipids, play critical roles in various biological functions, including cell signalling, immune response, and disease progression. Detailed observation of glycans in their native environment has been significantly advanced through metabolic labelling and fluorescent detection methods. Metabolic glycan labelling involves incorporating unnatural monosaccharide analogues into glycans during biosynthesis. These analogues are bioorthogonal, meaning they do not interfere with natural biochemical processes. Once integrated into glycans, these analogues can be detected through specific chemical reactions. One widely used method is azide-alkyne cycloaddition, often referred to as "click chemistry," which attaches fluorescent probes to the labelled glycans, enabling their visualization under a fluorescence microscope.^[45] A key fluorescent modality in this context involves azido sugars, such as *N*-azidoacetylglucosamine (GlcNAz) and *N*-azidoacetylmannosamine (ManNAz). These azido sugars are metabolised by the cell and incorporated into glycan structures. Subsequent treatment with a fluorescent alkyne, like a fluorophore-conjugated cyclooctyne, facilitates the visualisation of these glycans through a copper-free click reaction, which is biocompatible, and efficient.^[15] This approach is advantageous as it allows for the labelling and detection of glycans in live cells and tissues without significant cytotoxicity. In addition to click chemistry, other bioorthogonal reactions have been employed for fluorescent metabolic glycan labelling. The Staudinger ligation is one such method, where an azide-functionalized glycan reacts with a phosphine to form an amide bond, enabling the attachment of a fluorescent label (**Figure 1.15**). This reaction is mild and biocompatible, making it suitable for live-cell applications.^[10]

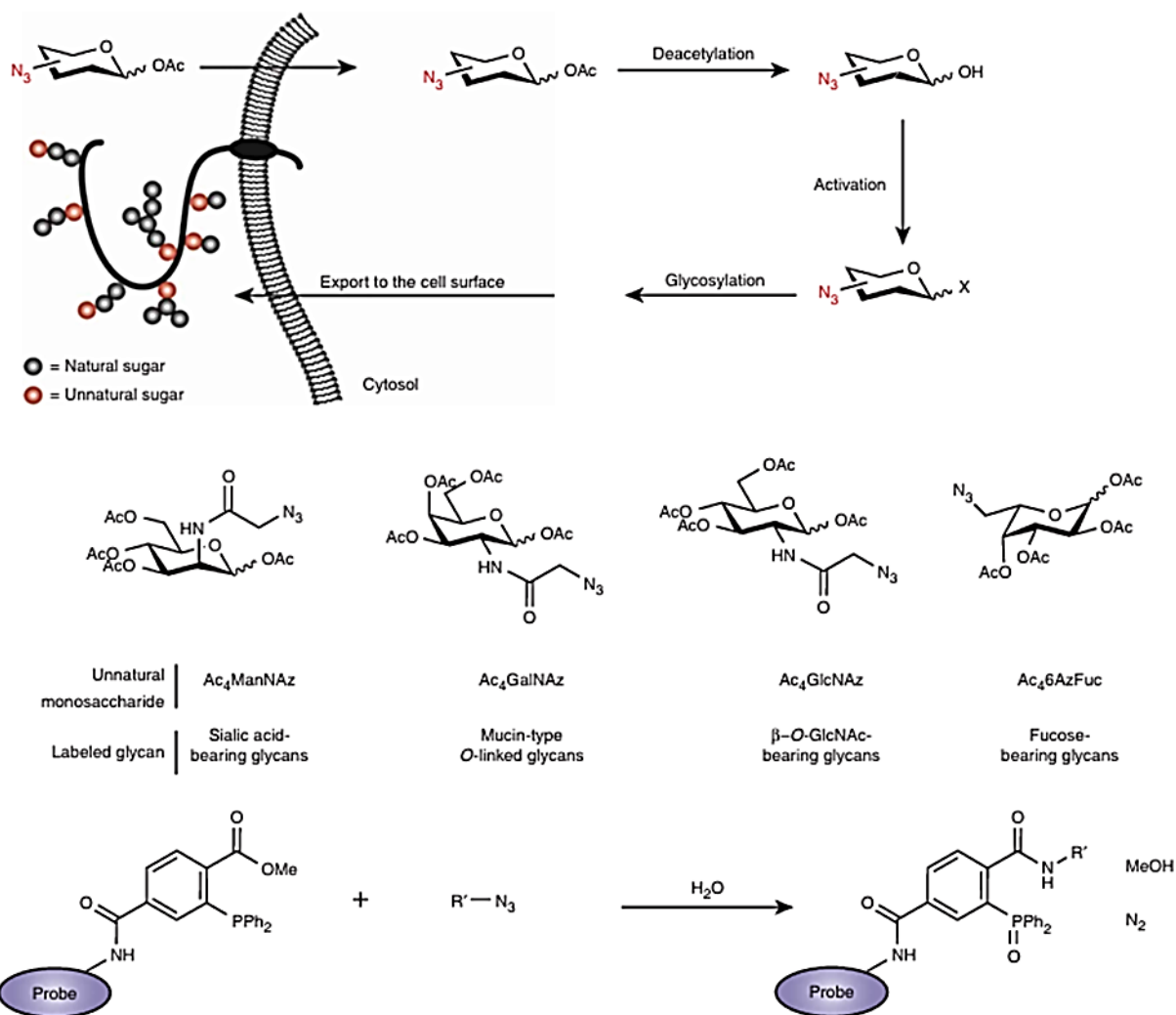


Figure 1.15: Metabolic glycan labelling through fluorescent modality (Adapted from Nat. Protoc, 2007, 2(11), 2930-2944)

Another important bioorthogonal reaction is the inverse electron-demand Diels-Alder (iEDDA) reaction, involving a strained alkene or alkyne and a tetrazine (**Figure 1.14**). This reaction is extremely fast and has high specificity, making it ideal for real-time imaging of glycans in complex biological systems. The iEDDA reaction's speed and bioorthogonality make it particularly useful for dynamic studies of glycan trafficking and interactions.^[46] Fluorescent metabolic labelling of glycans has provided significant insights into cellular glycosylation patterns and dynamics. For example, this technique has been used to investigate cancer biology, where altered glycosylation patterns are a hallmark. Visualising changes in glycan structures in cancer cells enables researchers to identify potential biomarkers for early diagnosis and targets for therapeutic intervention.^[47] Recent advancements in fluorophore technology have further enhanced the sensitivity and resolution of glycan imaging.

Fluorescent dyes such as fluorescein, rhodamine, and cyanine derivatives, along with newer, more photo stable fluorophores, offer diverse options for multi-colour labelling and detailed studies of glycan interactions and functions.^[48] In summary, the detection of metabolic glycan labelling *via* fluorescent modalities, employing various bioorthogonal reactions such as click chemistry, Staudinger ligation, and iEDDA reactions, is a powerful technique that has revolutionised the study of glycobiology. By combining the specificity of metabolic labelling with the sensitivity of fluorescence detection, this method offers a robust tool for visualising and understanding the complex roles of glycans in health and disease. Even though MGL through fluorescence modality evolved in the past several years it has its shortcomings due to the limited specificity of bulky fluorophore, photo bleaching of fluorescent derivative. Also, it needs an additional step of ligation (click reaction, Staudinger ligation etc.) to conjugate the fluorescent probe.

1.5.3. Raman-assisted metabolic labelling (RAML) techniques

Raman-assisted metabolic labelling (RAML) techniques have emerged as powerful tools in the field of cellular imaging, offering distinct advantages over traditional methods.^{[49][50]} Raman spectroscopy provides a label-free and non-invasive approach, allowing researchers to study live cells and tissues with minimal perturbation.^[51] RAML techniques offer a versatile and powerful approach to studying cellular processes. The label-free nature, multiplexing capability, and compatibility with live cells make these techniques indispensable in advancing our understanding of cellular metabolism and contributing to various fields, including cancer research, drug development, and regenerative medicine.^[52,53] One of the primary advantages of Raman-based techniques is their label-free nature. Unlike fluorescent labelling, Raman spectroscopy relies on the inherent vibrational modes of molecules, eliminating the need for exogenous labels. This feature minimises cellular perturbations, allowing for more accurate observations of native cellular processes. Raman spectroscopy enables the simultaneous detection of multiple biomolecules based on their unique spectral signatures. This multiplexing capability is particularly advantageous for studying complex cellular environments, as it allows the concurrent monitoring of various metabolic pathways and biomolecular interactions.^[16] Raman-based techniques, including Raman microscopy and coherent anti-stokes Raman scattering (CARS), enable real-time monitoring of dynamic cellular processes.^[54,55] This capability is invaluable for studying fast-paced events, such as cell division, migration, and responses to external stimuli. Raman imaging facilitates three-

dimensional visualisation of cellular structures and metabolic activities. Techniques like confocal Raman microscopy provide depth-resolved information, offering a comprehensive view of cellular processes within complex tissue environments. RAML techniques are increasingly being applied *in vivo* for studying animal models and human tissues. This expands the scope of research to more physiologically relevant conditions, providing insights into disease mechanisms and therapeutic interventions. Advancements in Raman-based technologies, such as surface-enhanced Raman scattering (SERS), stimulated Raman scattering (SRS) and coherent Raman imaging, continue to broaden the applications of metabolic labelling techniques. These technologies offer enhanced sensitivity and specificity, opening new avenues for exploring cellular metabolism at the molecular level. This review explores the principles of metabolic labelling and highlights different Raman modalities for its detection, emphasising their applications and advancements.

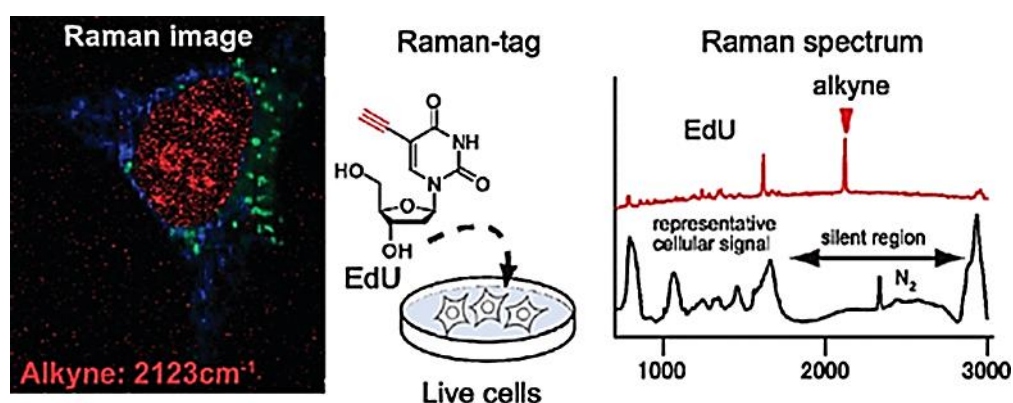


Figure 1.16: Metabolic labelling of DNA with EdU (Adapted from J. Am. Chem. Soc., 2011, 133, 102-6105)

Yamakoshi *et al.*, for the first time, has used the alkyne functional group as the chemical Raman reporter utilising EdU, a precursor of nucleic acids, for the visualisation of real time DNA synthesis inside the cells (**Figure 1.16**).^[56] Inspired by this work, Lin *et al.*, has reported the SERS detection of glycan modifications using *N*-acetyl mannosamine derivatives and exhibited the superiority of SERS platform over fluorescent modality (**Figure 1.17**).^[18]

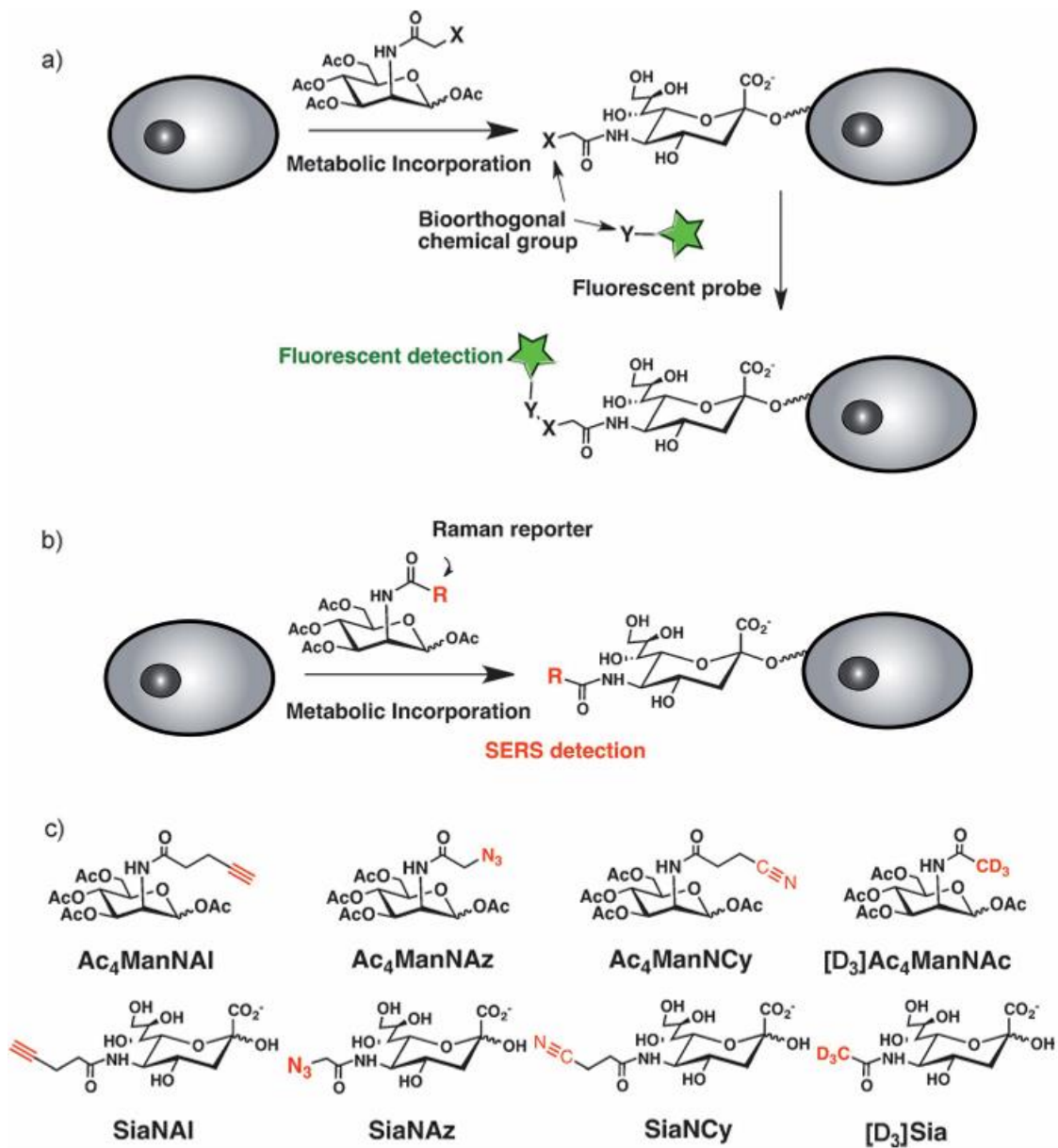


Figure 1.17: First report of SERS detection of glycans through metabolic glycan labelling (Adapted from J. Am. Chem. Soc. 2022, 144, 43, 19651–19667)

1.6. Vascular calcification and its involvement in chronic kidney disease

The accumulation of calcium phosphate salts in the vascular tissues characterises the pathological process known as vascular calcification (VC). It is often noticed in individuals who have long-term conditions with chronic kidney disease (CKD), significantly contributing to increased cardiovascular morbidity and mortality in this population. The process of VC in CKD is complex and involves multiple mechanisms, including disrupted mineral metabolism,

inflammation, and cellular differentiation. Hence, VC is also another area in biomedical field that requires much more attention.

1.6.1. Pathophysiology of VC in CKD

In CKD, there is an imbalance in calcium and phosphate homeostasis, often leading to hyperphosphatemia. This imbalance promotes the deposition of calcium-phosphate complexes in the vascular tissues.^[57] In patients with CKD, there is a high occurrence of chronic inflammation and oxidative stress, promoting vascular smooth muscle cell (VSMC) transformation into osteoblast-like cells, depositing calcium into the vascular walls (**Figure 1.18**).^[58] VSMCs undergo phenotypic changes under the influence of inflammatory cytokines and elevated phosphate levels, contributing to the calcification process.^[59]

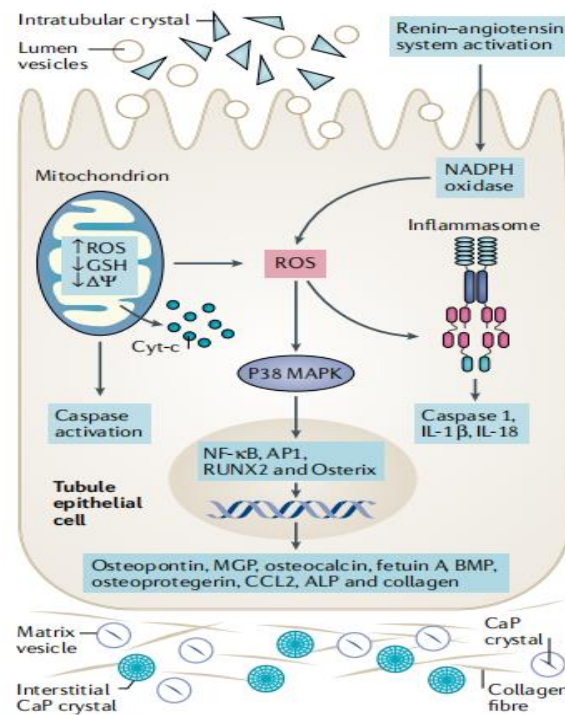


Figure 1.18: Pathophysiology of Vascular Calcification in CKD.

1.6.2. Involvement of calcium oxalate in VC

Calcium oxalate (CaOx), typically associated with kidney stones, also plays a role in VC (**Figure 1.19**). Elevated levels of oxalate can lead to the formation of CaOx crystals, which can deposit in vascular tissues, exacerbating the calcification process.^[60]

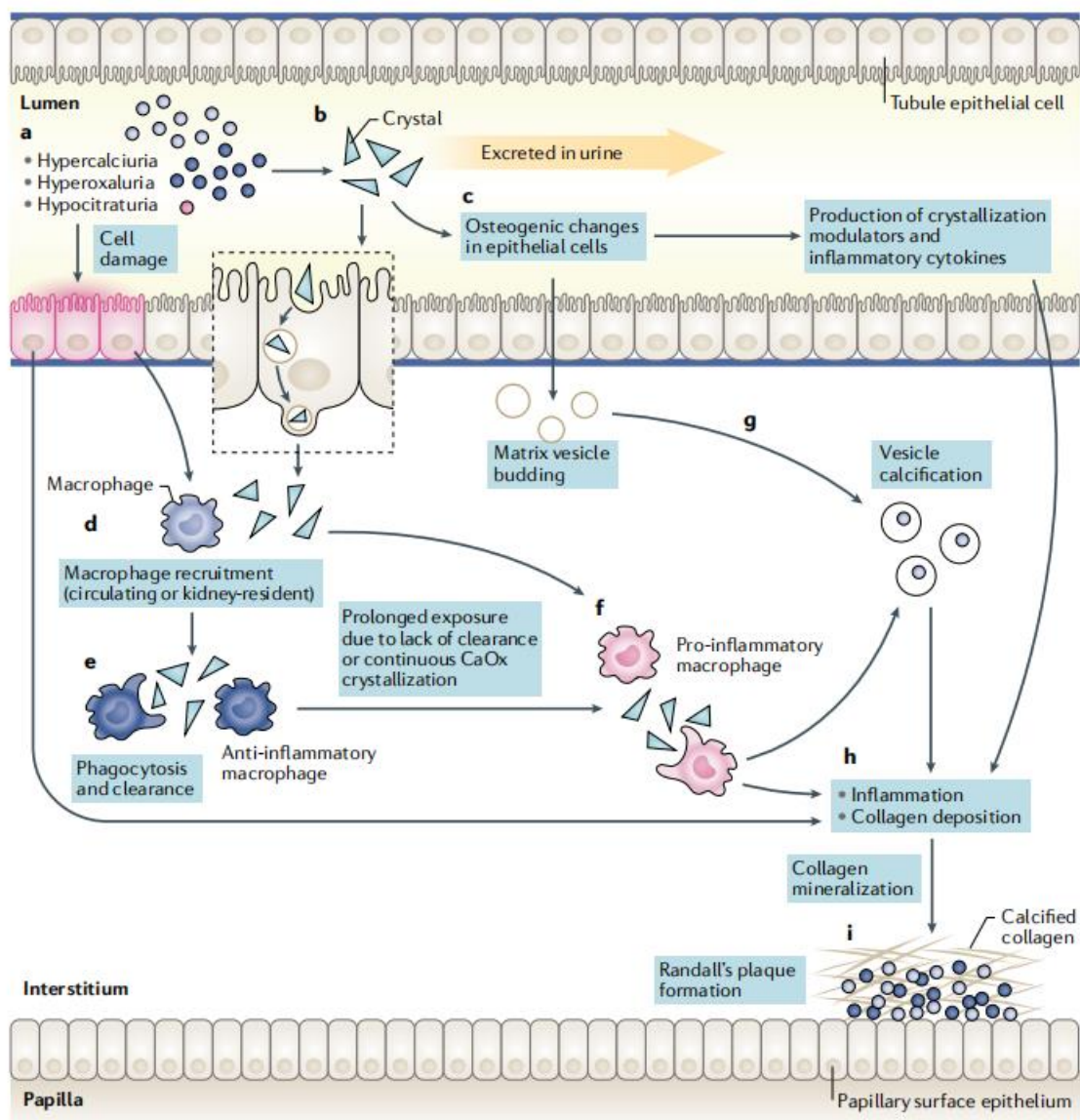


Figure 1.19: Proposed model of hyperoxaluria, hypercalciuria.

1.6.3. Therapeutic approaches and involvement of SERS in recognising VC

Some of the current therapeutic approaches towards VC are given here. Phosphate binders reduce serum phosphate levels by capturing dietary phosphate in the digestive system, thereby preventing its absorption. Commonly used phosphate binders include sevelamer and lanthanum carbonate.^[61] Vitamin K is essential for the inducing matrix Gla-protein (MGP), a potential inhibitor of VC. Vitamin K could reduce vascular calcification in CKD patients.^[62] Magnesium inhibits the precipitation of calcium-phosphate crystals and has been shown to reduce VC in animal models and CKD patients.^[63] Recent studies have explored inhibitors of calcium oxalate crystal formation, which could potentially reduce VC. Citrate and

pyrophosphate are among the compounds investigated for their inhibitory effects on calcium oxalate crystal formation (**Figure 1.20**).^[64] Still, all of them have inadequate evidence of *in vivo* inhibitory activity and are reported to be associated with gastrointestinal side effects.^[65] By leveraging surface enhanced Raman scattering (SERS), clinicians and researchers can detect subtle changes in biochemical compositions preceding the onset of nephropathic conditions, enabling early diagnosis and improved patient outcomes. SERS's high sensitivity and specificity allow for the detection of trace biomolecules, making it an invaluable tool in medical diagnostics. For instance, SERS has been employed to detect biomarkers associated with acute kidney injury (AKI), demonstrating its potential for early diagnosis in clinical applications.^[66]

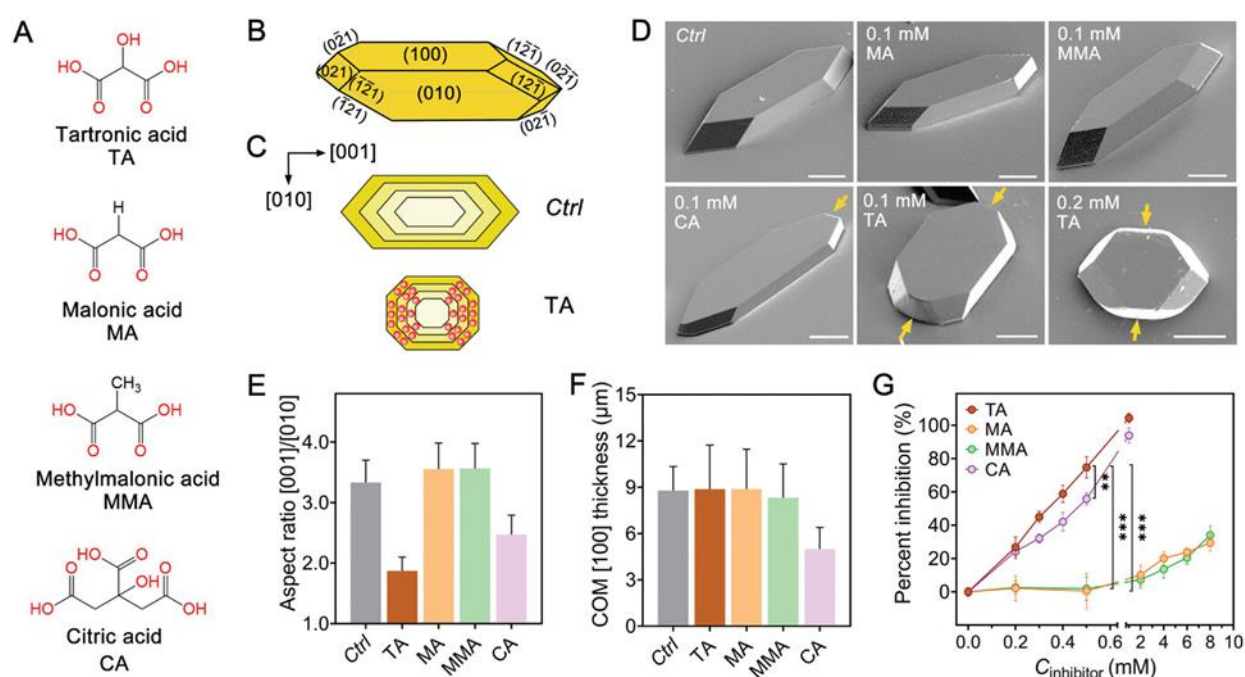


Figure 1.20: Potent CaOx inhibitors of citric acid derivatives. (Adapted from Adv. Sci. 2024, 11(21), e2400642).

1.7. Conclusions

The current advancements in SERS modality have made this platform widely for theranostics purposes in the biomedical fields. The comprehensive characterisation of cellular-level changes within their natural environment poses a significant challenge in the field of disease diagnostics and therapy. In this scenario, to address the current limitations, the most suitable option is the development of molecular probes with metabolic labelling capabilities. Metabolic glycan labelling using unnatural sugars has emerged as a facile but powerful tool

to label cell membranes with chemical tags. In this thesis, a systematic investigation of the design, synthesis, and evaluation of cell surface glycan probes is presented for the application of in cancer as well as during calcification. With the advancements of SERS imaging modalities, we have developed SERS based calcification profiling platform for the assessment of anti-calcification properties of nano-rhein. These approaches hold the promise of creating theranostically relevant probes for applications such as point-of-care diagnosis and personalised treatment.

1.8. Objective of the present investigation

The complex nature of cell-surface glycans makes it difficult to track metabolic changes in cells. In **chapter 2**, objective was to surmount this challenge by developing a metabolic glycan labelling combined with surface-enhanced Raman scattering (MGL-SERS) strategy to study the differences in glycosylation patterns in cancer cell lines. A new glycan precursor, an *N*-alkyl derivative of glucosamine (GlcNPhAlk), was introduced for glycan labelling for the first time. The extent of labelling was evaluated using Raman imaging and confirmed through fluorescence and Western blot analysis. This technique allowed us to compare the differences in cell surface glycan patterns in different cancer cells, and we found a direct relationship between glycan expression and metastatic potential. We also studied the impact of a sialyltransferase inhibitor, P-3F_{ax}-Neu5Ac, on the labelling of GlcNPhAlk, which indicated that GlcNPhAlk is incorporated into terminal glycans through the sialic acid biosynthetic pathway. This methodology helps us better understand how glycosylation contributes to the metastatic progression in cancer cells.

In **chapter 3**, the objective was to extend the investigation to the tolerance levels of the hexosamine biosynthetic pathway for structural alterations of the *N*-acyl, *N*-alkyl, and *N*-acyloxy substituents of mannosamine and glucosamine. A series of analogues with *N*-acyl, *N*-alkyl, and *N*-acyloxy groups of hexosamines (GlcNPhAlk, ManNPhAlk, GlcNAcPhAlk, ManNAcPhAlk, GlcNAcOPhAlk, and ManNAcPhOAlk) were synthesised and tested, and their metabolic conversion to cell surface glycans was examined using the MGL-SERS technique. Our findings indicated that the ManNAcPhAlk and ManNPhAlk are actively metabolically labelled, followed by GlcNPhAlk whereas GlcNAcOPhAlk, ManNAcPhOAlk and GlcNAcPhAlk are significantly underutilised by the biosynthetic machinery. This was further validated through far-western blot analysis using azide-PEG3-biotin, which yielded consistent results.

Identification of potent CaOx inhibitor and development of a calcification profiling platform with SERS was the objective of the **chapter 4**. For this, a simplest and fast sonochemical self-assembly technique was engineered to transform a bioactive herbal compound, rhein, isolated from *Cassia fistula* Linn into nano-rhein, aiming to augment its inhibitory efficacy towards CaOx. The anti-calcification properties of both rhein and nano-rhein were assessed through Alizarin Red S staining *in-vitro* model employing human embryonic kidney cells HEK-293. Furthermore, through the utilisation of SERS, a robust imaging platform to monitor calcification processes were established. This platform introduces a SERS-based Alizarin Red S assay for profiling CaOx inhibitors. By employing the metabolic glycan labeling technique alongside the SERS, changes in cell surface glycan expression during both calcification and decalcification processes subsequent to Rhein/Nano-Rhein treatment were identified. To deepen the understanding of cellular responses to CaOx and interpret morphological changes observed through cellular imaging, RNA sequencing experiment was conducted. Transcriptomic modifications induced by CaOx exposure and the mitigating effects of Rhein/Nano-Rhein were substantiated through comprehensive RNA sequencing followed by Reactome pathway analysis. This study offers intricate insights into the potential of rhein, particularly in its nano form, as a promising therapeutic agent for CaOx-induced nephropathies, shedding light on molecular mechanisms underlying its protective anti-inflammatory effects.

1.9. References

- [1] C. V Raman, *Indian J. Phys.* **1928**, 398, 387.
- [2] K. S. K. C.V. Raman, *Nature*, **1928**, 121, 501e502.
- [3] A. J. M. M. Fleischmann, P.J. Hendra, *Chem. Phys. Lett* **1974**, 26, 163.
- [4] A. Sujith, T. Itoh, H. Abe, *Anal Bioanal Chem* **2009**, 394, 1803.
- [5] N. Adarsh, A. N. Ramya, K. Maiti, *Chem. Eur.J* **2017**, 23, 14286.
- [6] S. Li, T. Chen, Y. Wang, L. Liu, F. Lv, Z. Li, Y. Huang, K. S. Schanze, S. Wang, *Angew. Chemie - Int. Ed.* **2017**, 56, 13455.
- [7] A. N. Ramya, M. M. Joseph, S. Maniganda, V. Karunakaran, T. T. Sreelekha, K. K. Maiti, *Small* **2017**, 13, 1.

- [8] N. Narayanan, V. Karunakaran, W. Paul, K. Venugopal, K. Sujathan, K. Kumar Maiti, *Biosens. Bioelectron.* **2015**, *70*, 145.
- [9] J. V Jokerst, A. J. Cole, D. Van De Sompel, S. S. Gambhir, *ACS Nano* **2012**, *6*, 10366.
- [10] E. Saxon, C. R. Bertozzi, *Science (80-.)*. **2007**, *287*, 2007.
- [11] V. V. Rostovtsev, L. G. Green, V. V. Fokin, K. B. Sharpless, *Angew. Chemie - Int. Ed.* **2002**, *41*, 2596.
- [12] N. J. Agard, J. A. Prescher, C. R. Bertozzi, *J. Am. Chem. Soc.* **2004**, *126*, 15046.
- [13] M. L. Blackman, M. Royzen, J. M. Fox, *J. Am. Chem. Soc.* **2008**, *130*, 13518.
- [14] P. E. Dawson, T. W. Muir, S. B. H. Kent, *Science (80-.)*. **1994**, *27*.
- [15] E. M. Sletten, C. R. Bertozzi, *Angew. Chemie - Int. Ed. Chem. Int. Ed.* **2009**, *48*, 6974.
- [16] K. Dodo, K. Fujita, M. Sodeoka, *J. Am. Chem. Soc.* **2022**, *144*, 19651.
- [17] H. Yamakoshi, K. Dodo, M. Okada, J. Ando, A. Palonpon, K. Fujita, S. Kawata, M. Sodeoka, *J. Am. Chem. Soc.* **2011**, *133*, 6102.
- [18] L. Lin, X. Tian, S. Hong, P. Dai, Q. You, R. Wang, L. Feng, C. Xie, Z. Tian, X. Chen, *Angew. Chemie - Int. Ed.* **2013**, *52*, 7266.
- [19] A. Varki, *Glycobiology* **2017**, *27*, 3.
- [20] K. Arora, P. M. Sherilraj, K. A. Abutwaibe, B. Dhruw, S. L. Mudavath, *Int. J. Biol. Macromol.* **2024**, *268*, 131511.
- [21] A. Purushothaman, M. Mohajeri, T. P. Lele, *J. Biol. Chem.* **2023**, *299*, 102935.
- [22] C. A. Reis, H. Osorio, L. Silva, C. Gomes, L. David, *J. Clin. Pathol.* **2010**, *63*, 322.
- [23] G. Y. Locker, S. Hamilton, J. Harris, J. M. Jessup, N. Kemeny, J. S. Macdonald, M. R. Somerfield, D. F. Hayes, R. C. B. Jr, *J. Clin. Oncol.* **2006**, *24*, 5313.
- [24] S. R. Stowell, T. Ju, R. D. Cummings, *Annu. Rev. Pathol. Mech. Dis.* **2015**, *10*, 473.
- [25] F. Bard, J. Chia, *Trends Cell Biol.* **2016**, *26*, 379.

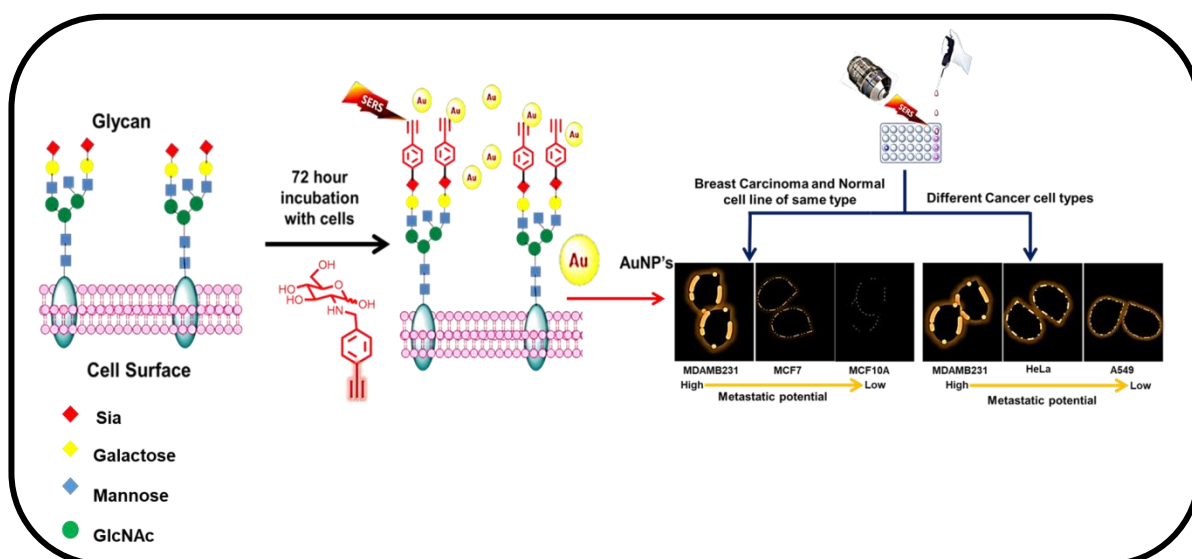
- [26] D. Thomas, A. Kumar, P. Radhakrishnan, *BBA - Rev. Cancer* **2021**, 1875, 188464.
- [27] L. R. Ruhaak, G. Zauner, C. Huhn, C. Bruggink, A. M. Deelder, M. Wuhrer, *Anal. Bioanal. Chem.* **2010**, 397, 3457.
- [28] E. Release, 1.
- [29] Y. Li, L. Wang, L. Ding, H. Ju, *Targets* **2023**, 2, 1.
- [30] N. I. Martin, S. I. Van Kasteren, *Org. Biomol. Chem.* **2021**, 19, 2856.
- [31] C. Bueschl, R. Krska, B. Kluger, R. Schuhmacher, *Anal. Bioanal. Chem.* **2013**, 405, 27.
- [32] C. Y. Jao, A. Salic, *Proc. Natl. Acad. Sci.* **2008**, 105, 15779.
- [33] R. J. Beynon, J. M. Pratt, *Mol. Cell. Proteomics* **2005**, 4, 857.
- [34] C.- Momethylase, **2002**, 297, 1873.
- [35] H. Y. Chen, M. Swaroop, S. Papal, A. K. Mondal, H. B. Song, L. Campello, G. J. Tawa, F. Regent, H. Shimada, K. Nagashima, N. De Val, S. G. Jacobson, **2023**, 1.
- [36] T. C. Branon, J. A. Bosch, A. D. Sanchez, N. D. Udeshi, T. Svinkina, S. A. Carr, J. L. Feldman, N. Perrimon, A. Y. Ting, **2018**, 36.
- [37] I. Chen, M. Howarth, W. Lin, A. Y. Ting, *Nat. Methods* **2005**, 2, 99.
- [38] S. Pujals, L. Albertazzi, **2019**.
- [39] B. Brenner, C. Sun, F. M. Raymo, H. F. Zhang, *Nano Converg.* **2023**, 10.
- [40] C. Lin, Y. Li, Y. Peng, S. Zhao, M. Xu, L. Zhang, Z. Huang, J. Shi, Y. Yang, *J. Nanobiotechnology* **2023**, 21, 1.
- [41] E. Smith, G. Dent, *Modern raman spectroscopy: A practical approach*, **2019**.
- [42] J. W. Lichtman, J. A. Conchello, *Nat. Methods* **2005**, 2, 910.
- [43] A. I. Pérez-Jiménez, D. Lyu, Z. Lu, G. Liu, B. Ren, *Chem. Sci.* **2020**, 11, 4563.

- [44] M. Vendrell, K. K. Maiti, K. Dhaliwal, Y. T. Chang, *Trends Biotechnol.* **2013**, *31*, 249.
- [45] Metabolic Labeling of Glycans with Azido Sugars for Visualization and Glycoproteomics, *Methods Enzymol.* **2006**, *415*, 230.
- [46] M. L. Blackman, M. Royzen, J. M. Fox, **2008**, 13518.
- [47] D. H. Dube, C. R. B. ã, *Curr. Opin. Chem. Biol.* **2003**, *7*, 616.
- [48] D. M. Patterson, L. A. Nazarova, J. A. Prescher, *ACS Chem. Biol.* **2014**, *9*, 592.
- [49] O. Terrones, J. Olazar-Intxausti, I. Anso, M. Lorizate, J. A. Nieto-Garai, F. X. Contreras, *Int. J. Mol. Sci.* **2023**, *24*, 2384.
- [50] J. Xu, T. Yu, C. E. Zois, J. X. Cheng, Y. Tang, A. L. Harris, W. E. Huang, *Cancers (Basel)*. **2021**, *13*, 1.
- [51] K. J. I. Ember, M. A. Hoeve, S. L. McAughtrie, M. S. Bergholt, B. J. Dwyer, M. M. Stevens, K. Faulds, S. J. Forbes, C. J. Campbell, *npj Regen. Med.* **2017**, *2*.
- [52] J. Du, Y. Su, C. Qian, D. Yuan, K. Miao, D. Lee, A. H. C. Ng, R. S. Wijker, A. Ribas, R. D. Levine, J. R. Heath, L. Wei, *Nat. Commun.* **2020**, *11*.
- [53] Y. Suzuki, K. Kobayashi, Y. Wakisaka, D. Deng, S. Tanaka, C. Huang, **2019**, *116*.
- [54] B. Kann, H. L. Offerhaus, M. Windbergs, C. Otto, *Adv. Drug Deliv. Rev.* **2015**, *89*, 71.
- [55] D. Boildieu, T. Guerenne-Del Ben, L. Duponchel, V. Sol, J. M. Petit, É. Champion, H. Kano, D. Helbert, A. Magnaudeix, P. Leproux, P. Carré, *Front. Cell Dev. Biol.* **2022**, *10*, 1.
- [56] H. Yamakoshi, K. Dodo, A. Palonpon, J. Ando, K. Fujita, S. Kawata, M. Sodeoka, *J. Am. Chem. Soc.* **2012**, *134*, 20681.
- [57] M. London, A. P. Gue, S. J. Marchais, F. Me, B. Pannier, H. Adda, *Nephrol. Dial. Transplant.* **2003**, *18*, 1731.
- [58] A. J. Nelson, P. Raggi, M. Wolf, A. M. Gold, G. M. Chertow, M. T. Roe, *JACC Basic to Transl. Sci.* **2020**, *5*, 398.

- [59] M. Abedin, Y. Tintut, L. L. Demer, *Arterioscler. Thromb. Vasc. Biol.* **2004**, *24*, 1161.
- [60] L. L. Demer, Y. Tintut, *Circulation* **2008**, 2938.
- [61] S. Chan, K. Au, R. S. Francis, D. W. Mudge, D. W. Johnson, P. I. Pillans, *Aust. Prescr.* **2017**, *40*, 9.
- [62] S. Roumeliotis, A. Duni, V. Vaios, A. Kitsos, V. Liakopoulos, E. Dounousi, *Nutrients* **2022**, *14*.
- [63] S. J. Zaslow, G. H. Oliveira-Paula, W. Chen, *Int. J. Mol. Sci.* **2024**, *25*.
- [64] A. Kletzmayer, S. R. Mulay, M. Motrapu, Z. Luo, H. J. Anders, M. E. Ivarsson, J. C. Leroux, *Adv. Sci.* **2020**, *7*.
- [65] Y. Su, S. Li, X. Li, J. Zhou, V. P. Chauhan, M. Li, Y. Su, C. Liu, Y. Ren, W. Yin, J. D. Rimer, T. Cai, **2024**, *2400642*, 1.
- [66] D. Li, L. Zhao, J. Qian, H. Liu, J. You, Z. Cheng, F. Yu, *RSC Adv.* **2022**, *12*, 15910.

CHAPTER 2

Exploring cell surface glycan imbalance via SERS-guided metabolic glycan labelling: assessing metastatic potential in cancer cells



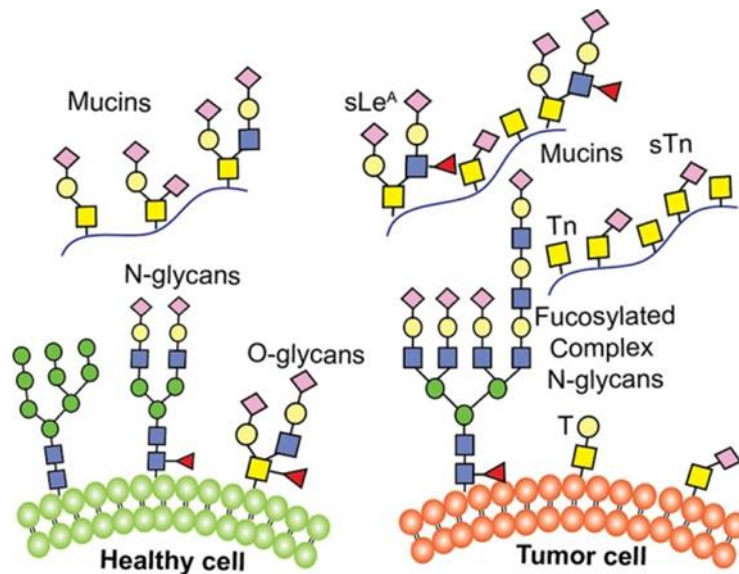
2.1. Abstract

The intrinsic complexities of cell-surface glycans impede tracking the metabolic changes in cells. The differential glycosylation pattern in cancer cell lines was elucidated by employing the MGL-SERS strategy, which couples metabolic glycan labelling (MGL) and surface-enhanced Raman scattering (SERS). For the first time, an *N*-alkyl glucosamine derivative (GlcNPhAlk) has been identified as a glycan labelling precursor. The extent of labelling was assessed by utilising Raman imaging and verified by complementary fluorescence and western blot analysis. MGL-SERS technique was implemented for a comparative evaluation of cell surface glycan imbalance in different cancer cells wherein a linear relationship between glycan expression and metastatic potential was established. Further, the effect of the sialyltransferase inhibitor, P-3Fax-Neu5Ac, on metabolic labelling of GlcNPhAlk proved the incorporation of GlcNPhAlk to the terminal glycans through the sialic acid biosynthetic pathway. Hence, this methodology unveils the phenomenon of metastatic progression in cancer cells with inherent glycosylation-related dysplasia.

2.2. Introduction

Glycosylation is a major post-translational modification prevalent in most eukaryotes. Notably, glycans cover the cell surface and play a decisive role in cell-cell interactions and cell migration during various physiological processes such as fertilization, embryogenesis and immune responses.^[1,2] Recognition of cell-surface glycans are mostly achieved by fluorescence imaging and colourimetric methods which have limited specificity, and sensitivity and are encountered problems including photobleaching.^[3,4] Even though in most of the instances Raman imaging is limited in its application upon comparison with fluorescence imaging in the case of metabolic glyco-engineering mediated labelling approaches, it can be counted as a robust method. This is mainly attributed to the high sensitivity and specificity of Raman imaging which could produce more accurate output than fluorescence or western blot. Western blot analysis is time-consuming and requires skilled technicians whereas fluorescence imaging techniques need an additional step of ligation (click reaction, Staudinger ligation etc.) to conjugate the fluorescent probe. In recent times, Raman imaging has been explored as an alternative technique for glycan detection since it is an ultrasensitive technique in terms of enhanced signal intensity. The inherent drawbacks from fluorescent modality in glycan labelling can be eliminated with the help of Raman spectroscopic techniques like coherent anti-stokes Raman scattering (CARS), stimulated Raman scattering (SRS) and surface-enhanced Raman scattering (SERS).^[5-7] SRS has been employed as an effective imaging modality for metabolic labelling with numerous advantages including enhanced tissue penetration, intrinsic 3D sectioning, minimal photo-toxicity, free of background signals and signal enhancement by a factor of 10^7 . Although few reports claimed that SERS could be used for imaging glycan still there is much more to be scrutinised for a better understanding in this field.^[8-10]

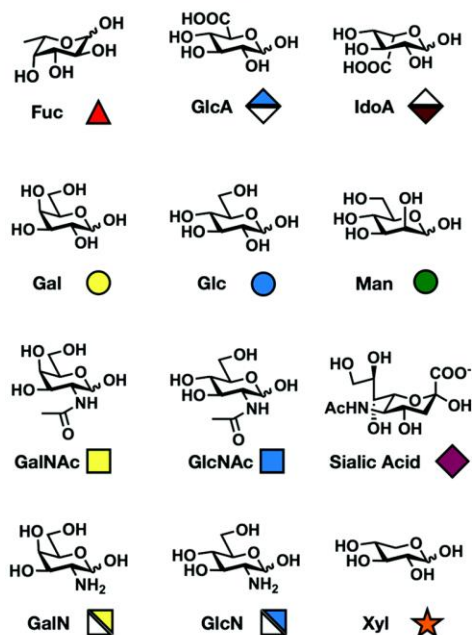
Glycans play a significant role in cancer progression and metastasis (**Figure 2.2**). Metastatic transformation is attributed to the efficiency of cancer cells to invade through the normal tissue surrounding them, engraftment and succeeding hematogenous or lymphatic spread.



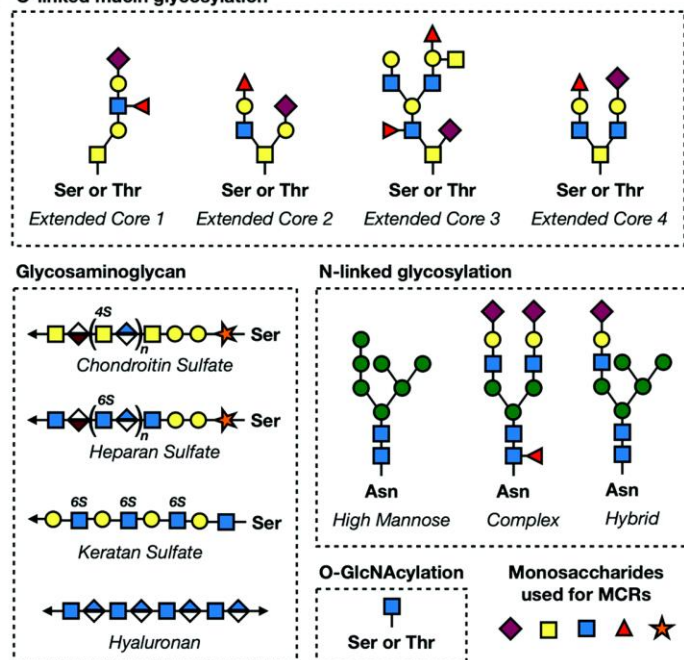
Scheme 2.1: Aberrant glycosylation in cancer cells.

Aberrant glycosylation is often associated with malignant cancers that can alter the antigenic and adhesive properties of cancer cells thereby facilitating metastatic advancement (**Scheme 2.1**).^[11,12] The overexpressed glycosyltransferase enzymes including MGAT5 (β -1,6-*N*-acetylglucosaminyltransferase V) play a key role in the biosynthesis of branched glycans and undoubtedly the expression will be proportional to the metastatic potential of the cells.^[13] Moreover, some reports differentiate the degree of tumour metastasis through the potentiometric detection of cell membrane sialic acid levels.^[14]

A. Monosaccharide Building Blocks



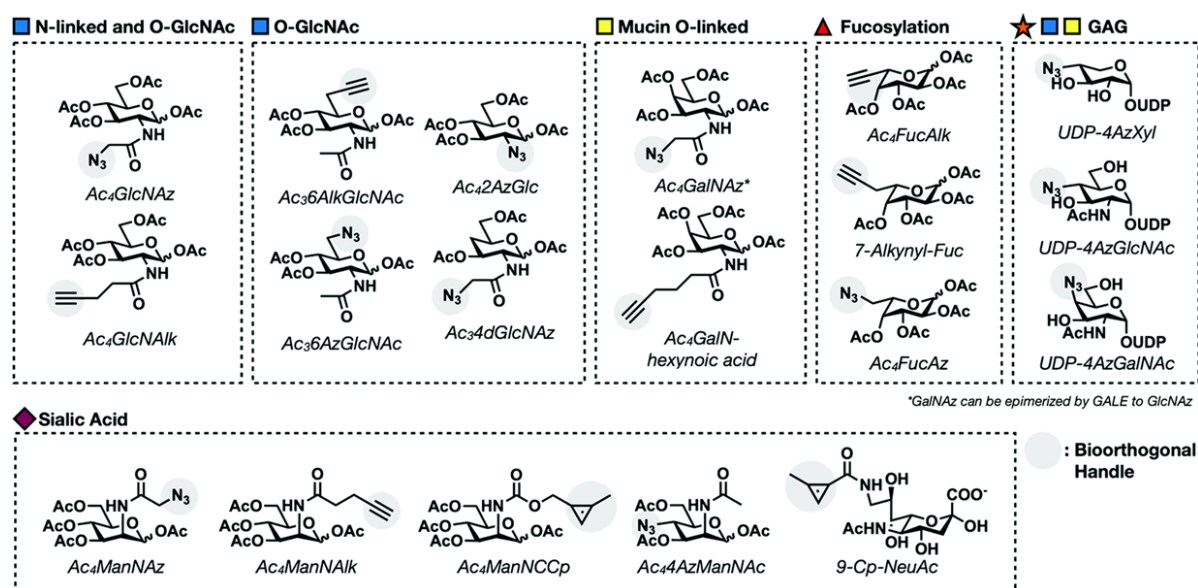
B. O-linked mucin glycosylation



Scheme 2.2: (A) Common mammalian monosaccharide building blocks and their geometric codes (B) Core structures for *O*-linked mucin, *N*-linked, GAG, and *O*-GlcNAc

2.2.1. An overview of metabolic labelling of glycans

Although glycan expression on cell surfaces has been attempted using SERS, the specificity in cell surface mapping and imaging is still a challenge.^[15,16] Utilising the Raman technique for glycan differentiation with aberrant glycosylation in different cancer cells based on their metastatic potential has not been explored. A facile SERS technique using bioorthogonal chemical reporter, GlcNPhAlk, as a glycan labelling entity has been introduced, which is the first *N*-alkyl monosaccharide analogue since all the reported glycan precursors (GPs) are of *N*-acyl group starting from *N*-acetyl mannosamine. Bertozzi and co-workers have extensively studied the substrate specificity of the sialic acid pathway and confirmed that the *N*-acetyl part is the critical determinant in selecting a sialic acid precursor.^[17] Moller *et al.* reported C4 modified *N*-acetyl mannosamine for metabolic oligosaccharide engineering applications keeping the *N*-acetyl group intact.^[18]

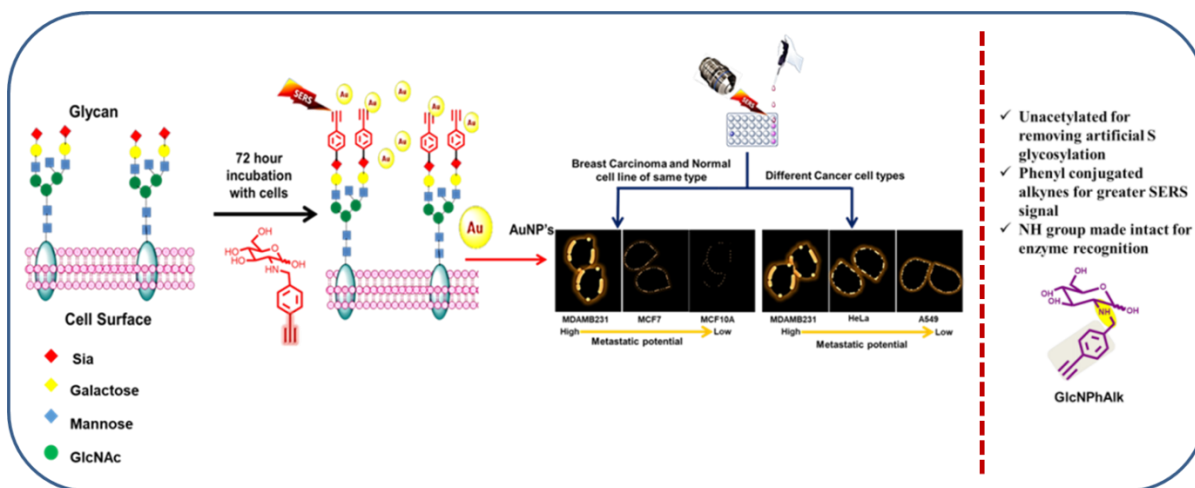


Scheme 2.3: Structures of some of the monosaccharide analogues used for glycan labelling reported to date

Both Bertozzi and Reutter's groups pioneered metabolic oligosaccharide engineering (MOE), a strategy that consists of the use of modified sugar analogues that are metabolically labelled and transformed into modified glycans. There have been many ground-breaking works on MOE and bioorthogonal chemistry for the development of glycan precursors for metabolic glycan labelling by both Bertozzi and Reutter and many others.^{[17][19-23]} These research

groups developed several approaches that have resulted in the plethora of bioorthogonal chemical reporters from various sugar analogues, including ManNAz, GalNAz, GlcNAz, and SiaNAz as well as their alkynyl counterparts having *N* acetyl functionality, which is of paramount importance in enzymatic recognition in the biosynthetic pathway of sialic acids (**Scheme 2.3**).^{[24–28][17,23]}

2.3. Aim and scope of the study: The present work replaces the keto group of *N*-acetyl part of the sugar unit with *N*-alkyl with the help of reductive amination reaction on glucosamine; it is anticipated that the NH bond will be intact for the enzyme activation through hydrogen bonding, which facilitates the glycan biosynthesis process to be transformed into a modified sialic acid. As glucosamine does not take part in any transformational changes that happen in the biosynthetic pathways of glycans, the decision was made to introduce the bioorthogonal functionality through *N*-alkyl linkage. Therefore, incorporating *N*-alkyl derivatives for glycan labelling enhances the versatility of glycan labelling molecules, which predominantly consist of *N*-acetyl compounds. Alkyne group was chosen as the bioorthogonal functionality since it has the maximum cross-sectional area in SERS when compared to other bioorthogonal functional groups, which is metabolically labelled at the terminal site of the glycan chain ended with sialic acid by biosynthetic pathway (**Scheme 2.1**).^[24,29,30] Colloidal gold nanoparticles (AuNPs) with a diameter of 35-40 nm were chosen as SERS substrate for acquiring maximum enhanced Raman fingerprint and imaging to elucidate the extent of metabolic labelling. Cancer cells with different metastatic potentials i.e., highly metastatic breast cancer cells MDA-MB-231, comparatively lower metastatic cervical cancer cells HeLa, non-small lung adenocarcinoma cells A549, another breast carcinoma cell line MCF-7 and finally a normal breast epithelial cell line MCF-10A with least metastatic potential were selected for the comparative study (**Scheme 2.4**).^[31–36] This carefully calibrated approach not only assesses *in situ* detection and imaging of glycans but also promotes semi-quantitative recording of the variation in glycan expression by their metastatic potential. The importance of identifying metastatic gradients is the principal goal of cancer theranostics that requires emerging imaging techniques to discriminate within cells and tissues. Such imaging technologies are of paramount interest in cancer diagnosis. Since metastasis remains a big barrier towards fruitful cancer treatment, the current investigation will be instrumental in designing glycan-based therapies against cancer.



Scheme 2.4: Schematic representation of MGL-SERS strategy and structural characteristics of synthesised glycan precursor

As expected, the probe was labelling the glycans at the cell surface confirmed by fluorescence imaging. An inhibition study using a Sialyltransferase inhibitor also suggested that GlcNPhAlk might be transforming to cell surface glycans through the sialic acid biosynthetic pathway. The MGL-SERS technique was utilised for evaluating glycan expression in various cancer cell lines with varying metastatic potential and the results suggested the linear relationship between the glycan expression and metastatic potential.

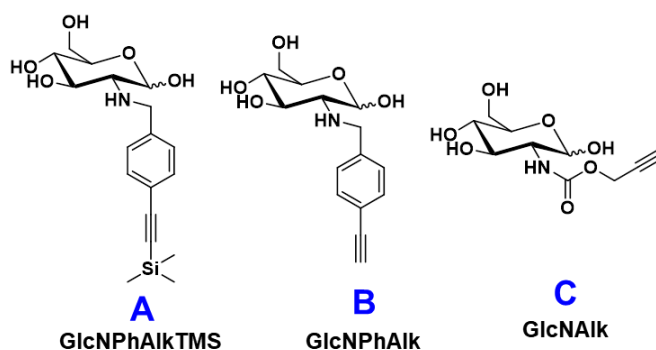


Figure 2.1: Structures of synthesised glycan precursors

2.4. Results and discussion

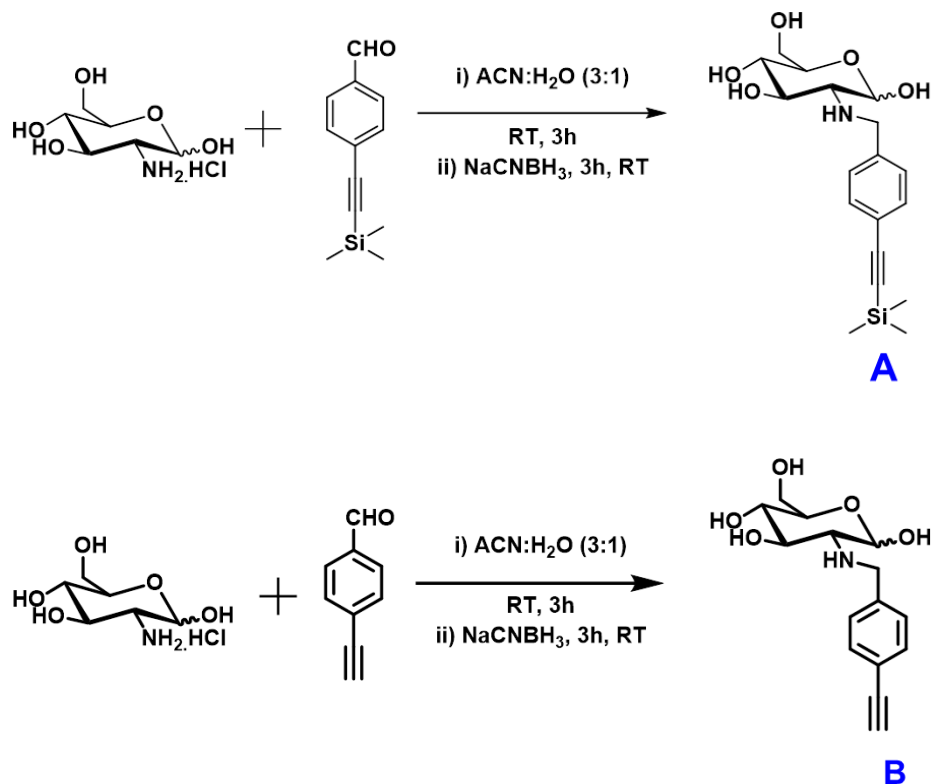
2.4.1. Synthesis and characterisation

To date, all the synthesised glycan labelling sugar analogues contain the *N*-acetyl group which was hypothesised to be essential for enzymatic recognition in sialic acid biosynthesis. Alkynyl-glucosamine derivatives GlcNPhAlk and GlcNPhAlkTMS were synthesized as probe molecules with *N*-alkyl groups anticipating that the NH bond, as a source of hydrogen bond,

is enough for enzymatic recognition. As a control, the acylated version of glucosamine (GlcNAIk) was also synthesised (**Figure 2.1 & Scheme 2.5**). All molecules were characterised with NMR and ESI-HRMS analyses (**Figure 2.2-2.7**). Although per-*O*-acetylated unnatural sugars are widely used to improve cell permeability, it leads to artificial *S*-glycosylation which compromises the specificity of metabolic glycan labelling in living cells.^[37] Hence to avoid false-positive results, unacetylated unnatural sugars were selected as the precursor for metabolic labelling.

2.4.1.1. General procedure for the synthesis of alkynylated glucosamine derivatives

To a stirred solution of D-glucosamine (500 mg, 2.3 mmol) in MeCN/H₂O (3:1, 12 ml) was added appropriate aldehydes (4.6 mmol) and the resulting mixture was stirred for 3 hours at room temperature. NaBH₃CN (6.9 mmol) was added and the reaction was stirred for a further 3 hours, at which point H₂O (25 ml) was added and the reaction mixture was extracted with ethyl acetate (EtOAc, 3 x 25 ml), and the organic layers were collected and washed with brine (25 ml), before being dried over Na₂SO₄ and concentrated in vacuum. The resulting residue was purified by column chromatography (CC) using EtOAc as the eluent to afford the desired compound as a yellow powder in 70% yield.



Scheme 2.5: Synthesis of GlcNPhAlkTMS, GlcNPhAlk respectively

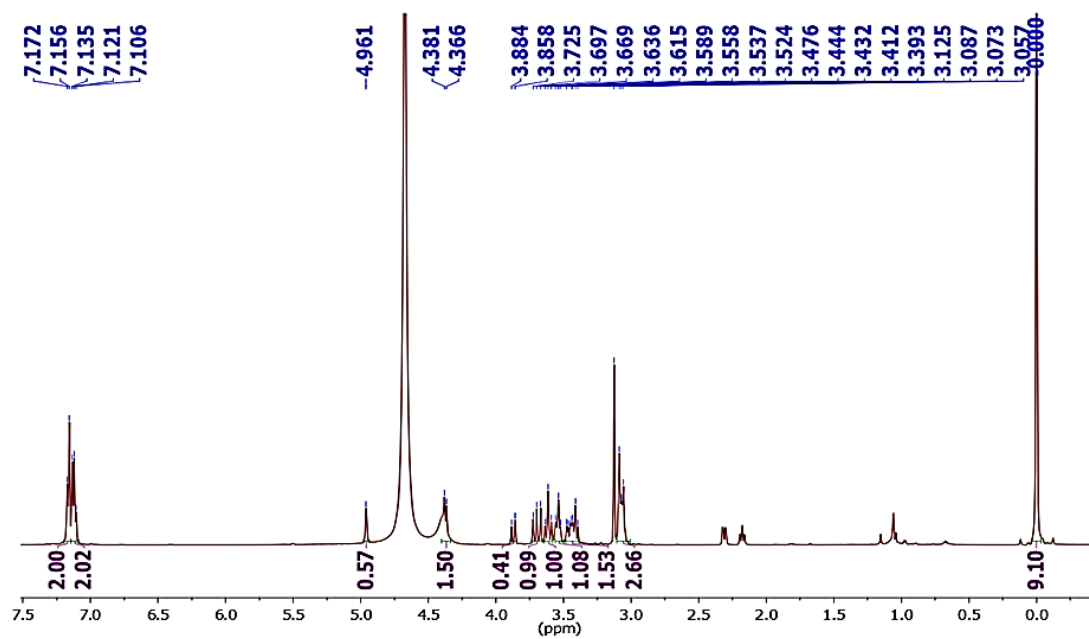


Figure 2.2: ^1H NMR spectrum of A

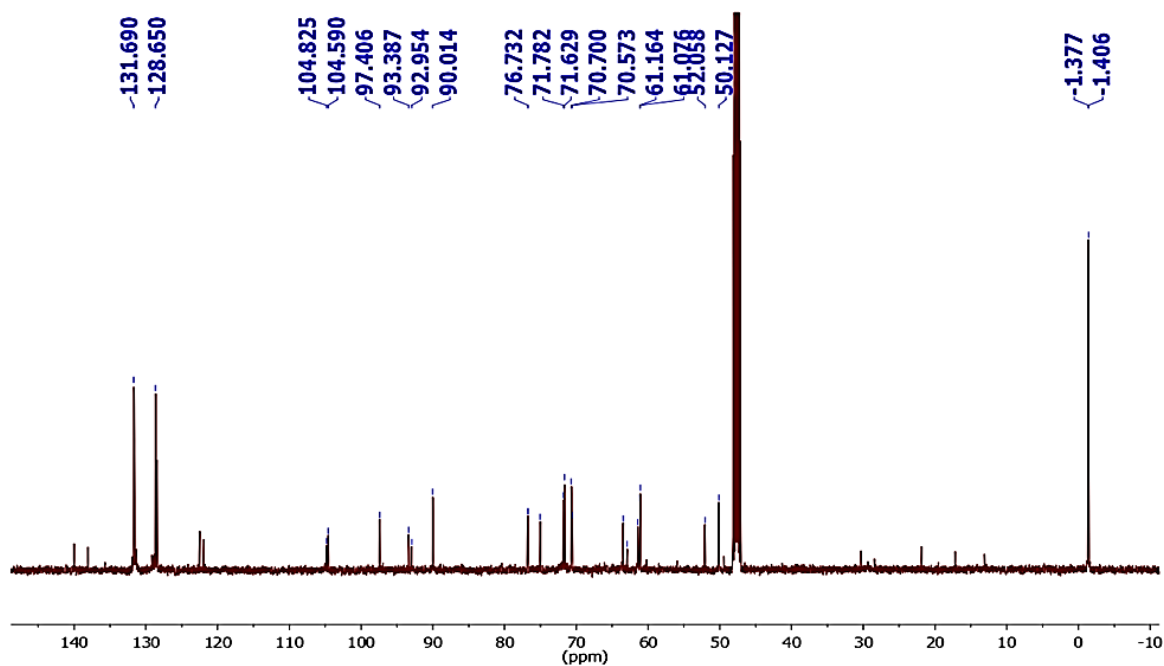


Figure 2.3: ^{13}C NMR spectrum of A

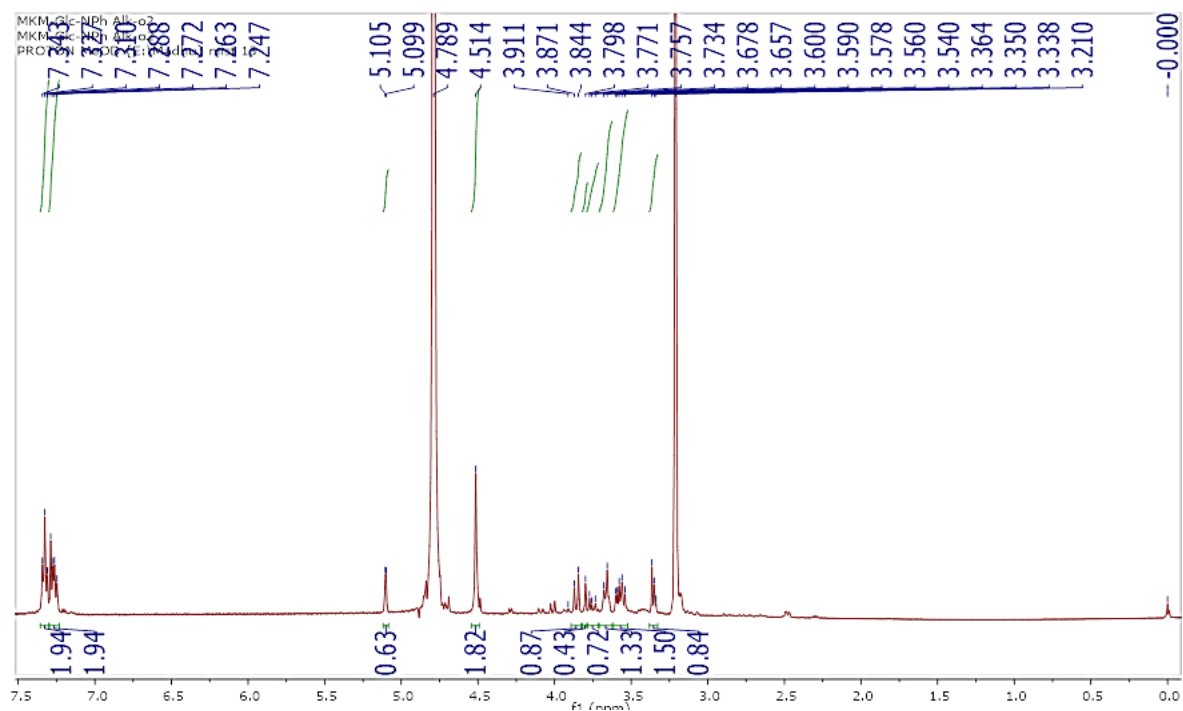


Figure 2.4: ^1H NMR spectrum of B

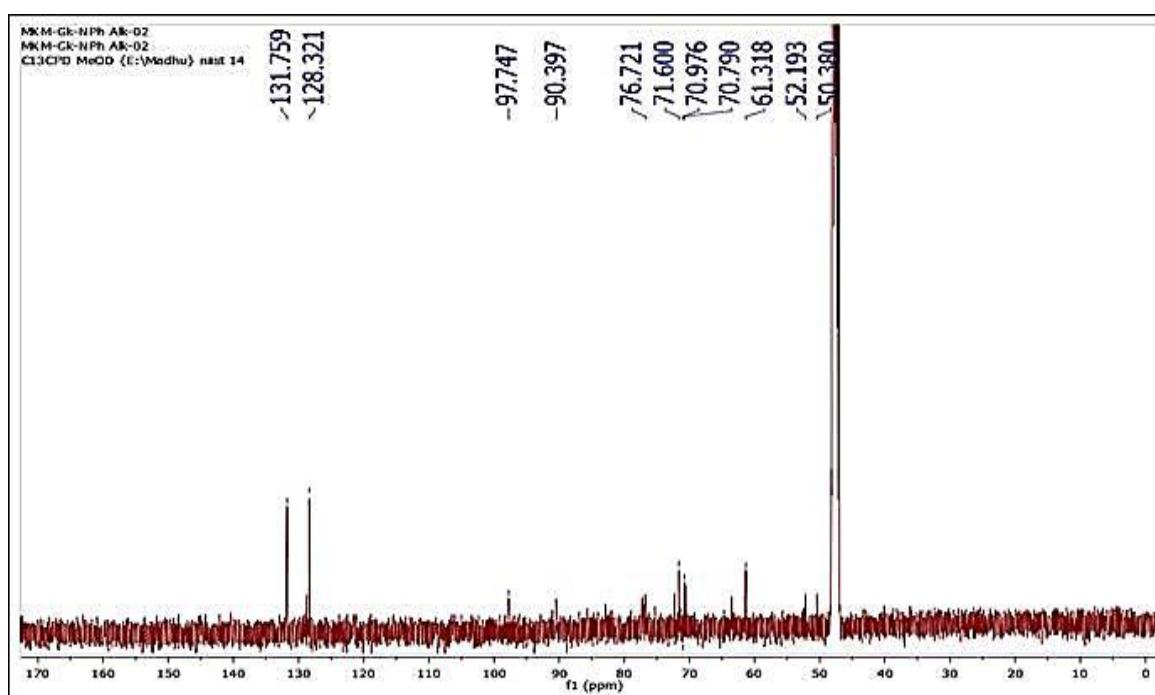
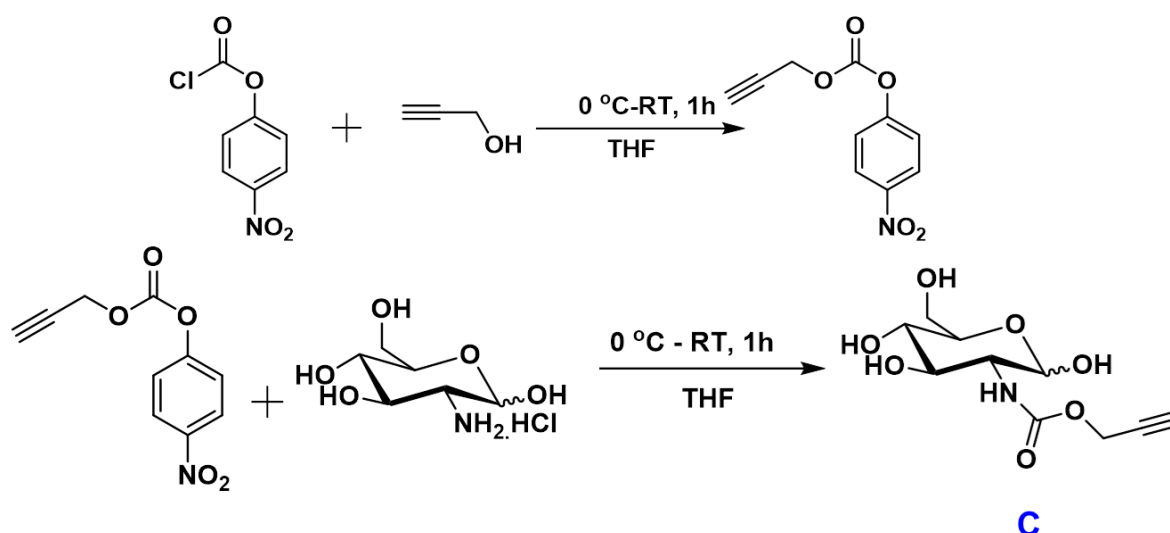


Figure 2.5: ^{13}C NMR spectrum of B

2.4.1.2 Synthesis of GlcNAIk (C)

To a stirred solution of prop-2-yn-1-ol (143 μl , 2.4 mmol) in tetrahydrofuran (THF) was added *p*-nitrochloroformate (500 mg, 2.4 mmol) and the resulting mixture was stirred for 1

hour at 0 °C. The reaction mixture was extracted with EtOAc (3 x 25 ml), and the organic layers were collected and washed with brine (25 ml), before being dried over anhydrous Na₂SO₄ and concentrated in a vacuum. The resulting residue was purified by CC with hexane: EtOAc (9:1) to afford the desired compound as a white powder in 91% yield. The resulting product (200 mg, 0.90 mmol) was stirred with glucosamine (194 mg, 0.90 mmol) in DMF and DIPEA (156 μL, 0.9 mmol) was added to the mixture and was stirred for 24 hours at room temperature. The reaction mixture was extracted with EtOAc (3 x 25 ml), and the organic layers were collected and washed with brine (25 ml), before being dried over anhydrous Na₂SO₄ and concentrated in a vacuum. The resulting residue was purified by CC using hexane : EtOAc (7:3) to afford the desired compound as a white powder in 76% yield.



Scheme 2.6: Synthesis of GlcNAIk

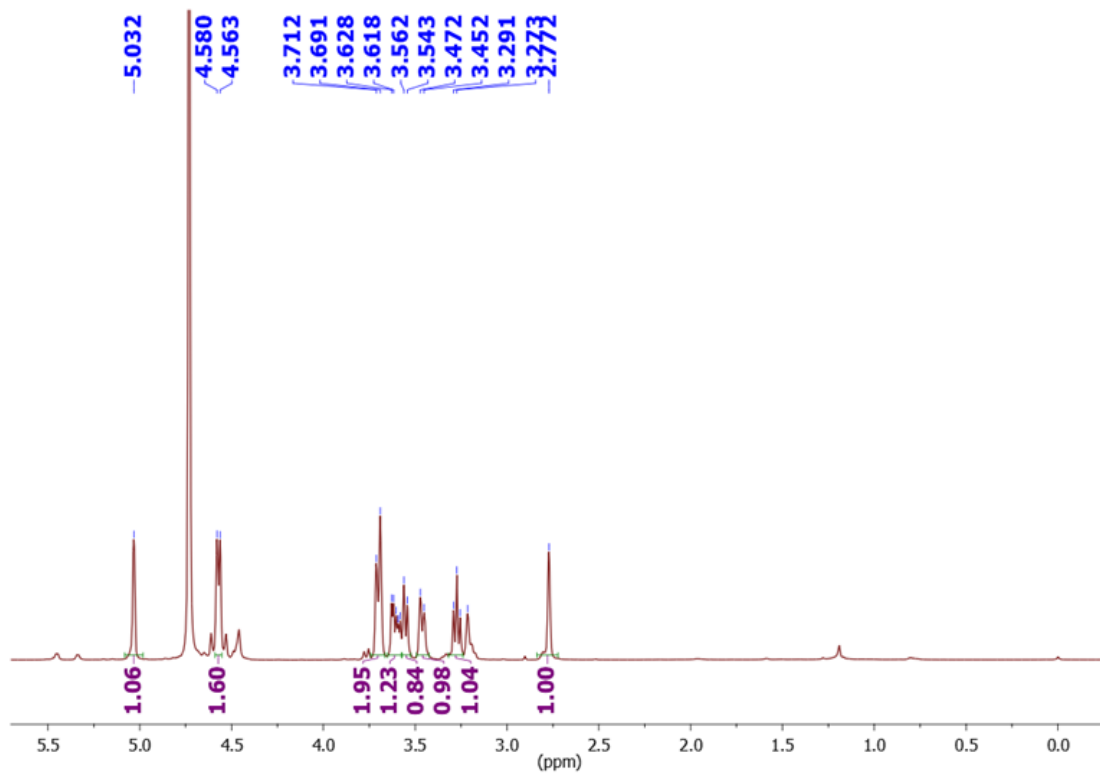


Figure 2.6: ^1H NMR spectrum of GlcNAk

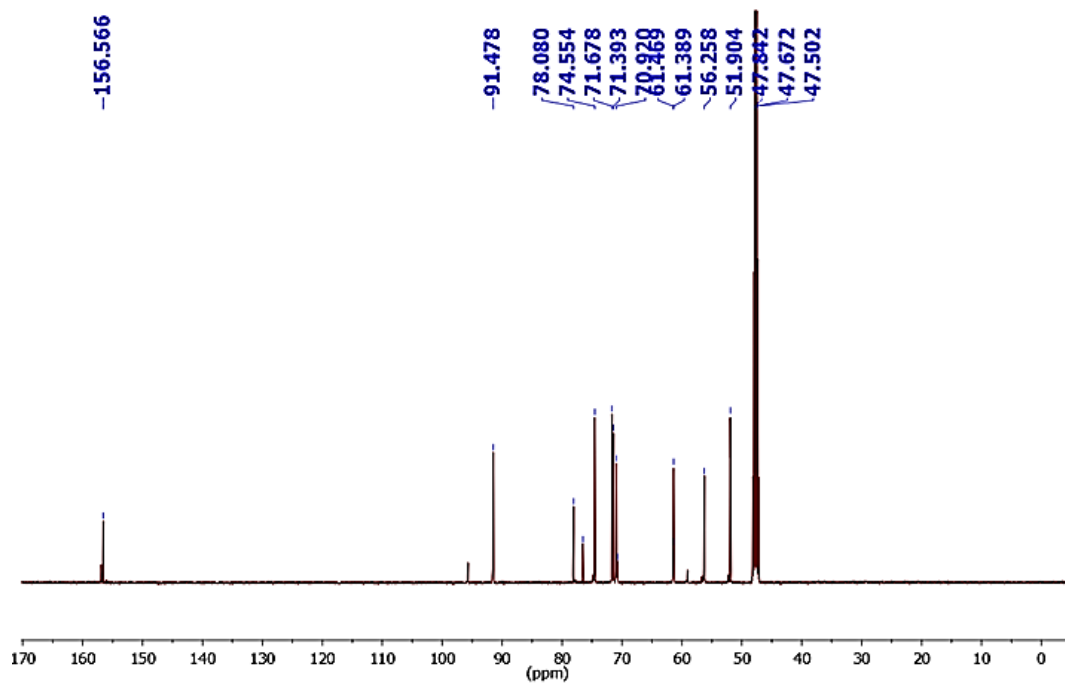


Figure 2.7: ^{13}C NMR spectrum of GlcNAk

2.4.2. SERS analysis of alkynylated glucosamine analogues

Using the hyperspectral Raman technique Yamakoshi and co-workers have reported Raman-tags conjugated with phenyl-ring performed as a better candidate for metabolic labelling.^[29] This strategy has been translated into the SERS modality by introducing phenyl-appended alkynes as bioorthogonal Raman-tags, and its Raman intensity in the solution state has been studied to foresee the efficiency of spectral fingerprint in the cell silent. At first, SERS analyses of various types of alkynes were performed. Hence, for that variety of compounds, having phenyl conjugated, non-conjugated, terminal and internal alkynes were selected as bioorthogonal Raman-tags and studied in solution state to foresee the efficiency of spectral fingerprint in the cell silent region. Quasi-spherical colloidal gold nanoparticles (AuNPs) of the size 35-40 nm were synthesised (**Figure 2.8**) for maximum SERS enhancement.^[38]

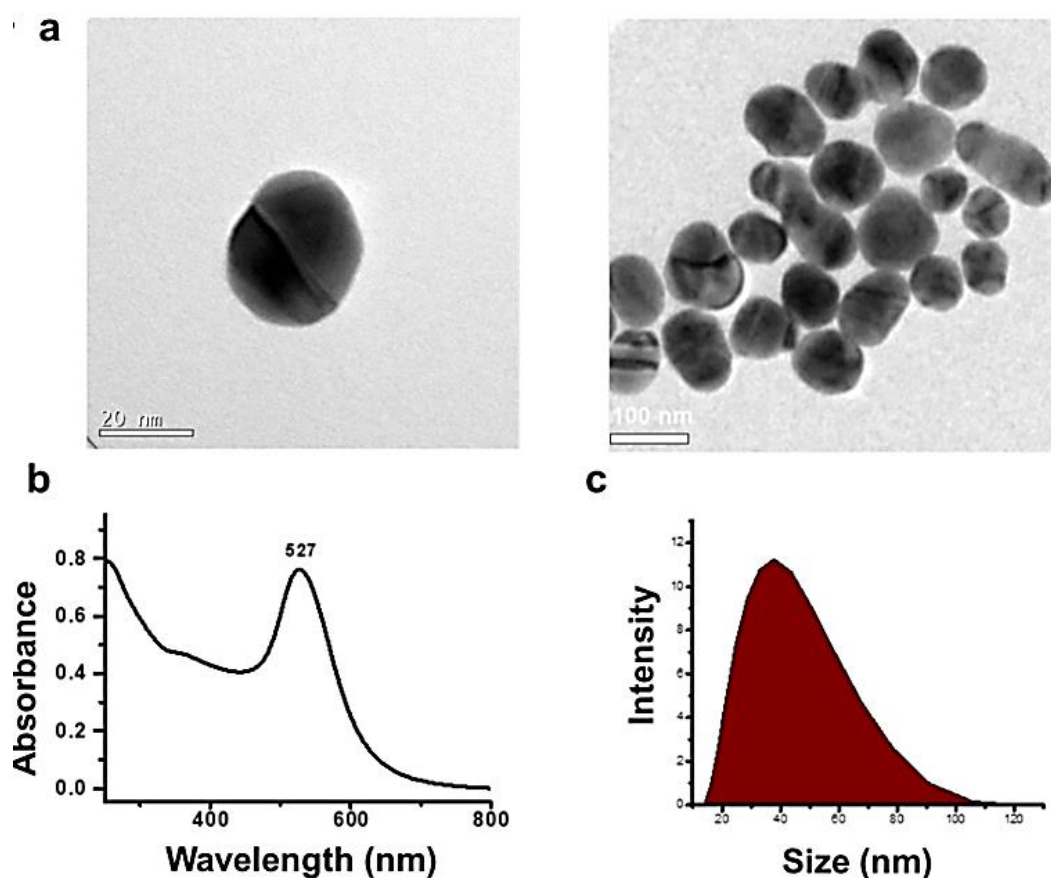


Figure 2.8: Characterisation data of synthesised AuNP's a) TEM analysis showing the spherical shape of AuNP's with average size 35-40 nm b) Absorption spectrum c) DLS data showing the particle size distribution of AuNP's with average size 40 nm.

These alkynes were mixed with 4-cyanobenzaldehyde (CB) which was taken as an internal standard due to the well-resolved Raman peak at 2230 cm^{-1} (**Figure 2.9**). The SERS spectra

of all the alkyne tags displayed a chemical shift near 2000 cm^{-1} with colloidal AuNPs. From the ratio of intensities of the sample and standard, RIC (relative Raman intensity vs CB) was calculated. Phenyl-conjugated alkynes produced a higher RIC value than the non-conjugated ones. The terminal alkynes showed more intense peaks than the internal alkynes in the SERS study (**Figure 2.9**).

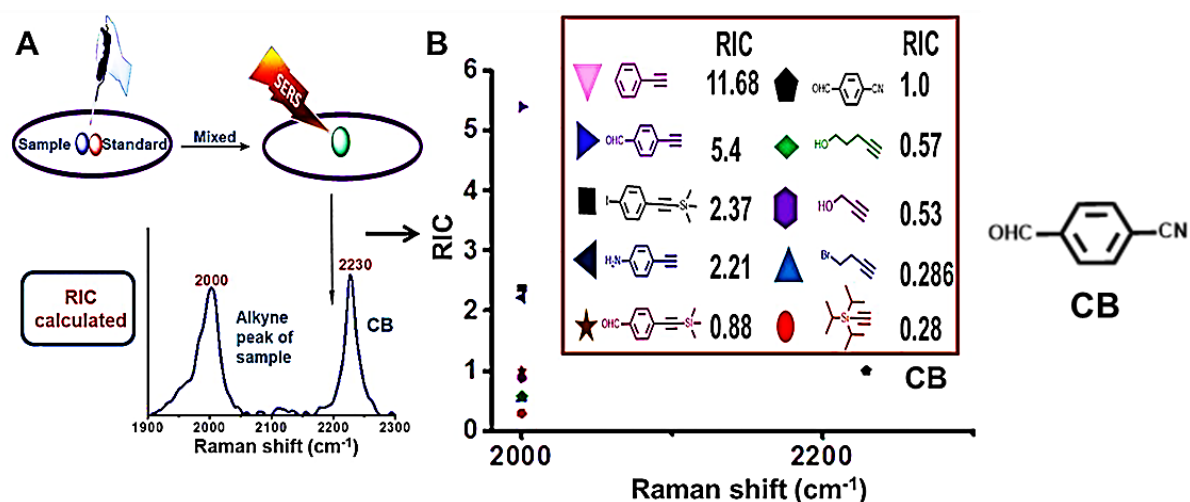


Figure 2.9: A) Schematic representation of SERS study of phenyl conjugated and unconjugated alkynes. B) Graph showing RIC (Relative intensity against 4-cyano benzaldehyde) values of different alkynes.

Three monosaccharide units (glucosamine moiety) as a metabolic labelling precursor with bioorthogonal alkyne groups GlcNPhAlkTMS, GlcNPhAlk, GlcNAlk were subjected to SERS analysis, in which both GlcNPhAlkTMS and GlcNPhAlk showed intense Raman peaks at 1165 cm^{-1} , 1596 cm^{-1} , 1991 cm^{-1} and has a broad signal around 2142 cm^{-1} corresponding to C–C skeletal stretch, C=C ring vibrations, and the last two peaks corresponding to C≡C stretching vibrations respectively (**Figure 2.10**).^[39–41]

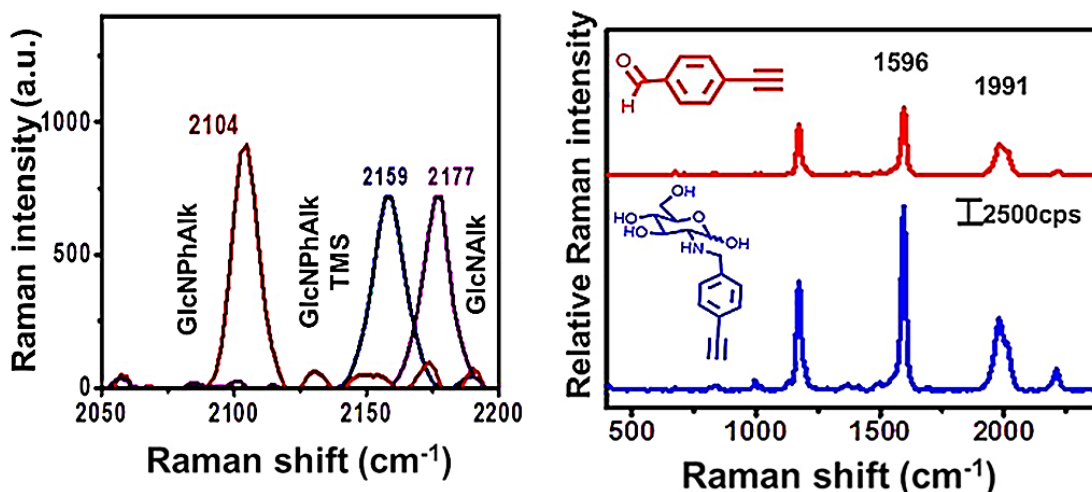


Figure 2.10: Bare Raman spectra of 3 GPs and SERS spectra of GlcNPhAlk and the aldehyde used for its synthesis.

Alkyne-centred compounds exhibited two peaks at 1991 cm^{-1} and 2142 cm^{-1} in the cell silent region due to the presence of two types of binding motifs for the molecule at the nanoparticle surface.^[39] It was further confirmed with the bare Raman spectra of both molecules, which showed only a single peak centred at 2100 cm^{-1} , whereas the SERS spectra of the third alkyne molecule, GlcNAIk, without phenyl group displayed a negligible peak in the cell silent region. However, the bare Raman spectrum of the compound demonstrated a peak around 2100 cm^{-1} , in the cell silent region (**Figure 2.11**). GlcNPhAlk produced an intense Raman peak compared to bare alkyne in the presence of AuNPs. Based on the above observation, it was decided to proceed with our studies with GlcNPhAlkTMS and GlcNPhAlk prevailing the most intense peaks at 1596 cm^{-1} and 1991 cm^{-1} . Out of these alkynes, phenyl appended alkynes produced a maximum Raman intensity peaks than the non-conjugated ones. Also, the peak intensity of terminal alkynes was higher than the internal alkynes in the SERS study. Based on these results two glycan tags GlcNPhAlk, and GlcNPhAlkTMS were synthesised using Borch reductive amination of D-glucosamine with their appropriate aldehydes as per the previous literature.^[42]

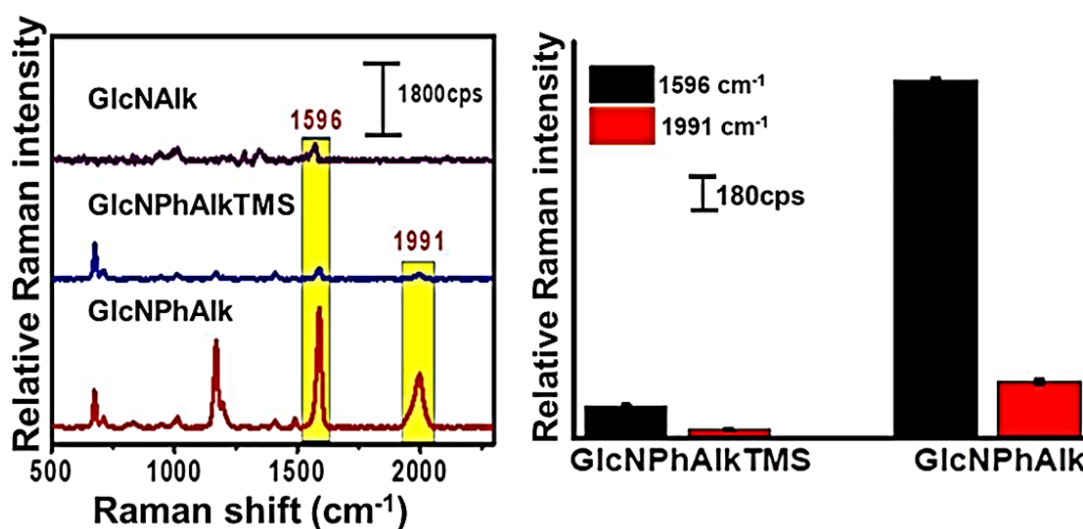


Figure 2.11: SERS spectra of 3 GPs and comparison of Raman Intensities of GPs (with and without TMS respectively) on AuNP.

2.4.3. Cytotoxicity studies of alkynylated compounds

MDA-MB-231, HeLa, A549 and MCF-10A cells were seeded into 96 well plates and incubated for 24 hours (at 37 °C 5% CO₂). Cells were then treated with varying concentrations of GlcNPhAlkTMS (**A**), GlcNPhAlk (**B**) and GlcNAIk (**C**) (20-200 μM). After 72 hour incubation, MTT (0.5 mg /ml) was added to each well and kept at 37 °C for 4 hours and finally, the so-formed formazan crystals were dissolved in DMSO and the optical density (OD) was measured at 570 nm using a microplate reader. Cytotoxic studies of all three GPs in normal and cancer cell lines confirmed the viability up to 100 μM concentrations (**Figure 2.12**).

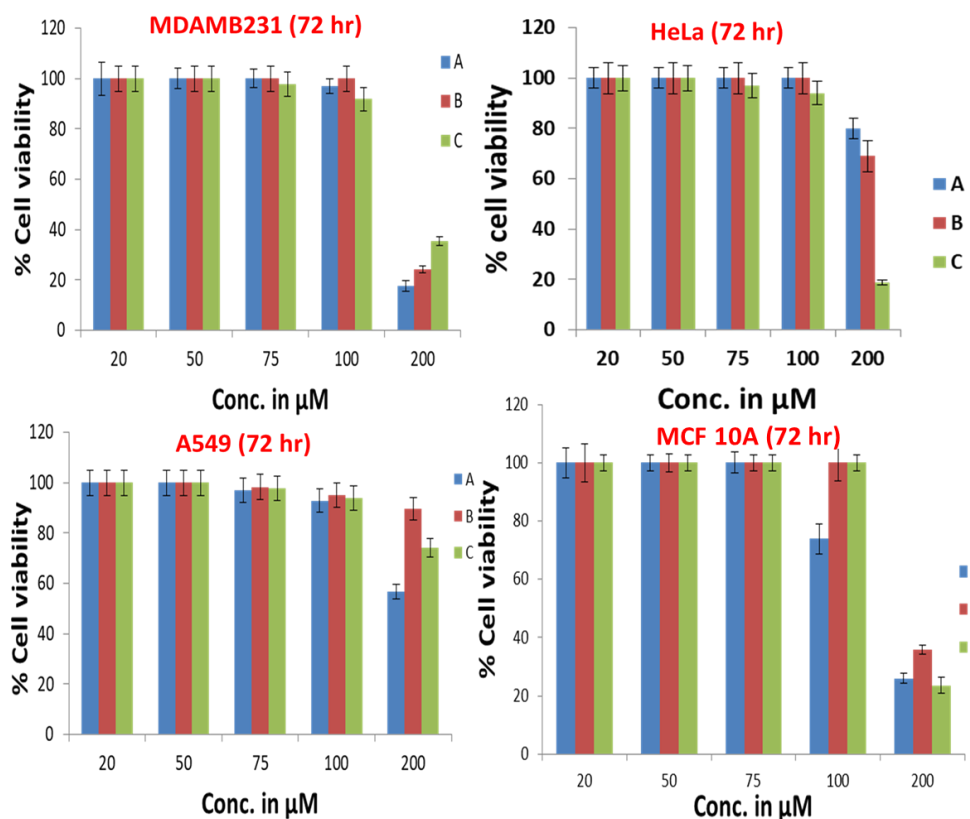


Figure 2.12: Cytotoxic studies on A) GlcNPhAlkTMS B) GlcNPhAlk and C) GlcNAIk

2.4.4. Metabolic glycan labelling of glucosamine analogues

Primarily our investigation was focused on the detection of cell surface glycans by SERS imaging and to find out the extent of metabolic labelling capability of aforesaid compounds. Cervical carcinoma HeLa cells were treated with GlcNPhAlkTMS and GlcNPhAlk for 72 hours to induce the biosynthetic pathway to incorporate into cell surface glycans. Cells without glycan tags were used as negative controls. After a treatment of 3 days, the cell culture medium was removed and washed thrice with PBS (phosphate-buffered saline), and SERS imaging was performed by incubating with colloidal AuNPs. SERS spectra of GlcNPhAlkTMS and GlcNPhAlk suggested that the intensity of GlcNPhAlk is six to eight folds higher than its counterpart with TMS, demonstrating GlcNPhAlk as the better candidate for glycan labelling (**Figure 2.11**). Cells incubated with GlcNPhAlk provided significant Raman-mapped images with greater sensitivity, specificity and repeatability when compared to GlcNPhAlkTMS-treated cells (**Figure 2.13**). Hence GlcNPhAlk was selected for further studies. Control images were also taken without labelling (**Figure 2.13**).

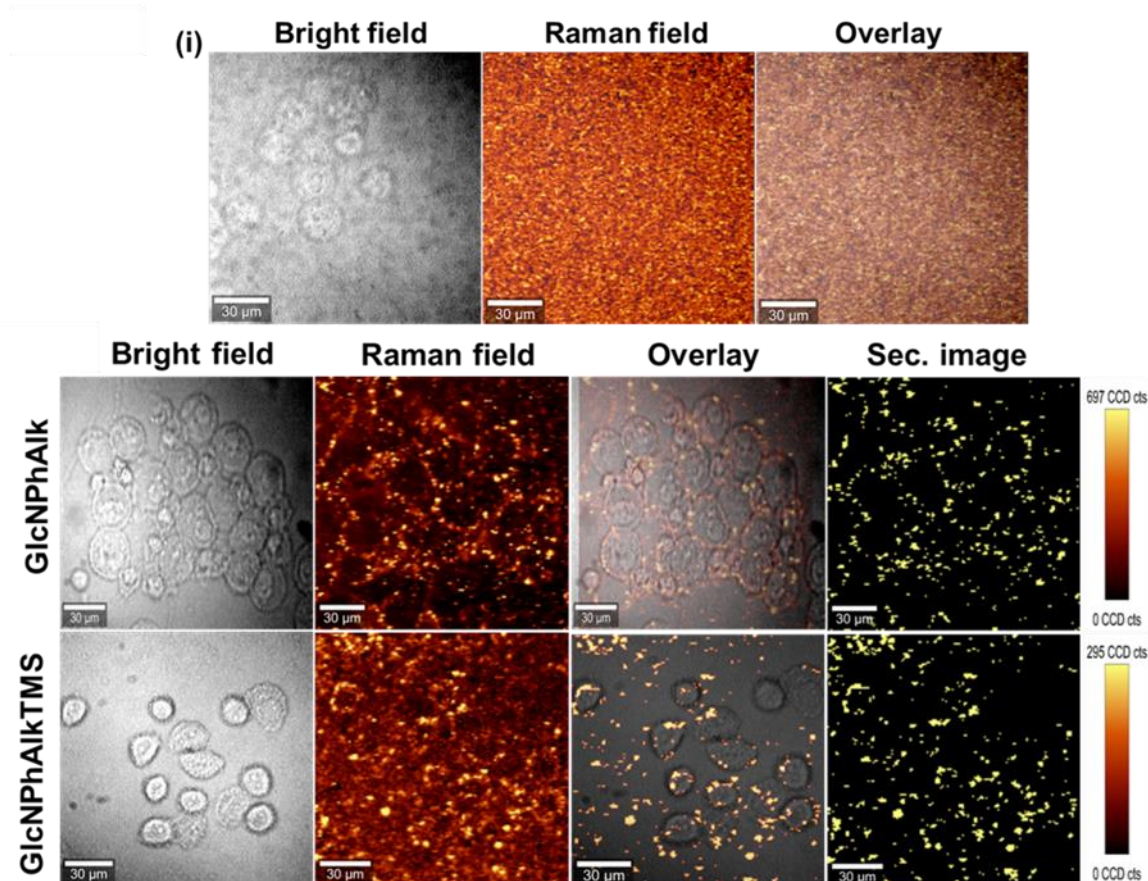


Figure 2.13: Images of HeLa cells without labelling and comparison of glycan labelling of GlcNPhAlk and GlcNPhAlkTMS respectively on HeLa cells.

2.4.5. Complementary glycan labelling through fluorescence and western blot Analysis

There have been numerous reports of azido or alkynyl sugars being used as bioorthogonal chemical reporters with the help of “click chemistry” for the labelling of glycans in cells and living animals^[43–46]. After the incorporation of azido/alkynyl sugars, they can be covalently labelled with various tags (e.g., biotin or fluorescent molecules) by chemical reactions such as Cu(I)-assisted [3+2] azide-alkyne cycloaddition (CuAAC), Staudinger ligation etc. The labelled glycans have been imaged and enriched using these techniques. Thus to confirm the the metabolic labelling of GlcNPhAlk, we decided to pursue fluorescent analysis using azidonaphthalimide probe (**Figure 2.14**) and chemiluminescent western blot analysis using biotin PEG azide both facilitated by CuAAC.^[7,44]

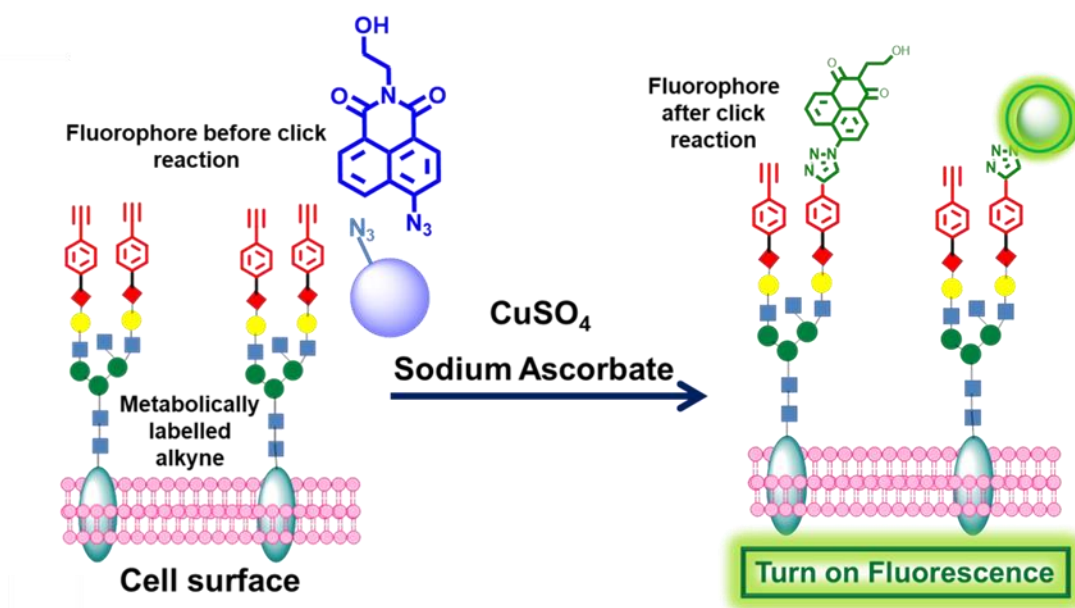
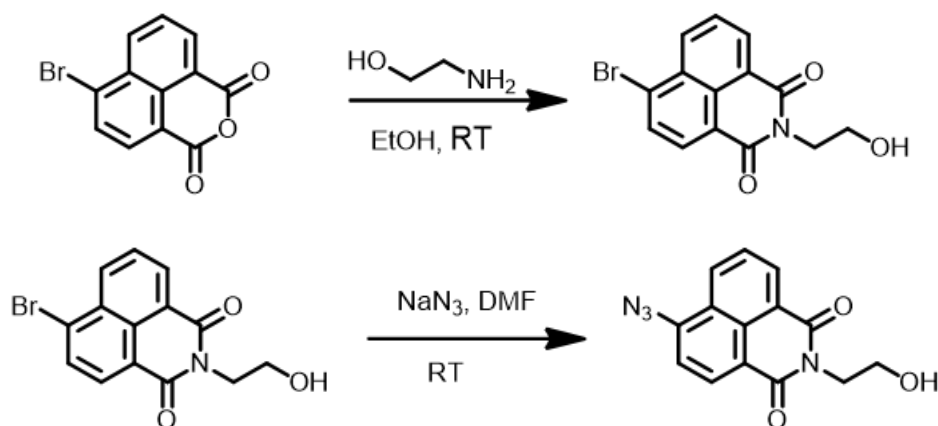


Figure 2.14: CuAAC based fluorescent detection of metabolically labelled alkyne glycans.

2.4.5.1. Synthesis of azidonaphthalimide derivative

4-bromo-1,8-naphthalic anhydride (500 mg, 1.8 mmol) was taken into a 100 ml round bottom flask containing 3 ml ethanolamine. A few ml of ethanol was added to it. The mixture was stirred at room temperature for 2 hours. The compound was filtered and dried under a vacuum. The product was used for the next step without further purification. The resulting product (500 mg) and sodium azide (234 mg, 3.6 mmol) were taken into a 100 ml round bottom flask containing 3 ml anhydrous DMF. The reaction mixture was stirred for 1 hour at room temperature and then poured into water and extracted three times with EtOAc. The combined organic layer was washed with brine and water, dried over anhydrous Na_2SO_4 . After removal of the solvent under reduced pressure, the residue was subjected to CC with EtOAc: Hexane (4:1) as the eluent over silica gel afforded the pure product in 80% yield (Scheme 2.7).



Scheme 2.7. Synthesis of azidonaphthalimide derivative

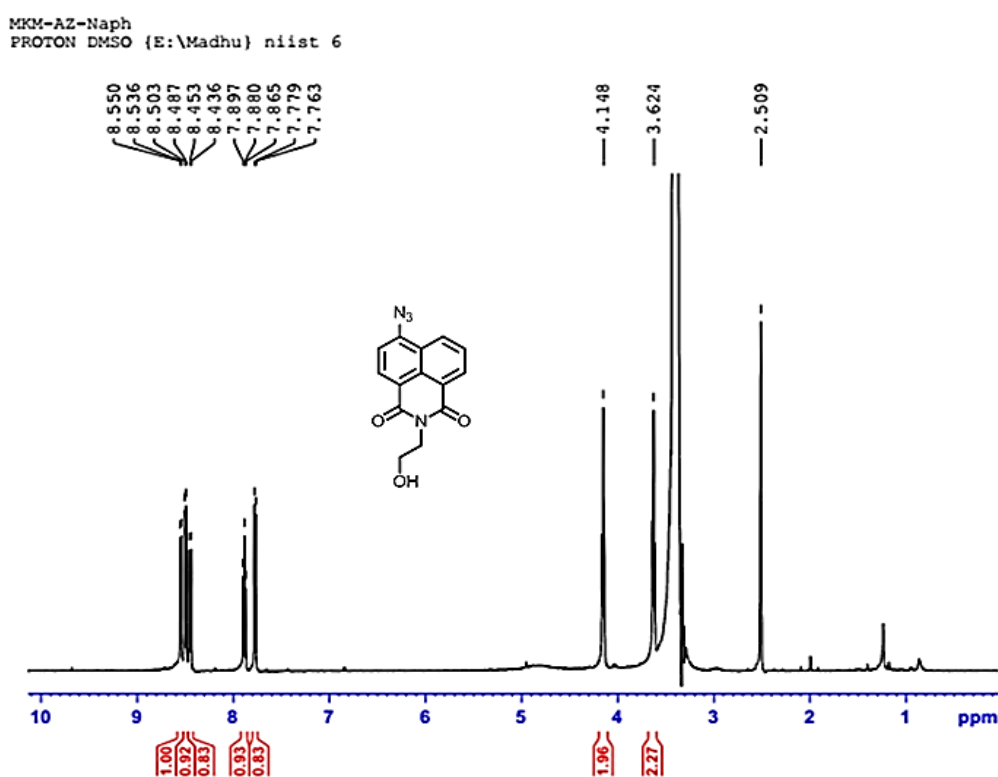


Figure 2.15: ^1H NMR spectrum of azidonaphthalimide fluorophore

2.4.5.2. Cu catalysed click reaction between alkynylated glucosamine and azido naphthalimide fluorophore.

The azidonaphthalimide derivative (final product) has very feeble fluorescence at λ_{max} 560 nm, as seen in the figure. But once it is made to react with the alkynylated glucosamine derivative its fluorescence gets enhanced with time and reaches a maximum at 50 minutes. After that, its fluorescence intensity decreases as shown in the figure (**Figure 2.16**). The compound has an excitation wavelength at λ_{max} 441 nm.

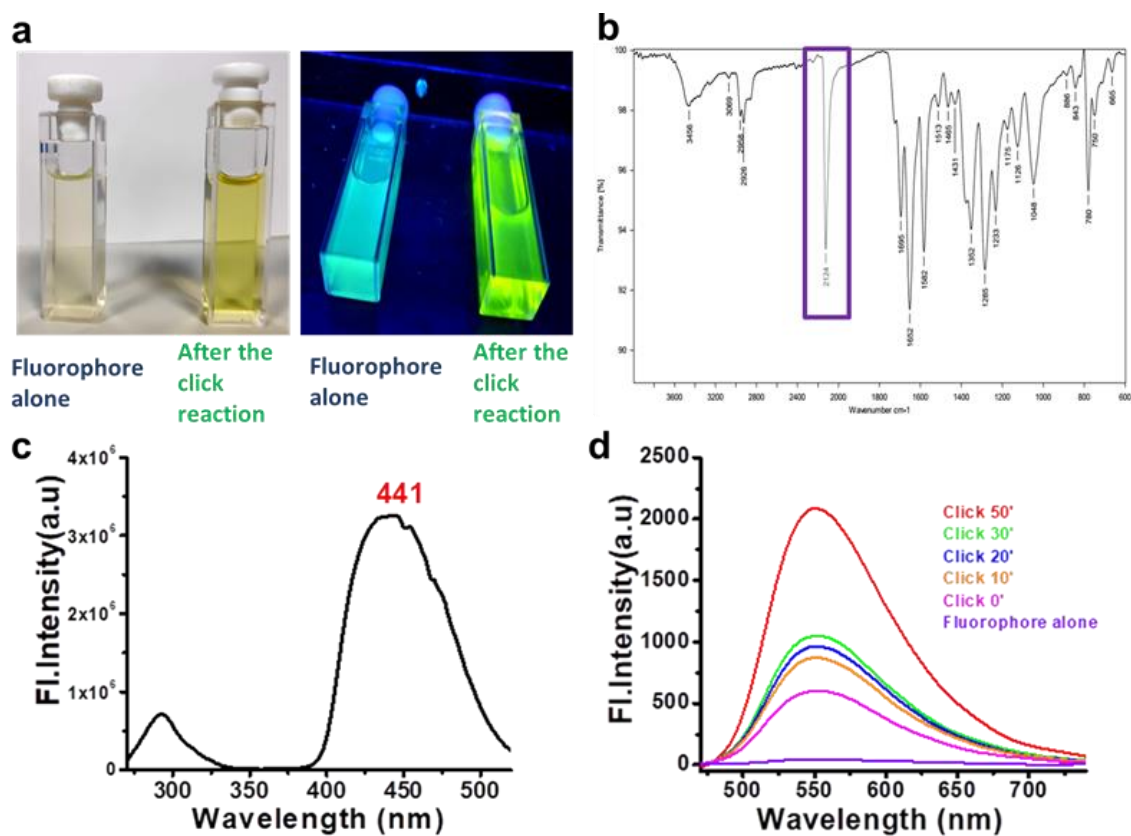


Figure 2.16: a) Naked eye and long UV vision of fluorophore alone and after the addition of GlcNPhAlk through CuAAC reaction b) IR spectrum of fluorophore showing azide peak at 2124 cm⁻¹ c) Excitation spectrum of fluorophore showing the excitation wavelength at 441 nm d) Emission spectrum of fluorophore with emission at 560 nm

Reactivity and click reaction-triggered fluorescence was tested by performing a [3+2] cycloaddition with GlcNPhAlk (**Figure 2.16 a**). The fluorescent intensity of the triazole cycloadduct was enhanced up to 30 times as it reacted with the GlcNPhAlk (**Figure 2.16 d**). This enhancement is due to the replacement of weak donors like azide by much better triazole donors. The emission maximum of click-product was centred at 560 nm when excited at 441 nm (**Figure 2.16 c**). Fluorescence labelling was performed in highly metastatic breast carcinoma MDA-MB-231 cells. Cells were incubated with GlcNPhAlk for 3 days and later azidonaphthalimide fluorophore tag was added followed by CuSO₄ and sodium ascorbate. After the incubation of 50 min, images were taken that indicated distinct labelling of the cell-surface (**Figure 2.17**). Another set of control experiments was also conducted with the same procedure with glucosamine instead of GlcNPhAlk, to confirm that the fluorescence is click activated turn on phenomenon.

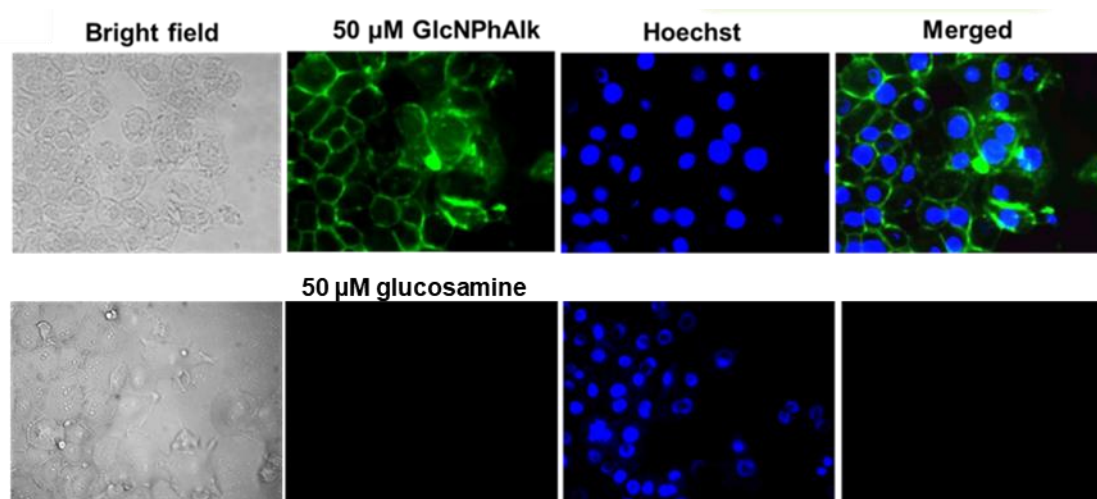


Figure 2.17: Confirmation of labelling through fluorescence in MDA-MB-231 cells for GlcNPhAlk and glucosamine respectively.

The extent of protein glycosylation by metabolically labelled alkyne tag was further evaluated by western blot analysis. The presence of metabolically anchored alkyne was confirmed in MDA-MB-231 cells treated with GlcNPhAlk using CuAAC. For this, cell lysate was extracted and treated with azide-PEG3-biotin in the presence of CuSO₄ and sodium ascorbate followed by horse radish peroxidase (HRP) conjugated streptavidin for chemiluminescent detection (**Figure 2.18**). A parallel experiment was carried out with glucosamine-treated cells taken as a negative control. Increased volumes of alkyne tagged glycoprotein were generated in the cell lysate of GlcNPhAlk treated MDA-MB-231 cells while no bands were visible in the cell lysate from glucosamine-treated cells indicating the detection of unique glycoproteins (**Figure 2.19**).

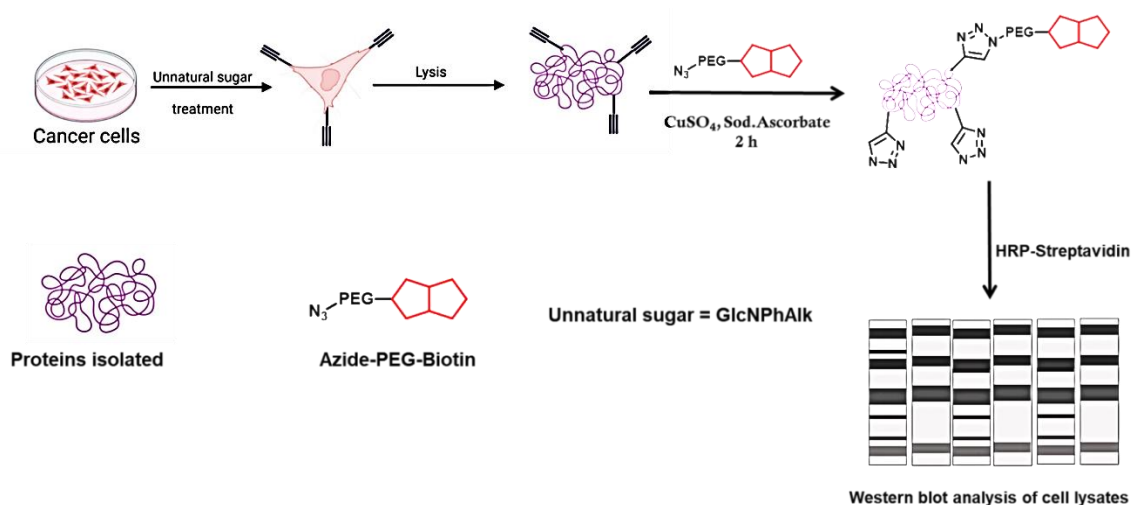


Figure 2.18: Schematic representation of western blotting and SERS analysis of cell lysates.

Also, the labelled alkyne was further confirmed by the SERS analysis of cell lysates collected from both the GlcNPhAlk and glucosamine-treated cells. Cell lysate obtained from GlcNPhAlk treatment displayed signature peaks at 1596 cm^{-1} and 1991 cm^{-1} which was absent in the cell lysates treated by glucosamine suggesting the alkyne group generation upon incubation of GlcNPhAlk with the cells (**Figure 2.21**).

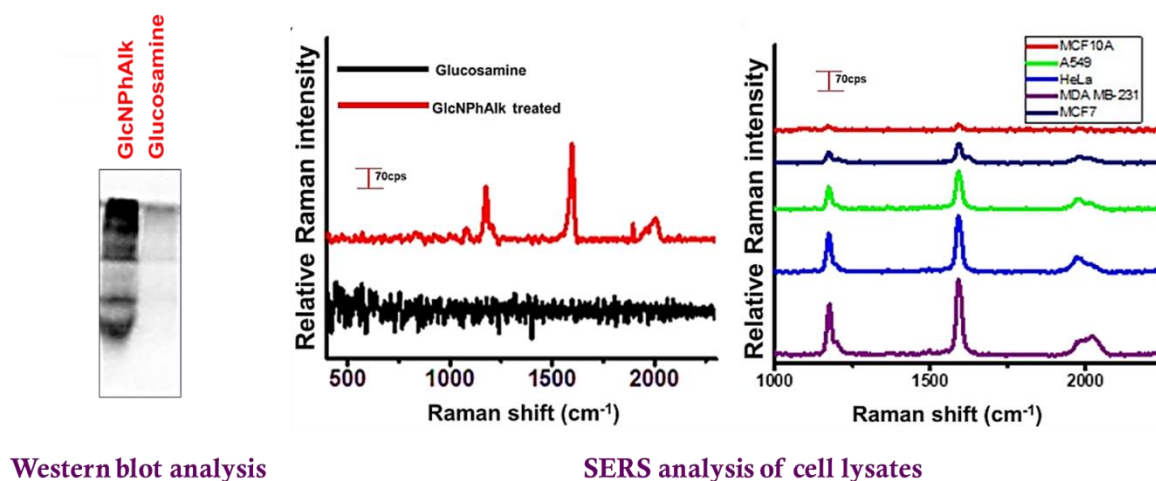


Figure 2.19: Western blotting and SERS analysis of cell lysates.

2.4.6. Metastatic potential and cell-surface glycosylation in cancer cells

Numerous glycosyltransferase enzymes have been reported as catalysts for glycosylation which is mostly located in the Golgi apparatus in cells. Besides, glycosylation plays a critical part in cancer progression and metastasis and epithelial-mesenchymal transition (EMT) in cancer cells.^[5,47–49] Metastatic transformation is attributed to the ability of cancer cells to grow into nearby normal tissue and then by moving through the walls of nearby lymph nodes or blood vessels finally invading the lymphatic system and spreading through the bloodstream to other parts of the body. As cancer malignancy is closely related to differential glycosylation in cells, semi-quantitation of this aberrant glycosylation in cancer cells is being performed for metastatic potential. Even though there have been previous attempts to imaging glycans using SERS techniques it was hugely hampered by the lack of specificity in cell surface mapping.^[15,16] The variation in the glycosylation within the cell surface is always associated with the metastatic potential of cell lines.^[12,14] Our major objective was to evaluate the glycosylation pattern in different cancer cells with varying metastatic capacities (**Figure 2.20**). For this, triple-negative breast cancer cells MDA-MB-231 with higher metastatic potential were compared to less metastatic breast carcinoma MCF-7 and the normal mammary epithelial cell line MCF-10A. Further, the experiment was extended to cervical

cancer cell line HeLa and non-small lung cancer cell line A549 based on their metastatic potential as verified in the literature reports.^[34–36]

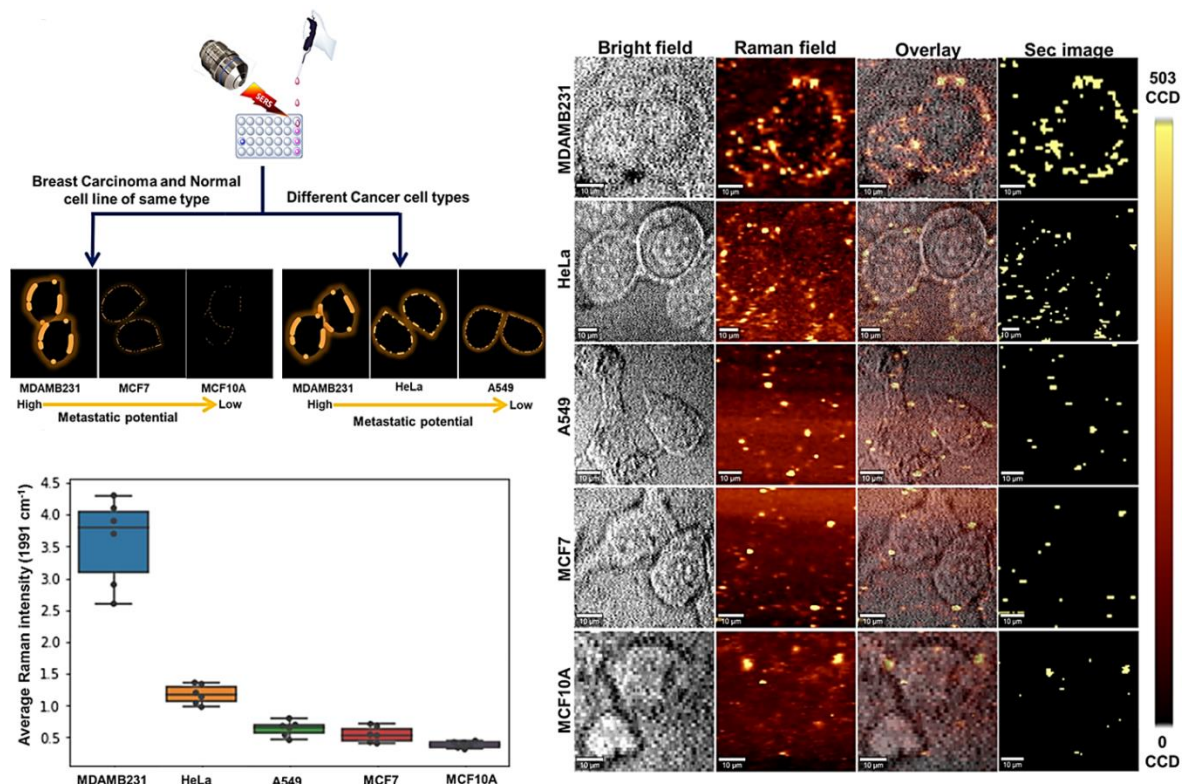


Figure 2.20: Schematic representation of MGL SERS technique employed upon variation of glycosylation in cells with respect to metastatic potential with representative images of variation of glycan expression in different cells MDA-MB-231, HeLa, A549, MCF-7 and MCF-10A respectively. (Average intensity of 1991 cm⁻¹ is displayed through boxplot with overlay points were also given)

The cells were subjected to metabolic labelling with GlcNPhAlk and investigated the glycosylation pattern in terms of alkyne-tagged sialic acid by SERS analysis as described earlier. From **Figure 2.20**, the extent of glycan labelling was found to be maximum for MDA-MB-231 while MCF-10A exhibited the minimum GlcNPhAlk incorporation. Labelling of glycans in other cells is in between MDA-MB-231 and MCF-10A in the order of MDA-MB-231 > HeLa > A549 > MCF-7 > MCF-10A. The same trend was also reflected in the average Raman peak intensity of GlcNPhAlk (1991 cm⁻¹) obtained from the image scan being expressed in the form of a boxplot (**Figure 2.20**). It demonstrates the comparative distribution of a continuous variable and jittered points indicate each measurement in a group. Secondary Raman images of five cells were constructed based on the peak intensity by applying a threshold number from the colour scale bars. Only signals above the assigned

threshold limit will appear as yellow spots, thus providing a much clear picture about the glycan expression in cell surface (**Figure 2.20**).

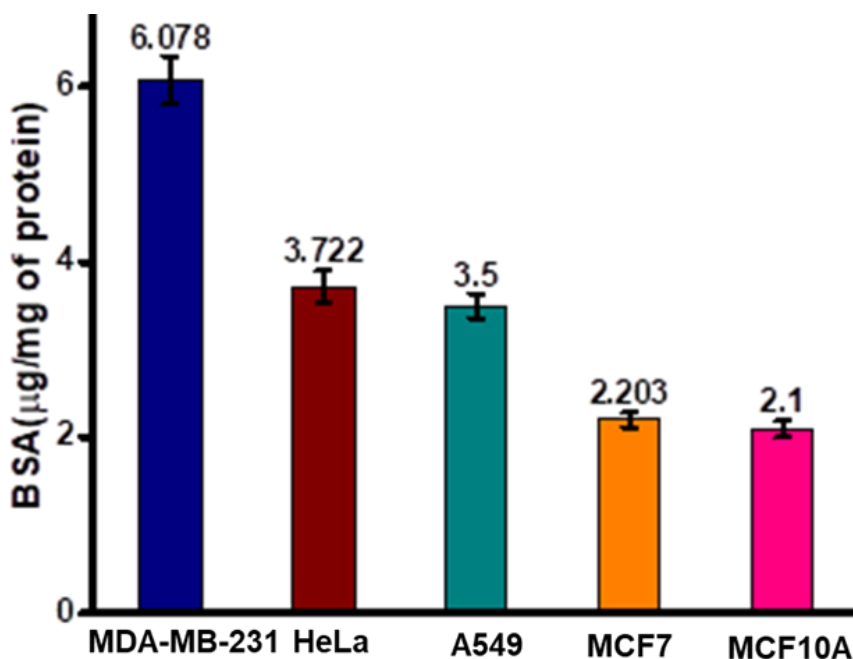


Figure 2.21: Sialic acid quantification by TBA method

Our results in **Figure 2.22** showed the direct correlation between glycan expression and metastasis which was further supported by the bound sialic acid estimation of the tested 5 cell lines using the thiobarbituric acid (TBA) method (**Figure 2.21**). Bound sialic acid expression in the cell lines is strongly correlated to the extent of glycan labelling revealed by SERS analysis (**Figure 2.20**). SERS intensities of cell lysates from these 5 cells also show the same trends (**Figure 2.20**). These data demonstrate the variance in glycosylation in cancer cells of different sources (MDA-MB-231, HeLa, A549) as well as breast normal and cancer cells of the same origin (MDA-MB-231, MCF-7, MCF-10A) (**Figure 2.20**). Hence, GlcNPhAlk is benchmarked as a highly sensitive glycan labelling probe that can be used to predict differential glycan expressions in various cell lines.

2.4.7. Glycosylation inhibition through SERS Assessment

The glycosylation inhibition effect through the SERS modality has been examined by using P-3Fax-Neu5Ac, a global sialyltransferase inhibitor, whose therapeutic potential has been well established in previous literature.^[50,51] There are several possible leaks to metabolic pathways as GlcNAc derivatives are not superior to bypass the NANS bottleneck and there are chances of converting to *O*-GlcNAc modified proteins which are mainly located in the nucleoplasmic region.

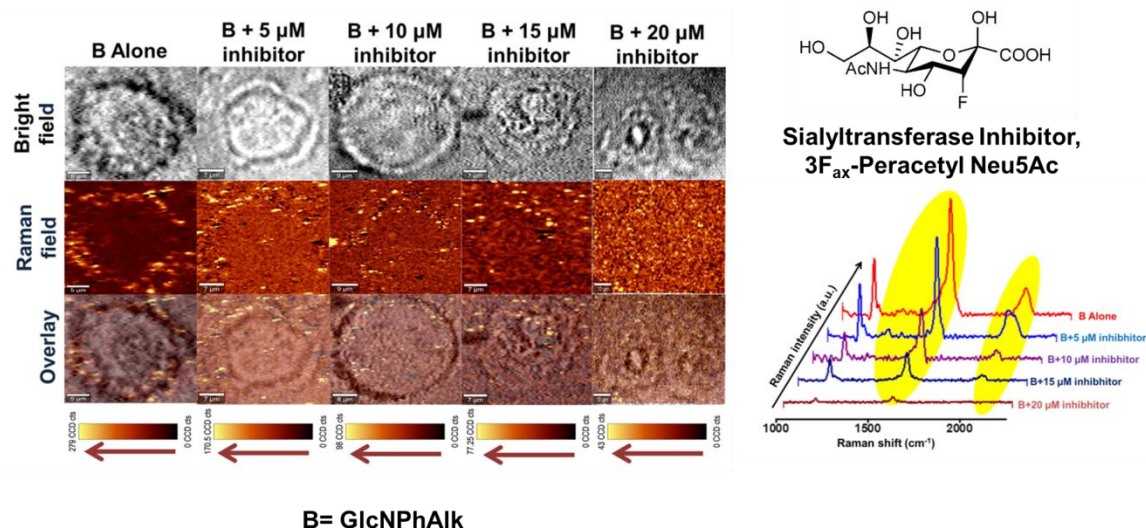


Figure 2.22: Inhibition studies of glycans using sialyltransferase inhibitor P-3F_{ax}-Neu5Ac on HeLa cells.

Since **Figure 2.21** clearly shows GlcNPhAlk labelling at the cell surface itself, therefore the involvement of *O*-GlcNAc transferase can be omitted.^[52,53] Sialyltransferase is the enzyme involved in the biosynthetic pathway of sialic acids where it activates the CMP sialic acid (Cytidine-5'-monophospho-*N*-acetylneuraminic acid) to glycosylate the proteins in the Golgi compartment. Hence P-3Fax-Neu5Ac must reduce the extent of sialylation if GlcNPhAlk is labelled through the sialic acid pathway. The inhibitor was added in different concentrations starting from 5 μM to 20 μM and incubated for 72 hours with the HeLa cells, along with GlcNPhAlk to verify the inhibition of glycosylation through SERS. The rate of inhibition was found to be directly proportional to the inhibitor concentration which not only proves the involvement of GlcNPhAlk through the sialic acid pathway but also confirms the efficiency of precise monitoring by SERS modality and it can be extended to the therapeutic applications for the glycan-based therapies against cancer (**Figure 2.22**).

2.5. Conclusion

In summary, the cell surface glycan labelling phenomenon has been demonstrated using a newly designed phenylalkynylated derivative of D-glucosamine, GlcNPhAlk as the metabolic precursor of sialic acid for glycan imaging. To the best of our knowledge, this is a pioneering study that emphasises metabolic glycan labelling capabilities of *N*-alkyl glucosamine through the SERS modality. This newly evolved sialic acid precursor strengthens the metabolic labelling chemistry since it is formed by the reductive amination reaction which was not

previously explored for MOE applications. A linear relationship of the cell surface glycan imbalance of different cancer cells concerning their metastatic potential was observed through SERS. A comparison of cancer cells with different metastatic potential from the same origin (MDA-MB-231, MCF-7, and MCF-10A) was also examined. The malignant breast carcinoma MDA-MB-231 cells with high metastatic potential reflected with highest Raman intensity in comparison to cervical carcinoma HeLa, lung adenocarcinoma A549 and breast carcinoma MCF-7 cells with relatively less metastatic capacity. The normal mammary epithelial cell line MCF10A registered the least glycan labelling when tagged with GlcNPhAlk. This metabolic labelling has been validated through fluorescent imaging as a complementary approach with the help of CuAAC and further confirmed its protein glycosylation by western blot analysis. Moreover, the inhibition of glycan biosynthesis in live cancer cells was proved through SERS using a global sialyl-transferase inhibitor, which validates the fact that the biosynthetic pathway of GlcNPhAlk is the same as that of sialic acid. Although selective tumour labelling *in vivo* is still a challenge, clinical translation of these strategies for cancer targeted therapies is highly anticipated. Finally, it is worth mentioning that SERS coupled with metabolic labelling strategy is a highly sensitive and effective imaging technique that can have translational application in both glycan-based cancer therapy and cancer immunotherapy.

2.6. Experimental section

2.6.1. Materials and methods

All chemicals and solvents were brought from Sigma Aldrich, Alfa Aesar, TCI and Merck and used without further purification. Global Sialyltransferase inhibitor P-3Fax-Neu5Ac was obtained from Calbiochem, Sigma Aldrich. ^1H NMR spectra were recorded on Bruker Advance 500 MHz NMR spectrometer, and chemical shifts are expressed in parts per million (ppm). Mass spectra were recorded under ESI/HRMS at 61800 resolution using Thermo scientific exactive, mass spectrometer. Absorption spectra were measured on a Shimadzu (UV-2450) UV-Vis. spectrophotometer, and the data analysis was performed using Microsoft excel and Origin 7. SERS measurements were carried out in a WITec Raman microscope (WITec Inc. Germany, alpha 300R) with a laser beam directed to the sample through 20x objective and a Peltier-cooled CCD detector. Samples were excited with a 633 nm excitation wavelength laser and stokes shifted Raman spectra were collected in the range of 400 to 4000 cm^{-1} with 1 cm^{-1} resolution. Prior to every measurement, a calibration with a silicon standard (Raman peak centered at 520 cm^{-1}) was performed. WITec Project plus (v 2.1) software

package was used for data evaluation. TEM measurements were performed (JEOL 2010) with an accelerating voltage of 200 KV. The sample was prepared by pipetting a drop of the aqueous solution of nanoparticles onto a 230 mesh copper grid coated with carbon and the sample was allowed to dry in air before the measurement.

2.6.2. Synthesis of gold nanoparticle

Gold nanoparticles were synthesised by the well-established citrate-reduction method (Turkevich Method).^[38] In short, 300 ml of deionised water was boiled at 100 °C with continuous stirring to which 300 µl of gold chloride solution (250 mM) in deionised water was added and allowed to stir for 10 minutes, after that 750 µl trisodium citrate solutions (100 mM) in deionized water was added and waited until the colour changes from yellow to black to purple. After this heating was stopped and allowed to cool to room temperature with continuous stirring. After 2 hours the solution was kept in refrigerator for further use.

2.6.3. Cellular studies

2.6.3.1. Cytotoxicity studies of alkynylated compounds

MDA-MB-231, HeLa, A549 and WI-38 cells were seed into 96 well plates and incubated for 24 hour (at 37 °C, 5% CO₂). Cells were then treated with varying concentrations of GlcNPhAlkTMS (**A**), GlcNPhAlk (**B**) and GlcNAlk (**C**) (20-200 µM). After 72 hour incubation, MTT (0.5 mg/ml) was added to each well and kept at 37 °C for 4 hours and finally the so formed formazan crystals were dissolved in DMSO and the OD was measured at 570 nm using a microplate reader.

2.6.3.2. Cell culture and metabolic labelling of cell surface glycans

Cells were cultured in Dulbecco's modified Eagle medium (DMEM) with 1% penicillin streptomycin (Gibco) and 10% fetal bovine serum (Gibco) with 5% CO₂ at 37 °C until they were confluent. The cells were then harvested by adding 0.25% EDTA trypsin of appropriate volume for 4 min, followed by the addition of DMEM of double that volume to neutralize the trypsin. The harvested cells were centrifuged at 1500 rpm for 3 min. The supernatant was removed and the cells were suspended with DMEM to achieve a cell concentration of 3000 cells/ml. The cell numbers were determined using a Petroff-Hausser cell counter. 100 µl of cell suspension was seeded per well in a sixteen well glass bottom chamber slide and allowed to grow for 24 hour. After the incubation, DMEM was removed from each well and the adhered cells were rinsed lightly with PBS, which was subsequently removed. Different

concentrations of GlcNPhAlk and GlcNPhAlk TMS were added to the wells from the stock solution of 50 mM of mentioned compounds in DMSO and left to incubate for 72 hours. The remaining wells were used as untreated control cells. Post-incubation washing was performed for all of the wells using HBSS buffer. All sixteen wells were washed thrice HBSS to remove excess compounds and unbound cells, and then leaving the cells ready for SERS sample preparation.^[24,51] Same procedure was repeated with the inhibition study and along with 100 μ M GlcNPhAlk different concentrations of sialyltransferase inhibitor (5 μ M to 20 μ M) was added and incubated for 3 days. SERS analysis was done after 3 washes with HBSS.^[30,50]

2.6.3.3. Thiobarbituric acid (TBA) method for sialic acid quantification

Protein concentration in cell lysates were determined by BCA protein assay kit (Thermo Pierce) according to the manufacturer's instruction and normalized to 1 mg/ml for each sample. Bound sialic acid (BSA) determination was quantified using TBA method. It was performed as follows: 100 μ l of pure standard sialic acid sample (2-10 μ g/well) and cell lysates were added to the 1.5 ml vials. Then, 100 μ l of 0.2 N H₂SO₄ (prepared from stock 36 N) was added to each vial and hydrolysed for 1 hour at 80 °C and cooled the vials at 20 °C for 20 min. Added 20 μ l of periodate reagent (prepared form stock of 0.2 M NaIO₄ in 9 M H₃PO₄). It was shaken and incubated for 20 min at 20 °C and added 100 μ l of arsenite reagent (10% NaAsO₂ with 0.1 N H₂SO₄ with 0.5 M Na₂SO₄). It is then shaken vigorously until the yellow brownish colour appears and disappears entirely. 250 μ l of TBA reagent added and heated in boiling water bath for 15 min. Vials then cooled to 20 °C and added 1 ml of cyclohexanone and centrifuged it for 7 min at 900 g. As the organic phase gets separated its OD is collected at 549 nm immediately by a microtiter plate reader (Biotek, USA).^[54]

2.6.3.4. Western blotting

MDA-MB-231 cells were seeded onto T-75 flasks at a density of 2 x 10⁶ cells per flask in 10 ml of media with or without GlcNPhAlk (100 μ M). After incubation for three days, the cells were washed twice with PBS (pH 7.4) and harvested with a cell scraper at 4 °C. They were pelleted by centrifugation at 1500 rpm for 5 min, and the cell pellets were re-suspended in 450 μ l of lysis buffer (Thermo) + Protease inhibitor cocktail (Sigma Aldrich, USA) incubation at 4 °C for 30 min with intermittent vortexing followed by repeated freeze thaw cycles of 5 min each for 5 times. After 1 min bath sonication at 4 °C, insoluble debris was removed by centrifugation for 20 min at 12000 rpm. Final supernatant concentrations were adjusted by bicinchoninic acid (BCA) protein assay (Pierce, USA) to be 1 mg/ml. Then, 20 μ l

of the lysate was incubated with azide-PEG3-biotin (2 μ l, 5 mM in PBS) for 1 hour at 37 °C along with CuSO₄ (1 mM, 1 μ l) and ascorbic acid (5mM, 1 μ l). Loading buffer was added to each sample, and samples were resolved on 10% SDS-PAGE gel after heating at 95 °C. Proteins were transferred to PVDF transfer membrane (Merck-Millipore), and the membrane was blocked with 5% bovine serum albumin (BSA) in PBST (0.1% Tween 20, pH 7.4) for 1 hour. Then, the membrane was incubated with streptavidin-HRP (diluted 1:1000 in PBST) (Sigma Aldrich, USA) overnight at 4 °C. The membrane was rinsed three times with PBST and developed by using ECL western blotting substrate (Takara, USA).^[55]

2.6.3.5. Live cell imaging

2.6.3.5.1. SERS evaluation of molecules and metabolic labelling

Cells were subjected to SERS spectral mapping mode of the confocal Raman microscope (alpha300R, WITec Inc. Germany). Spectrum at every pixel was taken (Scan rang 60 μ m X 60 μ m, 150 X 150 pixel) was taken by 20X objective. Sample was excited with a power of 10 mW from 633 nm laser and mapping was done using 600 g/mm grating is an integration time of 0.022 s using 1991 and 1580 cm^{-1} peak and the intensity modulated images were prepared by image processing option in control four software.

2.6.3.5.2. Comparative analysis method of Raman intensity of tags

Methanol solutions of 1mM the test compound (1 μ l of each) and internal standard (normally 1 M stock solution of 4-cyanobenzaldehyde (CB) were mixed on in a vial, to that added AuNP of 2.8×10^{10} particles/ml concentration of 18 μ l was added and mixed thoroughly and took Raman spectrum of the mixture quickly by using a Raman microscope. Finally, RIC (relative Raman intensity vs CB) was calculated from the intensity ratio and concentrations of the sample and standard. Since CB gives an intensive Raman peak (2230 cm^{-1}) at a different wavenumber from samples (around 2000 cm^{-1}), it can be used as an internal standard.^[29]

2.6.3.5.3. Generation of secondary images from Raman field images using commands

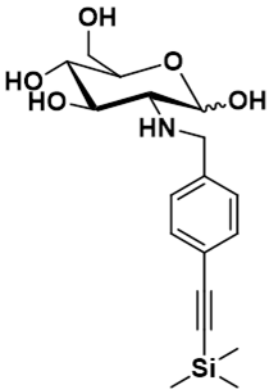
Secondary images from the Raman field images were able to be generated using the "calculator" command with the Project 4.1 software provided by WITec Inc., Germany. Here in secondary images as well as levelled colour scale bars of 5 cell lines are given. The half value of the maxima of the scale bar has been taken in all 3 cases (i.e., for MDA-MB-231, the value is 251, for HeLa, the value is 142, for A549, the value is 69, for MCF-7, the value is

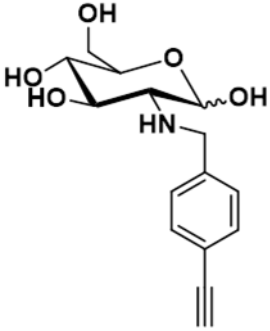
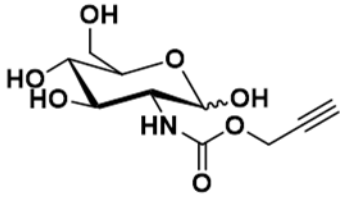
37.125, and for MCF10A, the value is 24.75. Using the command “Result = x1>value” secondary images were created.

2.6.3.5.4. Fluorescence microscopy and imaging

MDA-MB-231 cells were seeded to the 96 well plates (1000 cells/well) and maintained for 12 hour with 100 μ l DMEM (5%). From the stock solution of glycan tag; 50 μ M stock solution is made and added to the 96 well plates (100 μ l) and incubated for 24 hours (10% DMEM). Culture media (100 μ l) is replaced with fresh solution of glycan tag (100 μ l) and again incubated for 48 hour (10% DMEM). Media is removed (200 μ l), cells were washed with PBS for 3 times. Cells were maintained in serum-free media (100 μ l) for 4 hours. Freshly prepared fluorophore (30 μ M) in 5% DMEM is added (100 μ l) to each well followed by the addition of 7.5 μ l of 20 mM of CuSO₄ and 7.5 μ l of 100 mM of sodium ascorbate. After 45-60 min of incubation, cells were washed with PBS and took the images with or without counterstain with Hoechst and observed under an inverted fluorescent microscope (Olympus 1 \times 51, Singapore).^[24]

2.7. Spectral data

<p>Compound 1: GlcNPhAlkTMS</p> 	<p>Molecular formula: C₁₈H₂₇NO₅Si</p> <p>¹H NMR (500 MHz; CD₃OD): δ 7.28 (d, 2H, <i>J</i> = 8 Hz), 7.23 (d, 2H, <i>J</i> = 8 Hz), 4.49 (d, 2H, <i>J</i> = 7.5 Hz), 3.97 (m, 2H), 3.93 (m, 2H), 3.69 (m, 2H), 3.47 (d, 2H, <i>J</i> = 7.5 Hz), 0.12 (s, 9H) ppm</p> <p>¹³C NMR (125 MHz, CD₃OD): δ 139.9, 132.1, 127.5, 122.0, 90.3, 86, 76.7, 71.9, 70.6, 63.5, 61.2, 55.9, 1.4 ppm</p> <p>HR-ESIMS: 365.1744 (M+H)⁺</p>
<p>Compound 2: GlcNPhAlk</p>	<p>Molecular formula: C₁₅H₁₈NO₅</p> <p>¹H NMR (500 MHz, CD₃OD): δ 7.28 (d, 2H, <i>J</i> = 8 Hz), 7.23 (d, 2H, <i>J</i> = 8 Hz), 4.49 (d, 2H, <i>J</i> = 7.5 Hz), 3.97 (m, 2H), 3.93 (m, 2H), 3.69 (m, 2H), 3.47 (d, 2H, <i>J</i> = 7.5 Hz), 2.68 (s, 1H) ppm.</p> <p>¹³C NMR (125 MHz, CD₃OD): δ 139.9, 132.1,</p>

	<p>127.5, 122.0, 90.3, 86.0, 76.7, 71.9, 70.6, 63.5, 61.2, 55.9 ppm.</p> <p>HR-ESIMS: 294.13425 (M+H)⁺</p>
<p>Compound 3: GlcNAk</p> 	<p>Molecular formula: C₁₀H₁₅NO₇</p> <p>¹H NMR (500 MHz, CD₃OD): δ 5.03 (d, 1H, <i>J</i> = 8 Hz), 4.57 (d, 2H, <i>J</i> = 8.5 Hz), 3.70 (d, 2H, <i>J</i> = 11.5 Hz), 3.59 (m, 1H), 3.46 (d, 1H, <i>J</i> = 10 Hz), 3.27 (t, 2H, <i>J</i> = 8.5 Hz), 2.77 (s, 2H) ppm.</p> <p>¹³C NMR (125 MHz, CD₃OD): 155.6, 97.0, 86.0, 78.1, 76.7, 71.9, 70.6, 63.5, 61.2, 55.9 ppm.</p> <p>HR-ESIMS: 284.07513 (M+Na)⁺</p>

2.8. References

- [1] K. Ohtsubo, S. Takamatsu, M. T. Minowa, A. Yoshida, M. Takeuchi, J. D. Marth, *Cell* **2005**, *123*, 1307.
- [2] S. Cha, B. Ortega, H. Kurosu, K. P. Rosenblatt, M. Kuro-o, C. Huang, *Proc. Natl. Acad. Sci.* **2008**, *105*, 9805.
- [3] X. Song, B. Xia, S. R. Stowell, Y. Lasanajak, D. F. Smith, R. D. Cummings, *Chem. Biol.* **2009**, *16*, 36.
- [4] E. A. Halabi, D. Pinotsi, P. Rivera-fuentes, *Nat. Commun.* **2019**, *10*, 1.
- [5] Y. Liang, X. Jiang, R. Yuan, Y. Zhou, C. Ji, L. Yang, H. Chen, Q. Wang, *Anal. Chem.* **2016**, *89*, 538.
- [6] B. L. Fang Hu, Youyong Yuan, Wenbo Wu, Duo Mao, *Anal. Chem.* **2018**, *90*, 6718.

- [7] Hua Wang, R. Wang, J. Y. , Kaimin Cai, Hua He, Yang Liu, Z. Wang, X. Z. Ming Xu, Yiwen sun, I. t dobrucki , Qian Yin, Li tang, L. W. Dobrucki, eric J. Chaney, stephen a Boppart, timothy M. Fan, S. Lezmi, X. Chen, L. Yin2, J. Cheng, *Nat. Chem. Biol.* **2017**, *103*, 12371.
- [8] L. Wei, F. Hu, Y. Shen, Z. Chen, Y. Yu, C. Lin, M. C. Wang, W. Min, *Nat. Methods* **2014**, *11*, 410.
- [9] R. W. Liang Lin, Xiangdong Tian, Senlian Hong, Peng Dai, Qiancheng You, and X. C. Lianshun Feng, Can Xie, Zhong-Qun Tian, *Angew. Chemie - Int. Ed.* **2013**, *52*, 7266.
- [10] Y. Chen, L. Ding, W. Song, H. Ju, *Chem. Sci.* **2016**, *7*, 569.
- [11] F. M. Tuccillo, A. De Laurentiis, C. Palmieri, G. Fiume, P. Bonelli, A. Borrelli, P. Tassone, I. Scala, F. M. Buonaguro, I. Quinto, G. Scala, *Biomed Res. Int.* **2014**, *2014*.
- [12] D. H. Dube, C. R. Bertozzi, *Nat. Rev. Drug Discov.* **2005**, *4*, 477.
- [13] M. Granovsky, J. Fata, J. Pawling, W. J. Muller, R. Khokha, J. W. Dennis, *Nat. Med.* **2000**, *6*, 306.
- [14] A. Matsumoto, H. Cabral, N. Sato, K. Kataoka, Y. Miyahara, *Angew. Chemie - Int. Ed.* **2010**, *49*, 5494.
- [15] D. Craig, S. Mcaughtrie, J. Simpson, C. Mccraw, K. Faulds, D. Graham, *Anal. Chem.* **2014**, *86*, 4775.
- [16] M. Tabatabaei, G. Q. Wallace, F. A. Caetano, E. R. Gillies, S. S. G. Ferguson, F. Laguné-Labarthe, *Chem. Sci.* **2016**, *7*, 575.
- [17] C. L. Jacobs, S. Goon, K. J. Yarema, S. Hinderlich, H. C. Hang, D. H. Chai, C. R. Bertozzi, *Biochemistry* **2001**, *40*, 12864.
- [18] H. Möller, V. Böhrsch, J. Bentrop, J. Bender, S. Hinderlich, C. P. R. Hackenberger, *Angew. Chemie - Int. Ed.* **2012**, *51*, 5986.
- [19] N. J. Agard, J. A. Prescher, C. R. Bertozzi, *J. Am. Chem. Soc.* **2004**, *126*, 15046.
- [20] C. R. B. Lara K. Mahal, Kevin J. Yarema, **1997**, *276*, 1125.
- [21] E. Saxon, C. R. Bertozzi, *Science (80-.)*. **2000**, *287*, 2007.

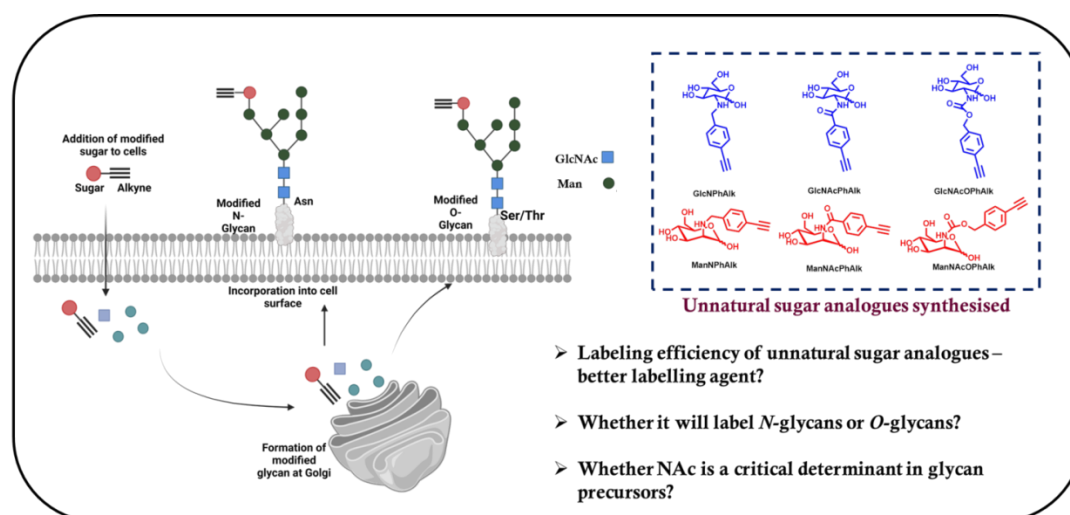
- [22] R. Zeitler, A. Giannis, S. Danneschewski, E. Henk, T. Henk, C. Bauer, *Eur. J. Biochem.* **1992**, *204*, 1165.
- [23] P. R. Wratil, R. Horstkorte, W. Reutter, *Angew. Chemie - Int. Ed.* **2016**, *55*, 9482.
- [24] S. T. Laughlin, C. R. Bertozzi, *Proc. Natl. Acad. Sci. U. S. A.* **2009**, *106*, 12.
- [25] P. V. Chang, X. Chen, C. Smyrniotis, A. Xenakis, T. Hu, C. R. Bertozzi, P. Wu, *Angew. Chemie - Int. Ed.* **2009**, *48*, 4030.
- [26] J. Vanbeselaere, D. Vicogne, G. Matthijs, C. Biot, F. Foulquier, Y. Guerardel, *Chem. Commun.* **2013**, *49*, 11293.
- [27] B. W. Zaro, Y. Y. Yang, H. C. Hang, M. R. Pratt, *Proc. Natl. Acad. Sci. U. S. A.* **2011**, *108*, 8146.
- [28] Y. Kizuka, S. Funayama, H. Shogomori, M. Nakano, K. Nakajima, R. Oka, S. Kitazume, Y. Yamaguchi, M. Sano, H. Korekane, T. L. Hsu, H. Y. Lee, C. H. Wong, N. Taniguchi, *Cell Chem. Biol.* **2016**, *23*, 782.
- [29] H. Yamakoshi, K. Dodo, A. Palonpon, J. Ando, K. Fujita, S. Kawata, M. Sodeoka, *J. Am. Chem. Soc.* **2012**, *134*, 20681.
- [30] R. Xie, S. Hong, L. Feng, J. Rong, X. Chen, *J. Am. Chem. Soc.* **2012**, *134*, 9914.
- [31] D. B. Agus, J. F. Alexander, W. Arap, S. Ashili, J. E. Aslan, R. H. Austin, V. Backman, K. J. Bethel, R. Bonneau, W. C. Chen, C. Chen-Tanyolac, N. C. Choi, S. A. Curley, M. Dallas, D. Damania, P. C. W. Davies, P. Decuzzi, L. Dickinson, L. Estevez-Salmeron, V. Estrella, M. Ferrari, C. Fischbach, J. Foo, S. I. Fraley, C. Frantz, A. Fuhrmann, P. Gascard, R. A. Gatenby, Y. Geng, S. Gerecht, R. J. Gillies, B. Godin, W. M. Grady, A. Greenfield, C. Hemphill, B. L. Hempstead, A. Hielscher, W. D. Hillis, E. C. Holland, A. Ibrahim-Hashim, T. Jacks, R. H. Johnson, A. Joo, J. E. Katz, L. Kelbauskas, C. Kesselman, M. R. King, K. Konstantopoulos, C. M. Kraning-Rush, P. Kuhn, K. Kung, B. Kwee, J. N. Lakins, G. Lambert, D. Liao, J. D. Licht, J. T. Liphardt, L. Liu, M. C. Lloyd, A. Lyubimova, P. Mallick, J. Marko, O. J. T. McCarty, D. R. Meldrum, F. Michor, S. M. Mumenthaler, V. Nandakumar, T. V. O'Halloran, S. Oh, R. Pasqualini, M. J. Paszek, K. G. Philips, C. S. Poultney, K. Rana, C. A. Reinhart-King, R. Ros, G. L. Semenza, P. Senechal, M. L. Shuler, S. Srinivasan, J. R. Staunton, Y. Stypula, H. Subramanian, T. D. Tlsty, G. W. Tormoen, Y. Tseng, A. Van

- Oudenaarden, S. S. Verbridge, J. C. Wan, V. M. Weaver, J. Widom, C. Will, D. Wirtz, J. Wojtkowiak, P. H. Wu, *Sci. Rep.* **2013**, *3*, 1449.
- [32] Y. L. Liu, C. K. Chou, M. Kim, R. Vasisht, Y. A. Kuo, P. Ang, C. Liu, E. P. Perillo, Y. A. Chen, K. Blocher, H. Horng, Y. I. Chen, D. T. Nguyen, T. E. Yankeelov, M. C. Hung, A. K. Dunn, H. C. Yeh, *Sci. Rep.* **2019**, *9*, 1.
- [33] C. C. Palsuledesai, J. D. Ochocki, M. M. Kuhns, Y. C. Wang, J. K. Warmka, D. S. Chernick, E. V. Wattenberg, L. Li, E. A. Arriaga, M. D. Distefano, *ACS Chem. Biol.* **2016**, *11*, 2820.
- [34] K. Liu, P. A. Newbury, B. S. Glicksberg, W. Z. D. Zeng, S. Paithankar, E. R. Andrechek, B. Chen, *Nat. Commun.* **2019**, *10*.
- [35] D. K. Mishra, R. A. Miller, K. A. Pence, M. P. Kim, *BMC Cancer* **2018**, *18*, 1.
- [36] Y. F. Tu, B. A. Kaiparettu, Y. Ma, L. J. C. Wong, *Biochim. Biophys. Acta - Bioenerg.* **2011**, *1807*, 1125.
- [37] W. Qin, K. Qin, X. Fan, L. Peng, W. Hong, Y. Zhu, P. Lv, Y. Du, R. Huang, M. Han, B. Cheng, Y. Liu, W. Zhou, C. Wang, X. Chen, *Angew. Chemie - Int. Ed.* **2018**, *57*, 1817.
- [38] P. C. S. A. J. H. JOHN TURKEVICH, *Discuss. Faraday Soc.* **1951**, *11*, 55.
- [39] c Y. R. and David C. Kennedy, a Craig S. McKay, ab Li-lin Tay, J. P. Pezacki, *ChemComm* **2011**, *47*, 3156.
- [40] M. Li, J. Wu, M. Ma, Z. Feng, Z. Mi, P. Rong, D. Liu, *Nanotheranostics* **2019**, *3*, 113.
- [41] Z. M. M. Ž. ć Snežzana Miljanić, Leo Frkanec, Tomislav Biljan, *J. Raman Spectrosc.* **2007**, *38*, 1538.
- [42] L. Carroll, T. H. Witney, E. O. Aboagye, *Med Chem. Commun* **2013**, *4*, 653.
- [43] J. M. Baskin, J. A. Prescher, S. T. Laughlin, N. J. Agard, P. V. Chang, I. A. Miller, A. Lo, J. A. Codelli, C. R. Bertozzi, *Proc. Natl. Acad. Sci. U. S. A.* **2007**, *104*, 16793.
- [44] T. L. Hsu, S. R. Hanson, K. Kishikawa, S. K. Wang, M. Sawa, C. H. Wong, *Proc. Natl. Acad. Sci. U. S. A.* **2007**, *104*, 2614.
- [45] D. Rabuka, S. C. Hubbard, S. T. Laughlin, S. P. Argade, C. R. Bertozzi, *J. Am. Chem.*

- Soc.* **2006**, *128*, 12078.
- [46] M. Sawa, T. Hsu, T. Itoh, M. Sugiyama, S. R. Hanson, P. K. Vogt, C. Wong, **2006**, *103*, 12371.
- [47] N. Taniguchi, Y. Kizuka, *Glycans and cancer: Role of N-Glycans in cancer biomarker, progression and metastasis, and therapeutics*, 1st ed., Vol. 126, Elsevier Inc., **2015**.
- [48] R. A. W. J. Raghu Kalluri, *Phys. Plasmas* **2010**, *To be subm*, 1420.
- [49] C. Y. Chen, Y. H. Jan, Y. H. Juan, C. J. Yang, M. S. Huang, C. J. Yu, P. C. Yang, M. Hsiao, T. L. Hsu, C. H. Wong, *Proc. Natl. Acad. Sci. U. S. A.* **2013**, *110*, 630.
- [50] C. Büll, T. J. Boltje, E. A. W. Van Dinther, T. Peters, A. M. A. De Graaf, J. H. W. Leusen, M. Kreutz, C. G. Figdor, M. H. Den Brok, G. J. Adema, *ACS Nano* **2015**, *9*, 733.
- [51] C. D. Rillahan, A. Antonopoulos, C. T. Lefort, R. Sonon, K. Ley, A. Dell, S. M. Haslam, J. C. Paulson, *Nat. Chem. Biol.* **2013**, *8*, 661.
- [52] S. R. Stowell, T. Ju, R. D. Cummings, *Annu. Rev. Pathol. Mech. Dis.* **2015**, *10*, 473.
- [53] J. Du, M. A. Meledeo, Z. Wang, H. S. Khanna, V. D. P. Paruchuri, K. J. Yarema, *Glycobiology* **2009**, *19*, 1382.
- [54] D. Surangkul, P. Pothacharoen, P. Kongtaweelert, *เข็ญงใหม □ เวชสาร* **2013**, *40*, 111.
- [55] S. Lee, H. Koo, J. H. Na, S. J. Han, H. S. Min, S. J. Lee, S. H. Kim, S. H. Yun, S. Y. Jeong, I. C. Kwon, K. Choi, K. Kim, *ACS Nano* **2014**, *8*, 2048.

CHAPTER 3

Investigation into the substrate promiscuity of hexosamine biosynthetic enzymes using unnatural sugar derivatives



3.1. Abstract

Unnatural forms of sialic acid can be introduced to mammalian cell surfaces by the metabolic transformation of unnatural derivatives of *N*-acetylhexosamine (ManNAc, GlcNAc). Previous studies have shown that mannosamine analogues with *N*-acyl groups that are uncomplicated, containing up to five carbon atoms long, can be recognised by the biosynthetic machinery and converted into sialoglycoconjugates on the cell surface. It has been reported that the *N*-alkyl glucosamine derivative (GlcNPhAlk) can also modify cell surface glycans. These structural changes to cell surface glycans can be used to investigate carbohydrate-dependent phenomena. In this study, it is aimed to explore the tolerance levels of the hexosamine biosynthetic pathway for structural alterations of the *N*-acyl, *N*-alkyl, and *N*-acyloxy substituents of mannosamine and glucosamine. A series of analogues has been synthesized with *N*-acyl, *N*-alkyl, and *N*-acyloxy groups of hexosamines (GlcNPhAlk, ManNPhAlk, GlcNAcPhAlk, ManNAcPhAlk, GlcNAcOPhAlk, and ManNAcOPhAlk), and examined their metabolic conversion to cell surface glycans using the MGL-SERS (metabolic glycan labelling coupled surface-enhanced Raman scattering) technique. The findings revealed that ManNAcPhAlk had the maximum labelling efficiency followed by ManNPhAlk and

GlcNPhAlk, while GlcNAcOPhAlk, ManNAcOPhAlk, and GlcNAcPhAlk are less efficiently metabolised by the biosynthetic machinery. This finding is further validated through far-western blot analysis using azide-PEG3-biotin, which consistently yielded the same results. Inhibitor studies using *N*-glycan and *O*-glycan inhibitors with MGL-SERS techniques revealed that all these analogues are mostly labelling *N*-glycans which was further substantiated by the same far-western blot analysis.

3.2. Introduction

Glycans have a significant impact on a variety of biological functions, particularly in cell-cell interactions and the interactions between cells and pathogens. These activities are largely dependent on the terminal monosaccharide components of glycoconjugates. In vertebrates, glycans commonly feature sialic acid, L-fucose (Fuc), or D-galactose (Gal) units at their nonreducing terminal and branching sites.^[1-3] Altering the structure of glycans has a significant impact on their biological characteristics. Structural changes in glycans can be achieved through enzyme inhibition, enzymatic treatment, and genetic alterations. Metabolic glycoengineering (MGE), also referred to as metabolic oligosaccharide engineering (MOE), has the potential to influence glycan structure both *in-vitro* and *in vivo*.^[4,5] Unnatural monosaccharides are introduced into cells or organisms, where they undergo metabolism and are transformed into glycoconjugates. Therefore, the enzymes involved in the biosynthetic pathway must be promiscuous, allowing them to accommodate changes in their substrates.

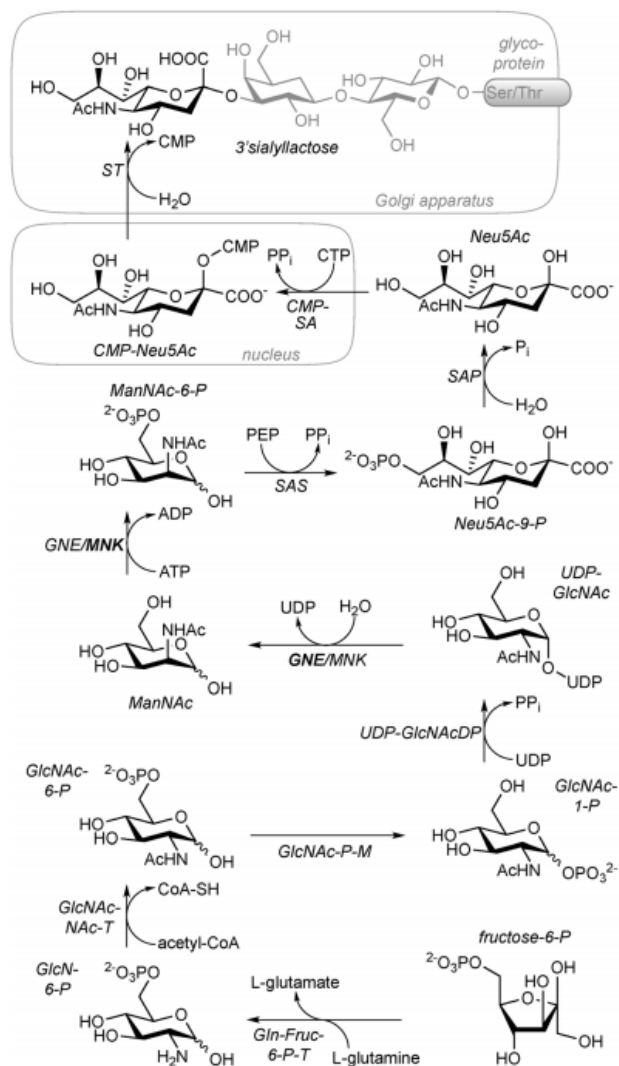
N-glycans and *O*-glycans are two major types of glycosylations found in proteins, each with distinct structures, functions, and cellular locations. *N*-glycans are connected to the nitrogen atom of the side chain amide of asparagine residues within the consensus sequence Asn-X-Ser/Thr (where X is any amino acid except proline, Asn-asparagine Ser-serine and Thr-threonine). They have a common pentasaccharide core consisting of two *N*-acetylglucosamine (GlcNAc) and three mannose residues, which can be further extended to form high-mannose, complex, and hybrid structures. Functionally, *N*-glycans are crucial for protein folding and stability within the endoplasmic reticulum (ER), participate in quality control mechanisms, and are involved in cell-cell adhesion, immune responses, and recognition processes. Their synthesis and processing occur in the ER and Golgi apparatus, and they are typically found on cell surfaces and in secreted glycoproteins.^[6]

In contrast, *O*-glycans are directed towards the oxygen atom within the hydroxyl groups of Ser/Thr residues, initiated by the addition of *N*-acetylgalactosamine (GalNAc). *O*-glycans

exhibit greater structural diversity than *N*-glycans, with various possible core structures and branching patterns. They are abundant in mucins, which form protective mucous barriers on epithelial surfaces, and play significant roles in cell signalling, communication, and immune responses. The addition of *O*-glycans primarily occurs in the Golgi apparatus, and they are commonly found on cell surface glycoproteins and secreted proteins, particularly on mucosal surfaces.^[7]

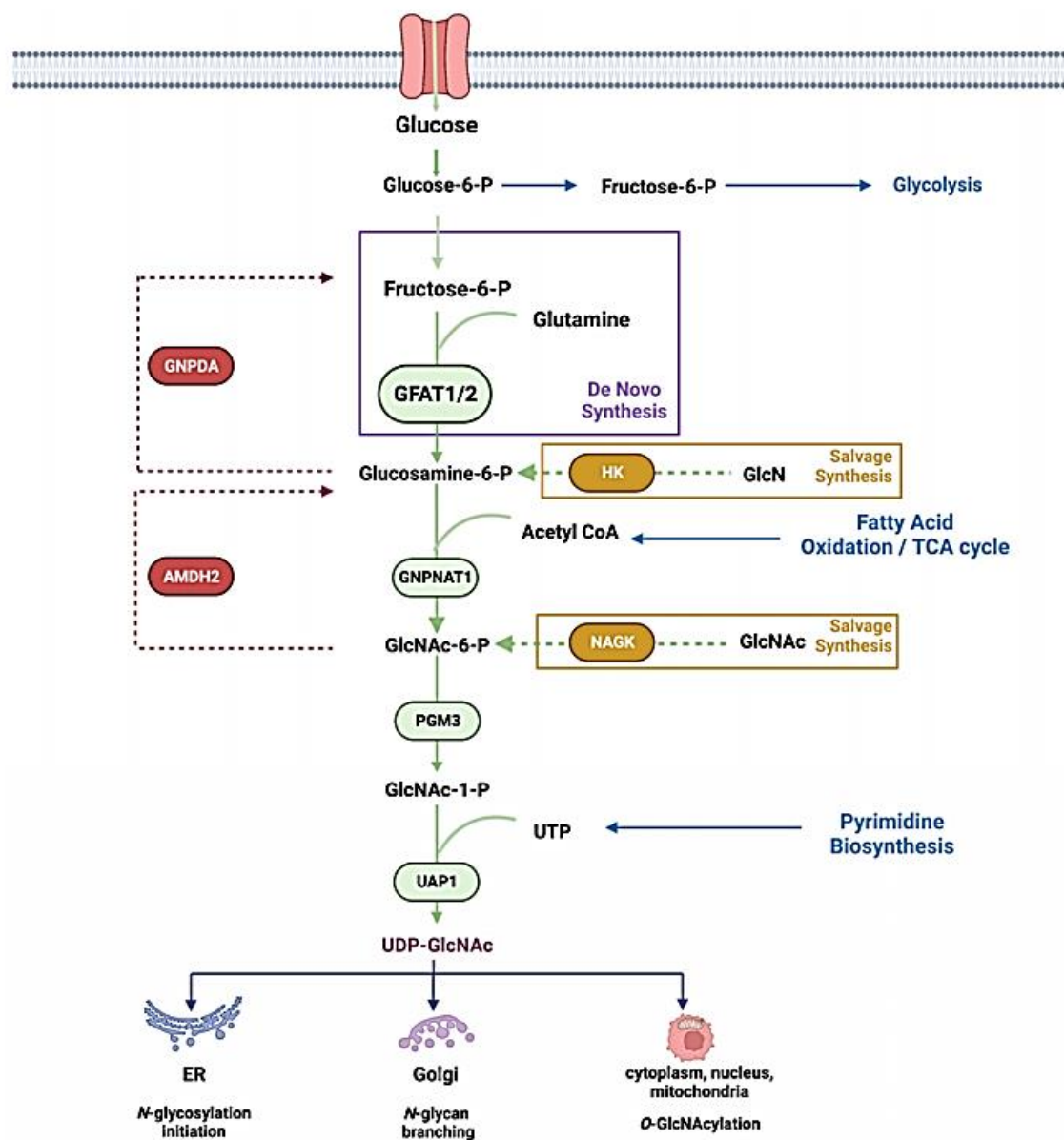
The Roseman-Warren pathway, initially utilized for the de novo synthesis of *N*-acetylneuraminic acid (Neu5Ac), begins with *D*-*N*-acetylmannosamine (ManNAc) as the precursor molecule. The enzymes in the Roseman-Warren pathway demonstrate flexibility by adjusting to alterations in the *N*-acyl side chains of their substrates. Introducing a mannosamine derivative with a modified *N*-acyl side chain to cells results in its conversion into an unnatural sialic acid, that is then displayed on the cell surface. In the past two decades, more than 20 artificial mannosamines have been developed as suitable materials for MGE. ManNAc analogues can be categorized into two types: aliphatic and bioorthogonal. Aliphatic analogues involve extending the *N*-acyl function with one or more methylene groups. MGE using aliphatic ManNAc analogues leads to the development of new biological properties and influences cell function in various ways. Conversely, bioorthogonal analogues modify the *N*-acyl side chain, which is not present in living systems but can be utilised in chemical processes. The reactive groups in bioorthogonal analogues can be utilised for labelling sialylated glycans with a fluorescent dye. MGE has been effectively applied to various monosaccharides, such as *D*-*N*-acetyl-galactosamine (GalNAc), *D*-*N*-acetylglucosamine (GlcNAc), 3-deoxy-*D*-manno-oct-2-ulosonic acid (KDO), and the sugar alcohol myo-inositol.^[8-19]

Fructose-6-phosphate (fructose-6-P) undergoes a conversion of approximately 2-5% from glycolysis to amino sugars as depicted in **scheme 3.1**.^[20] Through the catalysis of fructose-6-P amidotransferase (Gln-Fruc-6-P-T), glucosamine-6-P (GlcN-6-P) is aminated, leading to the formation of *N*-acetylglucosamine (GlcNAc) with acetyl-CoA serving as a cofactor. GlcNAc is obtained from endogenous glycoconjugates and nutrient digestion. Subsequently, it is phosphorylated to form GlcNAc-6-P and transformed into UDP-*N*-acetylglucosamine (UDP-GlcNAc), a key metabolite in the Roseman-Warren biosynthesis pathway.^[21-26]



Scheme 3.1: De novo biosynthesis of N-acetylneuraminic acid (Adapted from Angew. Chem. Int. Ed. 2016, 55, 2 – 33).

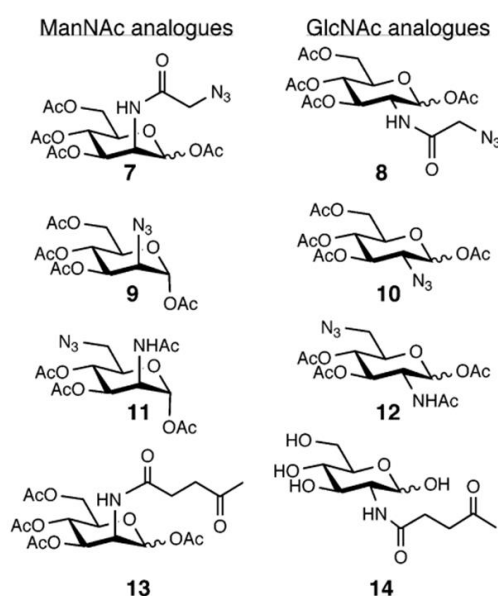
UDP-GlcNAc 2-epimerase/ManNAc-kinase (GNE/MNK) plays a pivotal role in the de novo synthesis of Neu5Ac.^[27–29] The enzyme orchestrates the biotransformation of UDP-GlcNAc through a two-step catalytic process, initially involving the 2-epimerization of UDP-GlcNAc to yield *N*-acetylmannosamine (ManNAc), followed by the subsequent phosphorylation of ManNAc to ManNAc-6-P. Notably, the process intermediates 2-acetamidoglucal, which results from an UDP anti elimination reaction.^[30]



Scheme 3.2: Hexosamine biosynthetic pathway depicting the formation of *N*-glycans and *O*-glycans from UDP-GlcNAc. (Adapted from Genes 2023, 14, 933.)

The hexosamine biosynthetic pathway (HBP) is a metabolic pathway that converts glucose into UDP-*N*-acetylglucosamine (UDP-GlcNAc), which is a crucial substrate for glycosylation processes, including the synthesis of glycoproteins and glycolipids [Scheme 3.2].^[31] The Roseman-Warren pathway produces sialic acids, such as Neu5Ac, while the hexosamine biosynthetic pathway generates UDP-GlcNAc. Despite being distinct, these pathways are interconnected within cellular metabolism. For example, intermediates from the hexosamine pathway can feed into the Roseman-Warren pathway. Specifically, UDP-GlcNAc produced

in the hexosamine pathway can be converted to ManNAc, an intermediate in the Roseman-Warren pathway. These biosynthetic pathways have been found to exhibit tolerance for non-natural substrates, making it an attractive option for engineering the metabolic cell surface. This method involves exposing cells or live animals to a synthetic monosaccharide that mimics to a natural precursor in the cell-surface glycan biosynthesis pathway but contains an unnatural chemical group. The modified monosaccharides are processed by biosynthetic enzymes within the cells through a pathway similar to that of the natural precursor. This results in the incorporation of the unnatural functional group into the cell-surface glycan. The sialic acid pathway has been particularly favoured in metabolic engineering due to its remarkable tolerance for non-natural chemical substituents in sialic acid and mannosamine precursors.^[4,32] Bertozzi and colleagues conducted a comprehensive investigation into the substrate specificity of the sialic acid pathway and confirmed that the *N*-acetyl moiety plays a significant role in selecting sialic acid precursors.^[33] Moller *et al.* reported the use of C4-modified *N*-acetyl mannosamine for applications in metabolic oligosaccharide engineering, preserving the integrity of the *N*-acetyl group.^[34]



Scheme 3.3: Structures of *N*-acetyl derivatives of hexosamines used to study MGE.
(Adapted from J. AM. CHEM. SOC. 2002, 124, 14893-14902.)

3.3. Aim and scope of the study: The efficiency of metabolic labelling of glycan precursors could change because of various factors, like substrate binding affinity to the enzymes involved in the biosynthetic pathway and the lipophilicity of the substrates. This study aims to investigate the labelling efficiency of a series of synthesised unnatural sugar analogues.

Specifically, labelling efficiencies has been compared with *N*-alkyl, *N*-acyl, and *N*-acyloxy derivatives of both glucosamine and mannosamine (GlcNPhAlk, ManNPhAlk, GlcNAcPhAlk, ManNAcPhAlk, GlcNAcOPhAlk, and ManNAcOPhAlk). The main goal is to determine whether *N*-acylation at the C-2 position is a critical factor in the biosynthetic pathway of glycans and to identify whether the unnatural sugars label *N*-glycans or *O*-glycans. Overall, the objective is to elucidate the substrate promiscuity of the enzymes involved in the hexosamine biosynthetic pathway through our MGL-SERS method, as detailed in the previous chapter, which was further confirmed by far-western blot analysis. Inhibitor studies were conducted to confirm whether the labelling is specific to *N*-glycans or *O*-glycans.

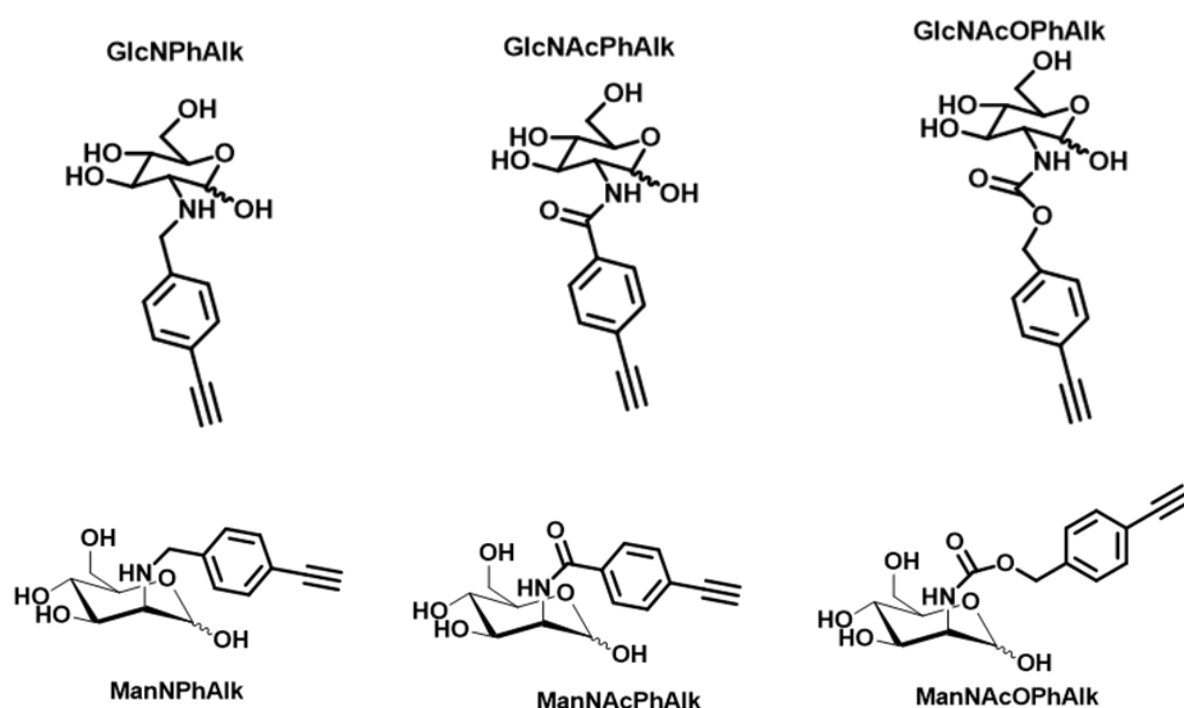


Figure 3.1: Structures of synthesised glycan precursors

3.4. Results and Discussion

3.4.1. Synthesis and characterisation of hexosamine derivatives

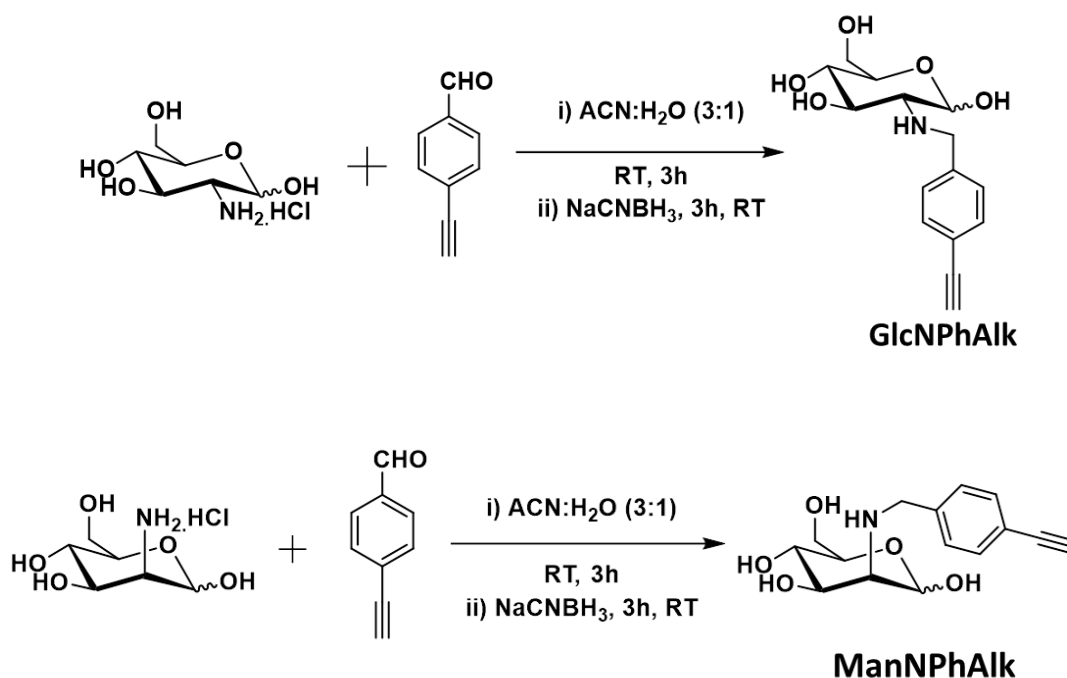
As per the literature, all synthesized analogues of glycan-labelling sugars retain the *N*-acetyl group, which is critical for the enzymatic recognition process within sialic acid biosynthesis.^[33] *N*-alkyl derivatives of hexosamines GlcNPhAlk and ManNPhAlk were synthesised using reductive amination reaction and *N*-acyl derivatives of glucosamine and mannosamine, GlcNAcPhAlk and ManNAcPhAlk, were prepared using acid amine coupling

with HBTU as the coupling agent respectively. GlcNAcOPhAlk and ManNAcOPhAlk, the *N*-acyloxy derivatives, were synthesised using *p*-Nitro chloroformate-appended ethynyl benzyl alcohol. All molecules were characterised with NMR and ESI-HRMS analyses (**Figure 3.2-3.13**). Although per-*O*-acetylated unnatural sugars are widely used to improve cell permeability, it leads to artificial *S*-glycosylation which compromises their specificity of metabolic glycan labelling in living cells.^[35] Hence to avoid false-positive results, unacetylated unnatural sugars were selected as the precursor for metabolic labelling.

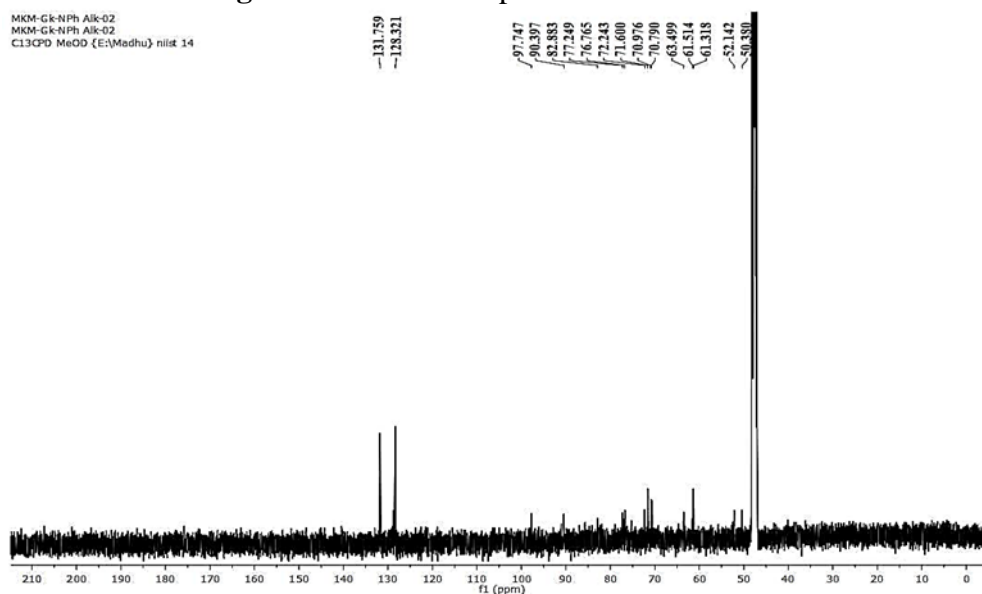
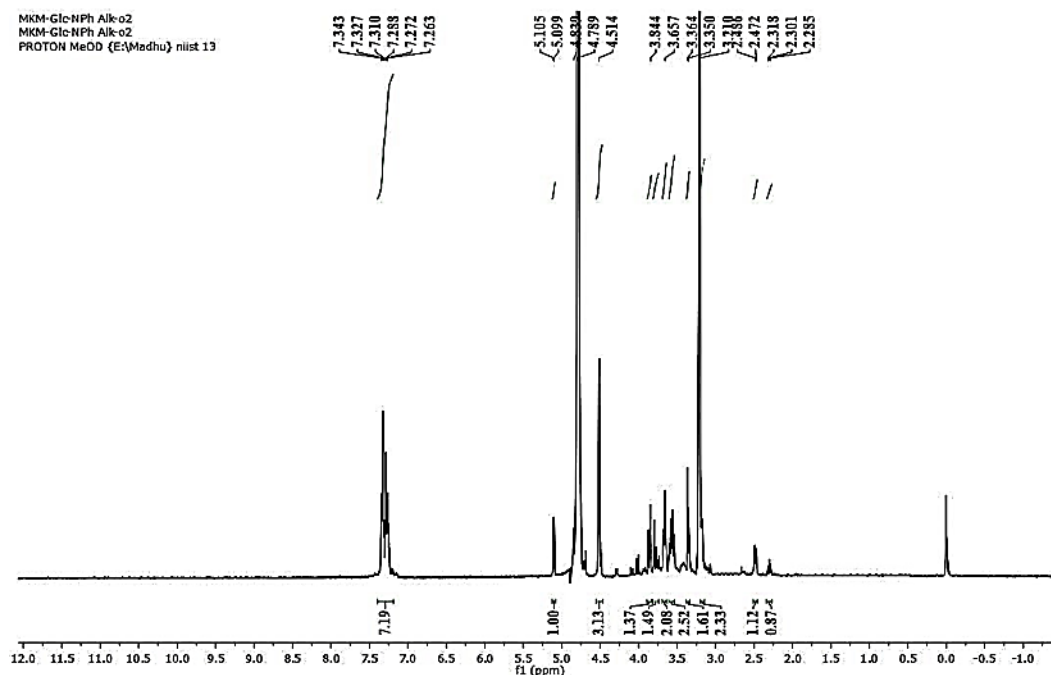
3.4.1.1. Synthesis of GlcNPhAlk, ManNPhAlk

N-alkyl derivatives of hexosamines GlcNPhAlk and ManNPhAlk were synthesised according to the procedure discussed in chapter 2 (**Scheme 2.5, Page number 40**).

The structure of the product, a mixture of the α and β anomers of GlcNPhAlk, was confirmed by spectral analysis, including ^1H NMR and ^{13}C NMR. In ^1H NMR spectrum, the anomeric protons appeared as a doublet at δ 5.10 ppm for the α anomer and at δ 4.79 ppm for the β anomer respectively. Unfortunately, we are unable to predict the ratio of α/β mixture, since the β proton merged with water peak of MeOD. Additionally, all aromatic protons resonated between δ 7.26 and 7.34 ppm (**Figure 3.2**). In the ^{13}C NMR spectrum, the anomeric carbons resonated at δ 97.7 ppm for the β anomer and δ 90.4 ppm for the α anomer, while the terminal alkyne carbon was resonated at δ 82.9 ppm (**Figure 3.3**).



Scheme 3.4: Synthesis of GlcNPhAlk, ManNPhAlk respectively



The structure assigned to the product (mixture of two anomers, α and β of ManNPhAlk) was confirmed by the spectral analysis including ^1H NMR and ^{13}C NMR. In ^1H NMR spectrum, the anomeric proton resonated at δ 5.10 ppm as doublet assigned to α proton and at δ 4.89 ppm (merged with water peak in MeOD) to β proton respectively. All the aromatic protons were resonated at δ 7.26 - 7.34 ppm (**Figure 3.4**). In ^{13}C NMR, the ester carbonyls resonated at δ 162.5-170.3 ppm. The anomeric carbons were resonated at δ 93.3 (β), 90.9 (α) ppm and terminal alkyne carbon at δ 82.6 ppm respectively (**Figure 3.5**).

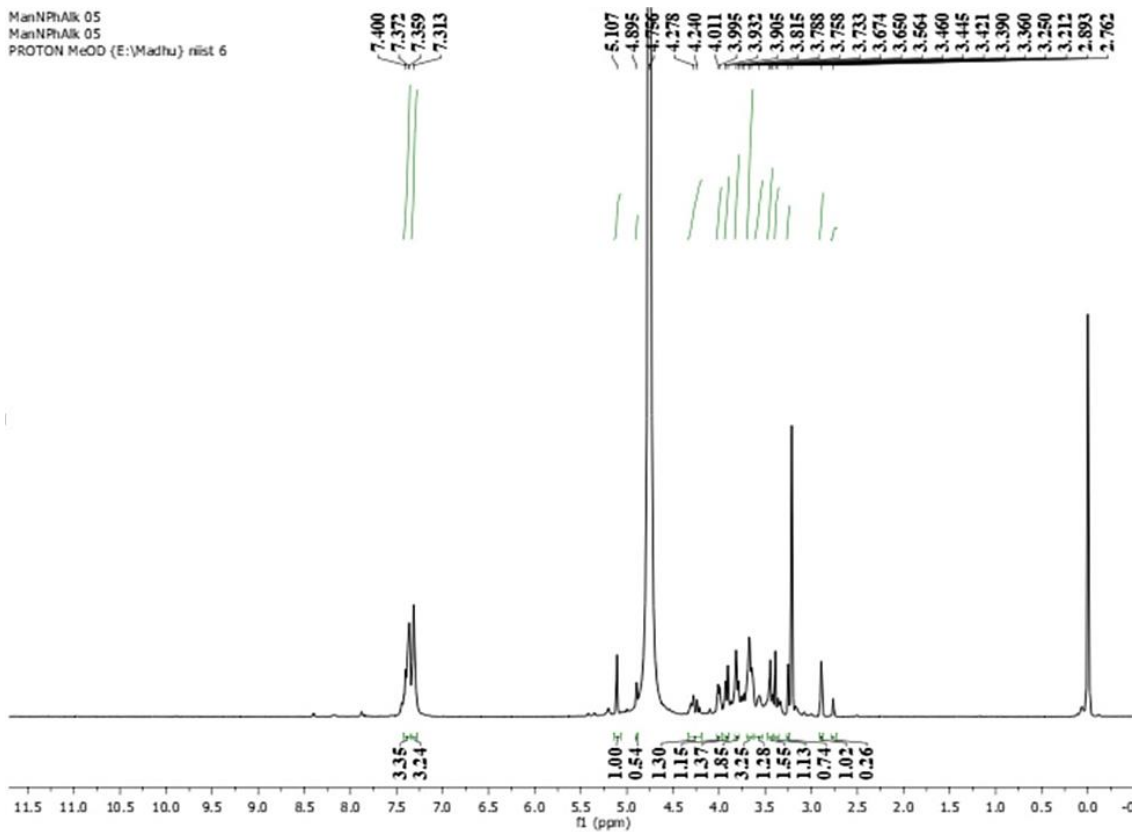


Figure 3.4: ^1H NMR spectrum of ManNPhAlk

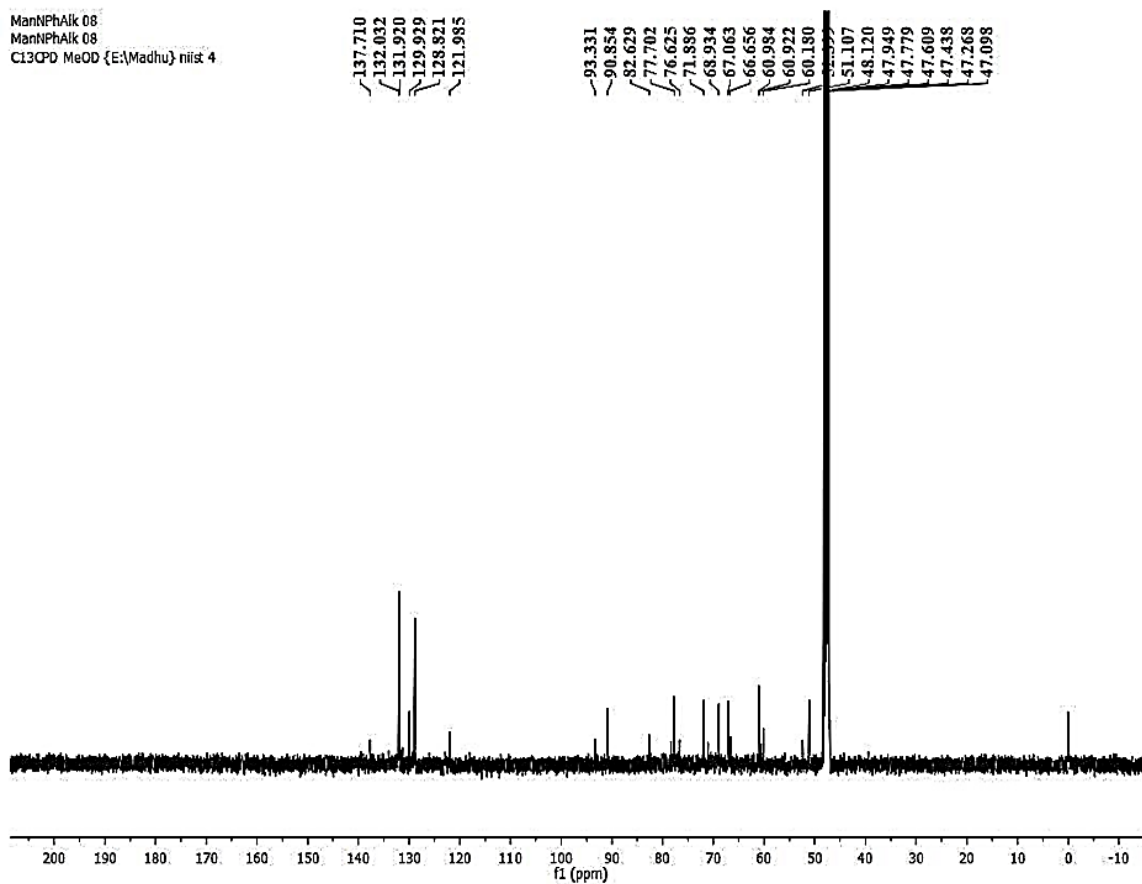
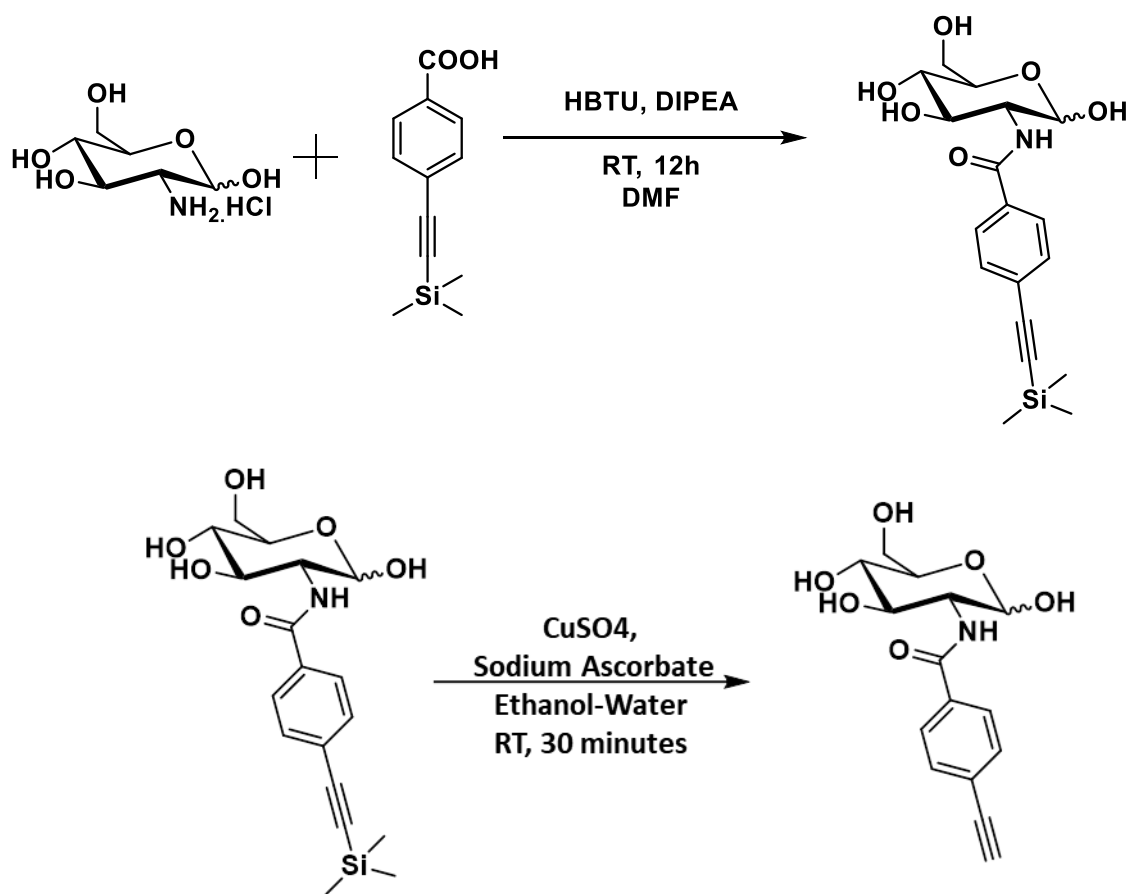


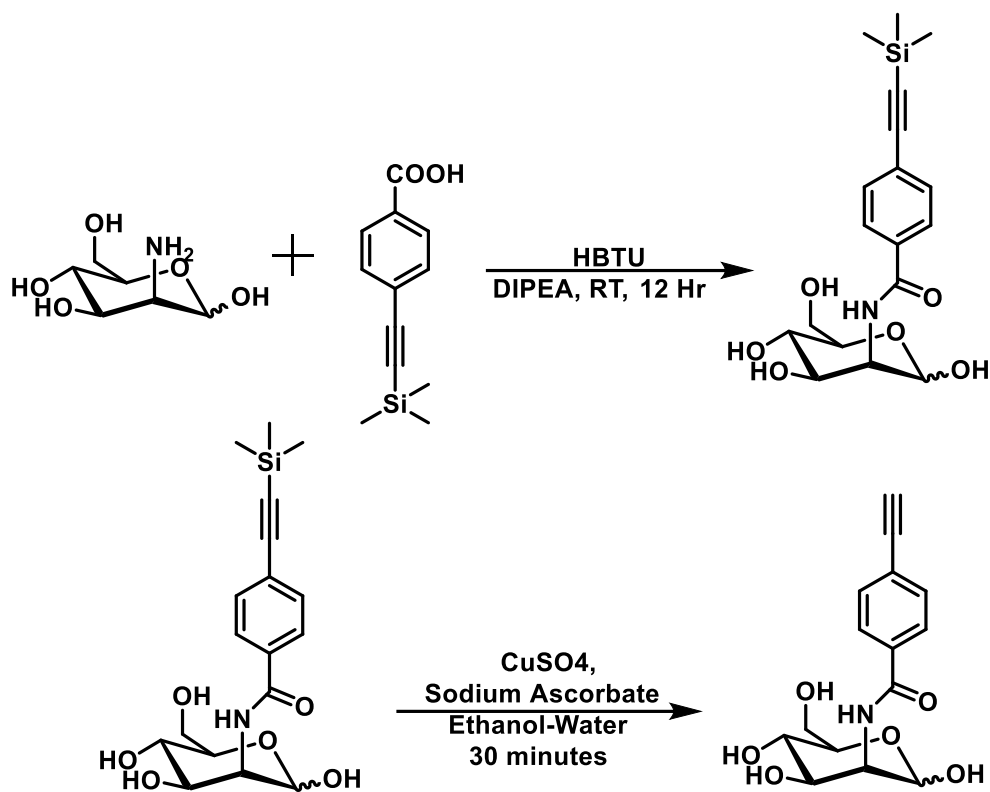
Figure 3.5: ^{13}C NMR spectrum of ManNPhAlk

3.4.1.2. Synthesis of GlcNAcPhAlk and ManNAcPhAlk

The synthetic strategy involves two steps. First step was the acid- amide coupling reaction between glucosamine (296.73 mg, 1.376 mmol) and trimethylsilane benzoic acid (300 mg, 1.376 mmol) in presence of the coupling agent is HBTU (521.848 mg, 1.376 mmol) and the base DIPEA (235.6 μ M) at room temperature. After completion of the reaction for 12 hours as indicated by thin layer chromatography (TLC), the reaction mixture was quenched with H₂O, washed with ethyl acetate (EtOAc), and dried with anhydrous Na₂SO₄. The product was separated by column chromatography (CC) using diverse gradient of EtOAc-hexane (9:1 to 10:0). Second step is the desilylation of the acetyl derivative of glucosamine (50 mg, 0.2471 mmol) with CuSO₄.5H₂O (39.43 mg, 0.2471 mmol) and sodium ascorbate (147 mg, 0.7413 mmol) in ethanol-water system for 30 minutes. The product was purified by CC using EtOAc- hexane (9:1) as the mobile phase (**Scheme 3.4**). The same procedure was repeated for the synthesis of mannosamine analogue also (**Scheme 3.5**).



Scheme 3.4: Synthesis of GlcNAcPhAlk



Scheme 3.5: Synthesis of ManNAcPhAlk

The structure assigned to the product is α/β anomers of GlcNAcPhAlk, which was confirmed with both ^1H NMR and ^{13}C NMR spectra. In ^1H NMR spectrum, the anomeric protons resonated at δ 5.15 ppm as apparent singlet and δ 4.67 ppm corresponding to both α and β anomers respectively. Here also, we are unable to report the exact ratio of the α/β mixture, since the β proton merged with water peak of MeOD. All the aromatic protons were resonated at δ 7.44 - 7.75 ppm (**Figure 3.6**). In ^{13}C NMR, the anomeric carbons were resonated at δ 95.6 (β), 91.1 (α) ppm and the terminal alkyne carbon at δ 82.2 ppm, and the amide carbonyl at δ 168.4 ppm respectively (**Figure 3.7**).

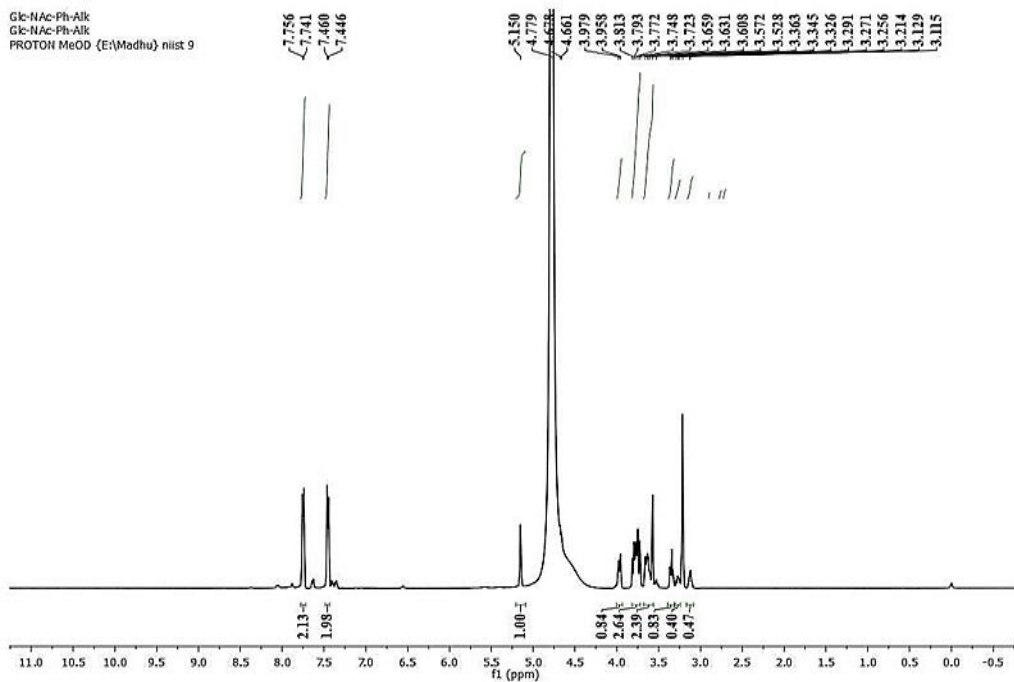


Figure 3.6: ^1H NMR spectrum of GlcNacPhAlk

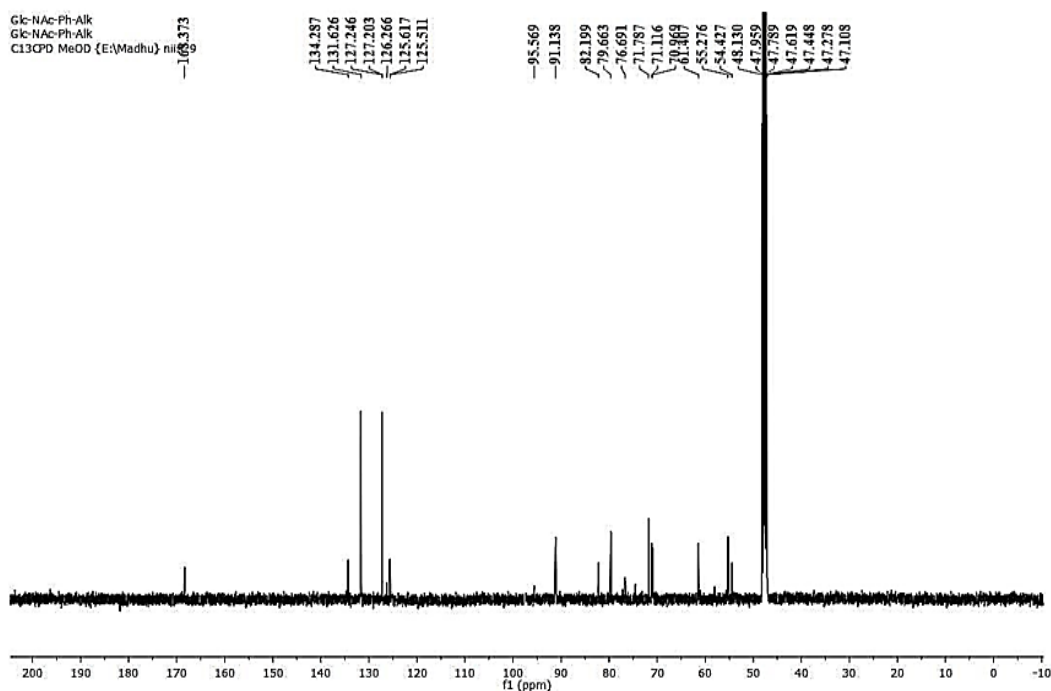


Figure 3.7: ^{13}C NMR spectrum of GlcNacPhAlk

The structure assigned to the product is α/β anomers of ManNacPhAlk, was confirmed by the spectral analysis including ^1H NMR and ^{13}C NMR. In ^1H NMR spectrum, the anomeric protons resonated at δ 5.04 ppm as apparent singlet (apps) and δ 4.67 ppm (merged with water peak of MeOD) corresponding to α and β protons respectively. Moreover, all the

aromatic protons were resonated at δ 7.53 - 7.87 ppm (**Figure 3.8**). In ^{13}C NMR, the anomeric carbons were resonated at δ 93.7 (β), 93.5 (α) ppm and terminal alkyne carbon at δ 82.4 ppm. The amide carbonyl is resonated at δ 169.3 ppm (**Figure 3.9**).

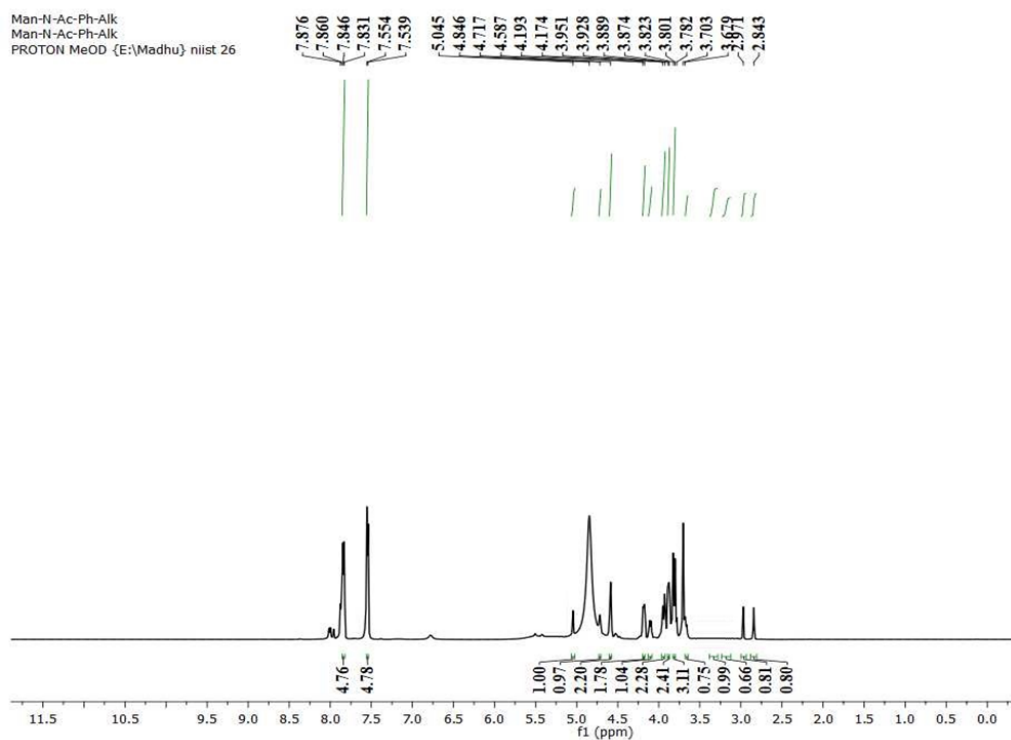


Figure 3.8: ^1H NMR spectrum of ManNacPhAlk

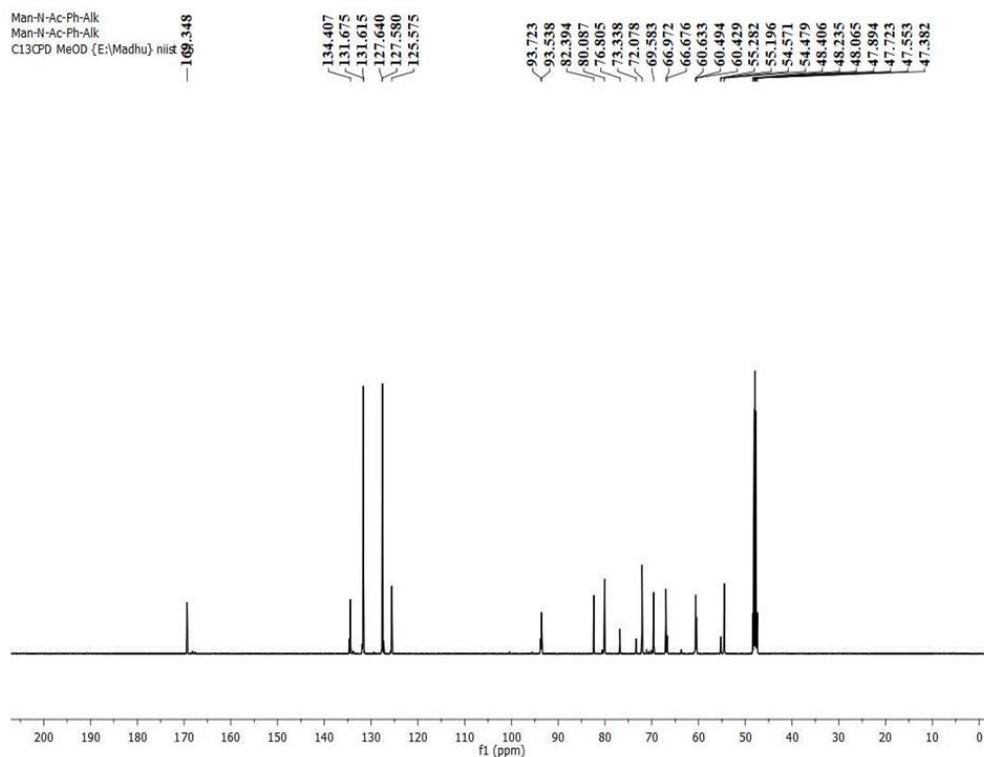
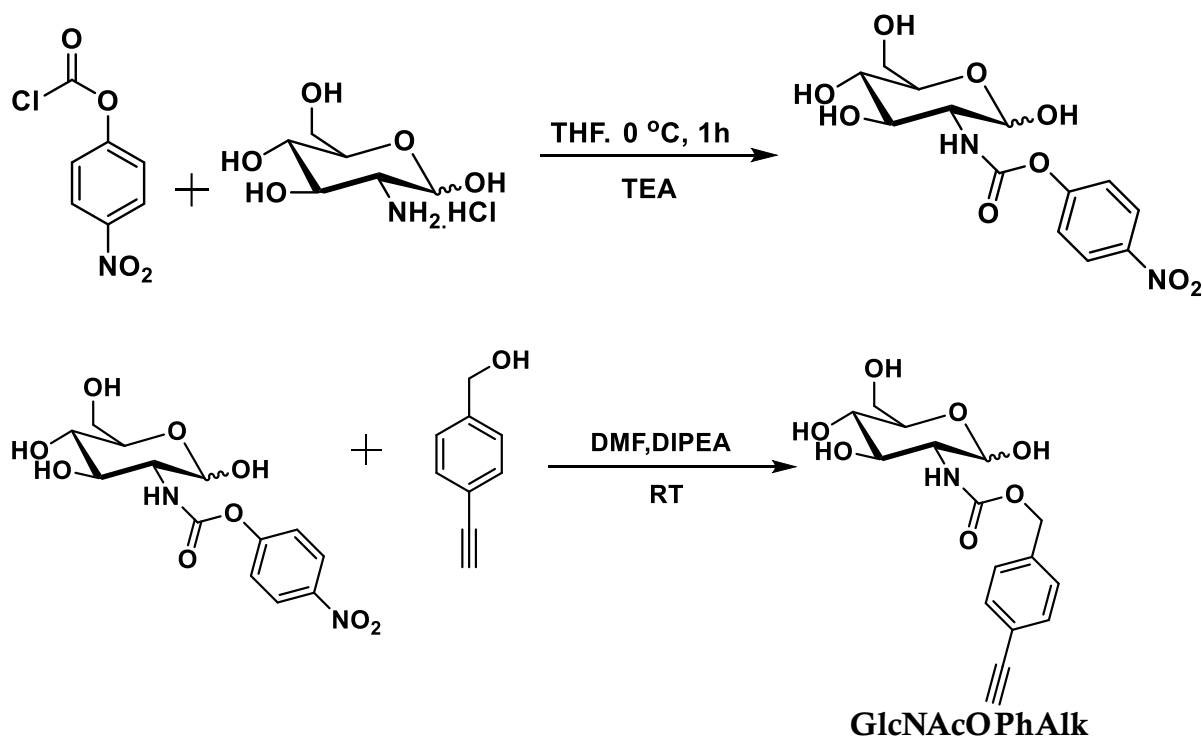


Figure 3.9: ^{13}C NMR spectrum of ManNacPhAlk

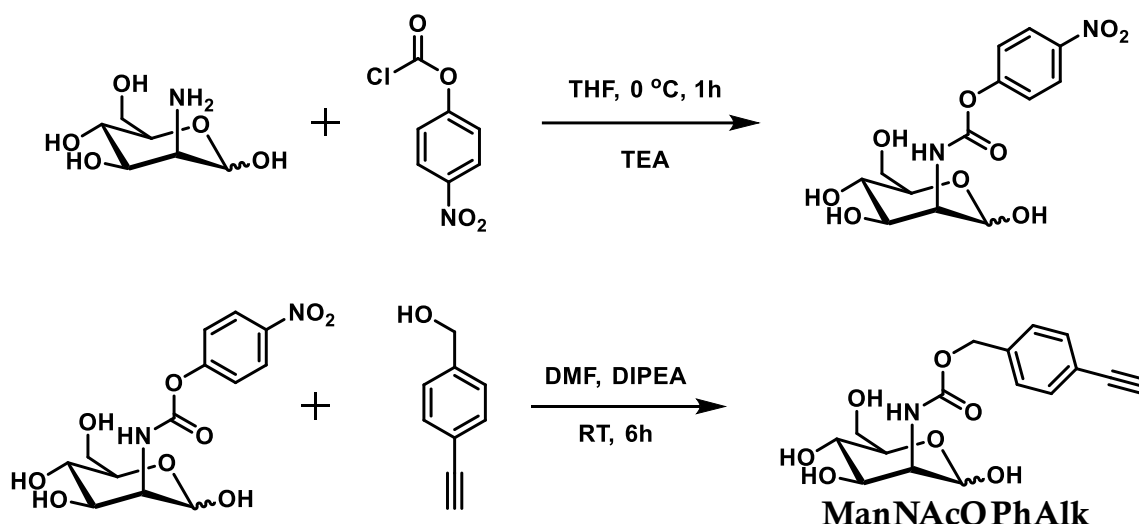
3.4.1.3. Synthesis of GlcNAcOPhAlk and ManNAcOPhAlk

The reaction proceeds through two steps. In first step, glucosamine (200 mg, 0.9275 mmol) was taken in a 100 ml round bottom flask. To this *p*-nitrochloroformate (373.89 mg, 1.8550 mmol) and triethylamine (129.09 ml, 0.9275 mmol) were added. THF was added as solvent. The reaction mixture was stirred at 0 °C for 1 hour and the product was separated by CC using EtOAc (100%) as the mobile phase. Finally, the product was dried under high vacuum and used for second step.

In the second step acyloxy derivative of glucosamine was reacted with ethynylbenzyl alcohol (100 mg, 0.7566 mmol) in the presence of DIPEA (0.7566 mmol) as base and DMF as solvent for 6 hours. Upon completion of the reaction as indicated by TLC, the product was purified by CC using EtOAc:hexane (1:9) as the eluent (**Scheme 3.6**). The same procedure was repeated for the synthesis of mannosamine analogue (**Scheme 3.7**).



Scheme 3.6: Synthesis of GlcNAcOPhAlk



Scheme 3.7: Synthesis of ManNAcOPhAlk

The structure assigned to the product of GlcNAcOPhAlk (α) was confirmed by the spectral analysis including ^1H NMR and ^{13}C NMR. In ^1H NMR spectrum, the anomeric proton is resonated as an app at δ 5.01 ppm corresponding to α configuration. Moreover, all the aromatic protons were resonated at δ 7.25 - 7.34 ppm (**Figure 3.10**). In ^{13}C NMR, carbons resonated at δ 95.5 (α), 86.7 and 157.3 ppm corresponding to anomeric carbon, terminal alkyne carbon and *N*-acyloxy carbonyl respectively (**Figure 3.11**).

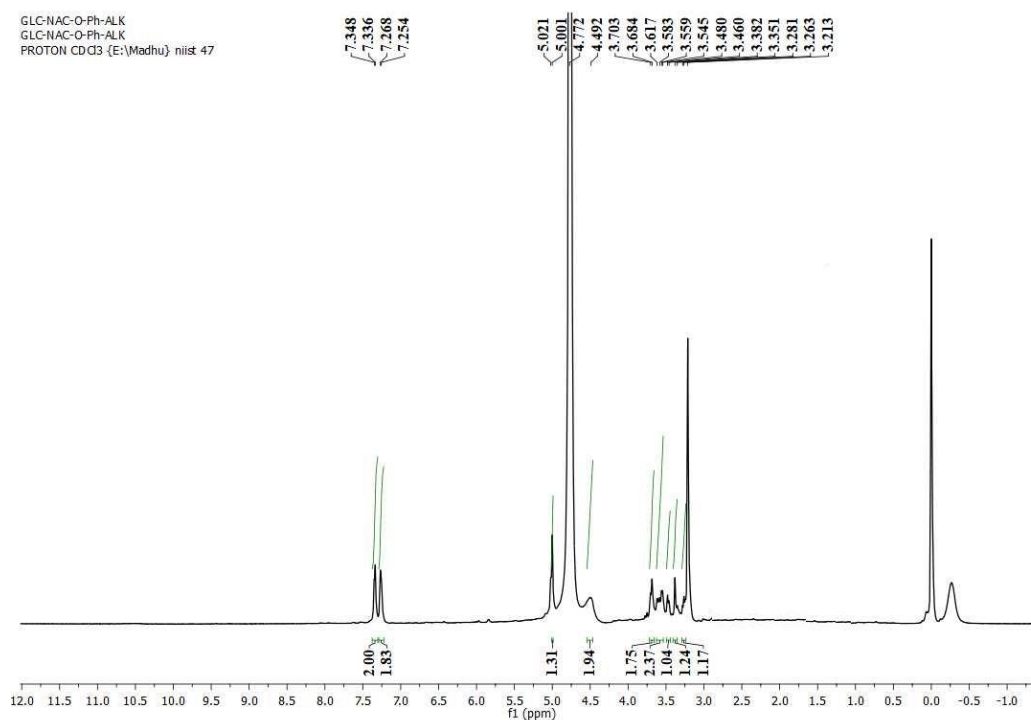


Figure 3.10: ^1H NMR spectrum of GlcNAcOPhAlk

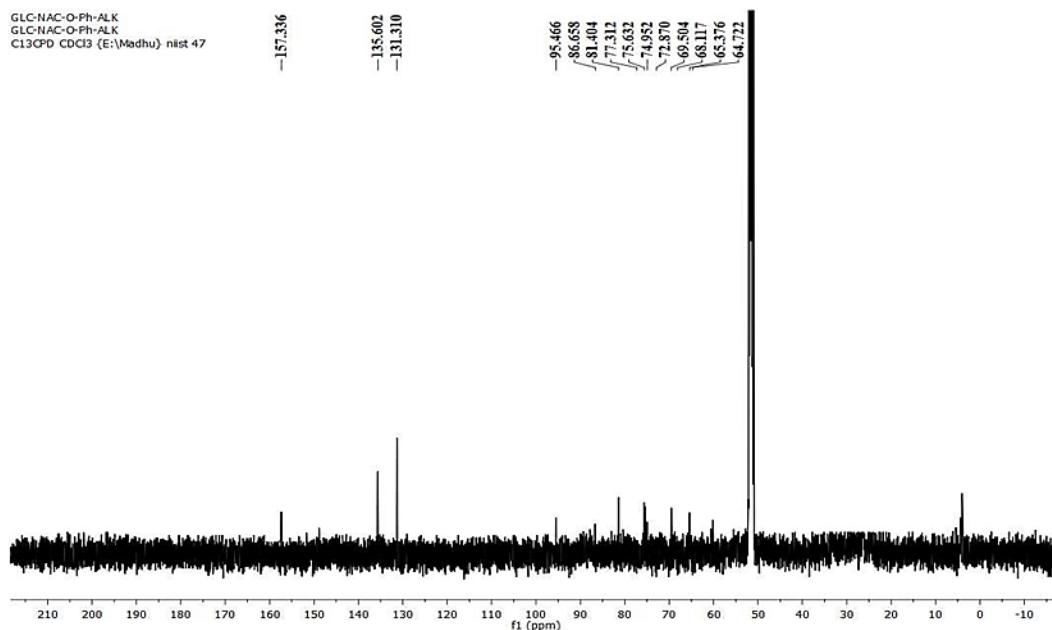


Figure 3.11: ^{13}C NMR spectrum of GlcNAcOPhAlk

The structure assigned to the product of ManNAcOPhAlk was confirmed by the spectral analysis including ^1H NMR and ^{13}C NMR. In ^1H NMR spectrum, the anomeric proton in α is resonated as a doublet in the region of δ 5.01 (merged with other sugar protons) ppm. Moreover, all the aromatic protons were resonated at δ 7.25 - 7.34 ppm (**Figure 3.12**). In ^{13}C NMR, the anomeric carbon is resonated at δ 95.5 (α) ppm and terminal alkyne carbon at δ 86.6 ppm. The *N*-acyloxy carbonyl is resonated at δ 157.3 ppm (Figure 3.13).

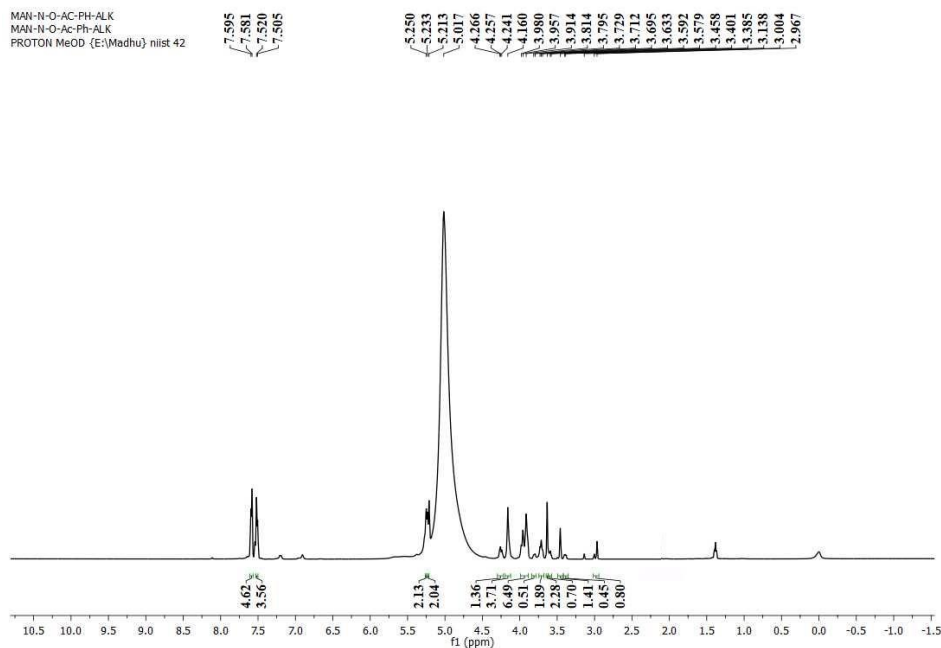


Figure 3.12: ^1H NMR spectrum of ManNAcOPhAlk

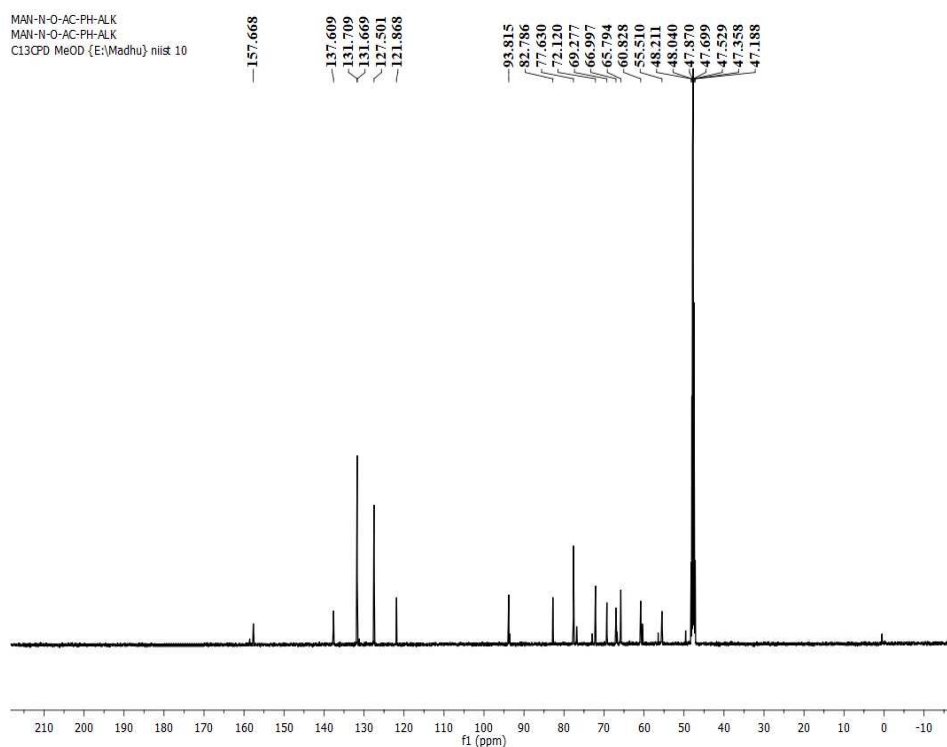


Figure 3.13: ^{13}C NMR spectrum of the ManNAcOPhAlk

3.4.2. SERS analysis of glycan precursors

Next, SERS signal strength of six unnatural sugars was measured. For that, quasi-spherical colloidal AuNP's of the size 35-40 nm were synthesised (**Figure 2.8, page number 45**) that can give maximum SERS enhancement.^[36] It was found that for 100 μM of all the

compounds SERS spectra as well as its signal strength were similar. Small changes in the *N*-acyl, *N*-alkyl and *N*-acyloxy parts of the hexosamine derivatives were not distinctive from SERS spectra. All of them showed major SERS peaks at 1596 cm^{-1} , 1991 cm^{-1} and 2142 cm^{-1} respectively. Peaks at 1991 cm^{-1} and 2142 cm^{-1} corresponds to alkyne functional group, and 1596 cm^{-1} corresponds to aromatic ring vibrations. SERS analysis confirmed that equal concentrations of glycan precursors produce equivalent SERS intensities, which is crucial for accurately evaluating the metabolic labelling efficiency of these analogues (**Figure 3.14**).

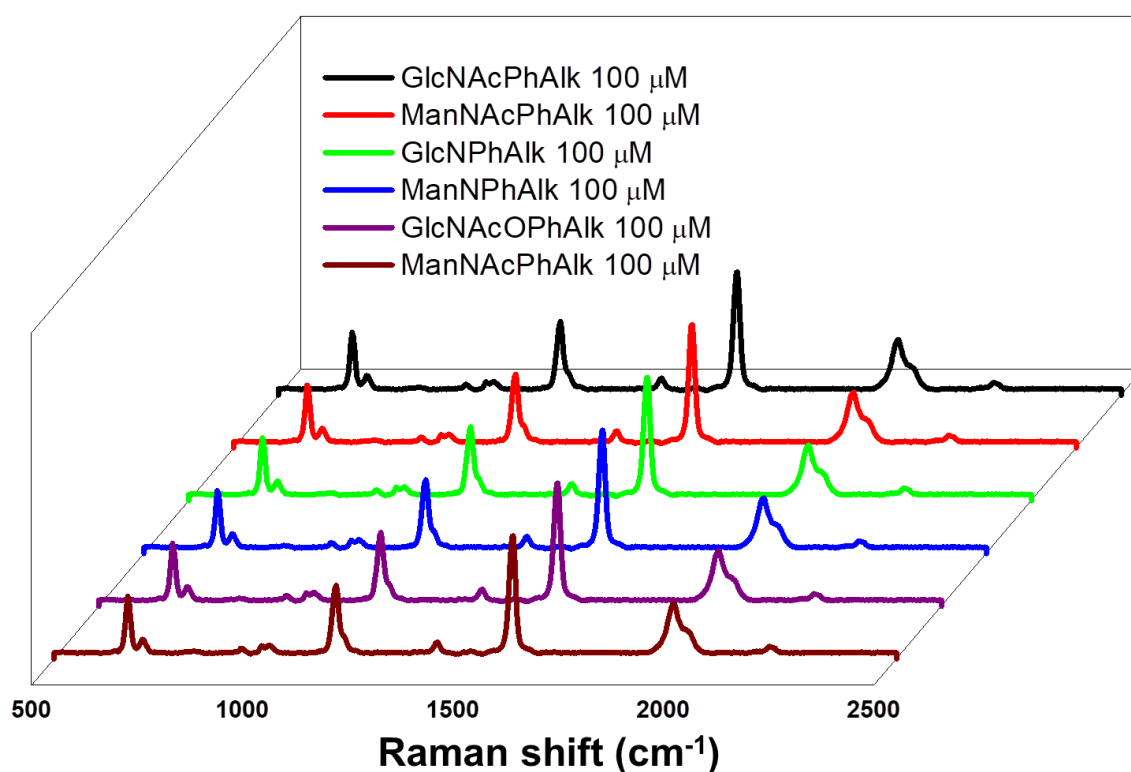


Figure 3.14: SERS spectra of 6 glycan precursors

3.4.3. Cytotoxicity studies of glycan precursors

HeLa cells were seed into 96 well plates and incubated for 24 hour (at 37 °C 5% CO_2). Cells were then treated with varying concentrations of GlcNPhAlk, ManNPhAlk, GlcNAcPhAlk, ManNAcPhAlk, GlcNAcOPhAlk, and ManNAcPhOAlk (10-200 μM). After 72 hour incubation, MTT (0.5 mg/ml) was added to each well and kept at 37 °C for 4 hour and finally the so formed formazan crystals were dissolved in DMSO and the optical density (OD) was measured at 570 nm using a microplate reader. Cytotoxic studies of all the six GPs in cancer cell lines confirmed the viability up to 100 μM concentrations (**Figure 3.15**).

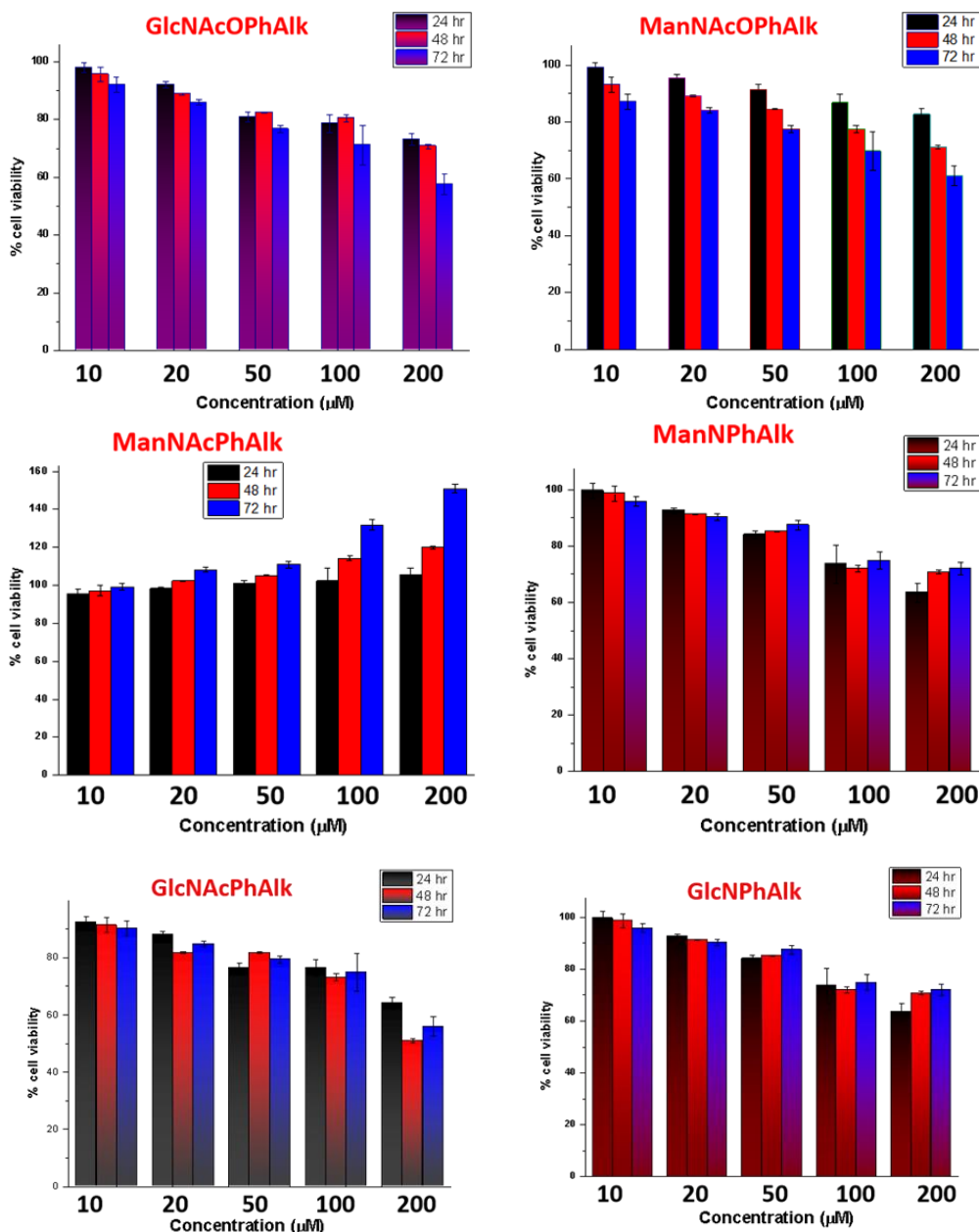


Figure 3.15: Cytotoxic studies on HeLa cell line by 6 glycan precursors.

3.4.4. Metabolic labelling of glycan precursors

Primarily the as-designed investigation was focused on the detection of cell surface glycans by SERS imaging and to find out the extent of metabolic labelling capability of aforesaid compounds with well-proven MGL-SERS strategy. Cervical carcinoma HeLa cells which were treated with GlcNPhAlk, ManNPhAlk, GlcNAcPhAlk, ManNAcPhAlk, GlcNAcOPhAlk, and ManNAcOPhAlk for 72 hours to induce the biosynthetic pathway to incorporate into cell surface glycans. Cells without glycan tags were used as negative controls. After a treatment of 3 days, the cell culture medium was removed and washed thrice

with PBS (phosphate-buffered saline), then SERS imaging was performed by incubating with colloidal AuNPs. Cells incubated with GlcNPhAlk, ManNPhAlk, GlcNAcPhAlk, ManNAcPhAlk, GlcNAcOPhAlk, and ManNAcOPhAlk provided significant Raman mapped images with greater sensitivity, specificity and repeatability (**Figure 3.16**). From the images it is seen as the ManNAcPhAlk had the maximum labelling efficiency, followed by N-alkyl derivatives of both mannosamine and glucosamine derivatives and least labelling was found to be for GlcNAcPhAlk.

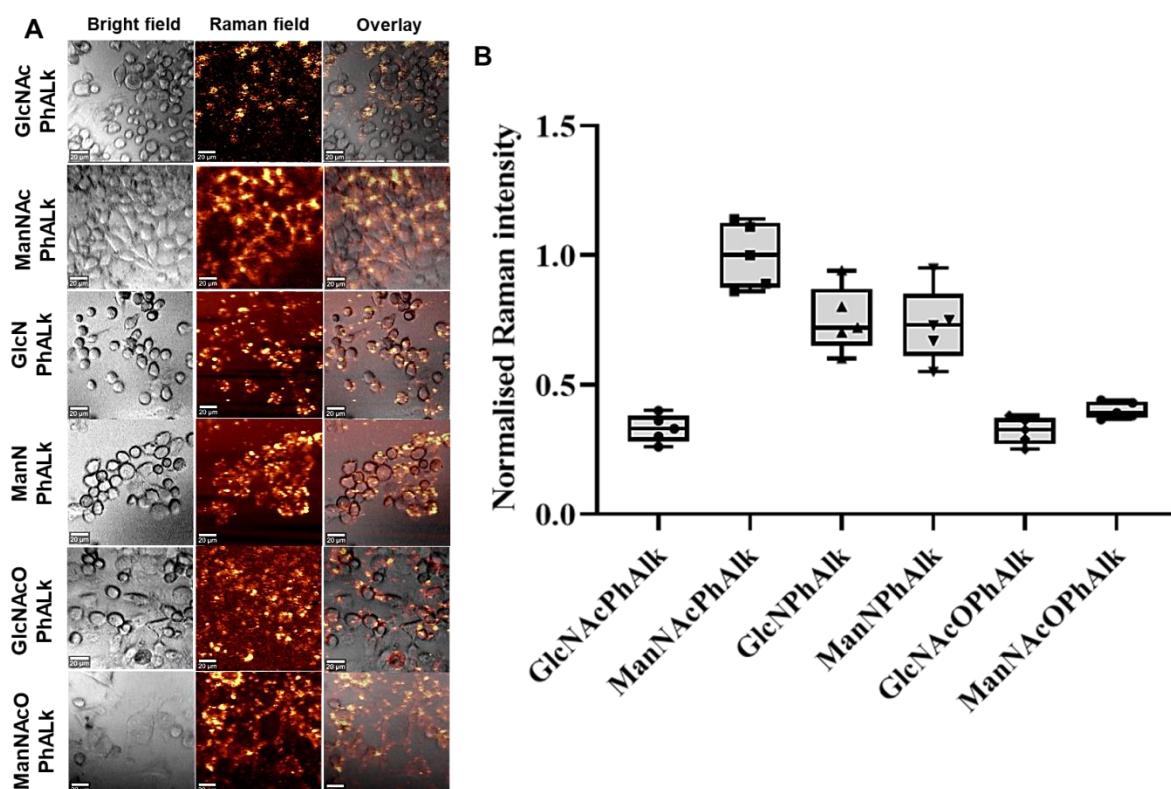


Figure 3.16: Metabolic glycan labelling of unnatural sugars. A) Bright field, Raman field and overlay representative images of 6GPs. B) Its average SERS intensities given as a box plot (n=5).

3.4.5. Inhibitor studies on metabolic labelling of glycan precursors

From the MGL-SERS method, it was found that all the six analogues were successfully labelling cell surface glycans with ManNAcPhAlk being the best candidate for labelling purposes. Since these glycosylations can be of two types, namely, *N*-glycans and *O*-glycans which varies in terms of structures, cellular functions and cellular locations. It is important to know whether the labelling precursors are indeed labelling *N*-glycans or *O*-glycans. For this purpose, labelling mechanisms of probes using glycosylation inhibitors were confirmed.

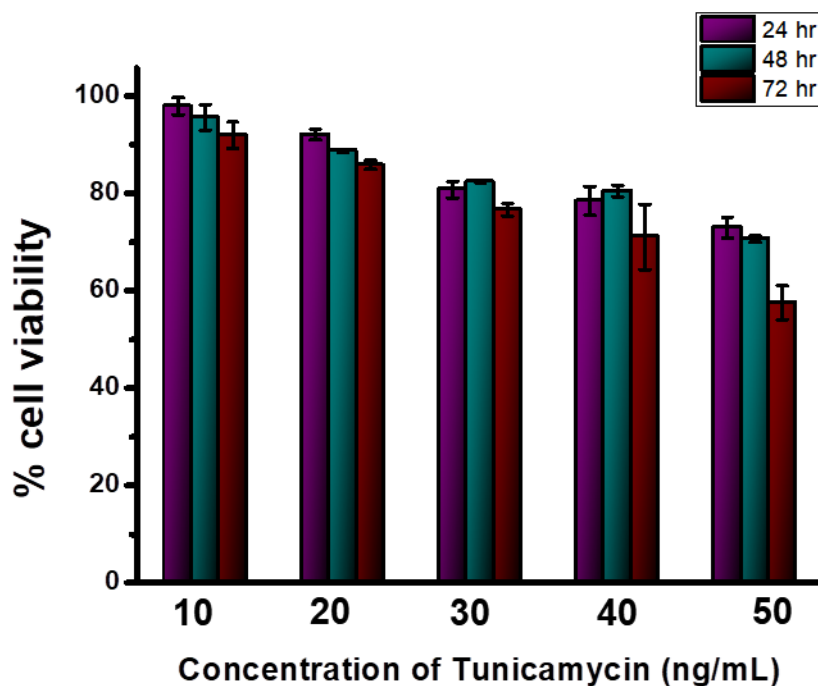


Figure 3.17: Cytotoxic studies on HeLa cell line by tunicamycin

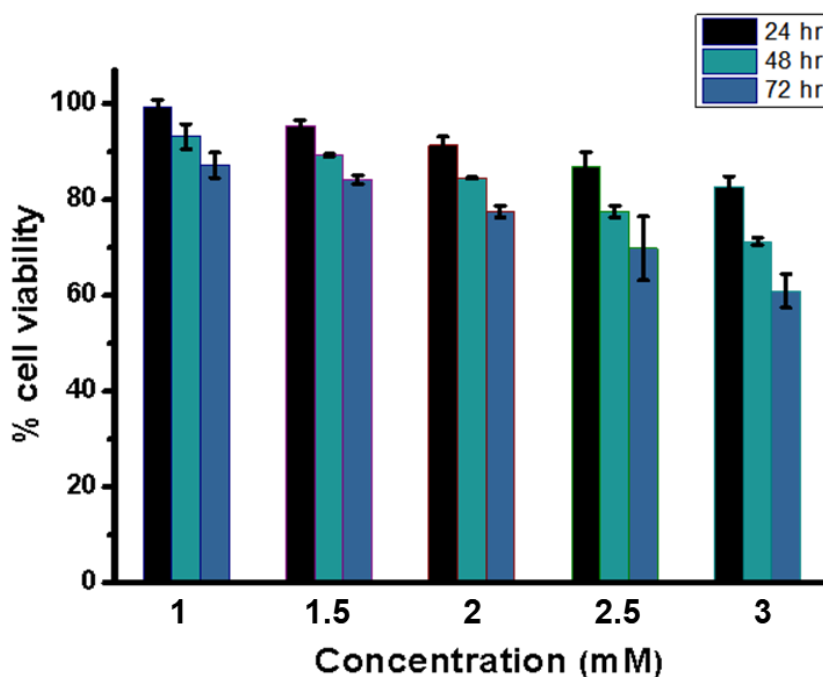


Figure 3.18: Cytotoxic studies on HeLa cell line by α -O-benzyl-N-acetyl galactosamine

Tunicamycin (Tun) is a commonly used *N*-glycosylation inhibitor, which targets GlcNAc phosphotransferase and prevents the assembly of GlcNAc-PP-dolichol at the first step of the *N*-linked glycosylation.^[33] On the other hand, α -O-benzyl-N-acetyl galactosamine (*O*-Bn) is a potent competitive inhibitor for *O*-glycosylation, with negligible activity against the incorporation of glucosamine or galactosamine. It is expected that a significant variance in

labelling efficiency between GPs will be resulted from treating cells with probes alongside one of these inhibitors. From the literature and MTT analysis, the treatment concentration were finalised with Tun to be 20 ng/ml and *O*-Bn to be 1.5 mM (**Figure 3.17 & 3.18**)

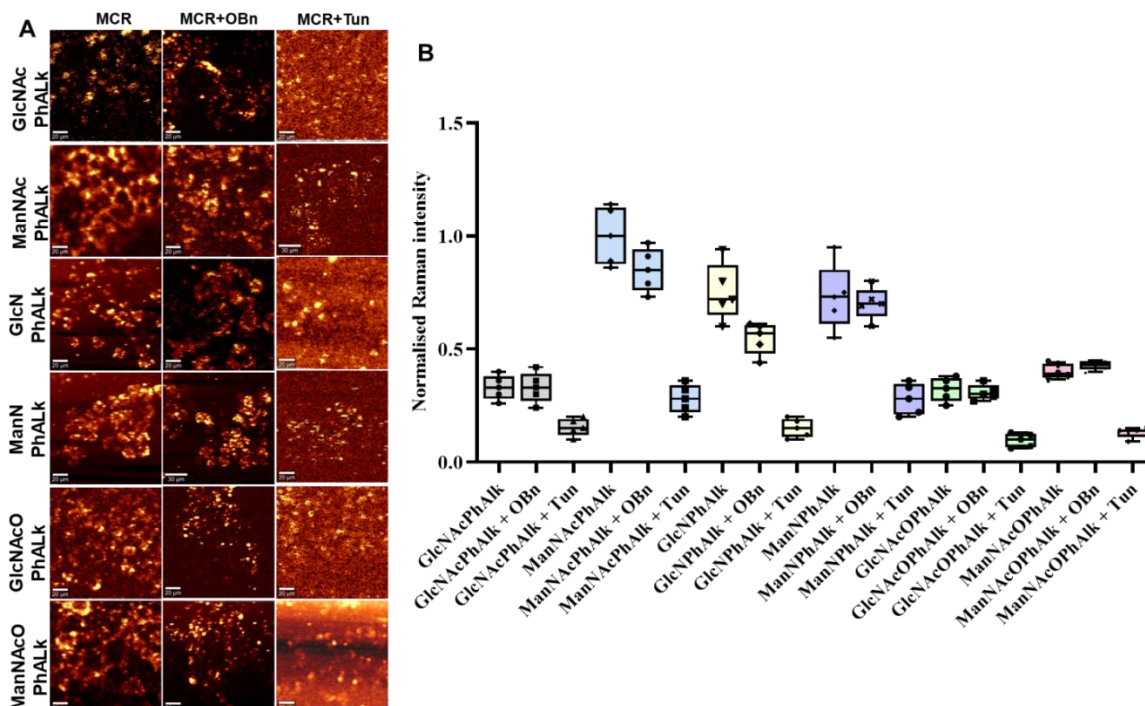


Figure 3.19: Inhibitor studies on metabolic glycan labelling of unnatural sugars. A) Representative Raman field images of GPs, GPs coincubated with 20 ng/mL Tun, GPs coincubated with 1.5 mM *O*-Bn. B) Its average SERS intensities given as a box plot (n=5).

Co-incubation of Tun with hexosamine derivatives led to a significant suppression of cell-surface alkyne expression compared to the control group (**Figure 3.19A**). This finding suggests that the metabolic product derived from hexosamine analogues are predominantly localised within *N*-linked oligosaccharides. The suppression of *O*-linked glycosylation, achieved through the application of *O*-BnGalNAc, was anticipated to exert a less pronounced influence on the manifestation of alkynyl sugar within primarily *N*-glycosylated HeLa cells.^[33,37] This presumption was corroborated by the empirical evidence presented in the figure (**Figure 3.19 B**).

3.4.6. Confirmation of protein glycosylation by far-western blot analysis

The extent of protein glycosylation by metabolically labelled alkyne tag was further evaluated by far-western blot analysis.^[38] The presence of metabolically anchored alkyne was confirmed in HeLa cells treated with six hexosamine derivatives using CuAAC. For this, cell lysate was extracted and treated with azide-PEG3-biotin in presence of CuSO₄·5H₂O and sodium ascorbate followed by horse radish peroxidase (HRP) conjugated streptavidin for chemiluminescent detection (**Figure 3.20**). A parallel experiment was carried out with D-glucosamine treated cells taken as a negative control. Multiple bands of alkyne tagged glycoprotein were generated in cell lysate of unnatural sugar analogues treated HeLa cells while no bands were visible in the cell lysate from glucosamine treated cells indicating the detection of unique glycoproteins (**Figure 3.21**).

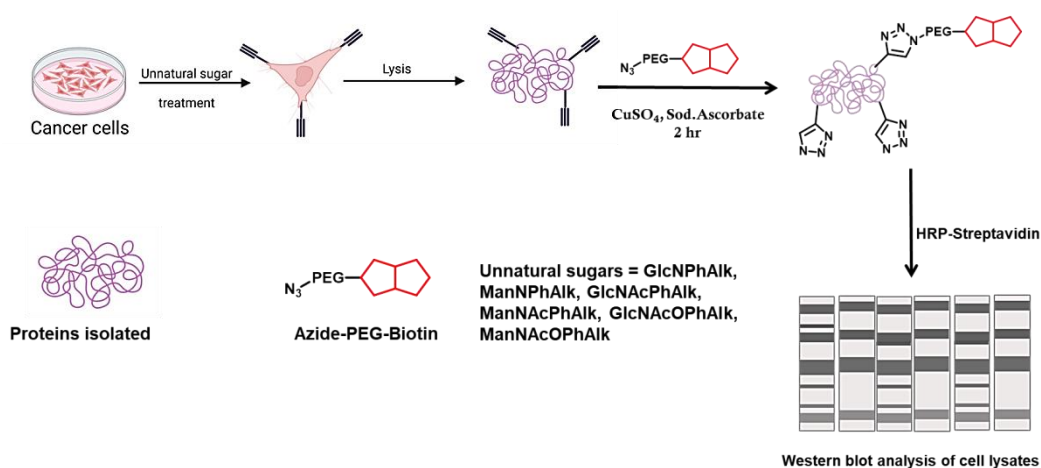


Figure 3.20: Schematic representation of far-western blotting.

It is worth noting that the different bands from the western blot analysis were quantified using Image J software. The results showed that they followed the same trend of labelling efficiency indicated by the MGL-SERS method, with ManNAcPhAlk being the most heavily protein glycosylated alkyne and GlcNAcPhAlk showing the least labelling efficiency.

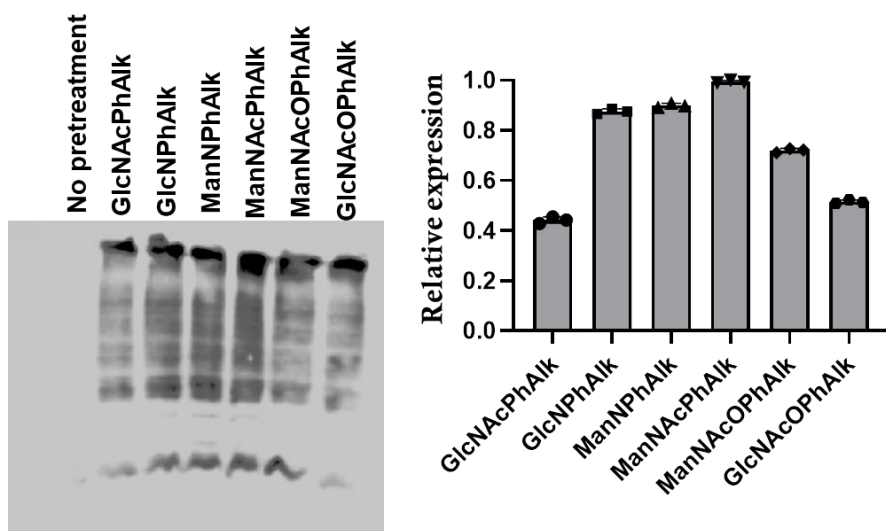


Figure 3.21: Western blot analysis of six GPs and their quantified relative expression.

3.4.7. Inhibitor studies on metabolic labelling of glycan precursors by far-western blot analysis

In western blot experiments, when Tun and hexosamine derivatives were used together, there was a notable decrease in the protein glycosylation expression induced by alkynyl sugars compared with the control group, similar to what we observed using the MGL-SERS method (**Figure 3.19A**). This outcome indicates that the metabolic products arising from hexosamine analogues predominantly occupy *N*-linked oligosaccharides (**Figure 3.22**).

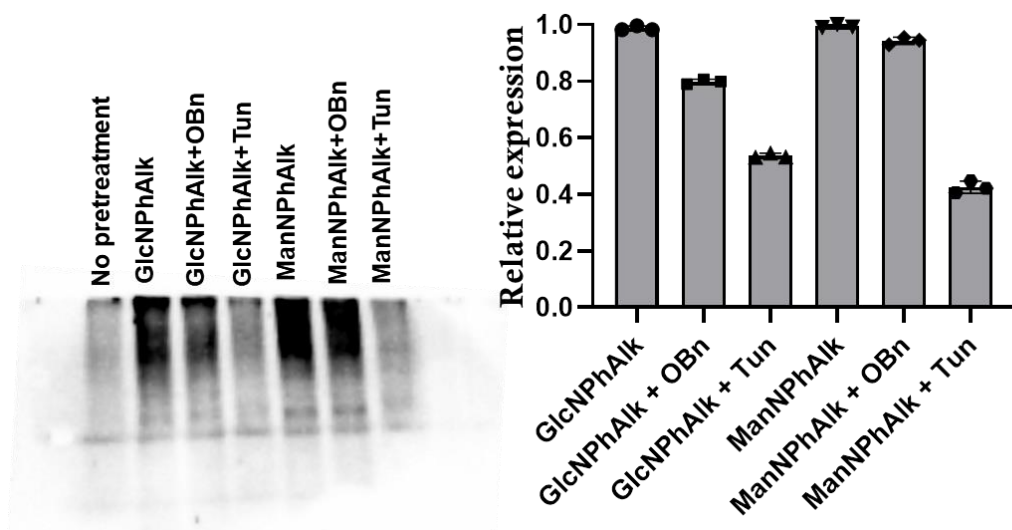


Figure 3.22: Western blot analysis of two *N*-alkyl GPs along with their inhibitors and their quantified relative expression.

Furthermore, the deliberate reduction of *O*-linked glycosylation with the use of *O*-BnGalNAc was expected to have a minimal impact on the presence of alkynyl sugar in mainly *N*-glycosylated HeLa cells. This initial hypothesis was validated by the data shown in the following figures (**Figure 3.22** - **Figure 3.24**).

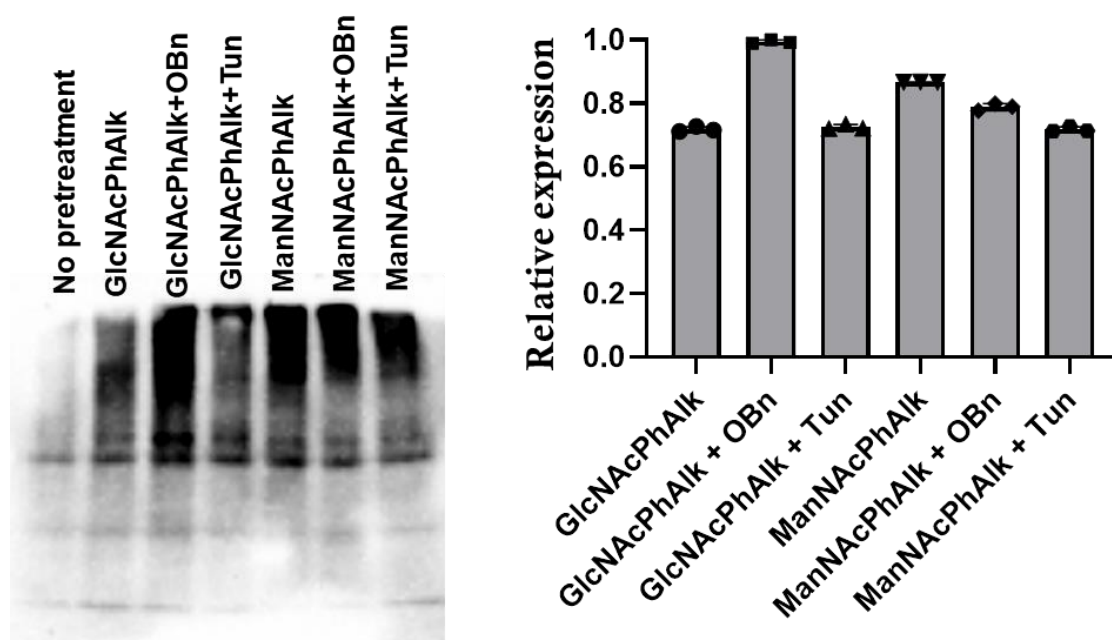


Figure 3.23: Western blot analysis of two *N*-acyl GPs along with their inhibitors and their quantified relative expression.

In reviewing the effects of different agents on protein glycosylation, it was observed that the application of Tun significantly reduced protein glycosylation more than when using *O*-Bn. This suggests that the attachment of these unnatural sugar moieties is occurring predominantly near *N*-glycosylated structures.

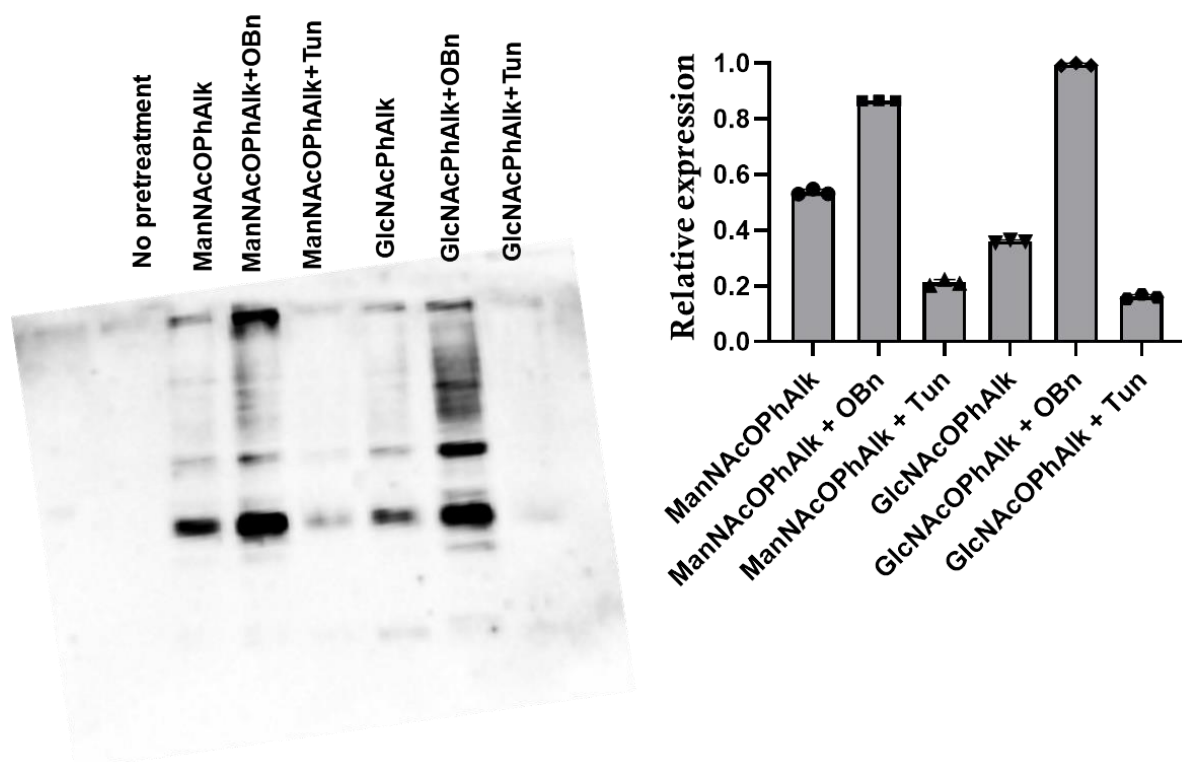


Figure 3.24: Western blot analysis of two *N*-acyloxy GPs along with their inhibitors and their quantified relative expression.

3.5. Conclusion

In summary, the current demonstration on the hexosamine biosynthetic pathway exhibits varying tolerance levels to structural alterations of *N*-acyl, *N*-alkyl, and *N*-acyloxy substituents in mannosamine and glucosamine analogues. Specifically, ManNAcPhAlk and ManNPhAlk are efficiently metabolised and incorporated into cell surface glycans, followed by GlcNPhAlk. In contrast, GlcNAcOPhAlk, ManNAcPhOAlk, and GlcNAcPhAlk are less efficiently utilised. These findings were consistently validated through MGL-SERS and far-western blot analyses. Furthermore, inhibitor studies confirmed that these analogues predominantly label *N*-glycans. This research provides valuable insights into the metabolic incorporation of unnatural sialic acid derivatives and their potential applications in investigating carbohydrate-dependent cellular phenomena.

3.6. Experimental section

3.6.1. General Experimental Methods:

All chemicals and solvents were brought from Sigma Aldrich, Alfa Aesar, TCI and Merck and used without further purification. Global Sialyltransferase inhibitor P-3Fax-Neu5Ac was obtained from Calbiochem, Sigma Aldrich. ¹H NMR spectra were recorded on Bruker Advance 500 MHz NMR spectrometer, and chemical shifts are expressed in parts per million (ppm). Mass spectra were recorded under ESI/HRMS at 61800 resolution using Thermo scientific exactive, mass spectrometer. Absorption spectra were measured on a Shimadzu (UV-2450) UV-Vis. spectrophotometer, and the data analysis was performed using Microsoft excel and Origin 7. SERS measurements were carried out in a WITec Raman microscope (WITec Inc. Germany, alpha 300R) with a laser beam directed to the sample through 20x objective and a Peltier cooled CCD detector. Samples were excited with 633 nm excitation wavelength laser and stokes shifted Raman spectra were collected in the range of 400 to 4000 cm⁻¹ with 1 cm⁻¹ resolution. Prior to every measurement, a calibration with a silicon standard (Raman peak centered at 520 cm⁻¹) was performed. WITec Project plus (v 2.1) software package was used for data evaluation. TEM measurements were performed (JEOL 2010) with an accelerating voltage of 200 KV. The sample was prepared by pipetting a drop of the aqueous solution of nanoparticles onto a 230 mesh copper grid coated with carbon and the sample was allowed to dry in air before the measurement.

3.6.2. Synthesis of gold nanoparticle

Gold nanoparticles were synthesised by the well-established citrate-reduction method (Turkevich Method).^[36] In short, 300 ml of deionised water was boiled at 100 °C with continuous stirring to which 300 µl of gold chloride solution (250 mM) in deionised water was added and allowed to stir for 10 minutes, after that 750 µl trisodium citrate solutions (100 mM) in deionized water was added and waited until the colour changes from yellow to black to purple. After this heating was stopped and allowed to cool to room temperature with continuous stirring. After 2 hours the solution was kept in refrigerator for further use.

3.6.3. Cellular studies

3.6.3.1. Cell culture and metabolic labelling of cell surface glycans

Cells were cultured in Dulbecco's modified Eagle medium (DMEM) with 1% penicillin streptomycin (Gibco) and 10% fetal bovine serum (Gibco) with 5% CO₂ at 37 °C until they were confluent. The cells were then harvested by adding 0.25% EDTA trypsin of appropriate volume for 4 min, followed by the addition of DMEM of double that volume to neutralize the trypsin. The harvested cells were centrifuged at 1500 rpm for 3 min. The supernatant was removed and the cells were suspended with DMEM to achieve a cell concentration of 3000 cells/ml. The cell numbers were determined using a Petroff-Hausser cell counter. Hundred microlitres of cell suspension was seeded per well in a sixteen well glass bottom chamber slide and allowed to grow for 24 hour. After the incubation, DMEM was removed from each well and the adhered cells were rinsed lightly with PBS, which was subsequently removed. 100 µM concentrations of GPs were added to the wells from the stock solution of 50 mM of mentioned compounds in DMSO and left to incubate for 72 hours. The remaining wells were used as untreated control cells. Post-incubation washing was performed for all of the wells using HBSS buffer. All sixteen wells were washed thrice HBSS to remove excess compounds and unbound cells, and then leaving the cells ready for SERS sample preparation.^[39,40]

3.6.3.2. Far-western blotting

HeLa cells were seeded onto T-75 flasks at a density of 2×10^6 cells per flask in 10 ml of media with or without GPs (100 µM). After incubation for three days, the cells were washed twice with PBS (pH 7.4) and harvested with a cell scraper at 4 °C. They were pelleted by centrifugation at 1500 rpm for 5 min, and the cell pellets were re-suspended in 450 µl of lysis buffer (Thermo) + Protease inhibitor cocktail (Sigma Aldrich, USA) incubation at 4 °C for 30 min with intermittent vortexing followed by repeated freeze thaw cycles of 5 min each for 5 times. After 1 min bath sonication at 4 °C, insoluble debris was removed by centrifugation for 20 min at 12000 rpm. Final supernatant concentrations were adjusted by bicinchoninic acid (BCA) protein assay (Pierce, USA) to be 1 mg/ml. Then, 20 µl of the lysate was incubated with azide-PEG3-biotin (2 µl, 5 mM in PBS) for 1 hour at 37 °C along with CuSO₄ (1 mM, 1 µl) and ascorbic acid (5mM, 1 µl). Loading buffer was added to each sample, and samples were resolved on 10% SDS-PAGE gel after heating at 95 °C. Proteins were transferred to PVDF transfer membrane (Merck-Millipore), and the membrane was blocked with 5% bovine serum albumin (BSA) in PBST (0.1% Tween20, pH 7.4) for 1 hour. Then, the membrane was incubated with streptavidin-HRP (diluted 1:1000 in PBST) (Sigma Aldrich,

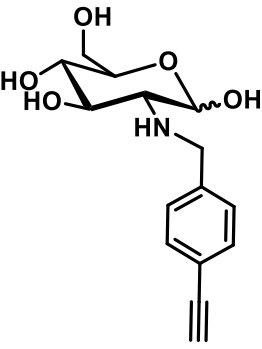
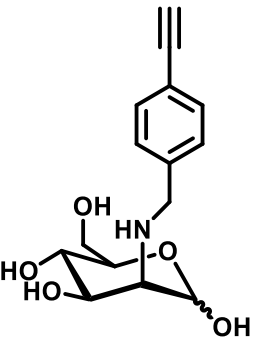
USA) overnight at 4 °C. The membrane was rinsed three times with PBST and developed by using ECL Western Blotting Substrate (Takara, USA).^[38]

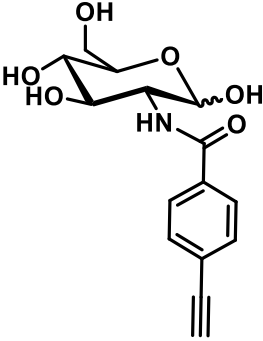
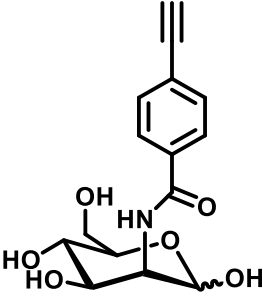
3.6.3.3. Live cell imaging

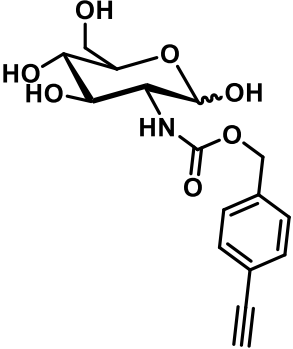
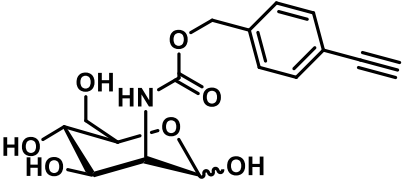
3.6.3.3.1. SERS evaluation of molecules and metabolic labelling

Cells were subjected to SERS spectral mapping mode of the confocal Raman microscope (alpha300R, WITec Inc. Germany). Spectrum at every pixel was taken (Scan range 60 μm X 60μm, 150 X 150 pixel) was taken by 20X objective. Sample was excited with a power of 10 mW from 633 nm laser and mapping was done using 600 g/mm grating is an integration time of 0.022 s using 1991 and 1596 cm⁻¹ peak and the intensity modulated images were prepared by image processing option in control four software.

3.7. Spectral data

<p>Compound 1: GlcNPhAlk</p> 	<p>Molecular formula: C₁₅H₁₈NO₅</p> <p>¹H NMR (500 MHz; CD₃OD): δ 7.26 - 7.34 (m, 8H), 5.10(d, 1H, J =3 Hz) 4.51 (s, 4H), 3.84(m, 2H), 3.65 (m, 2H), 3.35 (d, 2H, J= 7.5 Hz), 2.47(s,1H) ppm.</p> <p>¹³C NMR (125 MHz; CD₃OD): δ 131.7, 128.7, 128.3, 121.0, 97.7, 90.3, 82.8, 77.2, 72.2, 71.6, 70.9, 70.7, 63.4, 61.5, 52.1 ppm.</p> <p>HR-ESIMS: 294.13425 (M+H)⁺</p>
<p>Compound 2: ManNPhAlk</p> 	<p>Molecular formula: C₁₅H₁₈NO₅</p> <p>¹H NMR (500 MHz, CD₃OD): δ 7.404 – 7.37 (m, 4H), 7.33-7.31 (m, 4H), 5.10 (apparent s, 1H), 4.89 (apparent s, 1H), 4.27-4.24 (m, 2H), 4.11-3.99 (d, J = 8.0 Hz, 2H), 3.93-3.90 (t, J = 13.5 Hz, 2H), 3.81-</p>

	<p>3.78 (d, $J = 12.5$ Hz, 2H), 3.75-3.73 (d, $J = 12.5$ Hz, 2H), 3.67-3.65 (d, $J = 12.0$ Hz, 2H), 3.46-3.44 (d, $J = 7.5$ Hz, 1H), 3.39-3.36 (d, $J = 15.0$ Hz, 1H), 2.89 (s, 1H) ppm.</p> <p>^{13}C NMR (125 MHz, CD_3OD): δ 137.7, 132.0, 131.9, 129.9, 128.8, 121.9, 93.3, 90.8, 82.6, 77.7, 76.62, 71.9, 68.9, 67.0, 66.6, 60.9, 60.1, 52.5 ppm.</p> <p>HR-ESIMS: 294.13425 (M+H)⁺</p>
<p>Compound 3: GlcNAcPhAlk</p> 	<p>Molecular formula: $\text{C}_{15}\text{H}_{16}\text{NO}_6$</p> <p>$^1\text{H}$ NMR (500 MHz, CD_3OD): δ 7.75 (d, $J = 7.8$ Hz, 2H), 7.45 (d, $J = 7.7$ Hz, 2H), 5.15 (s, 1H), 3.97 (d, $J = 10.6$ Hz, 1H), 3.80 (d, $J = 10.3$ Hz, 1H), 3.76 (d, $J = 11.3$ Hz, 2H), 3.72 (s, 1H), 3.67 – 3.59 (m, 2H), 3.57 – 3.50 (m, 1H), 3.34 (dd, $J = 17.1, 7.7$ Hz, 1H), 3.31 – 3.24 (m, 1H), 3.12 (m, 1H) ppm.</p> <p>^{13}C NMR (125 MHz, CD_3OD): δ 168.3, 134.2, 131.6, 127.2, 127.2, 126.2, 95.5, 91.1, 82.1, 79.6, 76.6, 71.7, 70.9, 61.4, 55.2, 54.4, 48.1, 47.9 ppm.</p> <p>HR-ESIMS: 330.0963 (M+Na)⁺</p>
<p>Compound 4: ManNAcPhAlk</p> 	<p>Molecular formula: $\text{C}_{15}\text{H}_{16}\text{NO}_6$</p> <p>$^1\text{H}$ NMR (500 MHz, CD_3OD): δ 7.87 – 7.83 (m, 4H), 7.55 (d, $J = 7.5$ Hz, 4H), 5.04 (s, 1H), 5.05 (s, 1H), 4.72 (s, 1H), 4.59 (s, 2H), 4.19 (d, $J = 9.5$ Hz, 2H), 3.95-3.92 (t, $J = 12.5$ Hz, 2H), 3.88 – 3.77 (m, 2H), 3.70 (m, 2H), 2.97 (s, 1H), 2.84 (s, 1H) ppm.</p> <p>^{13}C NMR (125 MHz, CD_3OD): δ 169.3, 134.4, 131.6, 127.6, 127.5, 125.5, 93.7, 93.5, 82.3, 80.0,</p>

	<p>76.8, 73.3, 72.0, 69.5, 66.9, 66.6, 60.6, 60.4, 55.2, 54.4, 48.2, 47.8, 47.3 ppm.</p> <p>HR-ESIMS: 330.0963 (M+Na)⁺</p>
<p>Compound 5: GlcNAcOPhAlk</p> 	<p>Molecular formula: C₁₆H₁₈NO₇</p> <p>¹H NMR (500 MHz, CD₃OD): δ 7.34 – 7.33 (d, <i>J</i> = 6.0 Hz, 2H), 7.26-7.25 (d, <i>J</i> = 7.0 Hz, 2H), 5.02-5.00 (d, <i>J</i> = 10.0 Hz, 1H), 4.49 (s, 2H), 3.70 – 3.68 (d, <i>J</i> = 9.5 Hz, 2H), 3.61-3.58 (m, 2H), 3.55-3.54 (d, <i>J</i> = 7.0 Hz, 1H), 3.48-3.46 (d, <i>J</i> = 7.0 Hz, 1H), 3.35 (s, 1H), 3.28-3.26 (d, <i>J</i> = 10.0 Hz, 1H) ppm.</p> <p>¹³C NMR (125 MHz, CD₃OD): δ 157.3, 135.6, 131.3, 131.67, 127.50, 121.87, 95.4, 86.6, 81.4, 77.3, 75.6, 74.9, 72.8, 69.5, 68.1, 65.3, 64.7, 60.8, 60.4, 55.5 ppm.</p> <p>HR-ESIMS: 360.1065 (M+Na)⁺</p>
<p>Compound 6: ManNAcOPhAlk</p> 	<p>Molecular formula: C₁₆H₁₈NO₇</p> <p>¹H NMR (500 MHz, CD₃OD): δ 7.59 – 7.58 (d, <i>J</i> = 7.0 Hz, 2H), 7.52-7.50 (d, <i>J</i> = 7.5 Hz, 2H), 5.25-5.23 (d, <i>J</i> = 8.5 Hz, 1H), 5.21 (s, 1H), 4.26 – 4.24 (m, 1H), 4.16 (s, 1H), 3.98-3.95 (d, <i>J</i> = 11.5 Hz, 2H), 3.91 (2, 1H), 3.72-3.71 (d, <i>J</i> = 8.5 Hz, 1H), 3.71 (t, <i>J</i> = 8.5 Hz, 1H), 3.63 (s, 1H), 3.46 (s, 1H), 2.96 (s, 1H) ppm.</p> <p>¹³C NMR (125 MHz, CD₃OD): δ 157.6, 137.6, 131.7, 131.6, 127.5, 121.8, 93.8, 82.7, 77.6, 77.5, 72.1, 69.2, 67.00, 65.8, 65.7, 60.8, 55.5 ppm.</p> <p>HR-ESIMS: 360.1065 (M+Na)⁺</p>

3.8. References

- [1] G. Wiederschain, *Biochem.* **2009**, *74*, 819.
- [2] R. Schauer, *Curr. Opin. Struct. Biol.* **2009**, *19*, 507.
- [3] A. Varki, *Trends Mol. Med.* **2008**, *14*, 351.
- [4] J. Du, M. A. Meledeo, Z. Wang, H. S. Khanna, V. D. P. Paruchuri, K. J. Yarema, *Glycobiology* **2009**, *19*, 1382.
- [5] S. J. Luchansky, H. C. Hang, E. Saxon, J. R. Grunwell, C. Yu, D. H. Dube, C. R. Bertozzi, *Methods Enzymol.* **2003**, *362*, 249.
- [6] H. H. Freeze, H. Schachter, *Glycobiology* **2011**, *1*.
- [7] I. Brockhausen, *Biochim. Biophys. Acta - Gen. Subj.* **1999**, *1473*, 67.
- [8] N. Navabi, M. E. V. Johansson, S. Raghavan, S. K. Lindéna, *Infect. Immun.* **2013**, *81*, 829.
- [9] A. R. Burnham-Marusich, C. J. Snodgrass, A. M. Johnson, C. M. Kiyoshi, S. E. Buzby, M. R. Gruner, P. M. Berninsone, *PLoS One* **2012**, *7*.
- [10] R. Daniellou, D. R. J. Palmer, *Carbohydr. Res.* **2006**, *341*, 2145.
- [11] L. Lu, J. Gao, Z. Guo, *Angew. Chemie - Int. Ed.* **2015**, *54*, 9679.
- [12] H. C. Hang, C. Yu, D. L. Kato, C. R. Bertozzi, *Proc. Natl. Acad. Sci. U. S. A.* **2003**, *100*, 14846.
- [13] L. A. Marcaurelle, C. R. Bertozzi, *J. Am. Chem. Soc.* **2001**, *123*, 1587.
- [14] R. Sprung, A. Nandi, Y. Chen, S. C. Kim, D. Barma, J. R. Falck, Y. Zhao, *J. Proteome Res.* **2005**, *4*, 950.
- [15] K. N. Chuh, B. W. Zaro, F. Piller, V. Piller, M. R. Pratt, *J. Am. Chem. Soc.* **2014**, *136*, 12283.
- [16] C. Hart, L. G. Chase, M. Hajivandi, B. Agnew, *Methods Mol. Biol.* **2011**, *698*, 459.

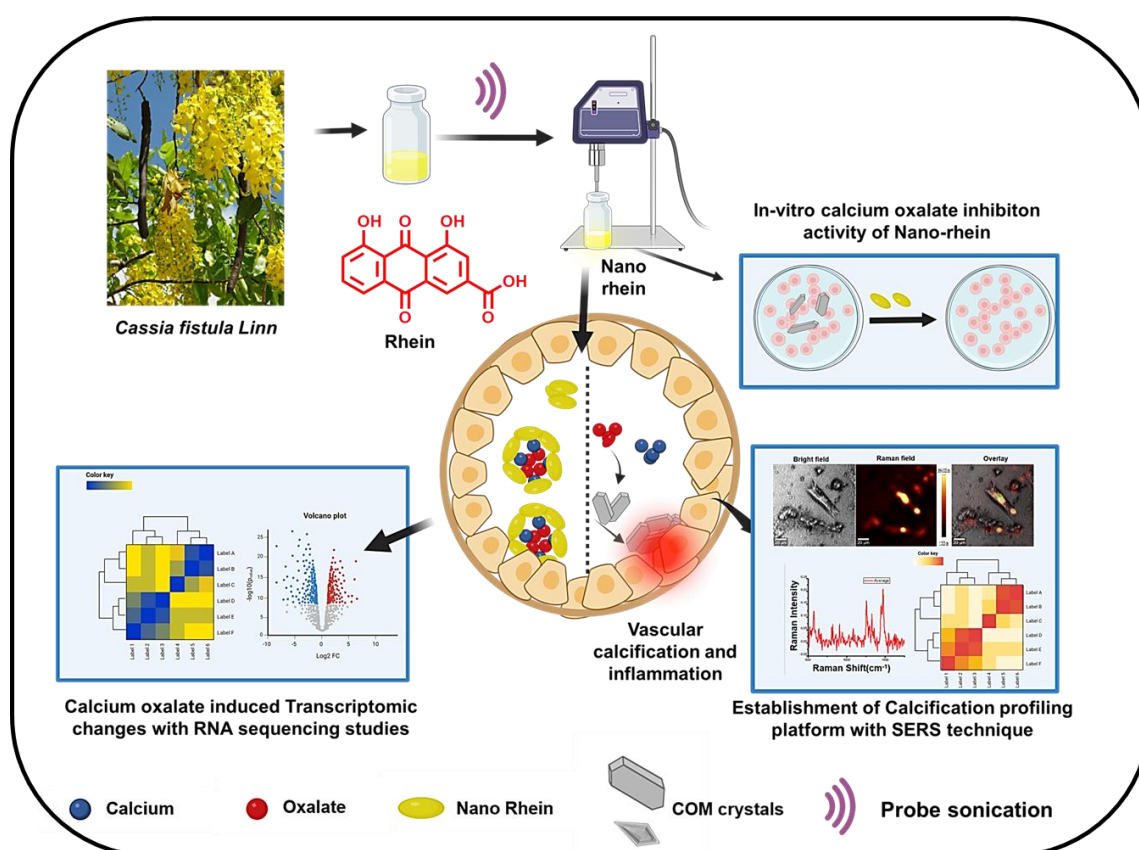
- [17] B. W. Zaro, H. C. Hang, M. R. Pratt, *951*, 57.
- [18] E. Fugier, A. Dumont, A. Malleron, E. Poquet, J. M. Pons, A. Baron, B. Vauzeilles, S. Dukan, *PLoS One* **2015**, *10*, 1.
- [19] M. M. n, Eunsung Mouradian, and K. H. Michael R. Bronsert, William G. Henderson, Robert Valuck, Patrick Hosokawa, *Bone* **2008**, *23*, 1.
- [20] Oken, *Bone* **2008**, *23*, 1.
- [21] E. Lansing, **1982**, *207*, 273.
- [22] L. Cenciotti, A. Mariotti, *Minerva Med.* **1960**, *51*, 4120.
- [23] S. Ghosh, S. Roseman, *Proc. Natl. Acad. Sci. U. S. A.* **1961**, *47*, 955.
- [24] S. Roseman, G. W. Jourdian, D. Watson, R. Rood, *Proc. Natl. Acad. Sci. U. S. A.* **1961**, *47*, 958.
- [25] L. Warren, R. S. Blacklow, *J. Biol. Chem.* **1962**, *237*, 3527.
- [26] L. Warren, **1961**, *4*, 232.
- [27] S. Hinderlich, R. Stäsche, R. Zeitler, W. Reutter, *J. Biol. Chem.* **1997**, *272*, 24313.
- [28] R. Stäsche, S. Hinderlich, C. Weise, K. Effertz, L. Lucka, P. Moormann, W. Reutter, *J. Biol. Chem.* **1997**, *272*, 24319.
- [29] K. Effertz, S. Hinderlich, W. Reutter, *J. Biol. Chem.* **1999**, *274*, 28771.
- [30] A. N. E. W. Metabolite, I. From, U. Of, A. P. With, **1979**, 583.
- [31] A. Paneque, H. Fortus, J. Zheng, G. Werlen, E. Jacinto, *Genes (Basel)*. **2023**, *14*.
- [32] C. Agatemor, M. J. Buettner, R. Ariss, K. Muthiah, C. T. Saeui, K. J. Yarema, *Nat. Rev. Chem.* **2019**, *3*, 605.
- [33] E. Saxon, S. J. Luchansky, H. C. Hang, C. Yu, S. C. Lee, C. R. Bertozzi, *J. Am. Chem. Soc.* **2002**, *124*, 14893.
- [34] H. Möller, V. Böhrsch, J. Bentrop, J. Bender, S. Hinderlich, C. P. R. Hackenberger,

Angew. Chemie - Int. Ed. **2012**, *51*, 5986.

- [35] W. Qin, K. Qin, X. Fan, L. Peng, W. Hong, Y. Zhu, P. Lv, Y. Du, R. Huang, M. Han, B. Cheng, Y. Liu, W. Zhou, C. Wang, X. Chen, *Angew. Chemie - Int. Ed.* **2018**, *57*, 1817.
- [36] J. Turkevich, J.; Stevenson, P. C.; Hillier, **1951**.
- [37] D. Chen, Y. Lin, Y. Fan, L. Li, C. Tan, J. Wang, H. Lin, J. Gao, *Angew. Chemie - Int. Ed.* **2023**, *62*.
- [38] S. Lee, H. Koo, J. H. Na, S. J. Han, H. S. Min, S. J. Lee, S. H. Kim, S. H. Yun, S. Y. Jeong, I. C. Kwon, K. Choi, K. Kim, *ACS Nano* **2014**, *8*, 2048.
- [39] C. D. Rillahan, A. Antonopoulos, C. T. Lefort, R. Sonon, K. Ley, A. Dell, S. M. Haslam, J. C. Paulson, *Nat. Chem. Biol.* **2013**, *8*, 661.
- [40] S. T. Laughlin, C. R. Bertozzi, *Proc. Natl. Acad. Sci. U. S. A.* **2009**, *106*, 12.

CHAPTER 4

Repurposing nano-dimensions of a small phyto molecule, rhein into nano-rhein, to investigate its efficacy on hypercalciuria-induced nephropathies by SERS-imaging



4.1. Abstract

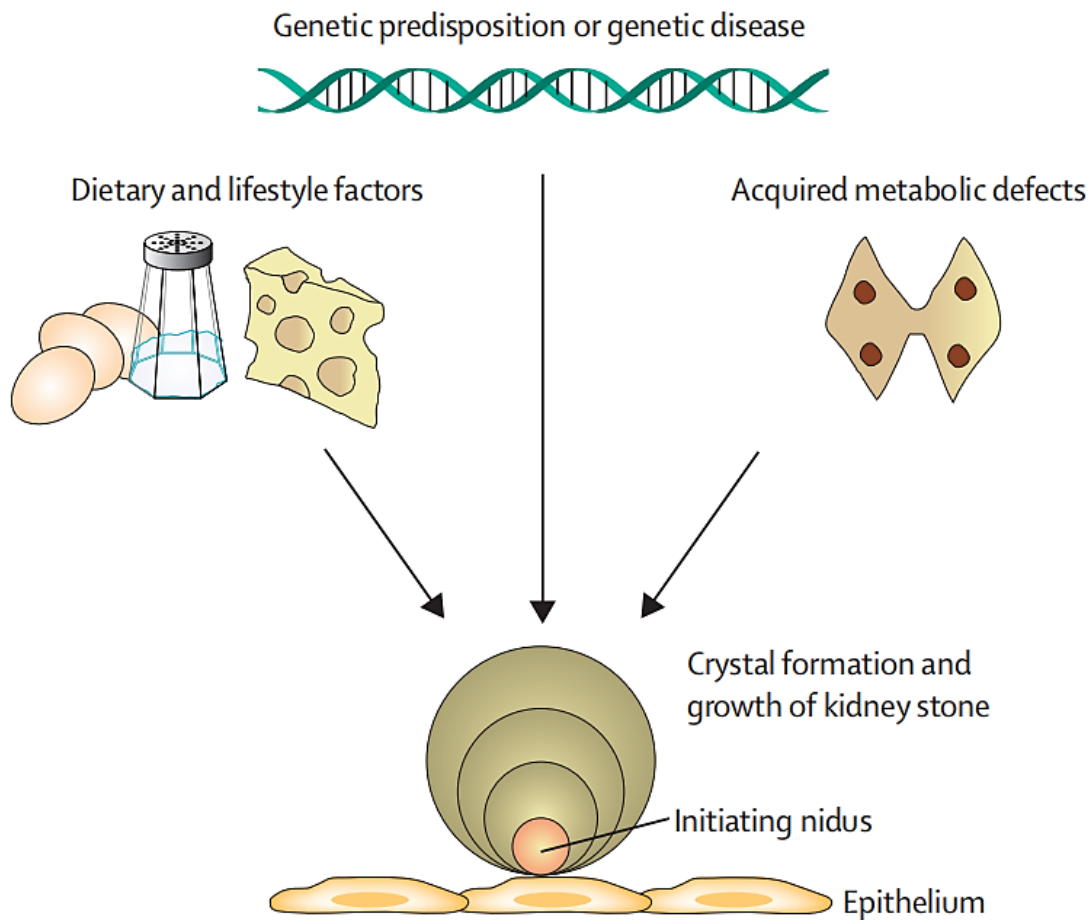
Renal disorders induced by calcium oxalate (CaOx) crystals potentiate a complex pathophysiological landscape devoid of effective pharmacological interventions. Although CaOx crystallization inhibitors have been suggested as a therapeutic approach in the past, the identification of potent molecules remains notably limited. A bioactive herbal compound, rhein, isolated from *Cassia fistula* Linn. (CF), known for its well-documented anti-inflammatory and anti-cancer properties, whereas its role as a CaOx inhibitor received inadequate scrutiny. The clinical viability of rhein is compromised by its inherent limitations

on poor aqueous solubility and low bioavailability. To surmount these challenges, the simplest and fastest sonochemical self-assembly technique was engineered to transform rhein into nano-rhein, aiming to augment its inhibitory efficacy towards CaOx. The anti-calcification properties of both rhein and nano-rhein were assessed through Alizarin Red S staining in an *in vitro* model employing human embryonic kidney cells HEK-293. Furthermore, a robust SERS imaging platform to monitor calcification and its growth retardation processes was redefined through the utilization of surface-enhanced Raman scattering (SERS), which otherwise had poor signal strength to the CaOx crystals in the Raman/SERS analysis. This newly evolved platform introduces a SERS-based-Alizarin Red S profiling of CaOx inhibition with a fold change of nearly 50 times by the treatment of nano-rhein. Subsequently, SERS imaging has been adopted to monitor the changes in the expression of cell surface glycans during calcification and decalcification processes after rhein/nano-rhein treatment. A comprehensive RNA sequencing was conducted to analyze the transcriptomic modifications induced by CaOx exposure, and the mitigating effects of rhein/nano-rhein were further substantiated by Reactome pathway analysis to deepen our understanding of cellular responses to CaOx and interpret changes observed through cellular imaging. It demonstrated that genes linked to inflammation and cell proliferation pathways, such as INHBA, TNFRSF12A, and FOS family, which are upregulated during calcification, become downregulated upon NR treatment. Therefore, for the first time, the current exploration offers intricate insights into the potential of rhein, particularly in its nano-form, as a promising therapeutic entity for CaOx-induced nephropathies, shedding light on molecular mechanisms underlying its protective anti-inflammatory effects.

4.2. Introduction

Vascular calcification (VC) stands as a prominent etiological contributor to cardiovascular pathologies, particularly in individuals grappling with chronic kidney disease (CKD), end-stage renal diseases (ERSD), and metabolic disorders.^[1] CKD represents a pathological state characterized by a gradual and progressive decline in renal function over time.^[2] This degeneration results in the accumulation of waste products and excess fluids within the body, giving rise to various systemic complications. Among these complications is the emergence of calcium oxalate (CaOx) crystals in the kidney tubules, a condition identified as Oxalate Nephropathy (ON).^[3] Hyperoxaluria, characterized by excessive oxalate excretion in the urine, often underlies the pathogenesis of ON.^[4] The surplus oxalate in the urine binds with

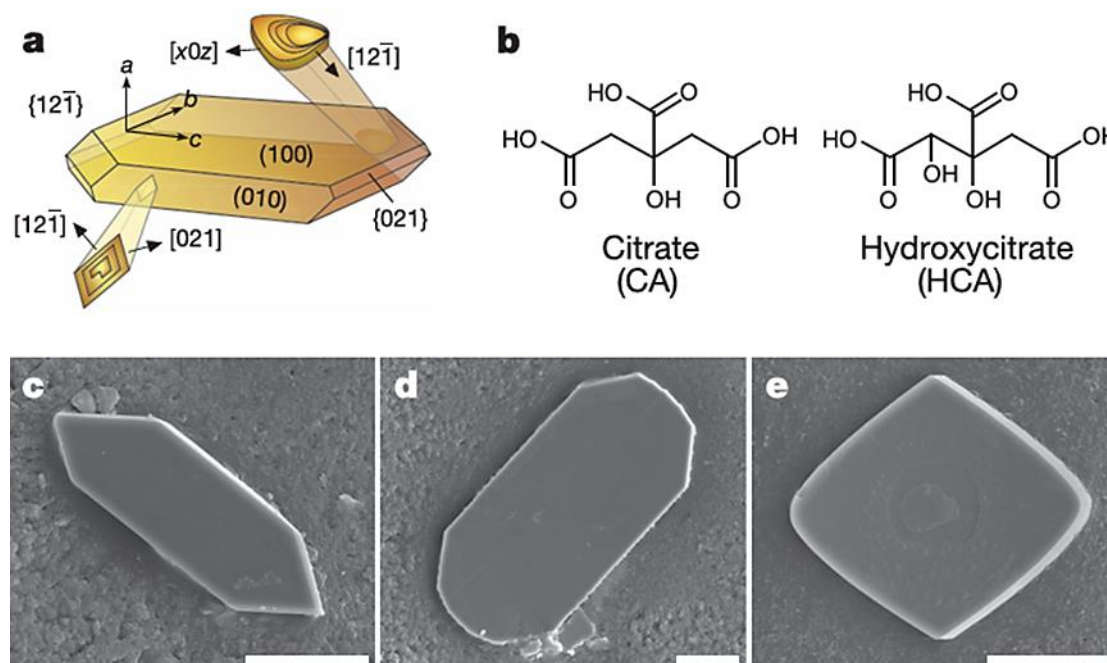
calcium, forming kidney stones and crystals, thereby contributing to the development of ON. The recurrence of kidney stones and crystals can inflict considerable damage on the kidneys,



Scheme 4.1: Pathogenesis of kidney stones (adapted from : *Lancet*, 2006, 367, 333–44)

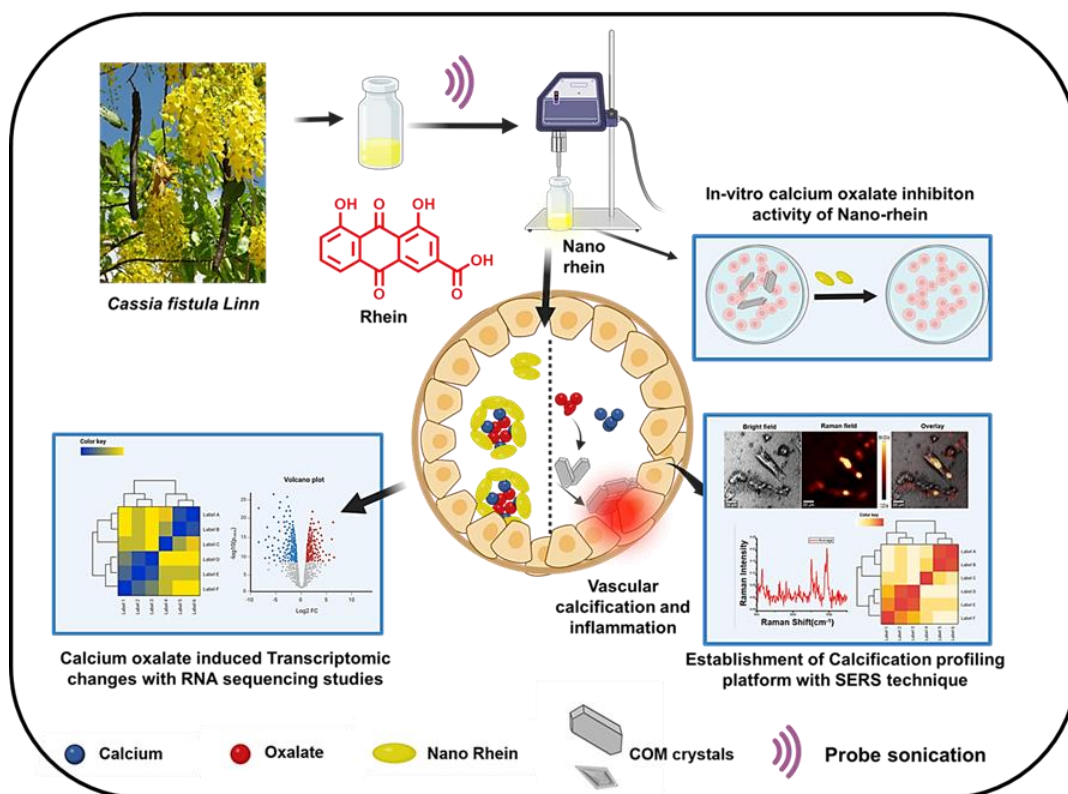
potentially culminating in kidney failure.^[5] In the context of CKD, the systemic levels of oxalate surge due to the kidneys serving as the primary route of oxalate excretion. Diminished Glomerular filtration rate (GFR) results in heightened concentrations of oxalate in plasma and glomerular ultra-filtrate, exposing the remaining tubular cells to increased oxalate concentrations. This exposure can prompt the formation of oxalate clumps or crystals, further exacerbating renal damage as these calcium oxalate crystals traverse through the renal system.^[6] Despite available treatments aimed at symptom management and slowing CKD progression, a definitive cure for the disease remains elusive. Consequently, there is a pressing need for research into innovative therapeutic strategies for CKD. Current therapeutic interventions under consideration encompass a spectrum of approaches, including the use of

phosphate binders, vitamin K, sodium thiosulphate, Myoinositol hexaphosphate (IP6), bisphosphonates, TNAP inhibitors, and Denosumab.^[7]



Scheme 4.2: Effect of inhibitors on COM crystallization. a) COM crystal habit with indexed faces. b) Molecular structures of CA and HCA. c–e) SEM images of COM crystals in the absence of inhibitor (control C) (c) and in the presence of $20 \mu\text{g ml}^{-1}$ CA (d) and in the presence of $20 \mu\text{g ml}^{-1}$ HCA (e). Scale bars, $20 \mu\text{m}$ (adapted from *Adv. Sci.*, 2024, 11, e2400642).

However, currently, there is no effective treatment to reduce or reverse calcifications. Nevertheless, some treatments can decelerate calcification's progression, such as phosphate binders, bisphosphonates, active vitamin D, sodium thiosulphate, and cinacalcet.^[1] Reports indicate that hydroxy-citrate, when ingested orally, is excreted via urine, positioning it as a promising therapeutic agent for stone treatment.^[8–10] Bio macromolecules, particularly polysaccharides enriched with acidic polyanionic groups, have been identified as potent inhibitors of CaOx calculus formation.^[11] Rhein, a lipophilic anthraquinone characterized as 4,5-dihydroxyanthraquinone-2-carboxylic acid, is abundantly present in various medicinal herbs.^[12] The biological activities of rhein, particularly those pertinent to human health, are currently under active investigation.



Scheme 4.3: Schematic representation of isolation of Rhein, Synthesis of Nanorhein, In-vitro anti calcium oxalate inhibition activity using Alizarin Red S assay, Development of calcification profiling platform using SERS technique and RNA sequencing and transcriptomic analysis.

4.3. Aim and scope of the study: Accumulating evidence indicates that rhein exhibits a plethora of pharmacological properties, encompassing hepatoprotective, nephroprotective, anti-inflammatory, antioxidant, anticancer, and antimicrobial activities.^[11–13] It has demonstrated inhibitory effects on a variety of cancers, including but not limited to, breast, cervical, colon, lung, and ovarian cancers, under both *in vitro* and *in vivo* conditions. Recent research has shed light on the ability of this compound to modulate diverse signaling pathways within cancer cells, thereby inhibiting angiogenesis and impeding the progression of various cancer types despite the therapeutic potential of rhein, its clinical application is significantly limited due to its poor aqueous solubility and low bioavailability, which is primarily attributed to the metabolism of glucuronidation in the liver^[11]. To overcome these limitations and enhance the therapeutic efficacy of rhein, several strategies have been exploited, including the development of polymeric microparticles and nanoparticles encapsulating rhein.^[14,15] However, these approaches often encounter challenges such as drug loss during the fabrication process and premature release of the payload, leading to lower

drug loading and potential systemic toxicity.^[14,16,17] It is proposed that a promising solution to these challenges could be the directed self-assembly of rhein into a nanoparticle form with the help of probe sonication, which may offer enhanced therapeutic efficacy. In the present investigation, rhein, an active compound isolated from *Cassia fistula* Linn. (CF), was found to self-assemble into nanoparticles through intermolecular π - π interactions and hydrogen bonding. Notably, these rhein nanoparticles, which are named nano-rhein (NR) exhibited superior anti-calcification properties compared to rhein in its free form while maintaining minimal cytotoxicity. A comprehensive evaluation of the molecular processes involved was conducted to elucidate the mechanisms underlying this enhanced CaOx inhibitor activity. The present findings emphasize that the nanoparticle of rhein is a much better candidate for CaOx inhibition than its molecular form of the compound. These characteristics position rhein nanoparticles as a promising therapeutic entity for the treatment of nephrocalcinosis. Further studies are warranted to fully understand the potential of these nanoparticles in clinical applications. As per our knowledge, it is the first time to report the CaOx inhibitory effects of rhein and its nano form using the SERS imaging technique.

4.4. Results and Discussion

4.4.1. Synthesis and morphological characterization of nano-rhein (NR)

Isolation of the rhein was achieved from ethanol extract of CF seeds and flowers (**Figure 4.19**). Anti-urolithiasis assessment conducted at both the extract and compound levels, utilizing Alizarin Red S (ARS) assays, has demonstrated the potent anti-calcification properties of the ethanolic extract of CF and the compound rhein (**Figure 4.5**). In this work, the sonochemical self-assembly of rhein molecules for enhanced inhibition of CaOx crystals was utilized (**Figure 4.1a**). Rhein NPs (NR) were characterized by DLS, TEM, SEM, and AFM imaging respectively (**Figure 4.1b-f**). Its morphology was found to be belt-like with an average size distribution of 280 nm. The absorption spectra revealed the characteristic peak associated with the anthraquinone core. DLS experiment demonstrated the stability of NR for up to 30 days at ambient temperature (**Figure 4.1c**).

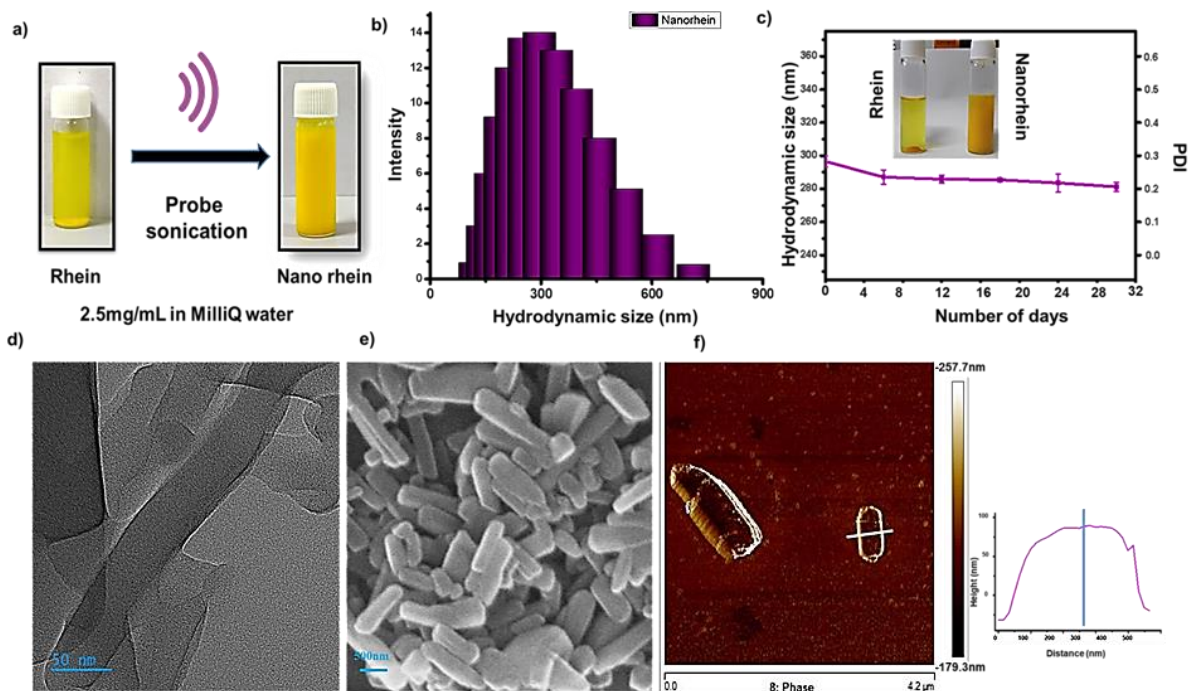


Figure 4.1: a) Synthetic procedure of nano rhein b) DLS spectrum of nano rhein c) Stability of rhein and nano rhein at room temperature d) TEM e) SEM and f) AFM images of nano rhein.

The hydrodynamic diameter measured was unchanged over 30 days, indicating the superior stability of NR at room temperature. In addition, the self-assembled NPs maintained colloidal stability in 50% FBS (fetal bovine serum) as observed with the SEM analysis (**Figure 4.2**).

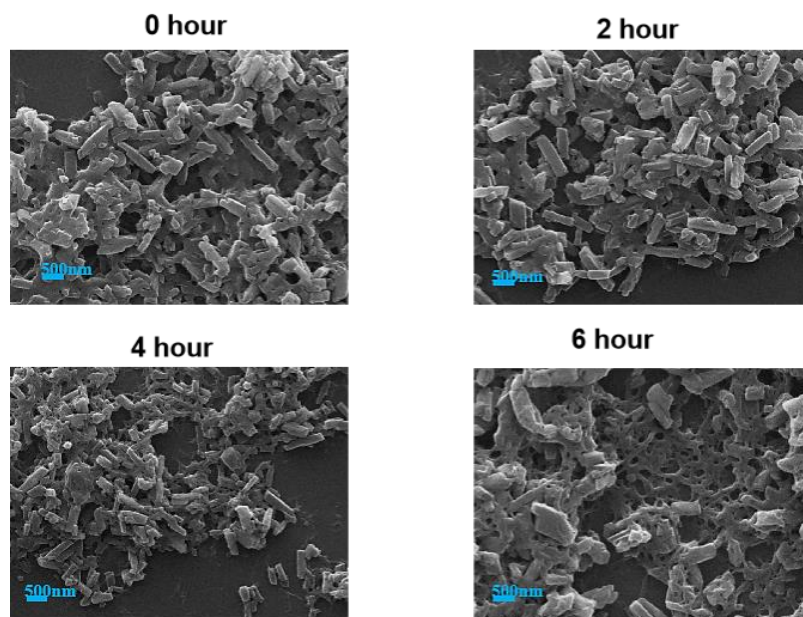
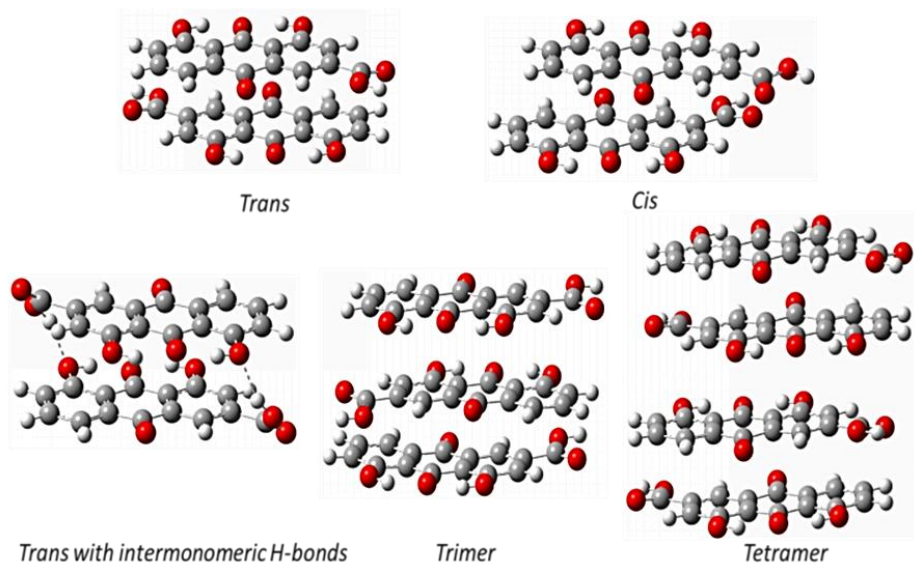
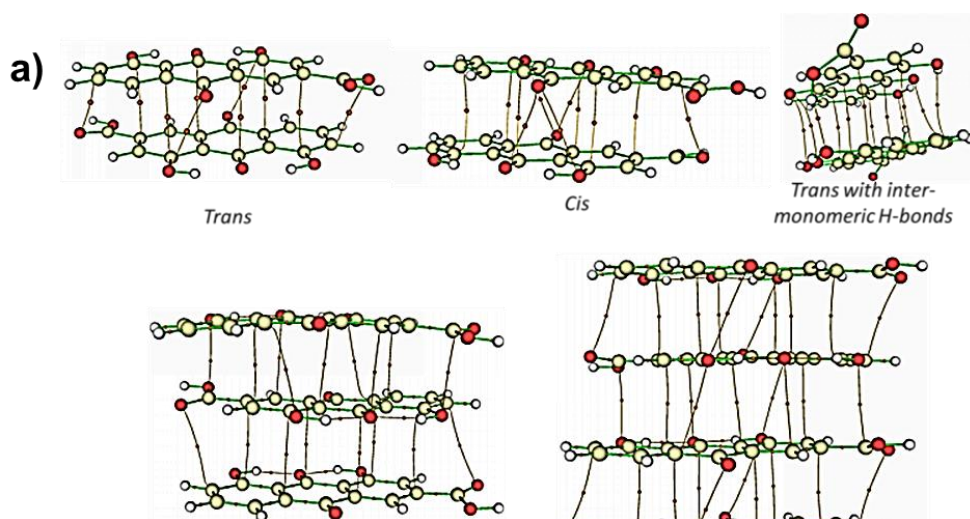


Figure 4.2: Stability of Nano Rhein in 50%FBS

Although no surfactants or excipients were applied, the NR displayed desirable stability without any precipitation and phase separation.

4.4.2 The self-assembly mechanism of rhein nanoparticles

The structure of rhein aggregates was examined using DFT calculations. All the calculations are performed using the Gaussian 09 suite of programs employing Minnesota hybrid density functional M06-2x at the 6-311+G(d,p) basis set. The stable structure of rhein dimeric form has been calculated resembling its stacking interactions (**Figure 4.3c**). Dimeric form with carboxyl functionalities lying in a trans manner is the most stable form over the cis (by 2.06 kcal/mol) or the ones with inter monomeric hydrogen bonds. This particular geometry was also found to have more stabilization energy due to dimer formation (-23.48 kcal/mol) (**Figure 4.3b**). The monomers are stacked by a distance of 3.23 Å in trans and 3.18 Å in cis conformer. From the perfect stacking arrangement, the central ring of one monomer is found to be displaced by an angle of 22° to the next. This slipping is slightly more in the case of the cis conformer, while it is reduced to 20° in the H-bonded conformer. The analysis aims to quantify the stacking interactions. The electron density and the laplacian of electron density calculated for the bond critical points between the monomers lie in the range specified for weak noncovalent interactions.^[18] All the C-C bond critical points calculated between the monomers had their electron density lying in the range 0.0075-0.0085 au (trans), 0.0074-0.0084 au (cis), and the laplacian of electron density lying in the range 0.025-0.026 au (trans), 0.021-0.025 au (cis) (**Figure 4.3a**).



c)

System	Energy (a.u.)	Stabilization Energy (kcal mol ⁻¹)	Stacking Energy [#] (kcal mol ⁻¹)
Trans- Rhein Dimer	-2055.471178	-23.48	-23.48
Cis-Rhein Dimer	-2055.467902	-21.42	-21.42
Trans-Rhein Trimer	-3083.219287	-43.08	-21.54
Trans-Rhein Tetramer	-4110.971402	-65.19	-21.73

[#] Stacking energy = Stabilization energy/n-1 where n is the number of rhein monomers involved in stacking

Figure 4.3: a) Bond critical points calculated between the monomers in various conformers of Rhein dimer b) Energy optimized structures of the monomers in various conformers of rhein dimer, trimer, and tetramer c) energy parameters of rhein oligomers

To further elucidate the self-assembly mechanism of NR, additional spectroscopy studies were conducted (**Figure 4.4**). Analysis of the FT-IR results revealed a characteristic absorption peak for the C=O peak at 1692 cm^{-1} shifted to 1631 cm^{-1} (**Figure 4.4a**). These alterations suggest the participation of hydrogen bonds in the self-assembly. The observed maximum redshift was associated with the existence of the anthraquinone excimer, primarily influencing the self-assembly process through π - π interactions.^[19] The results obtained from the X-ray diffraction (XRD) analysis provided further substantiation for our findings. A prominent peak was observed at a d-spacing value of 3.3 \AA . This peak is indicative of the characteristic intermolecular distance associated with π - π stacking interactions between the two molecules (**Figure 4.4a**).^[19] Notably, in the UV-visible spectrum, the peak underwent a bathochromic shift from 434 nm to 481 nm during the preparation of NR via the probe sonication method (**Figure 4.4c**). This shift can be attributed to the π - π interactions inherent to the anthraquinone structure. Furthermore, this observation suggests a transformation in the aggregate configuration from H-type to J-type aggregation, which is indicative of changes in the molecular arrangement and packing within the NR structure.^[19]

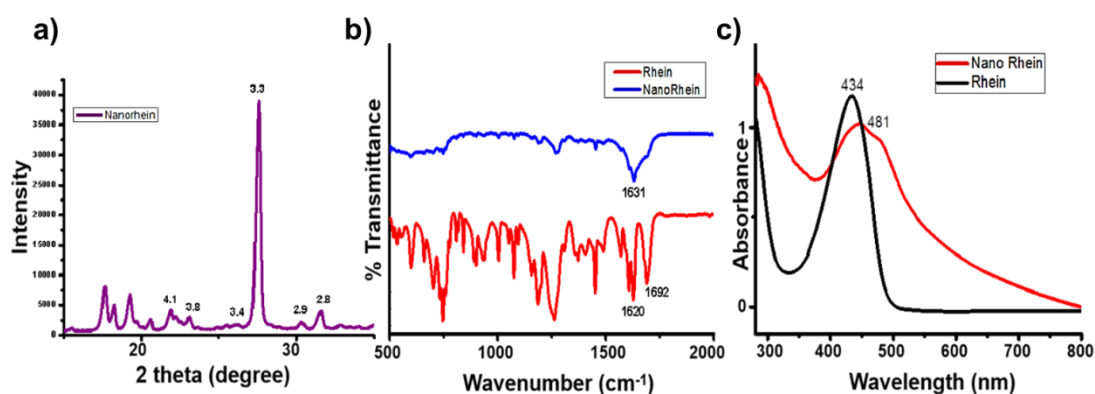


Figure 4.4: a) PXRD analysis of NR b) IR analysis of rhein and NR c) UV-Visible spectrum of rhein and NR.

4.4.3. Anti-calcification property of rhein and NR

Ethanol extracts derived from the flower and seed components of CF were found to be the most effective in ARS staining experiments (**Figure 4.5**). The ARS staining experiment is considered the gold standard for the quantification of calcium mineralization and is thus widely used among the scientific community.^[20]

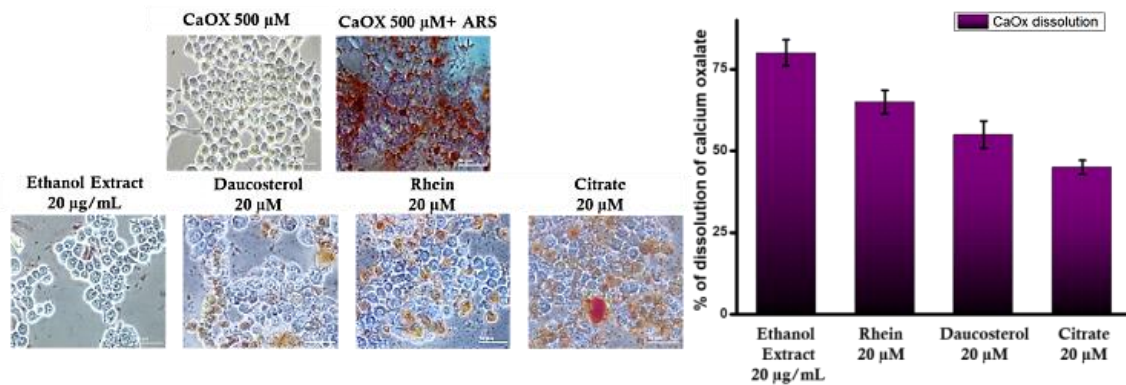


Figure 4.5: ARS staining for mineralization. The calcified minerals appear orange-red in color (original magnification x 40) Cells without incubation of CaOx; Cells treated with 1:1 CaOx; Cells treated with 20 μg/ml EtOH extract and then treated with CaOx; Cells treated with 20 μM Rhein and then treated with CaOx Cells treated with 20 μM Daucosterol and then treated with CaOx; Cells treated with 20 μM Citrate, standard and then treated with CaOx; and % of dissolution of both oxalate crystals of calcium for different compounds and extracts isolated from *Cassia fistula*.

Five compounds were isolated from these ethanol extracts, with the anthraquinone rhein being the most active one in the in-vitro anti-urolithiasis studies. In this study conducted at the compound level, rhein demonstrated superior activity compared to other compounds and even outperformed the positive control, citrate (**Figure 4.6**).

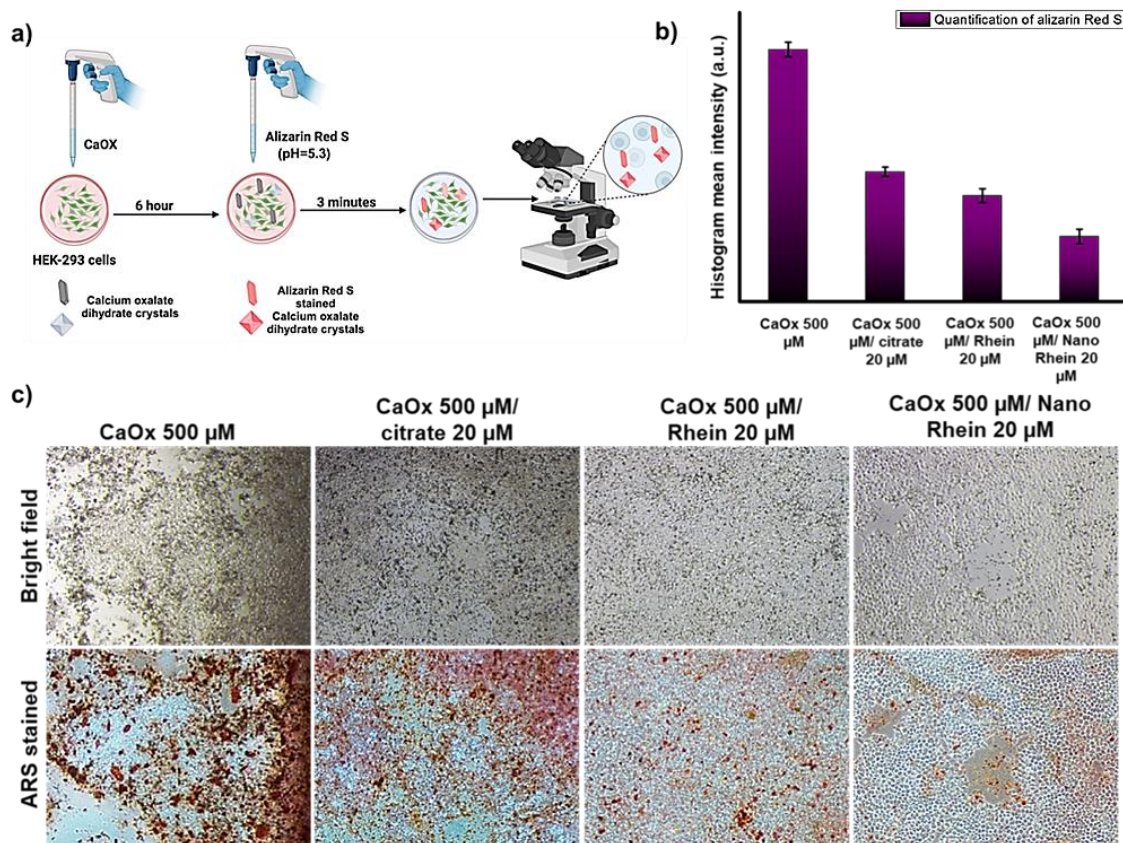


Figure 4.6: ARS staining experiment- Bright field images of a) CaOx 500 μM b) CaOx 500 μM/rhein 20 μM c) CaOx 500 μM/nano rhein 20 μM. Stained images of d) CaOx 500 μM e) CaOx 500 μM/rhein 20 μM and f) CaOx 500 μM/nano rhein 20 μM. Scale bar 200 μm

The cytotoxic potential of the investigated compounds was quantitatively assessed *via* the 3-(4, 5-dimethylthiazol-2-yl)-2,5-diphenyltetrazolium bromide (MTT) assay. The administration of both rhein nanoparticles and the rhein molecule was observed to exhibit negligible cytotoxic effects on the human embryonic kidney cells HEK-293. This observation was consistent across a concentration range of 20-50 μM, with the assessment conducted at the 24-hour mark post-administration. The lack of significant cytotoxicity suggests that these compounds, within the specified concentration range, maintain the viability of HEK-293 cells (**Figure 4.7**). Upon administration of the rhein compound at a concentration of 75 μM, a significant reduction in the viability of HEK-293 cells was observed, with a decrease of 29% compared to the NR. Intriguingly, the viability of HEK-293 cells remained unaffected across various concentrations when treated with NR. These findings indicate that the cytotoxicity exhibited by NR is notably lower than that of the rhein molecule.

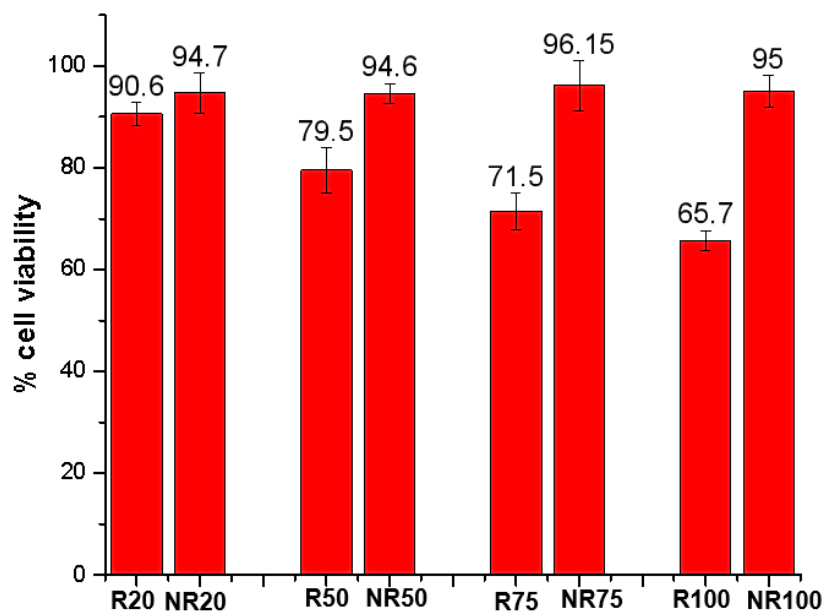


Figure 4.7: Comparison of results from MTT assays involving Rhein and NR

The biocompatibility of NR with varying concentrations of 10 μM to 200 μM was also assessed with hemolysis assay (**Figure 4.8**). This suggests that the transformation of rhein into nanoparticles could be a promising strategy for reducing its cytotoxic effects on HEK-293 cells, thereby potentially enhancing its therapeutic index.

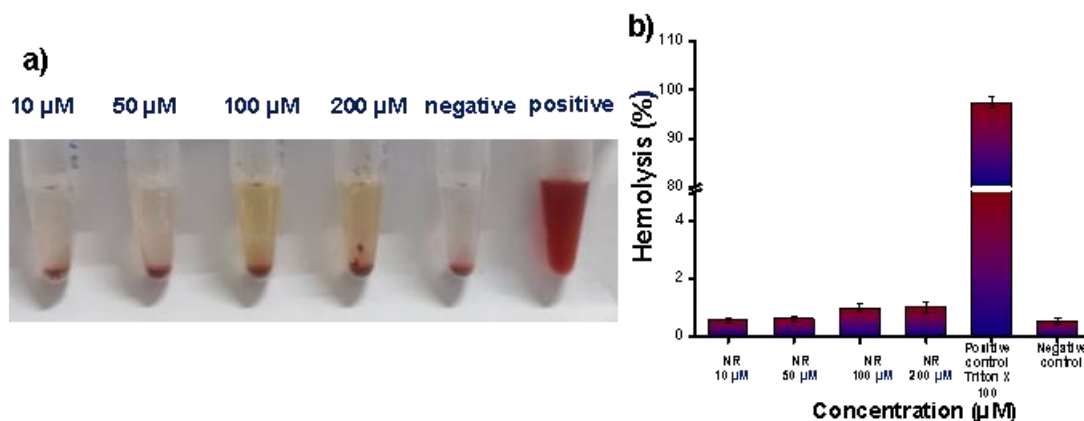


Figure 4.8: a) Hemolysis assay performed with each concentration of NR b) Graphical representation of calculated percentage hemolysis.

4.4.4. Mechanism of CaOx inhibition by NR

It is expected that carboxylate (COO^-) groups present in NR may have the ability to coordinate with Ca^{2+} ions and hydrogen bonding interactions can be established between the

hydroxyl (OH) groups in NR and the carboxylate ions in the oxalate groups of amorphous calcium-oxalate nanoparticles.^[9,21] To elucidate the mechanism of CaOx inhibition by NR, a Scanning Electron Microscopy (SEM) analysis was conducted (**Figure 4.9**).

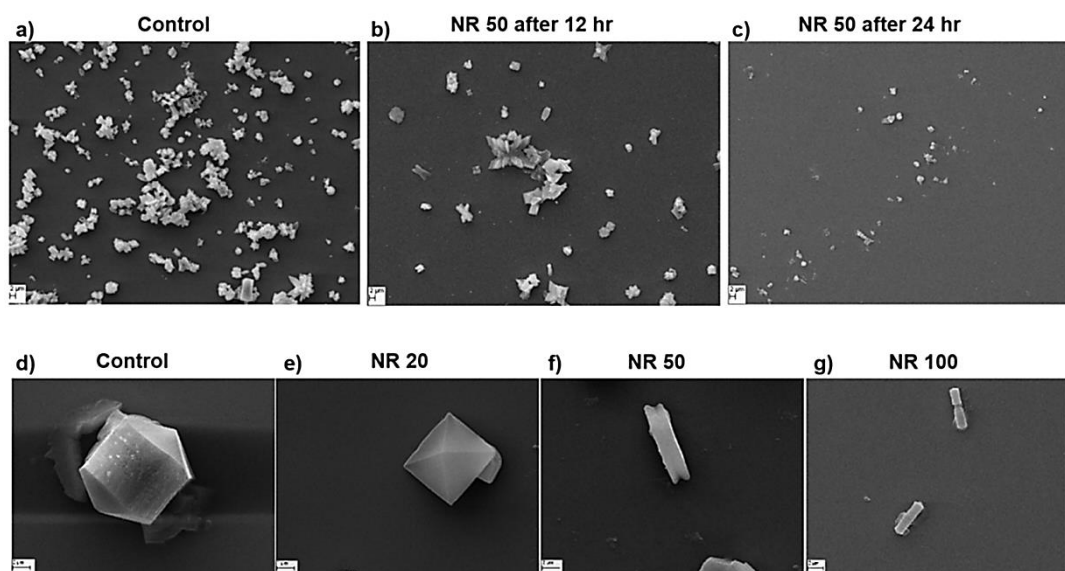


Figure 4.9: Mechanism of CaOx inhibition by NR-SEM images of a-c) Reduction of CaOx crystals on treatment with the NR, CaOx 1 mM as control, CaOx 500 μ M/NR 50 μ M 12hour, CaOx 500 μ M/NR 50 μ M 24 hour d-g) Conversion of calcium oxalate monohydrate (COM) crystals to calcium oxalate dihydrate (COD) and needle-like crystals on treatment with the CaOx 500 μ M as control, CaOx 500 μ M/NR 20 μ M 24 hour, CaOx 500 μ M/NR 50 μ M 24 hour, CaOx 500 μ M/NR 100 μ M 24 hour.

In a 12-well plate, CaCl_2 and $\text{Na}_2\text{C}_2\text{O}_4$ (NaOx) were added in situ to achieve a final concentration of 1 mM each. This was accomplished by diluting a 50 mM stock solution of each compound with Phosphate-Buffered Saline (PBS, pH=6.2). The formation of COM-type crystals was observed in the control and early incubation stages of CaOx and NR. However, as the incubation time increased, the crystal size began to shrink, transitioning from an octahedral shape to a linear one. This suggests that the addition of NR significantly inhibited the bulk crystallization of CaOx (**Figure 4.9 a, b and c**).

In addition, certain growth specific to the face of the crystal was observed. This could be due to the inhibitor's tendency to bind preferentially to a particular face of the crystal, which is determined by its unique molecular surface arrangement. This phenomenon was demonstrated by the transformation of COM crystals into a needle-like shape as the concentrations of NR's increased (**Figure 4.9 d, e, f, and g**). This was also confirmed with

the Raman spectral analysis where the NR-treated CaOx showed different patterns in both the Raman spectrum (**Figure 4.10**).

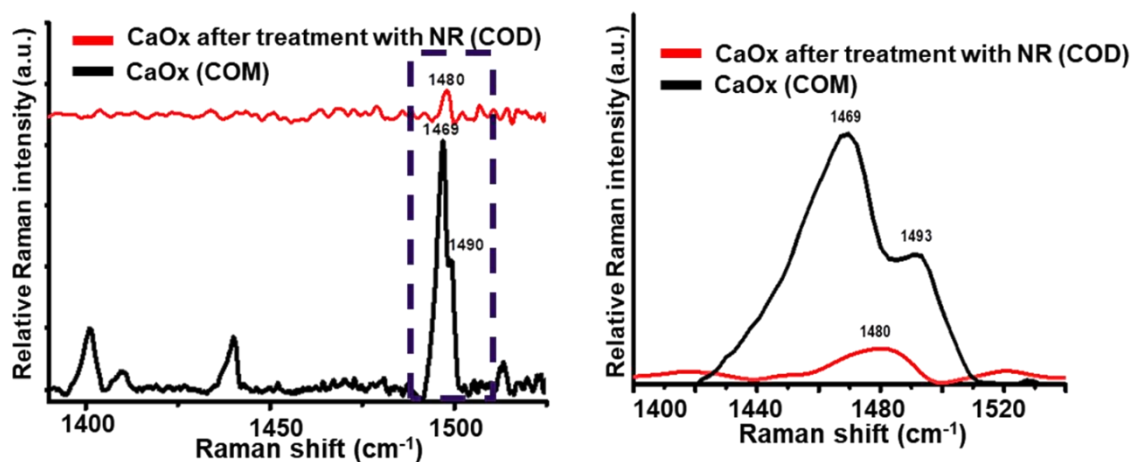


Figure 4.10: COD conversion experiments on NR-treated CaOx crystals Raman spectra of CaOx (COM) and NR-treated CaOx (COD), expanded view of the Raman spectrum

DFT studies showed that the preferable deprotonation at the carboxyl sites and the stabilization of the resulting anion by intramolecular hydrogen bonding would facilitate its salt formation with cations. The energy of formation for the calcium salt of deprotonated cis-rhein dimer from its anionic monomer is computed to be -440.29 kcal/mol. This value is comparable to the energy of the formation of stable calcium oxalate from its ions (-514.53 kcal/mol) (**Figure 4.11**).

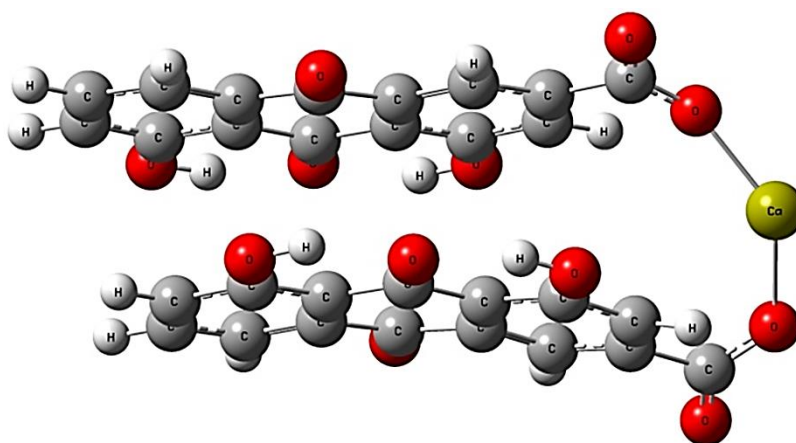


Figure 4.11: Energy optimized structure of Ca salt of rhein dimer (cis)

4.4.5. SERS-imaging platform for monitoring calcification processes

In this study, surface-enhanced Raman spectroscopy (SERS), an ultrasensitive analytical technique that intensifies the Raman scattering phenomenon of molecules adsorbed onto through nanostructures or coarse nano-metallic surfaces was utilized.^[22] This method enables the rapid detection of chemical species with high sensitivity and molecular-level specificity^[23]. Despite the potential of SERS in various applications, its use in *in-vitro* calcification image profiling platforms for analyzing CaOx inhibitors has been scarcely reported.

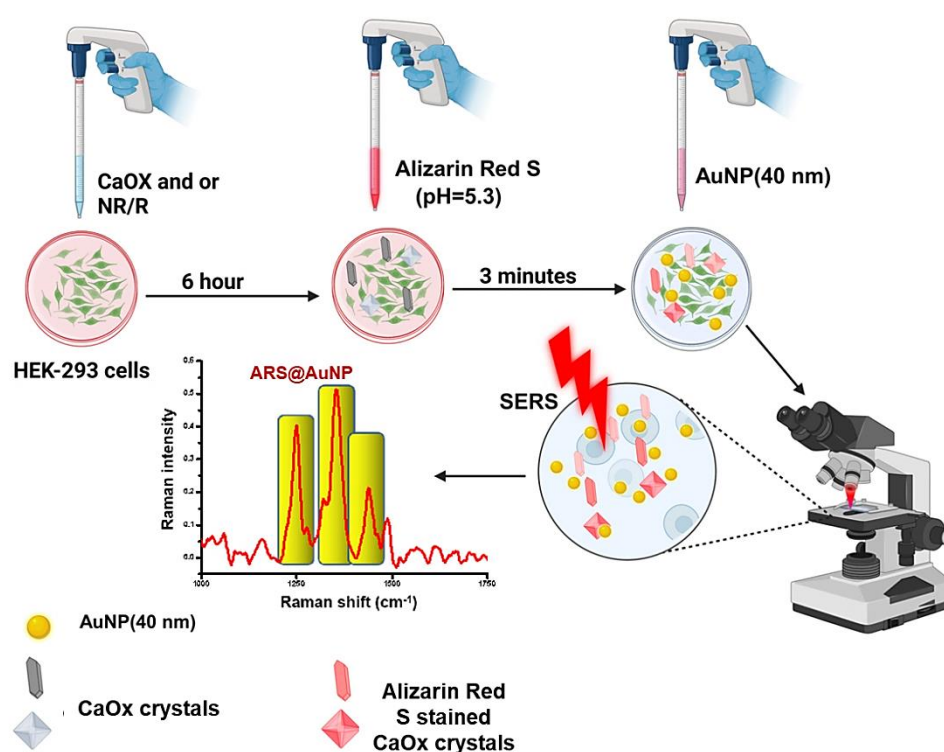


Figure 4.12: Schematic representation of SERS-based Alizarin Red SARS assay

For the first time, the SERS imaging platform has been evolved for profiling CaOx inhibitors and various calcification processes (**Figure 4.12**). A SERS-based ARS assay, wherein varying concentrations of CaOx crystals were crystallized by incubating calcium chloride (CaCl₂) and sodium oxalate (NaOx) for 24 hours in a 6-well plate seeded with cells was developed. Concurrently, rhein and NR were administered along with CaOx. Subsequently, the medium was removed from the plate, washed thrice with Phosphate-Buffered Saline (PBS), and incubated with ARS (pH=5.3) for 3 min for staining the CaOx crystals. The plate was then washed thrice again with PBS, incubated with 40 nm gold nanoparticles (AuNP) for

five min, and subjected to SERS imaging. ARS dye at pH 5.3 with the addition of 10% ammonium hydroxide seems to be giving much better SERS intensity than the normal ARS solution when incubated with the AuNP (**Figure 4.13**).

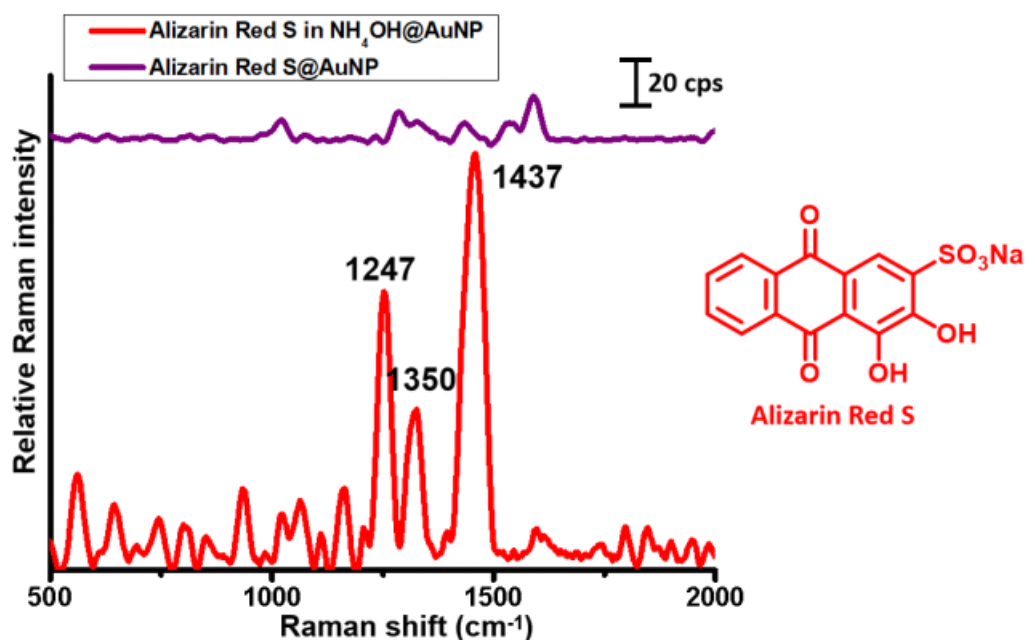


Figure 4.13: SERS data of ARS before and after addition of ammonium hydroxide

This prompted us to design the SERS-based ARS assay. Our results indicated that as the concentration of CaOx increased, the fingerprint SERS intensity of ARS also increased (**Figure 4.14a**). With this assay, the SERS intensities of stained ARS up to 10 μ M of CaOx were successfully analyzed and recorded its corresponding Raman images. The SERS intensities have been demonstrated as heat maps for each concentration of CaOx as well as for the CaOx treated with inhibitors to understand the effect of inhibitors on CaOx crystallization (**Figure 4.14b&c**). Interestingly, the crystallization on cells treated with 50 μ M NR resulted in a lower SERS intensity (50-fold less) compared to its CaOx counterpart (500 μ M), thereby demonstrating its superior anti-nephrolithiasis capability compared to the positive control, citrate (**4.14b**). By successfully identifying CaOx inhibitors using this SERS-based ARS assay, this technique could pave the way for the development of new therapeutic strategies for CaOx-induced nephropathies and other related disorders. It could also contribute to the broader field of nanomedicine by providing a powerful tool for the study of biological processes at the molecular level as the technique possesses high sensitivity compared to the original staining protocol and it represents a non-invasive modality.

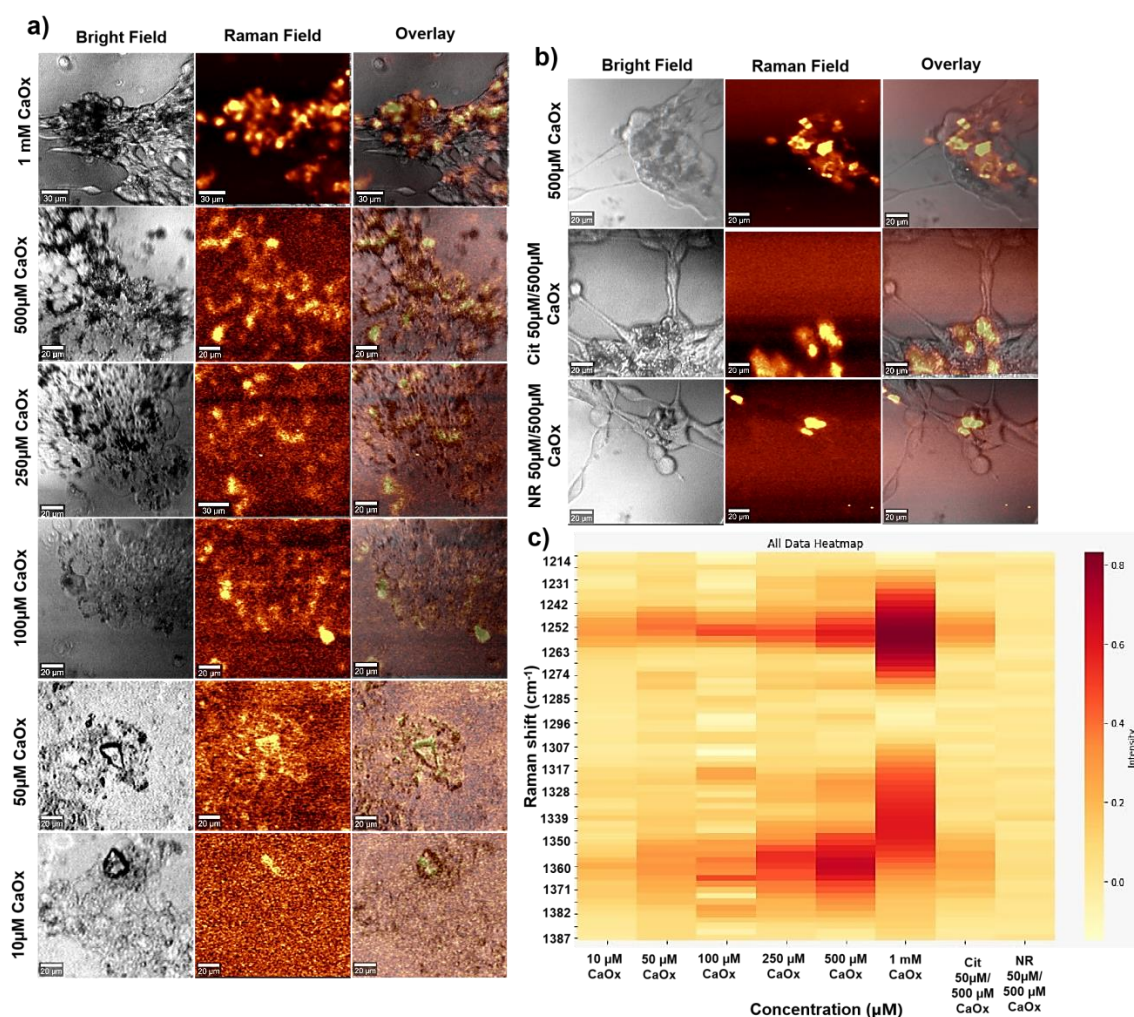


Figure 4.14: a) Representative images SERS images of various concentrations of CaOx as well as b) CaOx 500 μM, NR 50 μM / CaOx 500 μM, Cit 50 μM / CaOx 500 μM c) its SERS intensities represented as a Heatmap with each measurements being the average of five experiments.

The upregulation of cell surface markers during calcium crystallization and their expression levels during the anti-urolithic activity of rhein were investigated. It is well-established that these cell surface markers are upregulated during calcification as a defensive mechanism against calcium crystals.^[24–26] In our previous work, the compound GlcNPhAlk was utilized as a cell surface glycan marker to differentiate glycan expression in cancerous and normal cells.^[27,28] In the current study, metabolic glycan labeling of the GlcNPhAlk molecule was employed to understand glycan expression during the calcification process. Interestingly, increased labeling of cell surface glycans was observed as calcification progressed, indicating an upregulation of cell surface glycan upon calcium crystallization. However, when the NR

was administered alongside CaOx, glycan expression gradually declined (**Figure 4.15**). This suggests a potential role for NR in modulating glycan expression during calcification.

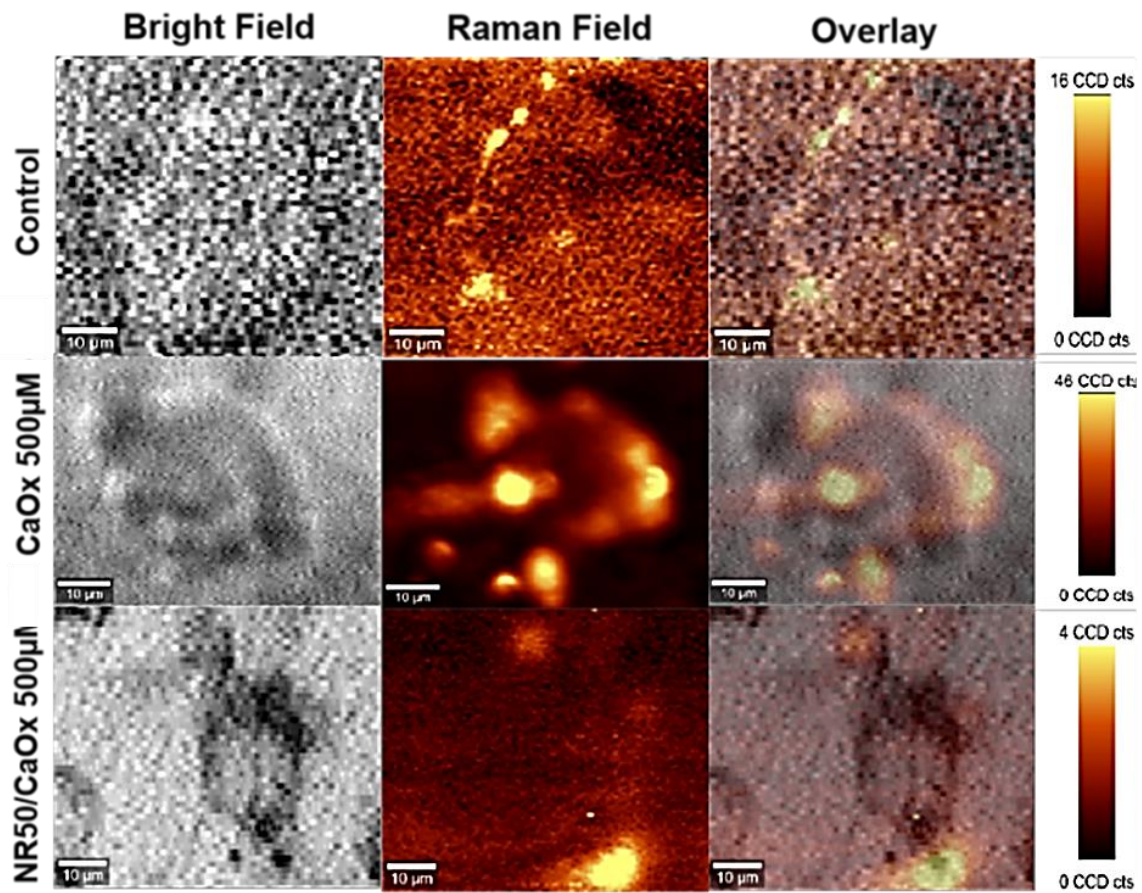


Figure 4.15: Upregulation of cell surface markers- Sialic acid; Bright field, Raman Field and Overlay images of Control, CaOx 500 μ M, CaOx 500 μ M/NR 50 μ M

4.4.6. Transcriptomic assessment of vascular calcification processes and anti-calcification responses by NR

To further understand the cellular response to CaOx and to interpret the associated cellular changes, an RNA sequencing experiment was performed. Cells were cultured as in the ARS imaging experiments and treated with 500 μ M CaOx spiked medium (positive ctrl), 500 μ M CaOx spiked medium premixed with 50 μ M NR, medium only (negative ctrl).. In ctrl versus CaOx samples, 137 differentially expressed genes with a fold change ≥ 0.5 and $p \leq 0.05$ were detected, similarly CaOx versus CaOx/NR contain 887 differentially expressed genes, respectively (**Table 4.1**).

Comparison	No.of. Upregulated genes	No.of. Downregulated genes
Control vs CaOx	103	34
CaOx vs CaOx/NR	522	365

Table 4.1: Table showing a number of upregulated and downregulated genes in all groupings.

Thereby the drastic change induced by CaOx treatment and the prevention thereof by NR were confirmed. Reactome pathway analysis of upregulated genes in control vs CaOx samples revealed enrichment in NGF-stimulated transcription, nuclear events (kinase and transcription factor activation), signaling by NTRKs, and signaling by Receptor Tyrosine Kinases (**Figure 4.16**). In our subsequent analysis, the expression levels of individual genes, with a specific focus on distinct gene groups were investigated. These included immune response pathways; particularly those associated with inflammatory responses, as well as extracellular matrix (ECM) proteins and cell cycle and proliferation processes. Our interest in these pathways stems from rhein's well-documented anti-inflammatory properties.^[11]

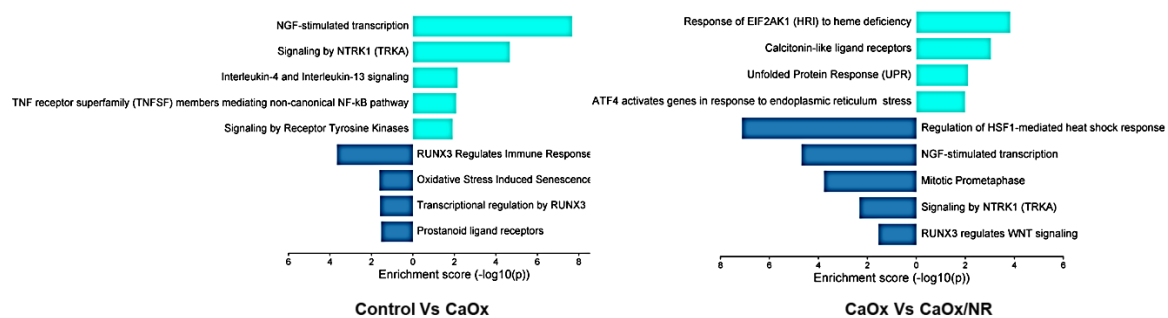


Figure 4.16: Reactome analysis of control vs CaOx, and CaOx vs CaOx / NR with $p < 0.05$

Furthermore, the induction of calcium oxalate (CaOx) crystals within cells is expected to trigger an immune response, which would be reflected in the observed differential gene expression. For that, expression levels of selected genes that are either reported in the literature to be involved in cellular response to CaOx and/or were found to be among the top deregulated genes in this study were compared. TNF receptor superfamily (TNFSF) members (TNFRSF12A, TNFRSF13C, TNFAIP3) mediating non-canonical NF- κ B pathway, Interleukin-6 signaling (IL6R) and TGF beta signaling pathways (INHBA) are assumed to play a role in the induction of an immune response in CaOx nephropathies.^[29,30] Indeed, elevated expression of TNF alpha and TGF beta signaling pathway genes, such a tumor

necrosis factor receptor superfamily, member 12A, tumor necrosis factor receptor superfamily, member 13C, TNF alpha-induced protein 3 and inhibin, beta A, a protein-coding gene that is a member of the transforming growth factor-beta (TGF- β) superfamily of proteins, in the CaOx group compared to all other groups were found (**Figure 4.17**). The FOS gene family contains 4 members: FOS, FOSB, FOSL1, and FOSL2. The FOS proteins have been implicated as regulators of cell proliferation, differentiation, and transformation which were also upregulated on CaOx crystallization and subsequently downregulated on treatment with the NR.^[31]

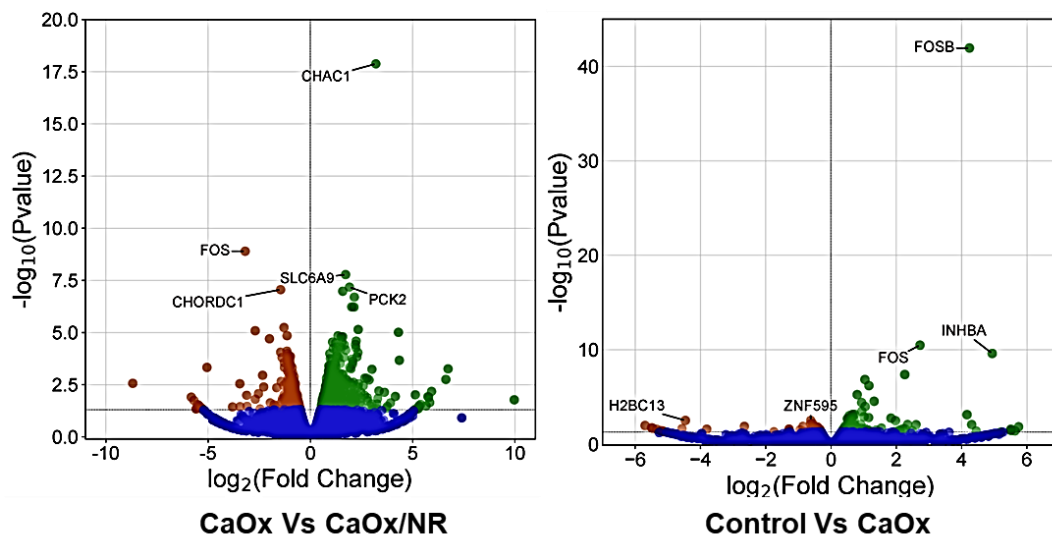


Figure 4.17: Volcano plots of differentially expressed genes between control vs CaOx, control vs CaOx/NR, and CaOx vs CaOx / NR with $p < 0.05$, $\log_2\text{ratio} \geq 0.5$, and respective expression levels in the other treatment groups are plotted (red—downregulated, green—upregulated)

To summarize, these results suggest that by reducing cell crystal interactions NR treatment can largely prevent CaOx-induced downstream responses, such as inflammatory signaling pathways as shown in the FPKM ratio of selected genes, especially genes like INHBA, FOS, FOSL1, FOSB, COL7A1, TNFRFS12A, and IL6R (**Figure 4.18**).

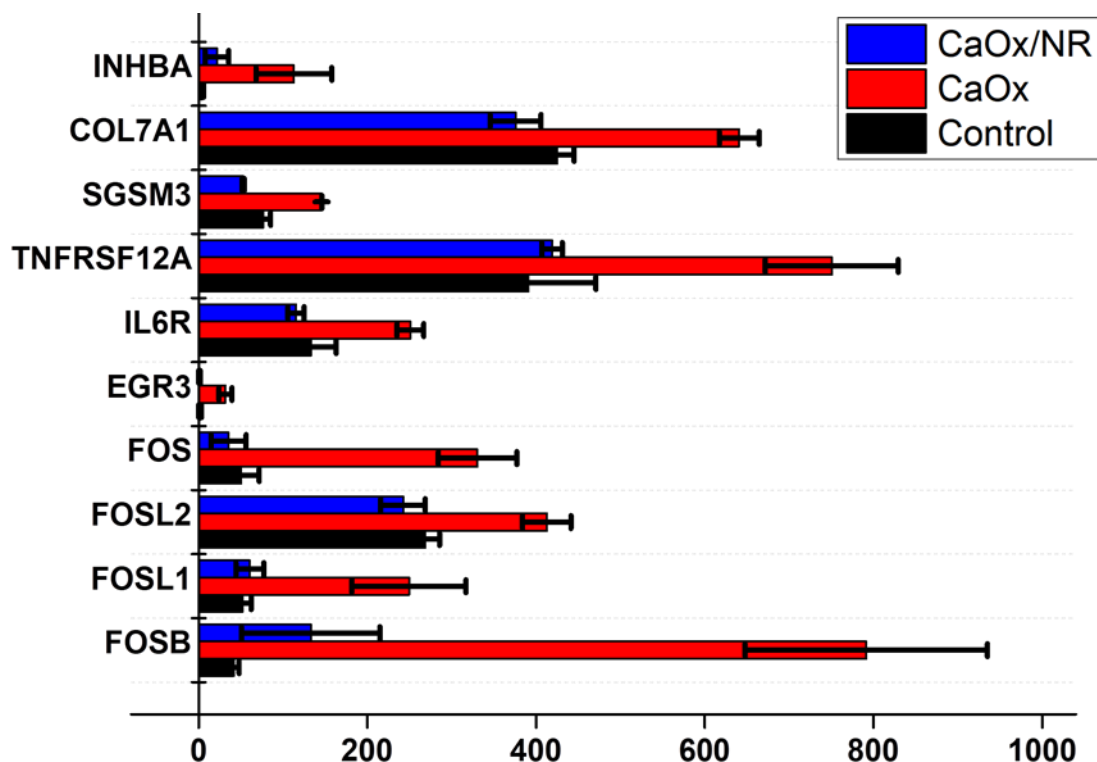


Figure 4.18: Normalized average count of gene transcripts (FPKM – fragments per kilobase of exon model per million reads mapped) involved in inflammatory responses, ECM composition, cell proliferation, and tissue homeostasis of the different treatment groups is plotted

4.5. Conclusion

In summary, the phytochemical rhein has been primarily isolated from *Cassia fistula* Linn., a plant known for its medicinal properties. Despite rhein's recognized anti-inflammatory and anti-cancer activities, its potential as an anti-urolithiasis agent has been unveiled. The therapeutic application of rhein is restricted due to its poor solubility and low bioavailability. To address these limitations, the simplest and fastest formulation of nano rhein was developed by direct sonochemical self-assembly technique, which enhanced its bioavailability and thereby its anti-urolithiasis activity. The efficacy of both rhein and nano rhein toward anti-calcification was confirmed via Alizarin Red S staining in an *in-vitro* system using HEK-293 cells. Additionally, the SERS-imaging capabilities have been harnessed to establish the SERS-based Alizarin Red S assay for monitoring calcification processes. This platform allowed profiling of calcium oxalate inhibition and revealed alterations in cell surface glycan expression during calcification and subsequent decalcification after rhein/nano-rhein treatment. RNA sequencing experiment was conducted

to further elucidate the cellular response to CaOx and interpret the associated morphological changes observed through cellular imaging. Finally, the transcriptomic alterations induced by CaOx treatment and the preventive effect of nano-rhein were confirmed through RNA sequencing and subsequent Reactome pathway analysis. Overall, this work provides a paradigm for discovering the potential of rhein, particularly in its nano form, as a promising upcoming therapeutic entity for CaOx-induced nephropathies.

4.6. Experimental section

4.6.1. Materials and methods

All the chemicals and solvents used in this study were procured from Sigma Aldrich, Alfa Aesar, TCI, and Merck, and were used as received without any additional purification. The ^1H NMR, ^{13}C NMR spectra were obtained using a Bruker Avance 500 MHz NMR spectrometer, with chemical shifts reported in parts per million (ppm). Mass spectra were acquired under ESI/HRMS at a resolution of 61800 using a Thermo scientific exactive mass spectrometer. The absorption spectra were recorded on a Shimadzu (UV-2450) UV-Vis. spectrophotometer, and the resulting data was analyzed using Microsoft Excel and Origin 7. SERS measurements were conducted using a WITec Raman microscope (WITec Inc. Germany, alpha 300R), which employed a laser beam directed at the sample through a 20x objective and a Peltier cooled CCD detector.

The samples were excited with a 633 nm wavelength laser, and the Stokes shifted Raman spectra were collected in the range of 400 to 4000 cm^{-1} with a resolution of 1 cm^{-1} . Before each measurement, the system was calibrated using a silicon standard with a Raman peak centered at 520 cm^{-1} . The WITec Project plus (v 2.1) software package was utilized for data evaluation. TEM measurements were carried out using a JEOL 2010 instrument with an accelerating voltage of 200 KV. The sample for TEM was prepared by placing a drop of the aqueous nanoparticle solution onto a 230 mesh copper grid coated with carbon, and allowing it to air dry prior to measurement.

4.6.2. Scanning Electron Microscopy (SEM)

It was employed to prepare CaOx crystals using a Bis-Tris buffer (comprising 50 mM Bis-Tris, 150 mM NaCl, pH 6.2) containing final concentrations of 1 mM NaOx, 2 mM CaCl_2 , and the specified concentration of the compound. Glass coverslips (12-mm round) were positioned at the base of 24-well plates. Initially, 20 \times stock solutions of CaCl_2 and inhibitor,

and 10× NaOx were prepared in Bis-Tris buffer. The assay mixture was prepared in Eppendorf tubes by adding 800 µl of Bis-Tris buffer, followed by the addition of 50 µl CaCl₂ (20× concentration) and 50 µl of inhibitor (20× concentration), and vortexing. Subsequently, 100 µl NaOx (10× final concentration) was added, the assay mixture was vortexed and immediately transferred to the prepared 24-well plate. Two wells per sample were prepared with 400 µl per well. Samples were incubated at 60 °C for one hour and then in room temperature for the specified duration. Representative images were captured using a Leica DM 6000B microscope (Leica Microsystems) in bright field mode before samples were rinsed once with double distilled water and air-dried at room temperature. Post-drying, samples were imaged again using bright-field microscopy to confirm minimal effects of the drying process on crystal morphology. After drying, glass coverslips were mounted on SEM stubs with silver paint and coated with a 6 nm layer of platinum/palladium using a CCU-010 Metal Sputter Coater (Safematic, Bad Ragaz, Switzerland). Samples were imaged using a Magellan 400 FEI SEM microscope (ThermoFisher Scientific) in the secondary electron mode using the TLD detector.

4.6.3. Cell based studies

4.6.3.1. Cytotoxicity studies of rhein and NR

HEK-293 cells were seeded into 96 well plates and incubated for 24 hour (at 37 °C 5% CO₂). Cells were then treated with varying concentrations of rhein and NR (20-200 µM). After 24 hour incubation, MTT (0.5 mg/ml) was added to each well and kept at 37 °C for 4 hours and finally the so formed formazan crystals were dissolved in DMSO and the OD was measured at 570 nm using a microplate reader.

4.6.3.2. Cell culture and metabolic labelling of cell surface glycans

Cells were cultured in Dulbecco's modified Eagle medium (DMEM) supplemented with 1% penicillin streptomycin and 10% fetal bovine serum, under a 5% CO₂ atmosphere at 37 °C until confluence was achieved. Confluent cells were harvested using 0.25% EDTA trypsin, which was subsequently neutralized with DMEM. The harvested cells were centrifuged, and the supernatant was discarded. The cells were then resuspended in DMEM to achieve a concentration of 3000 cells/ml. Cell count was determined using a Petroff-Hausser cell counter. A 100 µl aliquot of the cell suspension was seeded per well in a sixteen well glass bottom chamber slide and incubated for 24 hour. Cells are then treated with the CaOx 500 µM or NR 50µM/ CaOx 500 µM for another 24 hour incubation. Post-incubation, the cells

were rinsed with PBS and treated with 100 μ M of GlcNPhAlk and derived from a 50 mM stock solution in DMSO. The cells were then incubated for 60 hour. Control cells were left untreated. Following incubation, all wells were washed thrice with HBSS buffer to remove excess compounds and unbound cells. Post-incubation, the cells were washed thrice with HBSS and prepared for SERS analysis.

4.6.4. RNA Sequencing

Cells were cultured as described in the imaging assay and treated with a medium control (DMEM without any FBS), 500 μ M CaOx, and 500 μ M CaOx in a medium containing 50 μ M rhein nanoparticles (NR) in the medium for 24 hour. Total RNA was extracted using the RNeasy Mini Kit (74104) according to the manufacturer's instructions. The Qubit RNA BR Assay (Catalog number: Q10211) from Invitrogen was used to quantify RNA samples. For the assessment of RNA quality and integrity, the Agilent Tape Station system was used (Agilent, Cat# 5067-5576). Three wells per sample group were prepared, and the total RNA extracted from those three wells made them as the three technical replicates were pooled together for each biological replicate. Two biological replicates were used for the study. mRNA was purified, and the RNAseq library was prepared using the TrueSeq RNA kit (Illumina). Sequencing was performed on a Novaseq 6000 (Illumina). Reads were aligned to the reference human genome (hg38) using the STAR (2.4) tool. For the heatmap and hierarchical clustering of significantly different genes ($p \leq 0.05$, \log_2 fold change ≥ 1). The heatmap was plotted using R software. differentially expressed genes with $p \leq 0.05$, \log_2 fold change ≥ 0.5 . Reactome pathway analysis of differentially expressed genes was analyzed in the biological process functional database. The fragments per kilobase of the exon model per million reads mapped (FPKM) were used to compare the selected genes' expression levels, and two independent experiments were performed. RNA sequencing raw data can be made available to the corresponding author upon request.

4.6.5. Bioinformatics analyses

Biological pathways enrichment analysis and the biological interpretation of the DEGs was achieved using the Reactome pathway database. Reactome analyses were performed to identify the functions of the DEGs. Only pathways and functional groups with p-values less than 0.05 were discussed. Volcano plots and functional enrichment plots were created using the SR plot web tool.

4.6.6. DFT studies

The geometry and stability of rhein dimers are assessed by DFT calculations. All the calculations are done using Gaussian 09 suite of programs employing Minnesota hybrid density functional M06-2x at the 6-311+G(d,p) basis set.

4.6.7. Spectral data of Rhein

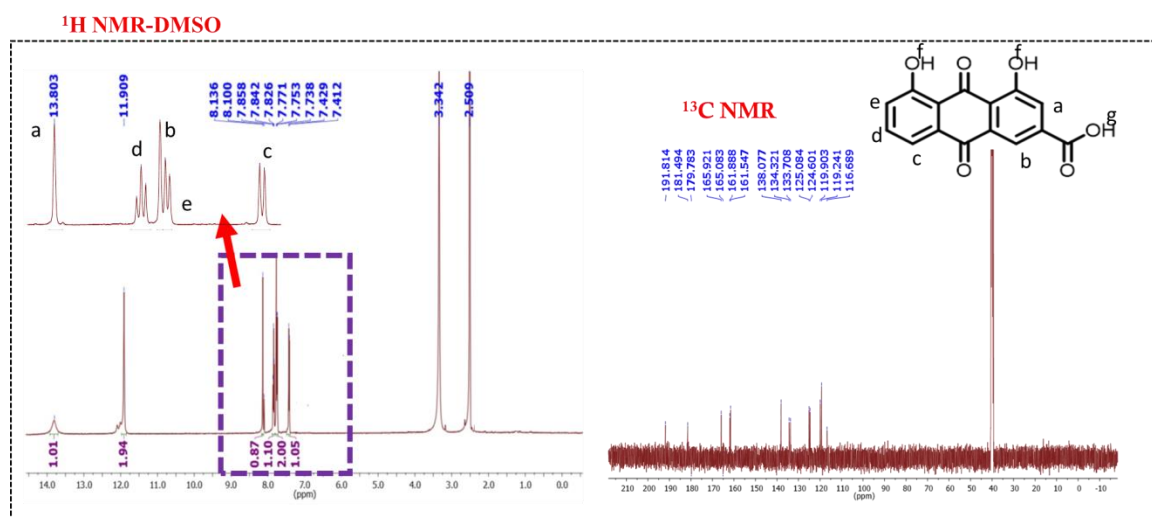


Figure 4.19: ¹H and ¹³C NMR spectra of Rhein molecule isolated from *Cassia fistula* Lin

Chemical Formula: C₁₅H₈O₆

¹H NMR (500 MHz, DMSO-d₆): δ 7.41 (d, *J* = 8.5 Hz, 1H), 7.74 (d, *J* = 7.5 Hz, 1H), 7.77 (s, 1H), 7.84 (t, *J* = 8.0 Hz, 1H), 8.10 (s, 1H), 11.91 (s, 2H), 13.80 (s, 1H) ppm.

¹³C NMR (125 MHz, DMSO-d₆): δ 116.7, 119.2, 119.9, 124.6, 125.1, 133.7, 134.3, 138.1, 161.5, 161.8, 165.1, 165.9, 181.4, 191.8 ppm.

ESI-HRMS, [M-H]⁻: 283.0248 (calculated), 283.0238 (observed).

4.7. References

- [1] A. Singh, S. Tandon, C. Tandon, *Mol. Biol. Rep.* **2021**, *48*, 887.
- [2] M. R. Hayden, S. C. Tyagi, L. Kolb, J. R. Sowers, R. Khanna, *Cardiovasc. Diabetol.* **2005**, *4*, 1.
- [3] W. Pan, W. Jie, H. Huang, *MedComm* **2023**, *4*, 1.
- [4] E. M. Worcester, F. L. Coe, *Semin. Nephrol.* **2008**, *28*, 120.

- [5] J. L. Rosenstock, T. M. J. Joab, M. V. Devita, Y. Yang, P. D. Sharma, V. Bijol, *Clin. Kidney J.* **2022**, *15*, 194.
- [6] S. R. Khan, *Urol. Res.* **2010**, *38*, 429.
- [7] M. Ketteler, G. A. Block, P. Evenepoel, M. Fukagawa, C. A. Herzog, L. McCann, S. M. Moe, R. Shroff, M. A. Tonelli, N. D. Toussaint, M. G. Vervloet, M. B. Leonard, *Kidney Int.* **2017**, *92*, 26.
- [8] R. D.M., S. R.F., *Aust. Prescr.* **2010**, *33*, 34.
- [9] J. Chung, I. Granja, M. G. Taylor, G. Mpourmpakis, J. R. Asplin, J. D. Rimer, *Nature* **2016**, *536*, 446.
- [10] D. Kim, J. D. Rimer, J. R. Asplin, *Urolithiasis* **2019**, *47*, 311.
- [11] G. M. Li, J. R. Chen, H. Q. Zhang, X. Y. Cao, C. Sun, F. Peng, Y. P. Yin, Z. Lin, L. Yu, Y. Chen, Y. L. Tang, X. F. Xie, C. Peng, *Evidence-based Complement. Altern. Med.* **2021**, 2021.
- [12] Y. X. Zhou, W. Xia, W. Yue, C. Peng, K. Rahman, H. Zhang, *Evidence-based Complement. Altern. Med.* **2015**, 2015.
- [13] C. Y. Li, L. Liu, Y. W. Zhao, J. Y. Chen, X. Y. Sun, J. M. Ouyang, *Oxid. Med. Cell. Longev.* **2021**, 2021.
- [14] Z. M. Mazayen, A. M. Ghoneim, R. S. Elbatany, E. B. Basalious, E. R. Bendas, *Futur. J. Pharm. Sci.* **2022**, 8.
- [15] Y. Zhuang, Y. Bai, Y. Hu, Y. Guo, L. Xu, W. Hu, L. Yang, C. Zhao, X. Li, H. Zhao, *Onco. Targets. Ther.* **2019**, *12*, 5281.
- [16] C. Pinto Reis, R. J. Neufeld, A. J. Ribeiro, F. Veiga, *Nanomedicine Nanotechnology, Biol. Med.* **2006**, *2*, 8.
- [17] B. Hu, F. Gao, C. Li, B. Zhang, M. An, M. Lu, Y. Liu, Y. Liu, *AMB Express* **2020**, *10*.
- [18] U. Koch, P. L. A. Popelier, *J. Phys. Chem.* **1995**, *99*, 9747.
- [19] J. Zheng, R. Fan, H. Wu, H. Yao, Y. Yan, J. Liu, L. Ran, Z. Sun, L. Yi, L. Dang, P. Gan, P. Zheng, T. Yang, Y. Zhang, T. Tang, Y. Wang, *Nat. Commun.* **2019**, *10*.
- [20] A. Bernar, J. V. Gebetsberger, M. Bauer, W. Streif, M. Schirmer, *Int. J. Mol. Sci.*

- 2023**, 24.
- [21] A. Kletzmayer, S. R. Mulay, M. Motrapu, Z. Luo, H. J. Anders, M. E. Ivarsson, J. C. Leroux, *Adv. Sci.* **2020**, 7, 1.
- [22] A. I. Pérez-Jiménez, D. Lyu, Z. Lu, G. Liu, B. Ren, *Chem. Sci.* **2020**, 11, 4563.
- [23] M. Murali, V. P. Murali, M. M. Joseph, S. Rajan, K. K. Maiti, *J. Photochem. Photobiol. B Biol.* **2022**, 234, 112506.
- [24] S. Gao, Y. Chao, N. Li, H. Li, H. Zhao, X. Liu, W. Chen, X. Dong, *Front. Med.* **2022**, 9.
- [25] A. Petrović, T. Kizivat, I. B. Čurčić, R. Smolić, M. Smolić, *Crystals* **2021**, 11.
- [26] X. Y. Sun, C. Y. Zhang, P. Bhadja, J. M. Ouyang, *CrystEngComm* **2018**, 20, 75.
- [27] F. Reggiori, H. J. Gabius, M. Aureli, W. Römer, S. Sonnino, E. L. Eskelinen, *Glycoconj. J.* **2021**, 38, 625.
- [28] K. P. Aggarwal, S. Narula, M. Kakkar, C. Tandon, *Biomed Res. Int.* **2013**, 2013.
- [29] S. R. Mulay, J. N. Eberhard, J. Desai, J. A. Marschner, S. V. R. Kumar, M. Weidenbusch, M. Grigorescu, M. Lech, N. Eltrich, L. Müller, W. Hans, M. H. De Angelis, V. Vielhauer, B. Hoppe, J. Asplin, N. Burzlaff, M. Herrmann, A. Evan, H. J. Anders, *J. Am. Soc. Nephrol.* **2017**, 28, 761.
- [30] M. B. Convento, E. A. Pessoa, E. Cruz, M. A. Da Glória, N. Schor, F. T. Borges, *Sci. Rep.* **2017**, 7, 1.
- [31] L. Cuarental, M. Ribagorda, M. I. Ceballos, A. Pintor-Chocano, S. M. Carriazo, A. Dopazo, E. Vazquez, B. Suarez-Alvarez, P. Cannata-Ortiz, A. B. Sanz, A. Ortiz, M. D. Sanchez-Niño, *Kidney Int.* **2023**, 103, 686.

ABSTRACT

Name of the student: **Mr. Madhukrishnan M.**

Registration no.: **10CC18A39004**

Faculty of Study: **Chemical Sciences**

Year of Submission: **2024**

AcSIR academic centre/CSIR Lab: **CSIR- National Institute for Interdisciplinary Science and Technology (CSIR-NIIST), TVM, Kerala**

Name of Supervisor: **Dr. Kaustabh Kumar Maiti**

Title of the thesis: **Design, synthesis and biological assessment of SERS guided cell surface glycan modifications and anti-calcification properties of nano-rhein**

Understanding biological processes is crucial for disease detection and treatment initiation. Raman imaging and spectroscopy offer high-sensitivity detection methods for biomolecules, facilitating the study of biological processes at a molecular level. Additionally, Surface-Enhanced Raman Spectroscopy (SERS) shows promise for non-invasive disease diagnosis, including vascular calcification. **Chapter 1** provides an overview of SERS advancements in biomedical applications, glycan recognition, and potential therapeutic strategies against kidney stones. **Chapter 2** delves into glycan patterns in cancer cell lines using MGL-SERS (metabolic glycan labeling coupled SERS), correlating glycan expression with metastatic potential. This work introduces an N-alkyl derivative of glucosamine (GlcNPhAlk) as a precursor for glycan labeling. **Chapter 3** explores the versatility of the hexosamine biosynthetic pathway using various glycan precursors. These precursors have been synthesized and tested using the MGL-SERS technique, with findings indicating differences in labeling efficiency. Inhibitor studies revealed that the analogues predominantly label N-glycans. **Chapter 4** focuses on developing nano-rhein to address calcium oxalate-induced nephropathies and establish an SERS-based calcification profiling platform. The study provides insights into the potential of rhein, particularly in its nano form, as a promising therapeutic agent for CaOx-induced nephropathies. Overall, the research highlights the effectiveness of SERS in understanding glycosylation and advancing disease treatment.

List of publications

Details of the Publications Emanating from the Thesis Work

1. Elucidating cell surface glycan imbalance through SERS guided metabolic glycan labelling: An appraisal of metastatic potential in cancer cells, **Madhukrishnan Murali**, Vishnu Priya Murali, Manu M. Joseph, Soumya Rajan, Kaustabh Kumar Maiti, *Journal of Photochemistry and Photobiology B: Biology*, Volume 234, **2022**, 112506, ISSN 1011-1344, doi:10.1016/j.jphotobiol.2022.112506.
2. Transforming nano-dimensions of a small herbal molecule, rhein into nano-rhein and unveiling its efficacy on hypercalciuria-induced nephropathies, **Madhukrishnan Murali**, Vishnu Priya Murali, Roopasree O Jayarajan, Daisy R Sherin , Jayadev S Arya , M M Vishnu Prasad,Elambalassery G. Jayasree and Kaustabh Kumar Maiti (communicated).
3. Substrate promiscuity analysis of hexosamine biosynthetic pathway enzymes with unnatural sugar derivatives, **Madhukrishnan Murali**, Vishnu Priya Murali, Abeesh P, Kaustabh Kumar Maiti (Manuscript under preparation).

Papers Published from Other Related Works

1. Putative biomimetic route to 8-oxabicyclo [3.2. 1] octane motif from a humulene sesquiterpenoid zerumbone, Kollery S Veena, Greeshma Gopalan, **Murali Madhukrishnan**, Sunil Varughese, Kokkuvayil Vasu Radhakrishnan, Ravi S Lankalapalli, *Organic Letters*, **2020**
2. A clinically feasible diagnostic spectro-histology built on SERS-nanotags for multiplex detection and grading of breast cancer biomarkers, Vishnu Priya Murali, Varsha Karunakaran, **M Madhukrishnan**, Asha Lekshmi, Shamna Kottarathil, Selvakumar Deepika, Valliamma N Saritha, Adukkadan N Ramya, Kozhiparambil G Raghu, Kunjuraman Sujathan, Kaustabh Kumar Maiti, *Biosensors and Bioelectronics*, 115177, Elsevier, **2023**
3. Detection of Sialic Acid and Imaging of Cell-Surface Glycan Using a Fluorescence–SERS Dual Probe, Palash Jana, Sudeep Koppayithodi, **Madhukrishnan Murali**, Monochura Saha, Kaustabh Kumar Maiti, and Subhajit Bandyopadhyay, *ACS Sensors* **2023**, 8 (4), 1693-1699.

Patents

1. Sers-nanotag and diagnostic kit for detecting breast cancer biomarkers, Inventor: Kaustabh Kumar Maiti, Vishnu Priya Murali, Varsha KARUNAKARAN, Deepika Selvakumar, Madhukrishnan Murali, Sujathan Kunjuraman, Saritha Valliamma Neelakantapillai, Asha Lekshmi, US Patent App. 18/041,283, 2023

List of Conference Presentations

1. Illustration of aberrations in glycans through SERS guided metabolic oligosaccharide engineering: rationale for its relation with metastatic potential in cancer cells. Madhukrishnan Murali, Vishnu Priya Murali, Manu M. Joseph , Soumya Rajan and Kaustabh Kumar Maiti* 5th International Conference on Nutraceuticals and Chronic Diseases on Pharmaceuticals and Nutraceuticals for Cancer and Other Chronic Diseases (INCD-2022), University of Delhi, Delhi on October 7-9. **(Oral presentation)**
2. Glycan imbalance in cancer cells monitored by SERS based metabolic labelling. **Madhukrishnan M**, Vishnu Priya Murali and Kaustabh Kumar Maiti* Recent trends in disease prevention and healthcare management (NS-DPHM-2022)) held at CSIR-NIIST, Thiruvananthapuram, Kerala **(Best Poster Award)**.

ILLUSTRATION OF ABERATIONS IN GLYCANS THROUGH SERS GUIDED METABOLIC OLIGOSACCHARIDE ENGINEERING: RATIONALE FOR ITS RELATION WITH METASTATIC POTENTIAL IN CANCER CELLS

Madhukrishnan Murali^{a,b} Vishnu Priya Murali^a, Manu M. Joseph^a, Soumya Rajan^c and Kaustabh Kumar Maiti^{*a,b}

[a] *Chemical Sciences & Technology Division (CSTD), Organic Chemistry Section, CSIR-National Institute for Interdisciplinary Science & Technology (CSIR-NIIST), Industrial Estate, Pappanamcode, Thiruvananthapuram- 695019, Kerala, India E-mail:madhumuralikrishnan08@gmail.com, kkmaiti@niist.res.in*

[b] *Academy of Scientific and Innovative Research (AcSIR), Ghaziabad-201002, India*

[c] *Government college, Kasargod-671123, Kerala, India*

Glycosylation is one of the most common post-translational modifications (PTMs) of proteins. Herein, we have coupled metabolic glycan labelling (MGL) and surface enhanced Raman scattering (SERS) i.e., MGL-SERS strategy to explore the differential glycosylation pattern in various cancer cell lines. We are reporting for the first time an N-alkyl derivative of glucosamine which is a vital nutraceutical used in treatments against cancer (GlcNPhAlk) as a glycan labelling precursor. The metabolic labelling capability of GlcNPhAlk was further confirmed using fluorescent imaging and its protein glycosylation was confirmed using chemiluminescent western blot analysis. MGL-SERS method was implemented for a comparative assessment of cell surface glycan imbalance in breast carcinoma cells MDAMB 231 and MCF 7 as well as in normal cell line MCF10A. Highly metastatic MDAMB-231 was found to be having maximum extent of glycan labelling compared to the other two. Further, we employed the same strategy in three different types of cancer cell lines, HeLa, A549 and MDAMB-231 with respect to their varying metastatic potential. A linear relationship between degree of glycan labelling and metastatic potential in cancer cells was. Further the effect of sialyl transferase inhibitor, P-3Fax-Neu5Ac, on metabolic labelling of GlcNPhAlk proved the incorporation of GlcNPhAlk to the terminal glycans through sialic acid biosynthetic pathway and showcased this strategy as a promising tool for glycosylation related dysplasia.

References

- (a) .Lu Wei1, Fanghao Hu1, Yihui Shen1, Zhixing Chen, Yong Yu, Chih-Chun Lin, Meng C Wang& Wei Min, *Live-cell imaging of alkynetagged small biomolecules by stimulated raman scattering*, VOL.11 NO.4 | APRIL 2014 | nature methods

GLYCAN IMBALANCE IN CANCER CELLS MONITORED BY SERS BASED METABOLIC LABELING

Madhukrishnan M, Vishnu Priya Murali and Kaustabh K. Maiti*

Chemical Sciences and Technology Division, CSIR- National Institute for Interdisciplinary
Science and Technology, Thiruvananthapuram, Kerala

e-mail: kkmaiti@niist.res.in

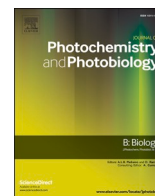
Glycans on the cell surfaces play a pivotal role in cellular recognition like cell–cell communication and host–pathogen interactions etc.[a,b] The extent of glycan imbalance causes genetic mutations which in turn reflected during the cell proliferation. The myriad functions of cell-surface glycans has rendered them attractive targets for in vivo molecular imaging. As a new insight, we report surface enhanced Raman scattering (SERS) imaging for the investigation of small biomolecules in live cells. We have utilized alkyne-bearing glucosamine core as a precursor for cell surface sialic acid biosynthesis pathway of glycans. The major focus of study is to evaluate the glycan imbalance in different cancer cells and normal cell lines by SERS imaging using alkyne fingerprint in the cell-silent region.

- (a) A. Varki, R. D. Cummings, J. D. Esko, H. H. Freeze, G. W. Hart, M. E. Etzler, *Essentials of Glycobiology*, 2nd ed., Cold Spring Harbor Laboratory Press, Cold Spring Harbor, NY, 2008.
- (b) Lu Wei¹, Fanghao Hu¹, Yihui Shen¹, Zhixing Chen, Yong Yu, Chih-Chun Lin, Meng C Wang & Wei Min, *Live-cell imaging of alkyne-tagged small biomolecules by stimulated raman scattering*, VOL.11 NO.4 | APRIL 2014 | nature methods



Contents lists available at ScienceDirect

Journal of Photochemistry & Photobiology, B: Biology

journal homepage: www.elsevier.com/locate/jphotobiol

Elucidating cell surface glycan imbalance through SERS guided metabolic glycan labelling: An appraisal of metastatic potential in cancer cells

Madhukrishnan Murali^{a,b}, Vishnu Priya Murali^a, Manu M. Joseph^a, Soumya Rajan^c,
Kaustabh Kumar Maiti^{a,b,*}

^a Chemical Sciences & Technology Division (CSTD), Organic Chemistry Section, CSIR- National Institute for Interdisciplinary Science & Technology (CSIR-NIIST), Industrial Estate, Pappanamcode, Thiruvananthapuram 695019, Kerala, India

^b Academy of Scientific and Innovative Research (AcSIR), Ghaziabad 201002, India

^c Government College, Kasargod 671123, Kerala, India

ARTICLE INFO

Keywords:

Metabolic labelling
SERS
Cell discrimination
Cancer
Metastatic potential
Glycan

ABSTRACT

The intrinsic complexities of cell-surface glycans impede tracking the metabolic changes in cells. By coupling metabolic glycan labelling (MGL) and surface-enhanced Raman scattering (SERS), we employed the MGL-SERS strategy to elucidate the differential glycosylation pattern in cancer cell lines. Herein, for the first time, we are reporting an N-alkyl derivative of glucosamine (GlcNPhAlk) as a glycan labelling precursor. The extent of labelling was assessed by utilizing Raman imaging and verified by complementary fluorescence and Western blot analysis. MGL-SERS technique was implemented for a comparative evaluation of cell surface glycan imbalance in different cancer cells wherein a linear relationship between glycan expression and metastatic potential was established. Further, the effect of sialyltransferase inhibitor, P-3Fax-Neu5Ac, on metabolic labelling of GlcNPhAlk proved the incorporation of GlcNPhAlk to the terminal glycans through the sialic acid biosynthetic pathway. Hence, this methodology unveils the phenomenon of metastatic progression in cancer cells with inherent glycosylation-related dysplasia.

1. Introduction

Glycosylation is a major post-translational modification prevalent in most eukaryotes. Notably, glycans cover the cell surface and play a decisive role in cell–cell interactions and cell migration during various physiological processes such as fertilization, embryogenesis and immune responses [1,2]. Recognition of cell-surface glycans are mostly achieved by fluorescence imaging [3] and colourimetric methods which have limited specificity, sensitivity and are accompanied by problems including photo bleaching [4]. Even though in most of the instances Raman imaging is limited in its application upon comparison with fluorescence imaging but in the case of metabolic glycoengineering mediated labelling approaches, it can be counted as a robust method. This is mainly attributed to the high sensitivity and specificity of Raman imaging which could produce more accurate output than fluorescence or Western blot. Western blot analysis is time-consuming and requires skilled technicians whereas fluorescence imaging techniques need an additional step of ligation (click reaction, Staudinger ligation etc.) to

conjugate the fluorescent probe. In recent times, Raman imaging has been explored as an alternative technique for glycan detection since it is an ultrasensitive technique in terms of enhanced signal intensity. The inherent drawbacks from fluorescent modality [5–7] in glycan labelling can be eliminated with the help of Raman spectroscopic techniques like coherent anti Stokes Raman scattering (CARS), stimulated Raman scattering (SRS) and surface-enhanced Raman scattering (SERS). SRS has been employed as an effective imaging modality for metabolic labelling with numerous advantages including enhanced tissue penetration, intrinsic 3D sectioning, minimal phototoxicity, free of background signals [8] and signal enhancement by a factor of 10^7 . Although few reports claimed that SERS could be used for imaging glycan [9,10] still there is much more to be scrutinized for better understanding in this field.

Glycans play a significant role in cancer progression and metastasis. Metastatic transformation is attributed to the efficiency of cancer cells to invade through the normal tissue surrounding them, engraftment and succeeding hematogenous or lymphatic spread. Aberrant glycosylation is often associated with malignant cancers that can alter the antigenic

* Corresponding author at: Chemical Sciences & Technology Division (CSTD), Organic Chemistry Section, CSIR- National Institute for Interdisciplinary Science & Technology (CSIR-NIIST), Industrial Estate, Pappanamcode, Thiruvananthapuram 695019, Kerala, India.

E-mail address: kkmaiti@niist.res.in (K.K. Maiti).

<https://doi.org/10.1016/j.jphotobiol.2022.112506>

Received 8 November 2021; Received in revised form 14 March 2022; Accepted 25 June 2022

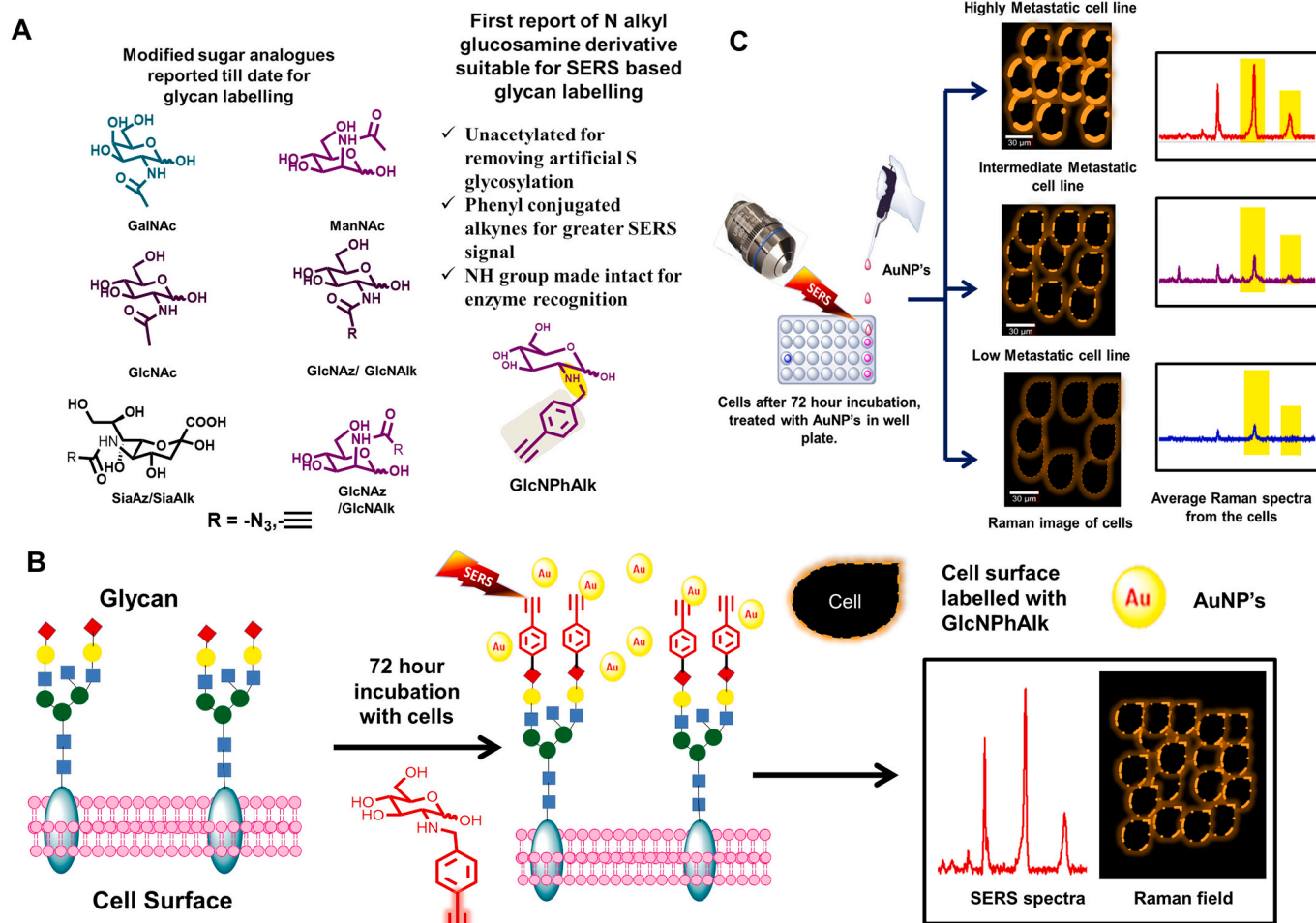
Available online 29 June 2022

1011-1344/© 2022 Elsevier B.V. All rights reserved.

and adhesive properties of cancer cells and thereby facilitating metastatic advancement [11,12]. The overexpressed glycosyltransferase enzymes including MGAT5 (β 1,6-*N*-acetylglucosaminyltransferase V) plays a key role in the biosynthesis of branched glycans and undoubtedly the expression will be proportional to the metastatic potential of the cells [13]. Moreover, some reports differentiate the degree of tumour metastasis through the potentiometric detection of cell membrane sialic acid levels [14]. Although glycan expression on cell surface has been attempted using SERS [15,16], the specificity in cell surface mapping and imaging is still a challenge. Utilizing the Raman technique for glycan differentiation with aberrant glycosylation in different cancer cells based on their metastatic potential has not been explored. Keeping this in mind, we have introduced a facile SERS technique using bio-orthogonal chemical reporter, GlcNPhAlk, as a glycan labelling entity which is the first *N*-alkyl monosaccharide analogue since all the reported glycan precursors are of *N*-acyl group starting from *N*-acetyl mannamine. Bertozzi and co-workers [17] have extensively studied the substrate specificity of the sialic acid pathway and confirmed that the *N*-acetyl part is the critical determinant in selecting sialic acid precursor. Moller et al. reported C4 modified *N*-acetyl mannamine for metabolic oligosaccharide engineering applications keeping the *N*-acetyl group intact [18].

Both Bertozzi and Reutter's groups pioneered the metabolic oligosaccharide engineering (MOE), a strategy that consists of the use of

modified sugar analogues that are metabolically labelled and transformed into modified glycans. The present work replaces the keto group of *N*-acyl part of the sugar unit with *N*-alkyl with the help of reductive amination reaction on glucosamine; hence we anticipate that the NH bond will be intact for the enzyme activation through hydrogen bonding that facilitates the glycan biosynthesis process to transform into a modified sialic acid. As the glucosamine does not take part in any transformational changes that happen in the biosynthetic pathways of glycans, we decided to introduce the bioorthogonal functionality through *N* alkyl linkage. Therefore the use of *N* alkyl derivatives for glycan labelling adds versatility to the numerous glycan labelling molecules which are mainly *N* acetyl ones. Alkyne group was chosen as the bioorthogonal functionality since it has the maximum cross-sectional area in SERS when compared to other bioorthogonal functional groups [19], which is metabolically labelled at the terminal site of the glycan chain ended with sialic acid by biosynthetic pathway [20,21] (Scheme 1A & B). Colloidal gold nanoparticles (AuNPs) with a diameter of 35–40 nm was chosen as SERS substrate for acquiring maximum enhanced Raman fingerprint and imaging to elucidate the extent of metabolic labelling. Cancer cells with different metastatic potentials i.e., highly metastatic breast cancer cells MDA-MB-231 [22,23], comparatively lower metastatic cervical cancer cells HeLa, non-small lung adenocarcinoma cells A549 [24], another breast carcinoma cell line MCF7 and finally a normal breast epithelial cell line MCF10A with least metastatic



Scheme 1. A) Structures of some of the monosaccharide analogues used for glycan labelling reported till date and the newly reporting *N* alkyl analogue of glucosamine GlcNPhAlk. B) Schematic representation of strategy MGLSERS adopted by coupling SERS with metabolic glycan labelling (MGL) to image glycan in cells using GlcNPhAlk as glycan precursor. C) schematic representation of variation of glycosylation in different cells through glycan imaging using SERS technique. Glycans being represented on the basis of Symbol Nomenclature for Glycans (SNFG) in which sialic acid is represented as red squares, GlcNAc by blue squares, Mannose by green rounds and galactose as yellow rounds.

potential were selected for the comparative study [23,25–27].

This carefully calibrated approach not only assesses in situ detection and imaging of glycans but also promoted semi-quantitative recording of the variation in glycan expression in accordance with their metastatic potential (Scheme 1C). The importance of identifying metastatic gradients is the principal goal of cancer theranostics that requires emerging imaging techniques to discriminate within cells and tissues. Such imaging technologies are of paramount interest in cancer diagnosis. Since metastasis remains a big barrier towards fruitful cancer treatment, the current investigation will be instrumental in designing glycan-based therapies against cancer.

2. Results and Discussion

There have been many ground-breaking works on metabolic oligosaccharide engineering (MOE) and bioorthogonal chemistry for the development of glycan precursors for metabolic glycan labelling by both Bertozzi and Reutter and many others [17,28–32]. These research groups developed several approaches that have been resulted in the plethora of bioorthogonal chemical reporters from various sugar analogues, including ManNAz, GalNAz, GlcNAz, and SiaNAz as well as their alkynyl counterparts [20,33–36] having N acetyl functionality, which is of paramount importance in enzymatic recognition in the biosynthetic pathway of sialic acids [17,32].

Present work introduces an N alkyl derivative, GlcNPhAlk for the first time in glycan imaging. We are anticipating the hydrogen bond

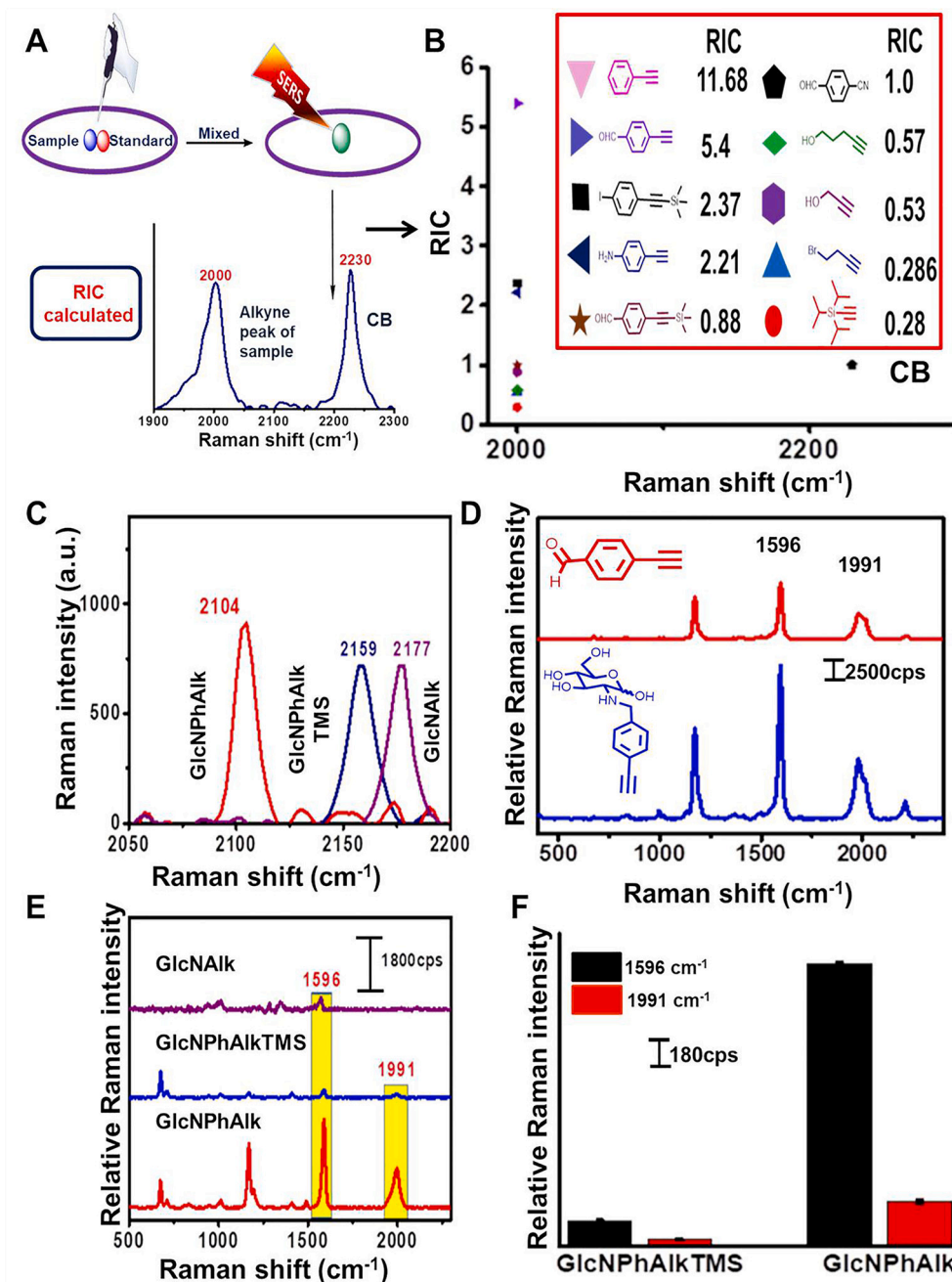


Fig. 1. Raman analysis of glycan precursors (GP). A) Schematic representation of SERS study of phenyl conjugated and unconjugated alkynes. B) Graph showing RIC (Relative intensity against Cyano benzaldehyde) values of different alkynes. C) Bare Raman spectra of 3 GPs. D) SERS spectra of GlcNPhAlk and the aldehyde used for its synthesis. E) SERS spectra of 3 GPs and F) comparison of Raman Intensities of GPs (with and without TMS respectively) on AuNP.

formation with the NH group of GlcNPhAlk which will be sufficient for the enzymatic recognition and decided to examine the labelling of GlcNPhAlk in cells. As expected, the probe was labelling the glycans at the cell surface confirmed by fluorescence imaging. An inhibition study using Sialyltransferase inhibitor also suggested that GlcNPhAlk might be transforming to cell surface glycans through the sialic acid biosynthetic pathway. MGL-SERS technique was utilized for evaluating glycan expression in various cancer cell lines with varying metastatic potential and the results suggested the linear relationship between the glycan expression and metastatic potential.

2.1. SERS Analysis of Alkynylated Glucosamine Analogues

Using hyperspectral Raman technique Yamakoshi and co-workers have reported Raman-tags conjugated with phenyl-ring performed as a better candidate for metabolic labelling [19]. We have translated this strategy into SERS modality, by introducing phenyl appended alkynes as bioorthogonal Raman-tags and studied its Raman intensity in solution state to foresee the efficiency of spectral fingerprint in the cell silent region. At first, SERS analyses of various types of alkynes were performed. Hence, for that variety of compounds, having phenyl conjugated, non-conjugated, terminal and internal alkynes were selected as bioorthogonal Raman-tags and studied in solution state to foresee the efficiency of spectral fingerprint in the cell silent region. Quasi-spherical colloidal AuNPs of the size 35–40 nm were synthesised (Fig. S4†) for maximum SERS enhancement [37]. These alkynes were mixed with cyano benzaldehyde (CB) which was taken as an internal standard due to the well-resolved Raman peak at 2230 cm^{-1} (Fig. 1A). The SERS spectra of all the alkyne tags displayed a chemical shift near 2000 cm^{-1} with colloidal AuNPs. From the ratio of intensities of sample and standard, RIC (relative Raman intensity v/s CB) was calculated. Phenyl conjugated alkynes produced a higher RIC value than the non-conjugated ones. Terminal alkynes showed more intense peaks than the internal alkynes in the SERS study (Fig. 1B). Three monosaccharide units (glucosamine moiety) as metabolic labelling precursor with bioorthogonal alkyne groups GlcNPhAlkTMS, GlcNPhAlk, GlcNAlk were subjected to SERS analysis, in which both GlcNPhAlkTMS and GlcNPhAlk showed intense Raman peaks at 1165 cm^{-1} , 1596 cm^{-1} , 1991 cm^{-1} and has a broad signal around 2142 cm^{-1} corresponding to C—C skeletal stretch, C=C ring vibrations, and the last two peaks corresponding to C≡C stretching vibrations respectively [38–40] (Fig. 1D, E). Alkyne centred compounds exhibited two peaks at 1991 cm^{-1} and 2142 cm^{-1} in the cell silent region due to the presence of two types of binding motifs for the molecule at the nanoparticle surface [39]. It was further confirmed with the bare Raman spectra of both molecules, which showed only a single peak centred at 2100 cm^{-1} , whereas the SERS spectra of the third alkyne molecule, GlcNAlk, without phenyl group displayed negligible peak in the cell silent region. However, the bare Raman spectrum of the compound demonstrated a peak around 2100 cm^{-1} , in the cell silent region (Fig. 1C). GlcNPhAlk produced an intense Raman peak compared to bare alkyne in the presence of AuNPs. Based on the above observation, we decided to proceed with our studies with GlcNPhAlkTMS and GlcNPhAlk prevailing the most intense peaks at 1596 cm^{-1} and 1991 cm^{-1} . Out of these alkynes, phenyl appended alkynes produced maximum Raman intensity than the non-conjugated ones. Also, the peak intensity of terminal alkynes was higher than the internal alkynes in the SERS study. Based on these results two glycan tags GlcNPhAlk, GlcNPhAlkTMS were synthesised using Borch reductive amination of glucosamine with their appropriate aldehydes as per the previous literature [41] (Scheme S1†).

2.2. Synthesis of Glycan Precursors: Alkynylated Glucosamine Analogues

To date, all the synthesised glycan labelling sugar analogues contain the *N*-acetyl group which was hypothesised to be essential for enzymatic recognition in sialic acid biosynthesis. We synthesised alkynyl-

glucosamine derivatives GlcNPhAlk and GlcNPhAlkTMS as probe molecules with *N* alkyl groups anticipating that NH bond, as a source of hydrogen bond, is enough for enzymatic recognition. As a control, the acylated version of glucosamine (GlcNAlk) was also synthesised (Scheme S1†). All molecules were characterised with NMR and HR-MS analyses (Fig. S3 a–†). Although per-*O*-acetylated unnatural sugars are widely used to improve cell permeability, it leads to artificial *S*-glycosylation which compromises their specificity of metabolic glycan labelling in living cells [42]. Hence to avoid false-positive results, unacetylated unnatural sugars were selected as the precursor for metabolic labelling. Cytotoxic studies of all the three glycan precursors in normal and cancer cell lines confirmed the viability up to $100\text{ }\mu\text{M}$ concentrations (Fig. S5).

2.3. Metabolic Glycan Labelling of Glucosamine Analogues

Primarily our investigation was focused on the detection of cell surface glycans by SERS imaging and to find out the extent of metabolic labelling capability of aforesaid compounds. So, we have initiated with, cervical carcinoma HeLa cells which were treated with GlcNPhAlkTMS and GlcNPhAlk for 72 h to induce the biosynthetic pathway to incorporate into cell-surface glycans. Cells without glycan tags were used as negative controls. After a treatment of 3 days, the cell culture medium was removed and washed thrice with PBS (phosphate-buffered saline), then SERS imaging was performed by incubating with colloidal AuNPs. SERS spectra of GlcNPhAlkTMS and GlcNPhAlk suggested that the intensity of GlcNPhAlk is six to eight folds higher than its counterpart with TMS, demonstrating GlcNPhAlk as the better candidate for glycan labelling (Fig. 1E&F). Cells incubated with GlcNPhAlk provided significant Raman mapped images with greater sensitivity, specificity and repeatability when compared to GlcNPhAlkTMS treated cells (Fig. 2A (ii)). Hence GlcNPhAlk was selected for further studies. Control images were also taken without labelling (Fig. 2A (i)).

2.4. Complementary Glycan Labelling through Fluorescence and Western Blot Analysis

There have been numerous reports of azido or alkynyl sugars being used as bioorthogonal chemical reporters with the help of “click chemistry” for the labelling of glycans in cells and living animals [43–46]. After the incorporation of azido/alkynyl sugars, they can be covalently labelled with various tags (e.g., biotin or fluorescent molecules) by chemical reactions such as Cu(I)-assisted [3 + 2] azide-alkyne cycloaddition (CuAAC), Staudinger ligation etc. The labelled glycans have been imaged and enriched using these techniques. Hence as a confirmation for metabolic labelling of GlcNPhAlk, we decided to pursue fluorescent analysis using azidonaphthalimide probe (Scheme S2, Fig. S3j†) and chemiluminescent Western blot analysis using biotin PEG azide both with the help of CuAAC [7,44]. Fluorescent analysis using azidonaphthalimide molecule proved that the glycan probe GlcNPhAlk is indeed labelling at the cell surface by *in vitro* studies (Fig. 2B, C). Confirmation of protein glycosylation was done by chemiluminescent Western blot analysis with the help of CuAAC between enriched alkynyl labelled proteins and azide PEG biotin resulting in the band formed from the cell lysates of GlcNPhAlk treated cells (Fig. 3A, B).

Azidonaphthalimide based fluorophore was synthesised since the counterpart contains alkyne functionality as a partner of the click reaction to form the triazole cycloadduct. Reactivity and click reaction triggered fluorescence was tested by performing a [3 + 2] cycloaddition with GlcNPhAlk (Fig. S7a†). The fluorescent intensity of the triazole cycloadduct was enhanced up to 30 times as it reacted with the GlcNPhAlk (Fig. S7d†). This enhancement is due to the replacement of weak donor like azide by much better triazole donor. The emission maximum of click-product was centred at 560 nm when excited at 441 nm (Fig. S7c†). Fluorescence labelling was performed in highly metastatic breast carcinoma MDA-MB-231 cells. Cells were incubated with

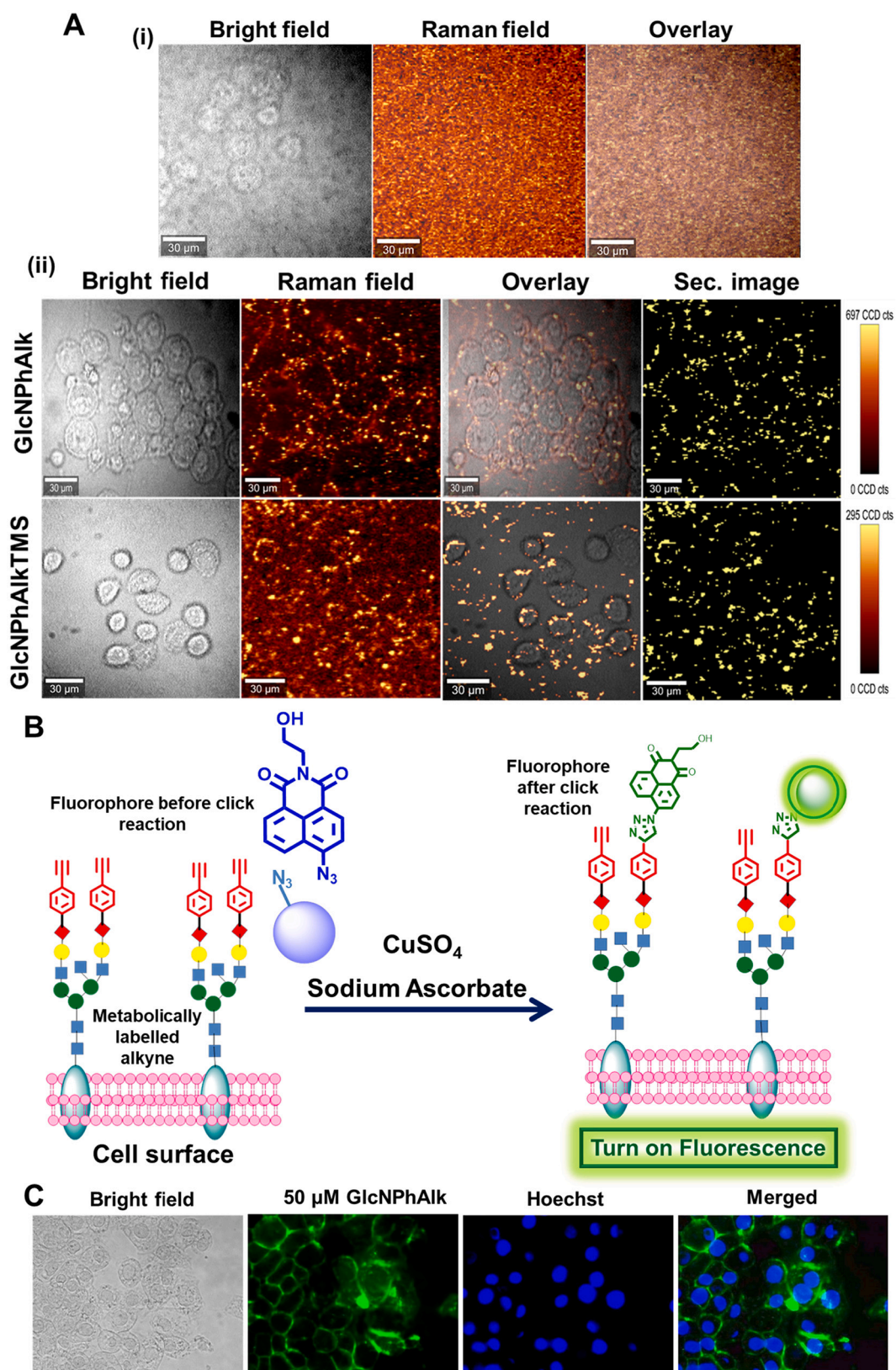


Fig. 2. A) (i) Images of HeLa cells without labelling (ii) Comparison of glycan labelling of GlcNPhAlk and GlcNPhAlkTMS respectively on HeLa cells. B) General scheme and C) confirmation of labelling through fluorescence in MDA-MB-231 cells.

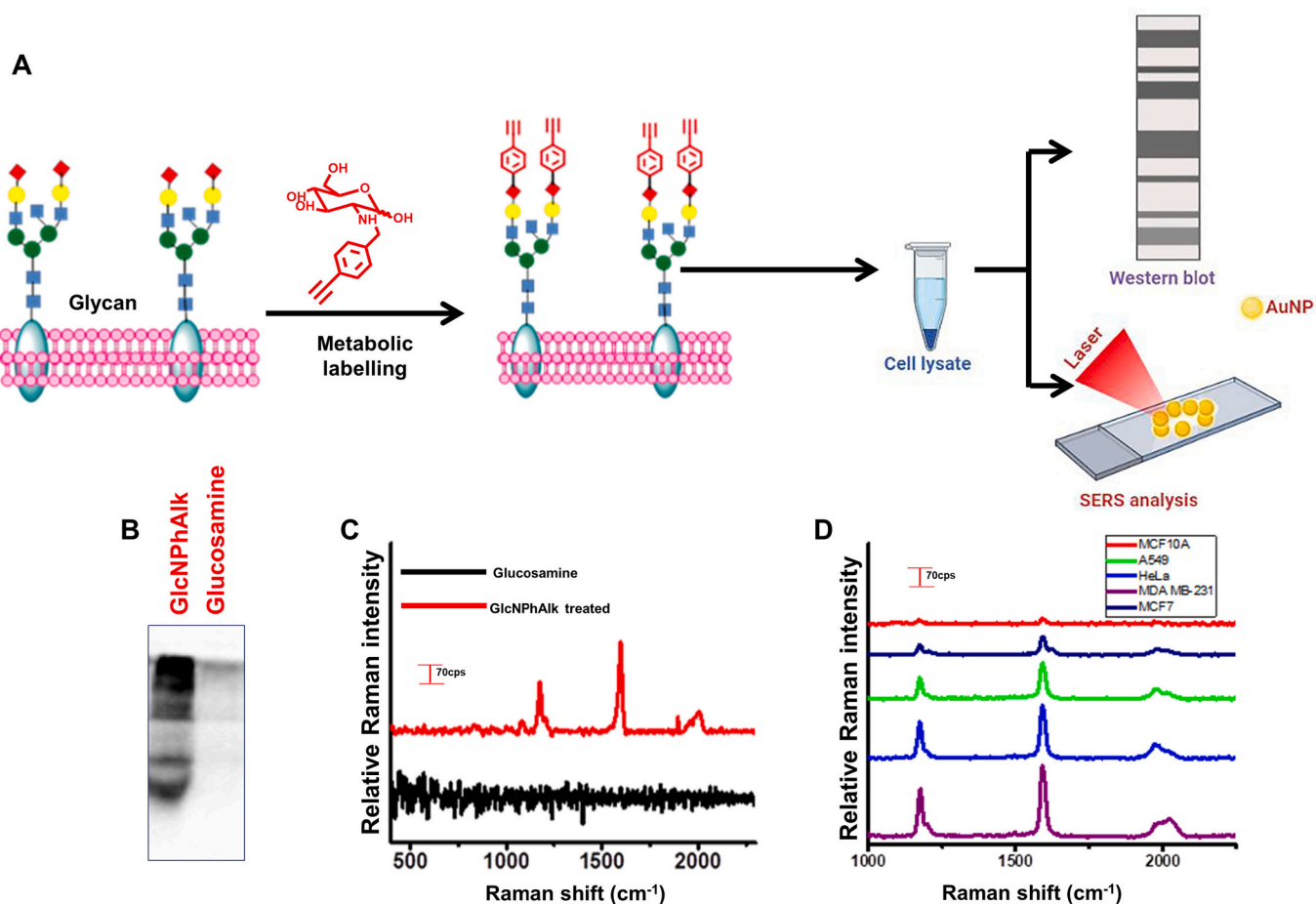


Fig. 3. A) Schematic representation of Western blotting and SERS analysis of cell lysates. B) Western blot analysis of MDA-MB 231 treated with GlcNPhAlk and C) corresponding SERS analysis of cell lysates. D) Quantification by SERS intensities of cell lysate.

GlcNPhAlk for 3 days and later azidonaphthalimide fluorophore tag was added followed by CuSO_4 and sodium ascorbate. After the incubation of 50 min, images were taken that indicated distinct labelling of cell-surface (Fig. 2C). Another set of control experiments was also conducted with the same procedure with glucosamine instead of GlcNPhAlk, to confirm that the fluorescence is click activated turn on phenomenon (Fig. S8†).

The extent of protein glycosylation by metabolically labelled alkyne tag was further evaluated by Western blot analysis. The presence of metabolically anchored alkyne was confirmed in MDA-MB-231 cells treated with GlcNPhAlk using CuAAC. For this, cell lysate was extracted and treated with azide-PEG3-biotin in presence of CuSO_4 and sodium ascorbate followed by horse radish peroxidase (HRP) conjugated streptavidin for chemiluminescent detection. A parallel experiment was carried out with glucosamine treated cells taken as a negative control. Increased volume of alkyne tagged glycoprotein were generated in cell lysate of GlcNPhAlk treated MDA-MB-231 cells while no bands were visible in the cell lysate from glucosamine treated cells indicating the detection of unique glycoproteins (Fig. 3A, B). Also, the labelled alkyne was further confirmed by the SERS analysis of cell lysates collected from both the GlcNPhAlk and glucosamine treated cells. Cell lysate obtained from GlcNPhAlk treatment displayed signature peaks at 1596 cm^{-1} and 1991 cm^{-1} which was absent in the cell lysates treated by glucosamine suggesting the alkyne group generation upon incubation of GlcNPhAlk with the cells (Fig. 3C).

2.5. Metastatic Potential and Cell-Surface Glycosylation in Cancer Cells

Numerous glycosyltransferase enzymes have been reported as catalysts for glycosylation which is mostly located in the Golgi apparatus in cells. Besides, glycosylation plays a critical part in cancer progression and metastasis and epithelial-mesenchymal transition (EMT) in cancer cells [11,47–49]. Metastatic transformation is attributed to the ability of cancer cells to grow into nearby normal tissue and then by moving through the walls of nearby lymph nodes or blood vessels and finally invading the lymphatic system and spreads through the bloodstream to other parts of the body.

As cancer malignancy is closely related to differential glycosylation in cells, we attempted the semi-quantitation of this aberrant glycosylation in cancer cells with respect to metastatic potential. Even though there have been previous attempts for imaging glycans using SERS techniques it was hugely hampered by the lack of specificity in cell surface mapping [15,16]. The variation in the glycosylation within the cell surface is always associated with the metastatic potential of cell lines [12,14]. Our major objective was to evaluate the glycosylation pattern in different cancer cells with varying metastatic capacity (Fig. 4A). For this, triple-negative breast cancer cells MDA-MB-231 with higher metastatic potential was compared to less metastatic breast carcinoma MCF7 and the normal mammary epithelial cell line MCF10A. Further, the experiment was extended to cervical cancer cell line HeLa and non-small lung cancer cell line A549 based on their metastatic potential as verified in the literature reports [25–27].

The cells were subjected to metabolic labelling with GlcNPhAlk and investigated the glycosylation pattern in terms of alkyne tagged sialic

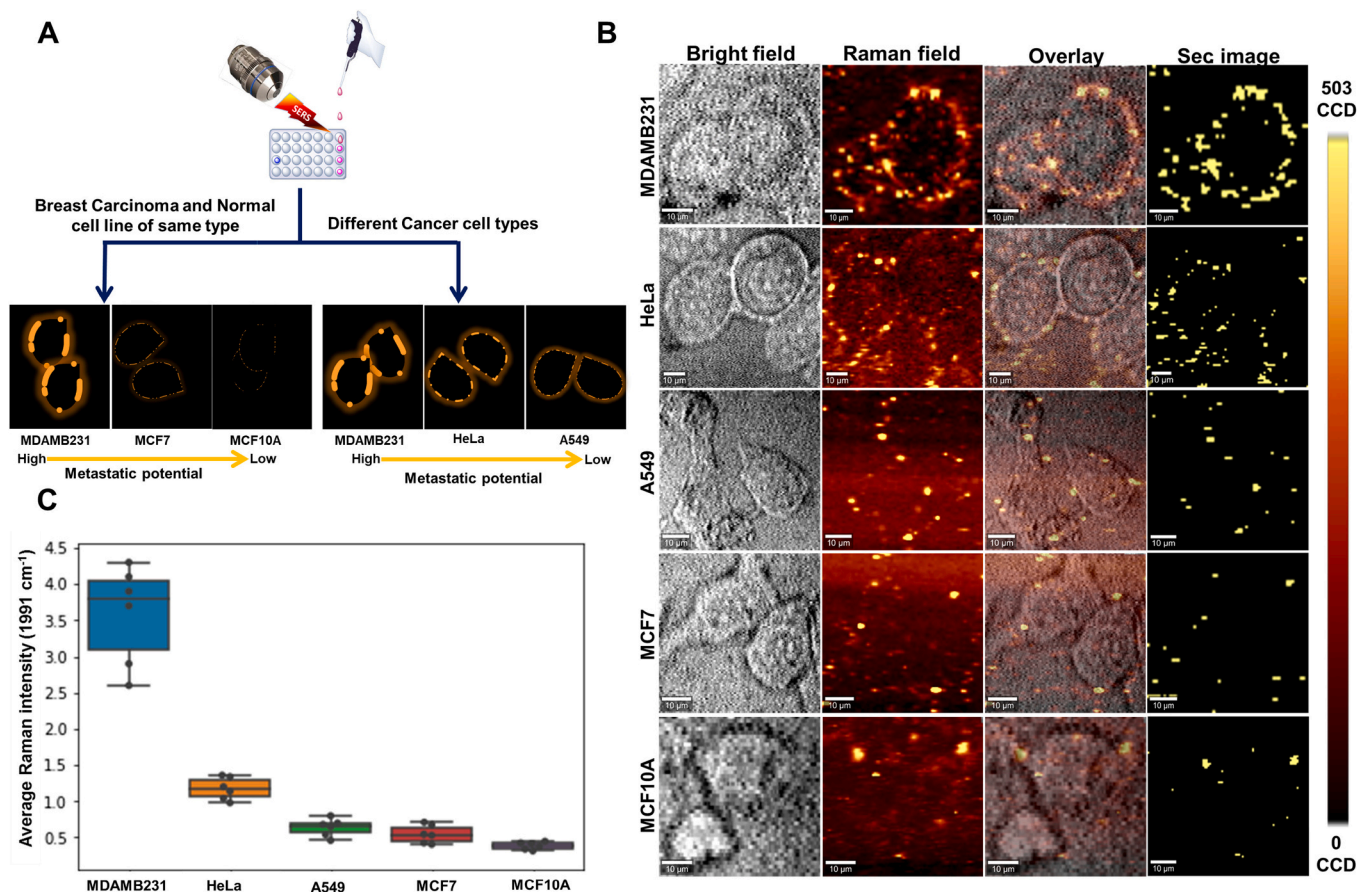


Fig. 4. A) Schematic representation of MGLSERS technique employed upon variation of glycosylation in cells with respect to metastatic potential B) Variation of glycan expression in different cells MDA-MB 231, HeLa, A549, MCF7 and MCF10A respectively. C) Average intensity of 1991 cm^{-1} is displayed through Boxplot with overlay points.

acid by SERS analysis as described earlier. From Fig. 4B & C, the extent of glycan labelling was found to be maximum for MDA-MB-231 while MCF10A exhibited the minimum GlcNPhAlk incorporation. Labelling of glycans in other cells are in between MDA-MB-231 and MCF10A in the order of MDA-MB-231 > HeLa > A549 > MCF7 > MCF10A. The same trend was also reflected in the average Raman peak intensity of GlcNPhAlk (1991 cm^{-1}) obtained from the image scan (Fig. 4B) being expressed in the form of a boxplot (Fig. 4C). It demonstrates the comparative distribution of a continuous variable and jittered points indicate each individual measurement in a group. Secondary Raman images of five cells were constructed based on the peak intensity by applying a threshold number from the colour scale bars. Only signals above the assigned threshold limit will appear as yellow spots, thus providing a much clear picture about the glycan expression in cell surface (Fig. 4B & Fig. S10†). Our results in Fig. 4B & C showed the direct correlation between glycan expression and metastasis which was further supported by the bound sialic acid estimation of the tested 5 cell lines using the thiobarbituric acid (TBA) method (Fig. S9†). Bound sialic acid expression in the cell lines are strongly correlated to the extent of glycan labelling revealed by SERS analysis (Fig. 4B). SERS intensities of cell lysates from these 5 cells also show the same trends (Fig. 3D). With these results, we have shown the variation in glycosylation in cancer cells of different origins (MDA-MB-231, HeLa, A549) as well as breast normal and cancer cells of the same origin (MDA-MB-231, MCF7, MCF10A) (Fig. 4A). Hence, GlcNPhAlk is benchmarked as a highly sensitive glycan labelling probe that can be used to predict the differential glycan expressions in various cell lines.

2.6. Glycosylation Inhibition through SERS Assessment

Finally, we have examined the glycosylation inhibition effect through the SERS modality by using P-3Fax-Neu5Ac, a global sialyltransferase inhibitor, whose therapeutic potential has been well established with previous literature [50,51]. There are several possible leaks to metabolic pathways as GlcNAc derivatives are not superior to bypass the NANS bottleneck and there are chances of converting to O-GlcNAc modified proteins which are mainly located in the nucleoplasmic region. Since Fig. 3B and C clearly show GlcNPhAlk labelling at the cell surface itself, therefore the involvement of O-GlcNAc transferase can be omitted [52,53]. Sialyltransferase is the enzyme involved in the biosynthetic pathway of sialic acids where it activates the CMP sialic acid (Cytidine-5'-monophospho-N-acetylneuraminic acid) to glycosylate the proteins in the Golgi compartment. Hence P-3Fax-Neu5Ac must reduce the extent of sialylation if GlcNPhAlk is labelled through the sialic acid pathway. The inhibitor was added in different concentrations starting from $5\text{ }\mu\text{M}$ to $20\text{ }\mu\text{M}$ and incubated for 72 h with the HeLa cells, along with GlcNPhAlk to verify the inhibition of glycosylation through SERS. The rate of inhibition was found to be directly proportional to the inhibitor concentration which not only proves the involvement of GlcNPhAlk through the sialic acid pathway but also confirms the efficiency of precise monitoring by SERS modality and it can be extended to the therapeutic applications for the glycan based therapies against cancer (Fig. 5A&B, Fig. S6†).

3. Conclusion

In summary, the cell surface glycan labelling phenomenon has been demonstrated using a newly designed phenylalkynylated derivative of

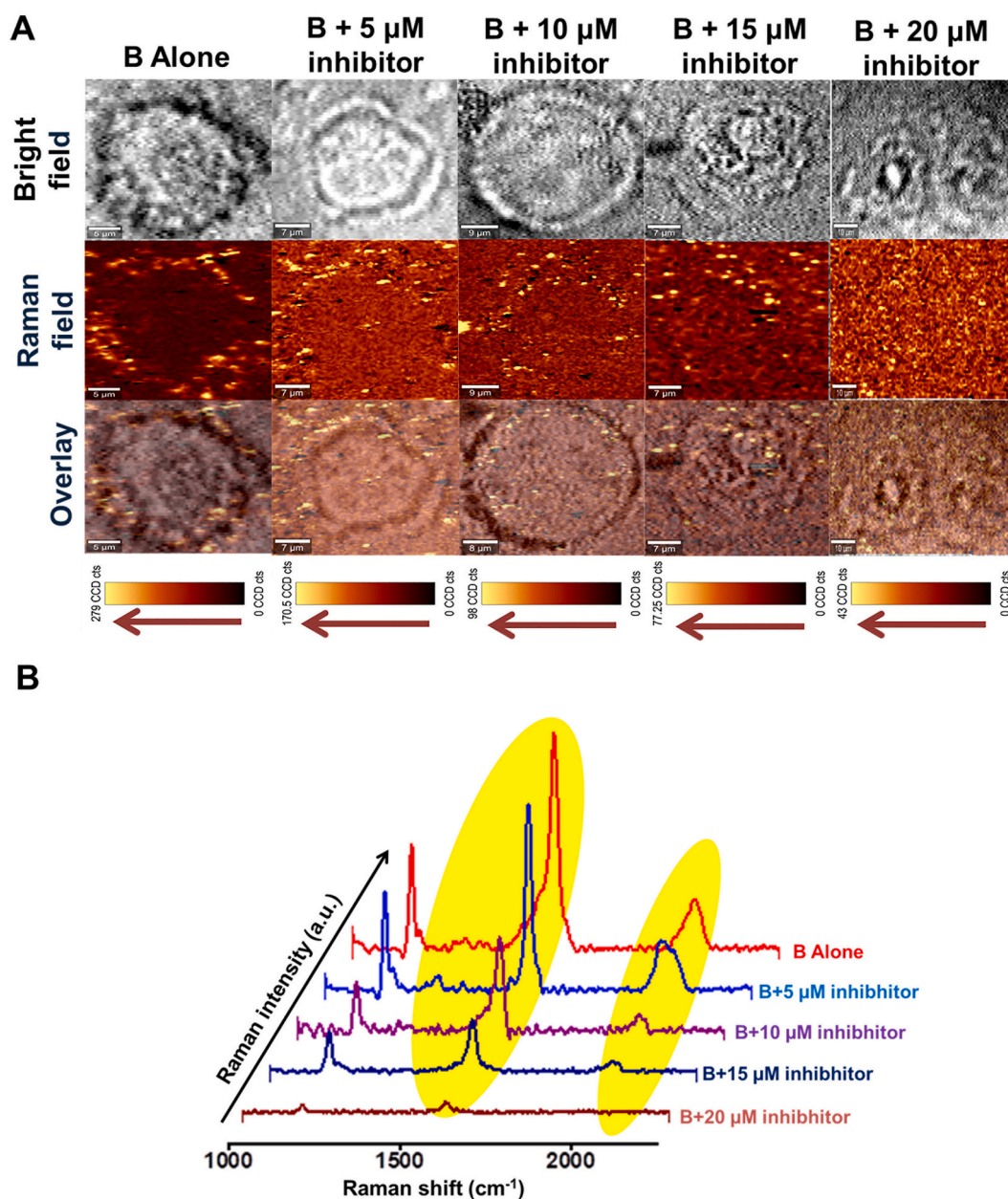


Fig. 5. A) Inhibition studies of glycans using sialyltransferase inhibitor P-3Fax-Neu5Ac on HeLa cells. B) Graphical representation of the average intensities 1596 and 1991 cm^{-1} of synthesised glycan alkyne tag.

glucosamine, GlcNPhAlk as the metabolic precursor of sialic acid for glycan imaging. As per our knowledge, this is a pioneering study that emphasizes metabolic glycan labelling capabilities of N-alkyl glucosamine through the SERS modality. This new sialic acid precursor also strengthens the metabolic labelling chemistry since it is formed by the reductive amination reaction which was not previously explored for MOE applications. We observed a linear relationship of the cell surface glycan imbalance of different cancer cells with respect to their metastatic potential through SERS. Comparison of cancer cells with different metastatic potential from the same origin (MDA-MB-231, MCF7, and MCF10 A) was also examined. Malignant breast carcinoma MDA-MB-231 cells with high metastatic potential reflected with highest Raman intensity in comparison to cervical carcinoma HeLa, lung adenocarcinoma A549 and breast carcinoma MCF7 cells with relatively less metastatic capacity. The normal mammary epithelial cell line MCF10A registered the least glycan labelling when tagged with GlcNPhAlk. This metabolic labelling has been validated through fluorescent imaging as a

complementary approach with the help of CuAAC and further confirmed its protein glycosylation by Western blot analysis. Moreover, we proved the inhibition of glycan biosynthesis in live cancer cells through SERS using a global sialyl-transferase inhibitor which validates the fact that the biosynthetic pathway of GlcNPhAlk is the same as of sialic acid. Although selective tumour labelling in vivo is still a challenge, clinical translation of these strategies for cancer targeted therapies is highly anticipated. Finally, it is worth mentioning that SERS coupled with metabolic labelling strategy is a highly sensitive and effective imaging technique that can have translational application in both glycan-based cancer therapy and cancer immunotherapy.

Author Contributions

The manuscript was written through contributions of all authors. All authors have given approval to the final version of the manuscript.

Author Statement

None. The manuscript is seen by all authors and approved for submission.

Declaration of Competing Interest

The authors declare that they have no known competing financial interests or personal relationships that could have appeared to influence the work reported in this paper.

Acknowledgment

K. K. M., M.M. and V.P.M thanks the CSIR mission mode project, Nano-biosensor and Microfluidics for Healthcare (HCP-0012). AcSIR Ph. D. student M.M thank UGC for research fellowship and V.P.M. thanks the CSIR Senior Project Associate (MLP0039). M.M.J. thanks CSIR for the Senior Research Associate (SRA) fellowship [13(9128-A) 2020-Pool].

Appendix A. Supplementary Data

Supplementary data to this article can be found online at <https://doi.org/10.1016/j.jphotobiol.2022.112506>.

References

- [1] K. Ohtsubo, S. Takamatsu, M.T. Minowa, A. Yoshida, M. Takeuchi, J.D. Marth, Dietary and genetic control of glucose transporter 2 glycosylation promotes insulin secretion in suppressing diabetes, *Cell*. 123 (2005) 1307–1321, <https://doi.org/10.1016/j.cell.2005.09.041>.
- [2] S. Cha, B. Ortega, H. Kurosu, K.P. Rosenblatt, M. Kuro-o, C. Huang, Removal of sialic acid involving klotho causes cell-surface retention of TRPV5 channel via binding to galectin-1, *Proc. Natl. Acad. Sci.* 105 (2008) 9805–9810.
- [3] X. Song, B. Xia, S.R. Stowell, Y. Lasanajak, D.F. Smith, R.D. Cummings, Novel fluorescent glycan microarray strategy reveals ligands for galectins, *Chem. Biol.* 16 (2009) 36–47, <https://doi.org/10.1016/j.chembiol.2008.11.004>.
- [4] E.A. Halabi, D. Pinotsi, P. Rivera-fuentes, Photoregulated fluxional fluorophores for live-cell super-resolution microscopy with no apparent photobleaching, *Nat. Commun.* 10 (2019) 1–10, <https://doi.org/10.1038/s41467-019-09217-7>.
- [5] Y. Liang, X. Jiang, R. Yuan, Y. Zhou, C. Ji, L. Yang, H. Chen, Q. Wang, Metabolism-based click-mediated platform for Specific imaging and Quantification of cell surface sialic acids, *Anal. Chem.* 89 (2016) 538–543, <https://doi.org/10.1021/acs.analchem.6b04141>.
- [6] B.L. Fang Hu, Youyong Yuan, Wenbo Wu, Duo Mao, Dual-responsive metabolic precursor and light-up AIEgen for cancer cell bioorthogonal labelling and precise ablation, *Anal. Chem.* 90 (2018) 6718–6724, <https://doi.org/10.1021/acs.analchem.8b00547>.
- [7] Hua Wang, R. Wang, Kaimin Cai, Hua He, Yang Liu, Z. Wang, X.Z. Ming Xu, Yiwen Sun, I.T. Dobrucki, Qian Yin, Li Tang, L.W. Dobrucki, Eric J. Chaney, Stephen A. Boppart, Timothy M. Fan, S. Lezmi, X. Chen, L. Yin, J. Cheng, Selective in vivo metabolic cell-labeling-mediated cancer targeting, *Nat. Chem. Biol.* 103 (2017) 12371–12376, <https://doi.org/10.1038/nchembio.2297>.
- [8] L. Wei, F. Hu, Y. Shen, Z. Chen, Y. Yu, C. Lin, M.C. Wang, W. Min, Live-cell imaging of alkyne-tagged small biomolecules by stimulated Raman scattering, *Nat. Methods* 11 (2014) 410–412, <https://doi.org/10.1038/nmeth.2878>.
- [9] Y. Chen, L. Ding, W. Song, H. Ju, Protein-specific Raman imaging of glycosylation on single cells with zone-controllable SERS effect, *Chem. Sci.* 7 (2016) 569–574, <https://doi.org/10.1039/c5sc03560k>.
- [10] R.W. Liang Lin, Xiangdong Tian, Senlian Hong, Peng Dai, Qiancheng You, X.C. Lianshun Feng, Can Xie, Zhong-Qun Tian, A bioorthogonal raman reporter strategy for SERS detection of glycans on live cells, *Angew. Chem. Int. Ed.* 52 (2013) 7266–7271, <https://doi.org/10.1002/anie.201301387>.
- [11] F.M. Tuccillo, A. De Laurentis, C. Palmieri, G. Fiume, P. Bonelli, A. Borrelli, P. Tassone, I. Scala, F.M. Buonaguro, I. Quinto, G. Scala, Aberrant glycosylation as biomarker for cancer: focus on CD43, *Biomed. Res. Int.* 2014 (2014), <https://doi.org/10.1155/2014/742831>.
- [12] D.H. Dube, C.R. Bertozzi, Glycans in cancer and inflammation - potential for therapeutics and diagnostics, *Nat. Rev. Drug Discov.* 4 (2005) 477–488, <https://doi.org/10.1038/nrd1751>.
- [13] M. Granovsky, J. Fata, J. Pawling, W.J. Muller, R. Khokha, J.W. Dennis, Suppression of tumor growth and metastasis in Mgat5-deficient mice, *Nat. Med.* 6 (2000) 306–312, <https://doi.org/10.1038/73163>.
- [14] A. Matsumoto, H. Cabral, N. Sato, K. Kataoka, Y. Miyahara, Assessment of tumor metastasis by the direct determination of cell membrane sialic acid expression, *Angew. Chem. Int. Ed.* 49 (2010) 5494–5497, <https://doi.org/10.1002/anie.201001220>.
- [15] D. Craig, S. Mcaughtrie, J. Simpson, C. McCraw, K. Faulds, D. Graham, Confocal SERS mapping of glycan expression for the Identification of cancerous cells, *Anal. Chem.* 86 (2014) 4775–4782.
- [16] M. Tabatabaei, G.Q. Wallace, F.A. Caetano, E.R. Gillies, S.S.G. Ferguson, F. Lagugn e-Labarthet, Controlled positioning of analytes and cells on a plasmonic platform for glycan sensing using surface enhanced Raman spectroscopy, *Chem. Sci.* 7 (2016) 575–582, <https://doi.org/10.1039/c5sc03332b>.
- [17] C.L. Jacobs, S. Goon, K.J. Yarema, S. Hinderlich, H.C. Hang, D.H. Chai, C. R. Bertozzi, Substrate specificity of the sialic acid biosynthetic pathway, *Biochemistry.* 40 (2001) 12864–12874, <https://doi.org/10.1021/bi010862s>.
- [18] H. M oller, V. B ohrsch, J. Bentrop, J. Bender, S. Hinderlich, C.P.R. Hackenberger, Glycan-specific metabolic oligosaccharide engineering of C7-substituted sialic acids, *Angew. Chem. Int. Ed.* 51 (2012) 5986–5990, <https://doi.org/10.1002/anie.201108809>.
- [19] H. Yamakoshi, K. Dodo, A. Palonpon, J. Ando, K. Fujita, S. Kawata, M. Sodeoka, Alkyne-tag Raman imaging for visualization of mobile small molecules in live cells, *J. Am. Chem. Soc.* 134 (2012) 20681–20689, <https://doi.org/10.1021/ja308529n>.
- [20] S.T. Laughlin, C.R. Bertozzi, Imaging the glycome, *Proc. Natl. Acad. Sci. U. S. A.* 106 (2009) 12–17, <https://doi.org/10.1073/pnas.0811481106>.
- [21] R. Xie, S. Hong, L. Feng, J. Rong, X. Chen, Cell-selective metabolic glycan labeling based on ligand-targeted liposomes, *J. Am. Chem. Soc.* 134 (2012) 9914–9917, <https://doi.org/10.1021/ja303853y>.
- [22] D.B. Agus, J.F. Alexander, W. Arap, S. Ashili, J.E. Aslan, R.H. Austin, V. Backman, K.J. Bethel, R. Bonneau, W.C. Chen, C. Chen-Tanyolac, N.C. Choi, S.A. Curley, M. Dallas, D. Damania, P.C.W. Davies, P. Decuzzi, L. Dickinson, L. Estevez-Salmeron, V. Estrella, M. Ferrari, C. Fischbach, J. Foo, S.I. Fraley, C. Frantz, A. Fuhrmann, P. Gascard, R.A. Gatenby, Y. Geng, S. Gerecht, R.J. Gillies, B. Godin, W.M. Grady, A. Greenfield, C. Hemphill, B.L. Hempstead, A. Hielscher, W.D. Hillis, E.C. Holland, A. Ibrahim-Hashim, T. Jacks, R.H. Johnson, A. Joo, J.E. Katz, L. Kelbauskas, C. Kesselman, M.R. King, K. Konstantopoulos, C.M. Kraning-Rush, P. Kuhn, K. Kung, B. Kwee, J.N. Lakins, G. Lambert, D. Liao, J.D. Licht, J. T. Liphardt, L. Liu, M.C. Lloyd, A. Lyubimova, P. Mallick, J. Marko, O.J.T. McCarty, D.R. Meldrum, F. Michor, S.M. Mumenthaler, V. Nandakumar, T.V. O'Halloran, S. Oh, R. Pasqualini, M.J. Paszek, K.G. Phillips, C.S. Poultnery, K. Rana, C. A. Reinhart-King, R. Ros, G.L. Semenza, P. Senechal, M.L. Shuler, S. Srinivasan, J. R. Staunton, Y. Stypula, H. Subramanian, T.D. Tlsty, G.W. Tormoen, Y. Tseng, A. Van Oudenaarden, S.S. Verbridge, J.C. Wan, V.M. Weaver, J. Widom, C. Will, D. Wirtz, J. Wojtkowiak, P.H. Wu, A physical sciences network characterization of non-tumorigenic and metastatic cells, *Sci. Rep.* 3 (2013) 1449, <https://doi.org/10.1038/srep01449>.
- [23] Y.L. Liu, C.K. Chou, M. Kim, R. Vasisht, Y.A. Kuo, P. Ang, C. Liu, E.P. Perillo, Y. A. Chen, K. Blocher, H. Hornig, Y.I. Chen, D.T. Nguyen, T.E. Yankeelov, M.C. Hung, A.K. Dunn, H.C. Yeh, Assessing metastatic potential of breast cancer cells based on EGFR dynamics, *Sci. Rep.* 9 (2019) 1–13, <https://doi.org/10.1038/s41598-018-37625-0>.
- [24] C.C. Palsuledesai, J.D. Ochocki, M.M. Kuhns, Y.C. Wang, J.K. Warmka, D. S. Chernick, E.V. Wattenberg, L. Li, E.A. Arriaga, M.D. Distefano, Metabolic labeling with an alkyne-modified isoprenoid analog facilitates imaging and quantification of the prenylome in cells, *ACS Chem. Biol.* 11 (2016) 2820–2828, <https://doi.org/10.1021/acscchembio.6b00421>.
- [25] K. Liu, P.A. Newbury, B.S. Glicksberg, W.Z.D. Zeng, S. Paithankar, E.R. Andrechek, B. Chen, Evaluating cell lines as models for metastatic breast cancer through integrative analysis of genomic data, *Nat. Commun.* 10 (2019), <https://doi.org/10.1038/s41467-019-10148-6>.
- [26] D.K. Mishra, R.A. Miller, K.A. Pence, M.P. Kim, Small cell and non small cell lung cancer form metastasis on cellular 4D lung model, *BMC Cancer* 18 (2018) 1–9, <https://doi.org/10.1186/s12885-018-4358-x>.
- [27] Y.F. Tu, B.A. Kaiparettu, Y. Ma, L.J.C. Wong, Mitochondria of highly metastatic breast cancer cell line MDA-MB-231 exhibits increased autophagic properties, *Biochim. Biophys. Acta Bioenerg.* 2011 (1807) 1125–1132, <https://doi.org/10.1016/j.bbambio.2011.04.015>.
- [28] N.J. Agard, J.A. Prescher, C.R. Bertozzi, A strain-promoted [3 + 2] azide-alkyne cycloaddition for covalent modification of biomolecules in living systems, *J. Am. Chem. Soc.* 126 (2004) 15046–15047, <https://doi.org/10.1021/ja044996f>.
- [29] C.R.B. Lara, K. Mahal, Kevin J. Yarema, Engineering Chemical Reactivity on Cell Surfaces Through Oligosaccharide Biosynthesis 276, 1997, pp. 1125–1128.
- [30] E. Saxon, C.R. Bertozzi, Cell surface engineering by a modified Staudinger reaction, *Science* (80-.). 287 (2000) 2007–2010, <https://doi.org/10.1126/science.287.5460.2007>.
- [31] R. Zeitler, A. Giannis, S. Danneschewski, E. Henk, T. Henk, C. Bauer, Inhibition of N-acetylglucosamine kinase and N-acetylmannosamine kinase, *Eur. J. Biochem.* 204 (1992) 1165–1168.
- [32] P.R. Wratil, R. Horstkorte, W. Reutter, Metabolic glycoengineering with N-acyl side chain modified mannosamines, *Angew. Chem. Int. Ed.* 55 (2016) 9482–9512, <https://doi.org/10.1002/anie.201601123>.
- [33] P.V. Chang, X. Chen, C. Smyrniotis, A. Xenakis, T. Hu, C.R. Bertozzi, P. Wu, Metabolic labeling of sialic acids in living animals with alkyne sugars, *Angew. Chem. Int. Ed.* 48 (2009) 4030–4033, <https://doi.org/10.1002/anie.200806319>.
- [34] J. Vanbeselaere, D. Vicogne, G. Matthijs, C. Biot, F. Foulquier, Y. Guerardel, Alkynyl monosaccharide analogues as a tool for evaluating Golgi glycosylation efficiency: application to congenital disorders of glycosylation (CDG), *Chem. Commun.* 49 (2013) 11293–11295, <https://doi.org/10.1039/c3cc45914d>.
- [35] B.W. Zaro, Y.Y. Yang, H.C. Hang, M.R. Pratt, Chemical reporters for fluorescent detection and identification of O-GlcNAc-modified proteins reveal glycosylation of the ubiquitin ligase NEDD4-1, *Proc. Natl. Acad. Sci. U. S. A.* 108 (2011) 8146–8151, <https://doi.org/10.1073/pnas.1102458108>.

- [36] Y. Kizuka, S. Funayama, H. Shogomori, M. Nakano, K. Nakajima, R. Oka, S. Kitazume, Y. Yamaguchi, M. Sano, H. Korekane, T.L. Hsu, H.Y. Lee, C.H. Wong, N. Taniguchi, High-sensitivity and low-toxicity fucose probe for glycan imaging and biomarker discovery, *Cell Chem. Biol.* 23 (2016) 782–792, <https://doi.org/10.1016/j.chembiol.2016.06.010>.
- [37] P.C.S.A.J.H. John Turkevich, A study of the nucleation and growth processes I in the synthesis of colloidal gold, *Discuss. Faraday Soc.* 11 (1951) 55–75.
- [38] M. Li, J. Wu, M. Ma, Z. Feng, Z. Mi, P. Rong, D. Liu, Alkyne-and nitrile-anchored gold nanoparticles for multiplex SERS imaging of biomarkers in cancer cells and tissues, *Nanotheranostics*. 3 (2019) 113–119, <https://doi.org/10.7150/ntno.30924>.
- [39] c Y.R. and David C. Kennedy, a Craig S. McKay, ab Li-lin Tay, J.P. Pezacki, Carbon-bonded silver nanoparticles: alkyne-functionalized ligands for SERS imaging of mammalian cells, *ChemComm.* 47 (2011) 3156–3158, <https://doi.org/10.1039/c0cc05331g>.
- [40] Z.M.M.Ž.Č. Snezzana Miljanić, Leo Frkanec, Tomislav Biljan, Recent advances in linear and nonlinear Raman spectroscopy I, *J. Raman Spectrosc.* 38 (2007) 1538–1553, <https://doi.org/10.1002/jrs>.
- [41] L. Carroll, T.H. Witney, E.O. Aboagye, Design and synthesis of novel 18F-radiolabelled glucosamine derivatives for cancer imaging †, *Med. Chem. Commun.* 4 (2013) 653–656, <https://doi.org/10.1039/c3md00023k>.
- [42] W. Qin, K. Qin, X. Fan, L. Peng, W. Hong, Y. Zhu, P. Lv, Y. Du, R. Huang, M. Han, B. Cheng, Y. Liu, W. Zhou, C. Wang, X. Chen, Artificial cysteine S-glycosylation induced by per-O-acetylated unnatural monosaccharides during metabolic glycan labeling, *Angew. Chem. Int. Ed.* 57 (2018) 1817–1820, <https://doi.org/10.1002/anie.201711710>.
- [43] J.M. Baskin, J.A. Prescher, S.T. Laughlin, N.J. Agard, P.V. Chang, I.A. Miller, A. Lo, J.A. Codelli, C.R. Bertozzi, Copper-free click chemistry for dynamic in vivo imaging, *Proc. Natl. Acad. Sci. U. S. A.* 104 (2007) 16793–16797, <https://doi.org/10.1073/pnas.0707090104>.
- [44] T.L. Hsu, S.R. Hanson, K. Kishikawa, S.K. Wang, M. Sawa, C.H. Wong, Alkynyl sugar analogs for the labeling and visualization of glycoconjugates in cells, *Proc. Natl. Acad. Sci. U. S. A.* 104 (2007) 2614–2619, <https://doi.org/10.1073/pnas.0611307104>.
- [45] D. Rabuka, S.C. Hubbard, S.T. Laughlin, S.P. Argade, C.R. Bertozzi, A chemical reporter strategy to probe glycoprotein fucosylation, *J. Am. Chem. Soc.* 128 (2006) 12078–12079, <https://doi.org/10.1021/ja064619y>.
- [46] M. Sawa, T. Hsu, T. Itoh, M. Sugiyama, S.R. Hanson, P.K. Vogt, C. Wong, Glycoproteomic probes for fluorescent imaging of fucosylated glycans in vivo 103, 2006, pp. 12371–12376.
- [47] N. Taniguchi, Y. Kizuka, Glycans and cancer: Role of N-Glycans in cancer biomarker, progression and metastasis, in: *And Therapeutics*, 1st ed, Elsevier Inc., 2015, <https://doi.org/10.1016/bs.acr.2014.11.001>.
- [48] R.A.W.J. Raghu Kalluri, Particle-in-cell simulations of a beam driven plasma, *Phys. Plasmas*. To be subm (2010) 1420–1428, <https://doi.org/10.1172/JCI39104.1420>.
- [49] C.Y. Chen, Y.H. Jan, Y.H. Juan, C.J. Yang, M.S. Huang, C.J. Yu, P.C. Yang, M. Hsiao, T.L. Hsu, C.H. Wong, Fucosyltransferase 8 as a functional regulator of nonsmall cell lung cancer, *Proc. Natl. Acad. Sci. U. S. A.* 110 (2013) 630–635, <https://doi.org/10.1073/pnas.1220425110>.
- [50] C. Büll, T.J. Boltje, E.A.W. Van Dinther, T. Peters, A.M.A. De Graaf, J.H.W. Leusen, M. Kreutz, C.G. Figdor, M.H. Den Brok, G.J. Adema, Targeted delivery of a sialic acid-blocking glycomimetic to cancer cells inhibits metastatic spread, *ACS Nano* 9 (2015) 733–745, <https://doi.org/10.1021/nn5061964>.
- [51] C.D. Rillahan, A. Antonopoulos, C.T. Lefort, R. Sonon, K. Ley, A. Dell, S.M. Haslam, J.C. Paulson, NIH public access, *Nat. Chem. Biol.* 8 (2013) 661–668, <https://doi.org/10.1038/nchembio.999.Global>.
- [52] J. Du, M.A. Meledeo, Z. Wang, H.S. Khanna, V.D.P. Paruchuri, K.J. Yarema, Metabolic glycoengineering: sialic acid and beyond, *Glycobiology*. 19 (2009) 1382–1401, <https://doi.org/10.1093/glycob/cwp115>.
- [53] S.R. Stowell, T. Ju, R.D. Cummings, Protein glycosylation in cancer, *Annu. Rev. Pathol. Mech. Dis.* 10 (2015) 473–510, <https://doi.org/10.1146/annurev-pathol-012414-040438>.